Faculdade de Engenharia da Universidade do Porto

Process Intensification for Butyl Acrylate Synthesis based on Sorption-Enhanced Reaction and Pervaporation-based Hybrid Processes

Dissertation presented to Faculdade de Engenharia da Universidade do Porto for the degree of PhD in Chemical and Biological Engineering

by

Dânia Sofia Martins Constantino

Supervisor: Professor Alírio E. Rodrigues

Co-supervisors: Dr. Ana M. Ribeiro and Dr. Rui P. Faria

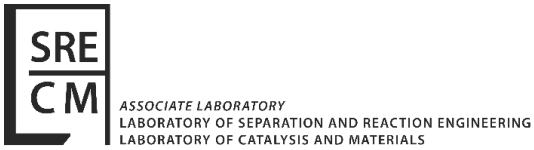

Laboratory of Separation and Reaction Engineering, Associate Laboratory LSRE-LCM

Department of Chemical engineering, Faculty of Engineering, University of Porto

2019

FEUP-LSRE/LCM - Universidade do Porto

This thesis was financially supported by Project POCI-01-0145-FEDER-006984 – Associate Laboratory LSRE-LCM funded by FEDER through COMPETE2020 Programa Operacional Competitividade e Internacionalização (POCI) – and by national funds through FCT – Fundação para a Ciência e Tecnologia, Associate Laboratory LSRE-LCM - UID/EQU/50020/2019 - funded by national funds through FCT/MCTES (PIDDAC), and Project NORTE-01-0145-FEDER-000006, supported by Norte Portugal Regional Operational Programme (NORTE 2020), under the Portugal 2020 Partnership Agreement, through the European Regional Development Fund (ERDF).

Acknowledgements

Some people were essential to accomplish this project, so my deepest acknowledgements are for them. First of all, I want to thank to Associate Laboratory of Separation and Reaction Engineering and Catalysis and Materials, namely to its Director, Professora Madalena Dias, for giving me this great opportunity that contributed for my personal and professional grow up, as well as all her availability and support to solve any bureaucratic issue, every time it was required.

Now, I would like to express my sincere gratitude to my supervisor, Professor Alírio Rodrigues, for the continuous support, guidance, motivation to do always more and better, and for his immense shared knowledge. His long and successful journey is impressive being an inspiration for all who worked or dealt with him, so I am privileged to be part of his work-team.

Then, I would like to thank to my co-supervisors, Dr Ana Mafalda Ribeiro and Dr Rui Pedro Faria, for all the support, guidance, friendship and availability for productive discussions about the main challenges that were emerging during this project, which were an asset to make important decisions when required. Their knowledge and abilities were crucial along this journey. Thank you for all comments and advices.

I cannot forget that I had the pleasure to start this project with Dr Carla Pereira, who impressed me by her great abilities and the way she faces each challenge. I am very grateful for her advices, motivation and friendship and I wish her the best of luck, mainly at this stage of her life.

I am deeply thankful to my dear friends, namely, Filipa, Vanessa, Raquel, Manuela and Mariana (the girl's team of the twelve o'clock), with whom I shared doubts, fears and laughs. Thank you girls for your patience and for your friendship.

My last acknowledgements, but not less important, go to my parents, by their dedication and patience, my brother, Luis Constantino and my husband, Wesley Souza, for all the emotional support and, finally, to the love of my life, my son, Santiago, who challenges me every day to be a better person.

"New ways of thinking—an integrated multidimensional approach to the problems of global sustainability—have long been needed, and it is up to us to decide whether the especially difficult challenges that we are facing today will jolt us into finding and accepting them."

by Peter H. Raven

Former president of the American Association for the Advancement of Science, 2002.

Resumo

A síntese de acrilato de butilo obtido através da esterificação do ácido acrílico e do n-butanol apresenta algumas limitações devido ao equilíbrio da reação e sobretudo à complexidade termodinâmica do sistema. Para além disso, existe um elevado risco de polimerização do ácido acrílico e do acrilato de butilo quando submetidos a elevadas temperaturas. Estas limitações fazem deste sistema um tema muito desafiante entre a comunidade científica no sentido de encontrar um processo capaz de ultrapassar estes inconvenientes, melhorando o processo convencional em termos ambientais e económicos.

Nesse sentido, o objetivo deste trabalho consistiu no estudo de diferentes estratégias de intensificação de processos para a síntese de acrilato de butilo com base na integração do processo de reação e separação numa só unidade por forma a ultrapassar a conversão de equilíbrio por remoção contínua da água (subproduto) recorrendo a técnicas cromatográficas (adsorção) e de pervaporação. Deste modo, as diferentes estratégias adotadas nesta investigação contemplaram: reatores cromatográficos de leito fixo, reatores cromatográficos de leito fixo com membranas integradas e, numa fase posterior, processos cíclicos de adsorção/ pervaporação, nomeadamente reatores cromatográficos de leito móvel simulado. Em todos os casos optou-se por usar a mesma fase estacionária, a resina de permuta iónica Amberlyst-15, de modo a facilitar a comparação dos diferentes processos estudados.

Assim, numa primeira fase, foram realizados experimentalmente estudos dinâmicos de adsorção e pervaporação, na ausência de reação, a fim de estimar os respetivos parâmetros de cada componente e de forma a ser possível prever e comparar o desempenho dos reatores de leito fixo e de leito fixo com membranas hidrofílicas integradas. Para isso, modelos matemáticos foram desenvolvidos para cada tecnologia, considerando fenómenos de transferência de massa, reação, adsorção e pervaporação, os

quais foram posteriormente estendidos para implementação de tecnologias de processos cíclicos, como o reator de leito móvel simulado e o reator de membranas de leito móvel simulado.

Os modelos matemáticos previamente desenvolvidos permitiram o estudo da otimização dos respetivos processos abordados neste trabalho e o dimensionamento dos mesmos à escala industrial.

A síntese experimental de acrilato de butilo foi também realizada no reator de leito móvel simulado à escala piloto disponível no laboratório (LICOSEP), variando alguns parâmetros de operação no sentido de validar o modelo matemático previamente desenvolvido no qual foram usados os parâmetros de adsorção multicomponente previamente determinados numa unidade de leito fixo na ausência de reação.

Numa fase final, foi realizada uma breve análise aos fatores energéticos e económicos envolvidos nos diferentes processos cíclicos à escala industrial de forma a avaliar a viabilidade e competitividade das estratégias de intensificação do processo propostas neste trabalho para a síntese de acrilato de butilo comparativamente aos diferentes processos apresentados na literatura.

Abstract

The butyl acrylate synthesis obtained from the esterification reaction between acrylic acid and n-butanol presents some limitations due to the reaction equilibrium and mainly due to the thermodynamic complex behaviour of the system. Furthermore, there is a high risk of polymerisation of acrylic acid and butyl acrylate when they are submitted to high temperatures. All these limitations make this system a very challenging subject among the scientific community towards finding a process that is able to overcome these drawbacks improving the conventional process regarding economic and environmental issues.

The main objective of this work was to study different process intensification strategies for the butyl acrylate synthesis based on the integration of reaction and separation in a single unit in order to overcome the equilibrium conversion by the continuous removal of water (by-product) using chromatographic (adsorption) and pervaporation techniques. Thus, the different strategies adopted in this research involved: fixed-bed chromatographic reactors, fixed-bed chromatographic reactors with integrated membranes and, at a later stage, cyclic adsorption/ pervaporation processes, namely simulated moving bed chromatographic reactors. In all cases, the same stationary phase was used, the Amberlyst-15 ion exchange resin, in order to perform a fair comparison between the different studied processes.

Thus, in a first stage, dynamic studies of adsorption and pervaporation were accomplished, in the absence of reaction, in order to estimate the respective parameters for each compound and to enable the prediction and comparison of the performance between the fixed-bed adsorptive reactor and the fixed-bed adsorptive reactor with integrated hydrophilic membranes. For that, mathematical models were developed for each technology, considering phenomena like mass transfer, reaction, adsorption and

pervaporation, which were then extended to model the other continuous processes, such as the simulated moving bed reactor and the simulating moving bed membrane reactor.

The mathematical models previously defined allowed to study the optimisation of the processes addressed in this work and to perform the respective scaling up to industrial scale.

The experimental butyl acrylate synthesis was also carried out in the simulate moving bed reactor pilot scale unit (LICOSEP) available in the laboratory, by changing some operating parameters in order to validate the mathematical model developed earlier using the multicomponent adsorption equilibrium parameters previously determined in a fixed-bed unit in absence of reaction.

Finally, a brief analysis to the energetic and economic factors involved in the different cyclic processes at industrial scale was performed aiming to evaluate the viability and competitiveness of the processes intensification strategies proposed in this work for the butyl acrylate synthesis comparatively to the different processes presented in the open literature.

Table of Contents

List of Figures

CHAPTER 2

CHAPTER 3

CHAPTER 4

CHAPTER 5

CHAPTER 6

CHAPTER 7

CHAPTER 8

List of Tables

CHAPTER 2

CHAPTER 3

CHAPTER 4

CHAPTER 5

CHAPTER 6

CHAPTER 7

CHAPTER 8

1. Introduction

This Chapter presents a brief introduction about process intensification, namely, for the synthesis of butyl acrylate, and the respective potential to overcome the drawbacks associated with its production, focusing, in particular, on adsorption/pervaporation based cyclic processes and on the global objectives of this work.

1.1. Motivation and Relevance

Numerous global market studies have predicted a considerable growth in the butyl acrylate (BAc) demand for long forecast periods mainly due to its resilient features which make it extremely important for several industrial applications. BAc is usually obtained from an esterification reaction between acrylic acid (AAc) and n-butanol having water as by-product. However, its conventional production involves a complex multistage process with homogeneous catalysis [1] and the subsequent processes (product purification) represents high operating and investment costs. Therefore, a Process Intensification (PI) study can bring great advantages for the production of this acrylic ester leading to a more compact design towards a more energy efficient and profitable process.

Over the last decades, PI is a subject that has been explored in chemical engineering research, being the key to find new paths towards more sustainable processes allowing a more efficient answer to the market demand of some products of industrial interest. Nowadays, it is possible to find different definitions for PI in the open literature. Gerven and Stankiewicz selected and gathered some of them in their recent review about fundamentals of PI [2] and, in summary, most of them are related with strategies that allow to drastically reduce the energy consumption and, consequently, improve the process efficiency by compacting the respective plant design. For that, innovation and creativity are a constant challenge in this field.

Multifunctional reactors, where reaction and separation steps are integrated into a single equipment, usually known as reactive separations, is one of the most relevant examples of PI. This concept leads to smaller, cleaner and more energy-efficient processes than the conventional ones [3, 4] since the reaction and separation take place simultaneously. Furthermore, it allows overtaking the equilibrium limitations by removing one of the products continuously and therefore improves the reaction conversion. Among the reactive separations, chromatographic reactors and reactive distillations are, currently, the most studied for systems that present limitations due to the reaction equilibrium like is the BAc system case. Although chromatography is more advantageous than distillation for complex molecules that are difficult to separate by evaporation process [5], like AAc and BAc, there are only a few studies concerning chromatographic reactors for BAc synthesis [6, 7]. Actually, the first report regarding the

application of such reactors to this particular system is one of the most relevant outcomes of the present thesis [8]. In this kind of technology, the separation process is accomplished by adsorption while the reaction step occurs simultaneously enabling operating at milder temperatures than reactive distillation. Definitely, this is a crucial factor in the BAc system since there is a high risk of polymerisation of BAc and AAc when they are exposed to high temperatures.

Meanwhile, a new concept based on chromatographic reactors was developed some years ago, the simulated moving bed reactor (SMBR) which combines reaction with chromatographic separation in a cyclic process. It consists of several fixed-bed chromatographic reactors connected in series forming a closed loop allowing operating in a continuous mode. It is based on the true moving bed (TMB) concept where a counter-current flow of the fluid and the solid phases is expected, which maximizes the mass transfer driving force, providing a better use of the adsorbent than in the batch mode [9]. However, this operation implies the motion of the solid, which is not readily feasible and can be overcome by the use of simulated moving bed (SMB) technology where the solid phase motion is simulated by periodically shifting the outlet and inlet streams at regular time intervals, the switching time. Moreover, this technology is also more advantageous with respect to batch preparative chromatography, particularly due to the continuous nature of the operation and to a more efficient use of the stationary and mobile phases, since it enables decreasing the desorbent requirements and improving the productivity per unit of time and unit of mass of stationary phase [9]. SMBR technology was already investigated for the synthesis of different oxygenated compounds like acetals and esters: diethylacetal [10], dimethylacetal [11], dibutoxyethane [12], dietoxybutane [13], and green solvents as the ethyl lactate [14], among others, where eluent savings and productivity improvements were reported.

More recently, a novel multifunctional reactor emerged from the integration of the SMB technology with hydrophilic membranes, the simulated moving bed membrane reactor, also known as PermSMBR. According to the literature [15,16,17], this new hybrid technology enables to improve the water removal in a continuous process, using different separation techniques simultaneously (adsorption and pervaporation), which was investigated for acetals and green solvents production leading to higher productivities with lower eluent consumption than SMBR.

1.2. Objectives and Outline

The present work focuses on the development of new sustainable alternative processes for BAc synthesis based on the simulated moving bed technology (SMB), namely, SMBR and PermSMBR processes, where different separation techniques, adsorption and/or pervaporation, are combined with reaction in the same equipment. For that, the knowledge of fundamental data, like adsorption equilibrium, reaction kinetics and pervaporation data, is crucial in order to be possible to implement a mathematical model able to predict the performance of the different reactors. This way, firstly, fixed-bed adsorptive reactors and fixed-bed adsorptive membrane reactors will be separately studied, which are, respectively, the fundamental units of each of the previous processes.

Therefore, this thesis comprises nine chapters where the different tasks required for the implementation of the SMBR and PermSMBR processes for BAc synthesis are described and the respective results are discussed.

The first Chapter evidences the motivation and relevance of the topic highlighting the main objectives of this work.

In the second Chapter, an overview of the most relevant patented processes and of alternative processes based on PI for BAc synthesis is reported. In addition, new PI approaches for esterification reactions are addressed.

The third Chapter is related with the dynamic study of the BAc synthesis in a fixed-bed adsorptive reactor (FBR) using Amberlyst-15 ion exchange resin (A-15) simultaneously as catalyst and as adsorbent, which is a very important step to determine the best operating conditions required to implement a SMBR process. Furthermore, a mathematical model able to describe the synthesis of BAc in a FBR is developed, where experimentally determined multicomponent adsorption equilibrium data are used together with the kinetic data obtained in batch conditions over A-15 by Ostaniewicz-Cydzik and her co-workers [18]. Then, the mathematical model is validated by reactive adsorption experiments conducted under different operating conditions.

The fourth Chapter concerns the study of the BAc synthesis in a fixed-bed membrane reactor (FBMR) considering the same catalyst/adsorbent material (A-15) and an hydrophilic pervaporation membrane, for which experimental pervaporation data are measured in the absence of reaction using a pilot scale unit. Afterwards, that data is

considered in the mathematical model developed to predict the performance of a FBMR to produce BAc at different operating conditions and for comparison with FBR results.

The synthesis of BAc in a SMBR is numerically investigated by developing a mathematical model taking into account the kinetic and the multicomponent adsorption equilibrium data previously determined and validated in the FBR study. This way, an optimisation study is performed in order to determine the ideal operating conditions. These data enabled to proceed to the scale up of the unit (SMBR) to industrial scale (IS) assessing its viability, comparing it with other alternative processes proposed in open literature. The experimental BAc synthesis in a pilot scale SMBR unit (LICOSEP) is also performed for validation of the mathematical model. All experimental and simulation data obtained at this stage are gathered in Chapter five.

Afterwards, a new PI configuration based on SMBR for BAc synthesis was created and explored, comprising a FBR followed by a SMBR, and its viability was also evaluated comparing it with other processes, including the conventional SMBR. The respective study at industrial scale is presented in Chapter six.

Chapter seven presents the PermSMBR process study for BAc synthesis. This technology is numerically investigated under different operating parameters and the ideal operating conditions are described. For that, a complex mathematical model is developed considering all pervaporation, adsorption and kinetic data used in the FBMR study. An optimisation study is carried out by studying different configurations and the respective performance is evaluated. The PermSMBR unit is scaled up to industrial scale in order to assess its feasibility and to compare with SMBR performance.

Additionally, a brief economic analysis is detailed in Chapter eight for all studied processes in this work and a comparison between the processes here suggested and the alternative processes that have been proposed in the literature is performed regarding the most relevant economic parameters.

Finally, the most relevant remarks and suggestions for future work are presented in Chapter nine.

1.3. References

1. Niesbach, A.; Kuhlmann, H.; Keller, T.; Lutze, P.; Górak, A., Optimisation of industrial-scale n-butyl acrylate production using reactive distillation. *Chem Eng Sci* **2013,** 100, 360-372.

2. Van Gerven, T.; Stankiewicz, A., Structure, Energy, Synergy, Time—The Fundamentals of Process Intensification. *Industrial & Engineering Chemistry Research* **2009,** 48, (5), 2465-2474.

3. Stankiewicz, A. I.; Moulijn, J. A., Process intensification: Transforming chemical engineering. *Chemical Engineering Progress* **2000,** 96, 22-33.

4. Stankiewicz, A., Reactive separations for process intensification: an industrial perspective. *Chem Eng Process* **2003,** 42, 137-144.

5. Lode, F.; Mazzotti, M.; Morbidelli, M., A New Reaction-Separation Unit: The Simulated Moving Bed Reactor. *CHIMIA International Journal for Chemistry* **2001,** 55, 883-886.

6. Moraru, M. D.; Bildea, C. S., Design and plantwide control of n-butyl acrylate production process. *Journal of Process Control* **2017,** 58, 46-62.

7. Moraru, M. D.; Bildea, C. S.; Milea, A., Design and Economic Evaluation of a Process for n-Butyl Acrylate Production. *U.P.B. Sci. Bull, Series B* **2016,** 78, 113.

8. Constantino, D. S. M.; Pereira, C. S. M.; Faria, R. P. V.; Ferreira, A. F. P.; Loureiro, J. M.; Rodrigues, A. E., Synthesis of butyl acrylate in a fixed-bed adsorptive reactor over Amberlyst 15. *AIChE Journal* **2015,** 61, (4), 1263-1274.

9. Mazzotti, M.; Storti, G.; Morbidelli, M., Optimal operation of simulated moving bed units for nonlinear chromatographic separations. *Journal of Chromatography A* **1997,** 769, (1), 3-24.

10. Silva, V. M. T. M.; Rodrigues, A. E., Novel process for diethylacetal synthesis. *AIChE Journal* **2005,** 51, (10), 2752-2768.

11. Pereira, C. S. M.; Gomes, P. S.; Gandi, G. K.; Silva, V. M. T. M.; Rodrigues, A. E., Multifunctional Reactor for the Synthesis of Dimethylacetal. *Industrial & Engineering Chemistry Research* **2007,** 47, (10), 3515-3524.

12. Graça, N. S.; Pais, L. S.; Silva, V. M. T. M.; Rodrigues, A. E., Analysis of the synthesis of 1,1-dibutoxyethane in a simulated moving-bed adsorptive reactor. *Chemical Engineering and Processing: Process Intensification* **2011,** 50, (11–12), 1214-1225.

13. Graça, N.; Rodrigues, A., Application of membrane technology for the enhancement of 1, 1-diethoxybutane synthesis. *Chemical Engineering and Processing: Process Intensification* **2017,** 117, 45-57.

14. Pereira, C. S. M.; Zabka, M.; Silva, V. M. T. M.; Rodrigues, A. E., A novel process for the ethyl lactate synthesis in a simulated moving bed reactor (SMBR). *Chem Eng Sci* **2009,** 64, (14), 3301-3310.

15. Pereira, C. S. M.; Rodrigues, A. E., Process intensification: New technologies (SMBR and PermSMBR) for the synthesis of acetals. *Catalysis Today* **2013,** 218–219, 148-152.

16. Silva, V. M. T. M.; Pereira, C. S. M.; Rodrigues, A. E., PermSMBR—A new hybrid technology: Application on green solvent and biofuel production. *AIChE Journal* **2011,** 57, (7), 1840-1851.

17. Rodrigues, A.; Pereira, C.; Minceva, M.; Pais, L. S.; Ribeiro, A.; Ribeiro, A. M.; Silva, M.; Graça, N.; Santos, J. C., *Simulated Moving Bed Technology: Principles, Design and Process Applications*. Elsevier Science 2015.

18. Ostaniewicz-Cydzik, A. M.; Pereira, C. S. M.; Molga, E.; Rodrigues, A. E., Reaction Kinetics and Thermodynamic Equilibrium for Butyl Acrylate Synthesis from n-Butanol and Acrylic Acid. *Industrial & Engineering Chemistry Research* **2014,** 53, (16), 6647-6654.

2. State-of-the-Art

In this Chapter, the most relevant data about the global butyl acrylate market and respective applications are presented as well as an overview on the patented and alternative processes integration strategies for the butyl acrylate synthesis suggested in open literature. New process intensification approaches are also addressed.

This Chapter is adapted from Constantino, D. S. M.; Faria, R. P. V.; Ribeiro, A. M.; Rodrigues, A. E., "Butyl Acrylate Production: a Review on Process Intensification Strategies". *Chemical Engineering and Processing: Process Intensification*, **2019**, 142. DOI 10.1016/j.cep.2019.107563

2.1. Introduction

Beyond several processes that were already patented for the BAc synthesis, process integration based strategies have been investigated along the last decades aiming to find the best solution in terms of industrial implementation that may be able to keep up with the market progress.

Process intensification methods are illustrated in Figure 2.1, including: multifunctional reactors resulting from the integration of reaction and separation techniques, new hybrid separations and use of alternative energy sources [1]. Multifunctional reactors, where reaction and separation steps are integrated into a single equipment, are one of the most relevant examples of PI for reactive systems, allowing to reduce the energy demand and investment costs on the required equipment and, consequently, leading to more sustainable processes which is one of the biggest Process Engineering challenges. This way, reactive separation attracts the researchers' attention because it leads to smaller, cleaner and more energy-efficient processes than the conventional multistage processes [1, 2], since reaction and separation take place simultaneously allowing to overcome the equilibrium limitations by continuously removing one of the products and leading to reaction conversion improvement. Among the reactive separations, chromatographic reactors and reactive distillations are currently the most studied methods for systems that comprise equilibrium-limited reactions as it is the case of BAc.

In this Chapter, an overview of the patented processes and process integration based strategies is presented showing the main achievements along the time that have contributed to improve BAc synthesis. In addition, new approaches based on PI that have been successfully applied for different esterification reactions are addressed, for the first time, as alternative processes for the BAc production, aiming to achieve higher yields and lower energy requirements than the conventional process and even than the other PI alternatives available in the open literature.

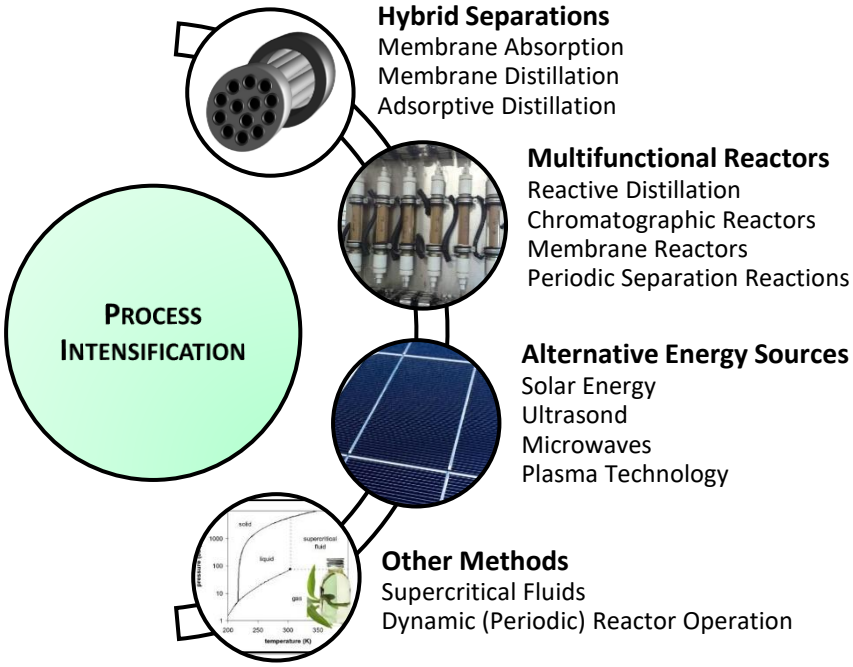

Figure 2.1. Process intensification methods [1].

2.2. Market and Applications

BAc is a clear colorless liquid with a strong characteristic odor, which presents a low solubility in water (0.2 % wt. at 293 K) and a very similar boiling point to that of AAc (see Table 2.1). It is a very important acrylic monomer with a wide application field, due to its properties such as low temperature flexibility, adhesion, hardness, water and oil resistance, among others. Additional properties of all species involved in this system can be observed in Table 2.1 and properties related with their safety including toxicity, storage and stability, among others, are presented in *Appendix A (Material Safety Data)*. All these properties make this chemical compound an attractive feedstock for paint and coating formulations and for several other products like adhesives [3] (including pressure-sensitive adhesives (PSAs)) [4, 5], varnishes, finishes of papers and textiles. [6] It has also been useful in the production of sealants, plastics, elastomers [7], and mostly to produce coatings and copolymers [8-12]. Cleaning products, antioxidant agents, amphoteric surfactants and aqueous resins are other uses of this chemical compound. Figure 2.2 illustrates the main application areas of BAc with surface coatings representing the major

one. Market research studies have reported a significant growth of the global demand of BAc during the last decade and this trend is expected to increase even further in the upcoming years. According to the market analysis [13], the global production capacity increased about 80 % from 2005 to 2013 pointing out to 3.45 million t.year^{-1} in 2013. A representation of the global production capacity can be observed in Figure 2.3 in terms of the manufactures and respective geography. The data corresponds to the most recent information available in open literature (related to 2013) and shows that BAc has been mostly produced in China. Nevertheless, the largest manufacturer, in that year, was Dow Chemical, located in the USA and Germany, with 14.7 % of the global market followed by BASF with 12.6 % and Arkema with 9.4 % [13]. The demand has increased mainly in Asia Pacific which is the largest consumer at about 1.44 million t.year^{-1}, followed by the USA at 476,000 t.year^{-1} and Western Europe at 446,000 t.year^{-1}, respectively. The most recent publications [14] point out that the global BAc market will reach around $ 8.1 billion by 2026 expanding at a Compound Annual Growth Rate (CAGR) of 5.0 % from 2018 to 2026 and expecting to reach 4.84 million tonnes by 2026. This market growth is due to the increase of the BAc usage in the manufacture of water-based coatings which are likely to replace solvent-based coatings. Moreover, the development of the automotive and construction industries boosts the global BAc market [14].

Table 2.1. Properties of all compounds involved in the butyl acrylate synthesis [15, 16].

Properties	AAc	n-Butanol	BAc	Water
Molecular mass - MM (g.mol^{-1})	72.06	74.12	128.17	18.02
Density (at 293 K)- ρ (g.cm^{-3})	1.050	0.810	0.900	1.030
Melting temperature - T_f (K)	286.2	183.9	208.6	273.2
Normal boiling temperature - T_b (K)	414.2	390.8	421.0	373.2
Critical temperature - T_c (K)	615.0	563.1	598.0	647.1
Critical pressure - P_c (bar)	56.60	44.14	29.10	220.6
Critical volume - V_c (cm^3.mol^{-1})	208.0	273.0	428.0	55.94
Acentric factor - w	0.540	0.590	0.480	0.350

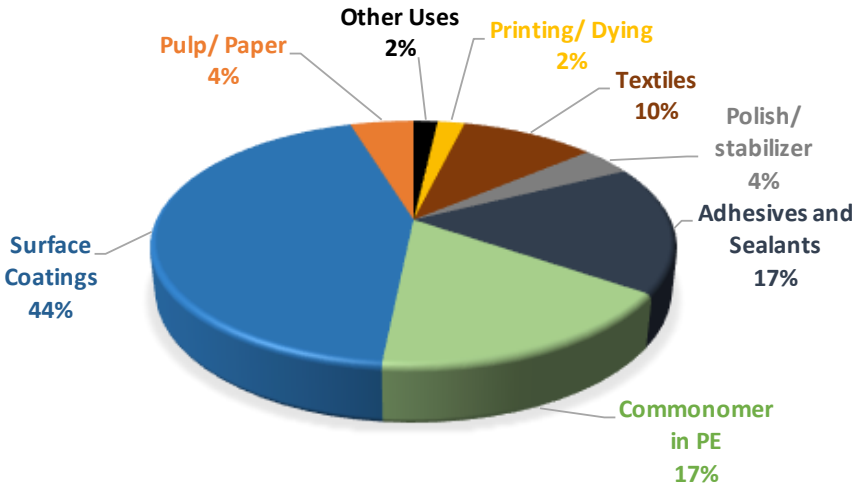

Figure 2.2. Global butyl acrylate applications (data from 2013) [13].

Figure 2.3. Global butyl acrylate production capacity (data from 2013) [13].

2.3. Conventional Synthesis Processes and Challenges

Although different routes can be followed to produce BAc, including acetylene-carbon monoxide mixtures in the presence of n-butanol at high pressures [17, 18], mass efficiency

has been a general concern in the selection of the employed synthesis reaction, favouring the paths that lead to water as the only by-product. In this way, BAc is, usually, obtained from an equilibrium limited esterification reaction between AAc and n-Butanol, in acidic medium, having water as the by-product, as can be seen in Figure 2.4. The reaction enthalpy value of 13.4 $kJmol^{-1}$, which can be obtained from the enthalpy of formation of the respective products ($\Delta H_{f,BAc}$ = -375.3 $kJmol^{-1}$, $\Delta H_{f,water}$ = -241.81 $kJmol^{-1}$) [15, 19] and reactants ($\Delta H_{f,n\text{-}butanol}$ = -274.6 $kJmol^{-1}$, $\Delta H_{f,,AAc}$ = -355.91 $kJmol^{-1}$) [19], indicates this is an endothermic reaction. According to the publications related with this system, numerous drawbacks have been associated, namely, it presents very slow reaction kinetic [15], a complex thermodynamic behaviour with several azeotropes (see Table 2.2) and high risk of polymerisation of AAc and BAc when they are exposed to high temperatures [20]. The mechanism of the polymerisation reactions is available in the open literature and it should be avoided during the esterification and separation processes, since it is highly exothermic which can lead to an uncontrolled self-accelerating reaction when high temperatures are used. Moreover, the equilibrium reaction conversion is low, according to the literature it is about 60 % at 363 K [15]. So, all these limitations make the BAc synthesis and its purification a very challenging process, since commercially a high purity is required (≥ 99.5 wt. %).

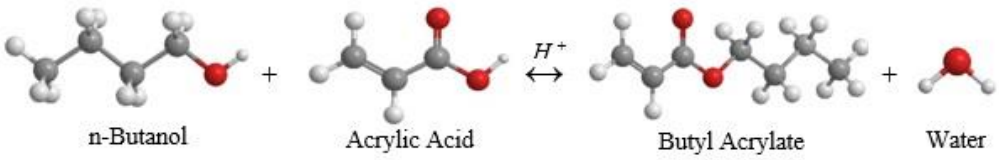

Figure 2.4. Esterification reaction for the synthesis of butyl acrylate.

Table 2.2. Azeotropic data of the butyl acrylate system (P = 0.267 bar) [20].

Reference	Type	Compounds	T_b (K)	x_{AAc}	x_{BAc}	$x_{n\text{-}Butanol}$	x_{Water}
Calculated (UNIQUAC_HOC) [20]	Homogeneous	AAc and BAc	379	0.37	0.63	-	-
Gmehling, 2004 [21]	Heterogeneous	BAc and water	335	-	0.18	-	0.82
Gmehling, 2004 [21]	Homogeneous	n-butanol and BAc	356	-	0.12	0.88	-
Gmehling, 2004 [21]	Heterogeneous	n-butanol and water	335	-	-	0.19	0.81
Gmehling, 2004 [21]	Heterogeneous	n-butanol, BAc and water	333	-	0.09	0.15	0.76

Conventionally, the BAc production is conducted in a homogeneously catalysed multistage process, shown in Figure 2.5, using two reactors with a total residence time of approximately three hours and three distillation columns which are used for the recovery of the reactants as well as for product purification [22]. Usually, the alcohol is used in excess and the water that is formed in the esterification is removed by distillation as well as its azeotrope with BAc and n-butanol to keep a high rate of AAc conversion. The separation of AAc from water, excess alcohol and BAc is not a simple task resulting in contamination of BAc containing, typically, 1-3% of AAc in a continuous process. Hence, there are reactant recovery problems leading to a significant energy use. In this manner, further improvements in the BAc production are required, namely, methods to make more efficient use of the water, driving to an easier separation of BAc from AAc and recycling unreacted AAc using less energy [23]. Besides that, liquid catalysts such as sulfuric acid, hydrofluoric acid, and para-toluenesulfonic acid are toxic and corrosive while the solid acids are less toxic and facilitate the recovery and recycling of the catalysts. Therefore, many researchers have tried to improve this process with heterogeneous catalysts (reducing the system toxicity) and integrated processes aiming to attain a more efficient eco-friendly process either by increasing the process and/or the material use efficiencies.

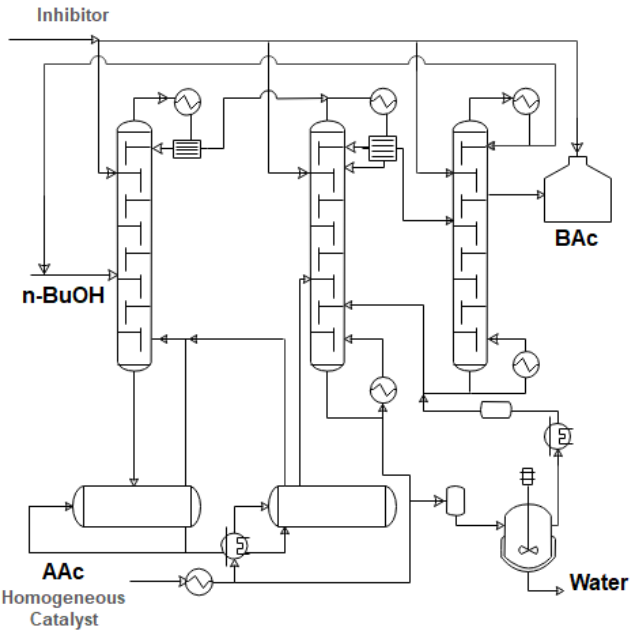

Figure 2.5. Conventional process for butyl acrylate synthesis [22].

2.4. Patent Processes Overview

There are numerous patented processes in the literature related to the BAc synthesis. A summary of those inventions is described in Table 2.3. Most of them focus on a first stage involving a reactor, where the esterification reaction between AAc and n-butanol in an acidic medium is carried out, followed by several distillation processes with recycling in order to extract the BAc from the organic phases. Usually, homogeneous catalysts are used, as sulphuric acid for instance but, heterogeneous catalysis is also reported, through the use of ion exchange resins (A-15, for instance). In summary, excess of one reactant, the alcohol commonly, is reported as a technique to overcome the reaction equilibrium limitations and the reaction and separation are performed in different steps.

Table 2.3. Patented processes for butyl acrylate production.

Source	Summary
Hoechst Aktiengesellschaft (Erpenbach et al., 1977) [24]	The production of BAc is claimed by reacting AAc with n-butanol in liquid phase over an acid cation exchanger catalyst (A-15, for instance). The authors report a continuous feed in the reaction zone, which is filled with the catalyst, using a molar ratio (AAc/n-butanol) from 1:1 to 1:2.5, at 353 K to 403 K, under a pressure from 3 to 15 atm with reaction periods within the range of 20-90 minutes. The esterification reaction is performed in a single reaction zone and the final mixture comprising a ternary mixture of BAc/ n-butanol/water is led through a three zones distillation sequence from which the respective organic phases are recovered. After the second distillation, a n-Butanol/BAc azeotrope is obtained being condensed and recycled to the reaction zone. At the end, pure BAc is obtained at the bottom of the third distillation zone, with yield between 94 % and 97 %.
Rohm and Haas (Bauer, Jr. et al, 2001) [23]	Two new process components are disclosed, one being related with the hydrolytic recovery of valuable reactants from their higher boiling adducts, and a second component related with an improved distillation of a crude product yielding BAc substantially free of AAc. A reaction conversion of 60 %, at least, is obtained in the esterification reaction using a feed molar ratio of 1 to 1.1-1.7 (AAc/n-butanol). The hydrolysis reactor is kept between 363 K and 413 K with a residence time of 0.5 to 20 hours in a continuous acid-catalysed process under 6.7 to 133.3 kPa while the cracking reactor is maintained at the same temperature with the same residence time under 2.7 to 26.7 kPa. The authors report a highly efficient continuous process for BAc synthesis comprising one esterification reactor, one hydrolytic reactor, one cracking reactor and a separation column to extract AAc providing an n-Butanol/BAc mixture which returns to the first reactor during subsequent conventional processing and final BAc isolation.
Celanese International Corporation (Jawaid and Schepp, 2001) [25]	A process for producing BAc is claimed where a feed molar ratio of 0.85 to 1.3 moles (n-butanol/AAc) is used and a polymerisation inhibitor is considered to be mixed with the AAc in the feed zone. The reaction vessel operates at a temperature between 293 K and 423 K under a pressure range of about 6.7 to 53.3 kPa. The finished product (BAc) is withdrawn as a vapour side stream from the finishing tower presenting a purity between 99.00 and 99.99 wt. %.

Table 2.3-Continued. Patented processes for butyl acrylate production.

Source	Summary
BASF Aktiengesellschaft (Aichinger, H. et al., 2001) [26]	The invention comprises at least two reactors for producing BAc over sulphuric acid or a mono-C4—C12-alkyl sulphate as catalyst. The first reactor operates, preferably, between 353 and 383 K, with the water content of the feed mixture being below 3% wt. (based on the total amount of starting materials) and the respective optimum conversion is reached after a residence time of about 1 hour, being at least 40 %, where the reaction is carried out while a single phase is observed. After that, at least one more reactor is used between 363 and 403 K. The water formed is removed by distillation in a stream containing a maximum residual amount of alcohol of 5 %.
BASF Aktiengesellschaft (Deckert, P. and Herbst, H, 2002) [27]	The reaction mixture removed from the esterification zone is first fed to a three-stage pre-purification and then worked up by rectification for BAc isolation. The reaction occurs, preferably, between 353 K and 403 K and between 0.1 and 0.8 bar (according to the authors, reduced pressures facilitates the removal of water by rectification). In the first pre-purification stage the catalyst is separated by extraction and washing with water. Then, the strongly acidic components are neutralized and extracted by reactive extraction using an aqueous alkali solution. After passing the remaining organic reaction mixture in an additional separation zone, the resulting alkyl ester is isolated. In the third stage, residual salts and aqueous foreign-phase fractions are removed by extraction with water from the organic reaction mixture that remained after the second pre-purification stage, before it is passed on into the separation zone comprising further rectification units.
Union Carbide Chemicals & Plastics Technology Corporation (Ho, F. and Julka, V., 2003) [28]	The esterification reaction is performed between 363 K and 413 K under a pressure range between 0.1 and 1.5 bar and using a feed molar ratio of 0.8-1.2 to 1 (n-Butanol/AAc). A splitter distillation column is used to perform a separation between lights, which include dibutylether, butyl acetate, n-butanol and lower boiling components (overhead fraction) and acrylate and heavier components (bottom fraction). The bottom fraction is removed from the splitter distillation column and the heavier compounds are separated by introducing that fraction into a distillation column to provide an overhead product containing BAc and a bottom product containing heavier components.
Arkema (Riondel, A. and Bessalem, J., 2005) [29]	This process encompasses a reactor charged with AAc, phenothiazine (PTZ) stabilizer, 96% of sulphuric acid and the BAc/n-butanol mixture from the top column wherein the water formed is entrained by distillation in the form of a heteroazeotropic mixture with n-butanol being then separated in a decanter after condensation. The esterification reaction is conducted preferably with an initial n-butanol/AAc molar ratio of 0.92, which rises to 1.12 following completion of the deferred introduction of n-Butanol. Initially, it is conducted with a temperature of 353 K for 30 minutes with regulation of the pressure, which varies from 0.293 bar to 0.227 bar and, then, maintaining this pressure the temperature is allowed to increase up to 373 K. The final product obtained contains at least 99.8 wt. % of BAc.
Rohm and Hass (Cooper, C. and Zamarripa, R., 2005) [30]	The authors report two process units running in parallel with interconnections designed to maximize yield and purity of the products from both units. A method for combining parts of the two units into a single process unit for improved yield and purity is also detailed. Both processes encompass an esterification reactor and a dehydration distillation column. The first process unit involves a hydrolysis reactor, a cracking reactor and an AAc separation column and the second process unit contains a bleed stripper, a recycle tank and a neutralization and acidification system. The feed molar ratio of AAc and n-butanol for esterification reactor is preferably from 1:1.25 to 1:1.45 over an acid catalyst. The AAc conversion is at least 60 %. The cracking reactor is kept preferably from 383 to 398 K under a pressure of 2.7 to 26.7 kPa and a residence time of 0.5 to 20 hours, based on the fed reactor bleed stream, is employed. The final product (BAc) presents reduced levels of AAc and n-butyl acetate.

2.5. Toward Process Intensification: Multifunctional Reactors

Nowadays, it is possible to find different descriptions for PI in the open literature, which is one of the latest trends in Chemical Engineering and Process Technology. Gerven and Stankiewicz [31] gathered some of them in their recent review about fundamentals of PI and, in summary, most of them are related with strategies that allow to drastically reduce the energy consumption and to improve the process efficiency by compacting the respective plant design or/and reducing wastes. For that, innovation and creativity are a constant challenge in this field with process integration being one of the most relevant strategies for the PI. Different studies have been conducted aiming to find more sustainable alternative processes for the BAc synthesis. The first studies emerged about two decades ago concerning heterogeneous catalysis where fundamental data as equilibrium and kinetic constants, activation energy and vaporisation enthalpy for the BAc system were reported [15, 32-35]. Meanwhile, studies involving multifunctional reactors started to appear, which are units where the reaction and separation occur simultaneously allowing to reduce the operating and investment costs, such as: reactive distillation (RD) [6, 36], fixed-bed adsorptive reactor (FBR)[37, 38] and pervaporation based hybrid process (combining reaction with membrane technology) [39]. The most relevant strategies and operating conditions are summarized in Table 2.4 as well as the principal results obtained.

Table 2.4. Summary of heterogeneously catalysed butyl acrylate synthesis and process intensification strategies.

Source	Processes/ Materials	Conditions	Remarks/ Results
Pascale Dupont et al., 1995 [32]	Flow and batch conditions; Heteropolyacids supported on activated carbon: $H_3PW_{12}O_{40}$ (HPW); Inhibitor in batch: PTZ (0.16 wt. % of the total reactants); in dynamic flow: PTZ (0.1 wt. %).	T = 353 K; P = 0.2 bar; $r_{A/B}$ = 0.75 (batch); $r_{A/B}$ = 1.34 (flow).	X_{AAc} = 98.0 % (removing water from the oganic phase, in batch conditions); The activity per proton of the HPW/carbon is higher than conventional resins but smaller than pure HPW; Occurs deactivation in batch conditions.
Xin Xen et al., 1999 [40]	Three neck flask with water-cooler condenser; Screening of catalysts including: A-15, Amberlite 200C, Nafion-H, Nafion-SiO_2,Solid oxides and Liquids.	T = 353 K; $r_{A/B}$ = 1.	The highest conversion was obtained with Nafion-H; X_{AAc} = 61.1 %; The highest selectivity to BAc was obtained wit Amberlite 200C; Selectivity to BAc = 95.6 %.
Schwarzer, S. and Hoffman U., 2002 [36]	Batch; Tube Reactor + RD *Kinetic:* Lewatit K 2621 *Equilibrium:* Toluene Sulfonic Acid.	*Kinetic:* T = 393 K, P = 2 bar; $r_{A/B}$ = 1.3 - 2.1; *Equilibrium:* T = 293 - 373 K; P = 1 bar.	K_{eq} = exp (- 8.805 + 0.05743 × (T/K) – 6.429 × 10^{-5} × $(T/K)^2$ + 3.821 × 10^{-9} × (T/K)); ΔH = 14.27 kJmol^{-1}; X_{AAc} = 62 %; BAc fraction = Máx. 93 %; LHHW model was considered.
Zeng, K. et al., 2006 [6]	RD with decanter; Kinetic parameters from Schwarzer, S. and Hoffman U., 2002 [36].	T = 363 - 428 K; $T_{Decanter}$ = 313 K; P = 1.1 bar.	BAc ≥ 99.83 mol. %; Water ≥ 95.90 mol. %.
Skrzypek, J. et al., 2009 [33]	Batch; Heterolpolyacids: $H_3PW_{12}O_{40}$ (catalyst A) $H_3PMo_{12}O_{40}$ (catalyst B) Inhibitor: HME.	T = 343 - 373 K; $r_{A/B}$ = 3.0, 5.0 and 10.0; Catalysts (wt. %) = 1.23 - 9.84 (Cat. A) 3.12 - 12.48 (Cat. B).	Cat. A: Ea = 66.00 ± 0.4 kJmol^{-1}; $k_{c,0}$ = 1.12 × 10^4 ($m^{4.5}$ $mol^{-1.5}$ min^{-1}); Cat. B: Ea = 72.30 ± 0.8 kJmol^{-1} $k_{c,0}$ = 9.82 × 10^4 ($m^{4.5}$ $mol^{-1.5}$ min^{-1}); K_{eq} = 9.603×10^5 × × exp (-31400/(RT)); ΔH = 31.40 kJmol^{-1}.

Table 2.4-Continued. Summary of heterogeneously catalysed butyl acrylate synthesis and process intensification strategies.

Source	Processes/ Materials	Conditions	Remarks/ Results
Sert E., et al., 2012 [34]	Batch; Zirconia supported by Tungstophoric acid (25 wt. % loading).	T = 358 K; Calcination T = 923.15 K; $r_{(A/B)}$ = 1.	ΔH = 15.20 kJmol^{-1}; X_{AAc} = 33%.
Sert E., et al., 2013 [35]	Batch; A-15, A-131, Dowex 50Wx-400.	T = 338 K, 348 K and 358 K; $r_{A/B}$ = 1, 2 and 3.	Ea = 57.40 kJmol^{-1}; K_{eq}= exp (2134/T-1.799); X_{AAc} = 88.8% (over A-131 at 338 K).
Niesbach, A. et al., 2012 [20]	RD; A-46; Inhibitors: 2 wt.% PTZ and 2 wt.% HME (top feed); 1000 ppm PTZ (AAc feed).	T = 380 - 393 K; P = 0.30 - 0.40 bar; $r_{A/B}$ = 1.10 - 3.26; Cat. (dry) = 0.205 kgm^{-1}.	Ea = 81.26 kJmol^{-1}; ΔH = 15.70 kJmol^{-1}; K_{eq} = exp (-1888.66/T(K) + 8.17); X_{AAc} = 38.69 %; LHHW model was considered.
Sert E. and Atalay F., 2014 [39]	Pervaporation-esterification hybrid process; Pervap 2201; A-131.	T = 358 K; r(A/B) = 8; catalyst loading of 10 g.L^{-1}; S/V ratio = 70 m^{-1}.	X_{AAc} = 96.3 %; High selectivity to water in the n-butanol/AAc/BAc/water system; Pervaporation and reaction rate increasing with the operating temperature.
Ostaniewicz C. et al., 2014 [15]	Batch; A-15.	T = 323 - 363 K; $r_{(A/B)}$ = 2 to 3; Cat. = 1 - 3.5 wt. %.	kc = 1.52 × 107 × exp (– 66 988/(RT)) (mol·g_{cat}^{-1}·min^{-1}); Ks,water = 1.589; Keq = exp (-1490/T(K) + 7.21); ΔH = 12.39 ± 4.80 kJmol^{-1}; ΔS = 59.98 ± 13.87 J.mol^{-1}·K^{-1}; LHHW model was considered.

2.5.1. Reactive distillation

There are numerous studies concerning reactive distillation (RD) process for different equilibrium limited reactions with particular emphasis on esterifications [22, 41-43]. Besides

esterification cases, other successful commercial applications of RD include etherifications [44-46], cumene [47] and ethylene glycol [48] production and olefin metathesis [49]. Generally, this is the first option for an industrial application due to its practical implementation and to the deep knowledge about the industrial application of distillation processes available in the literature [50]. A RD process comprises reaction and separation in the same operation unit and its operating principle is based on the continuous separation of the products through the differences in the species volatilities while reaction occurs. Commonly, a solid catalyst like an ion exchange resin, for instance, is used as packing material in the reaction zone as represented in Figure 2.6. Depending on the volatilities, the products can be separated either from the top or the bottom of the column enabling to shift the equilibrium towards the forward reaction. However, high temperatures are required in systems that present low volatilities as the BAc system case, which is harmful for this system since some of the species present tend to polymerize at high temperatures. Because of this, the use of inhibitors is crucial for the process.

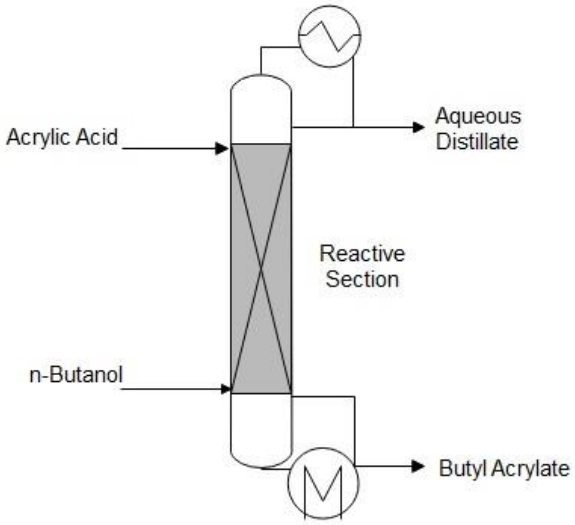

Figure 2.6. Schematic representation of a reactive distillation unit for the butyl acrylate synthesis.

The literature reports some studies searching for new alternatives to the conventional BAc production process and, so far, the most of them, concern RD technology. As can be observed in Table 2.4, Schwarzer and Hoffman [36] studied experimentally the reaction equilibrium and measured kinetic data using a macroporous acid ion exchange resin, Lewatit K 2621, and those data were then used to simulate a process involving a catalytic

tubular reactor and a RD column at 393 K. The maximum molar ester fraction reached was 93 % after optimisation.

Zeng K. et al. [6], investigated theoretically the design and control of a RD column with an overhead decanter providing for the first time a control strategy for an industrial application to produce high purity BAc (99.83 mol %) using the kinetic data from Schwarzer's and Hoffman's work [36]. However, these publications were only concerned with the production of BAc in an RD column on a theoretical basis. Moreover, the polymerisation risk of the heat-sensitive compounds (BAc and AAc) was not considered in the simulation study.

Niesbach et al. [51] were pioneers in the study of the inhibition period of AAc and BAc polymerisation, which is the time taken for a significant extent of polymerisation to occur, concluding that this process is dependent on the amount of inhibitor added, the temperature and the gas phase composition. The conventional chemicals, commonly called inhibitors, that are used to stabilize AAc and other acrylates are hydroquinone monomethyl ether (HME) and phenothiazine (PTZ). In that study, they also reported that the required amount of PTZ to avoid the polymerisation reaction is defined by the AAc, because the poly-acrylic acid formation is faster than the poly-butyl acrylate one and PTZ was found to be a more effective inhibitor than HME, as it does not depend on the presence of oxygen.

Meanwhile, Niesbach and his co-workers [20], investigated experimentally, for the first time, the BAc synthesis using a pilot-scale RD column. This research team changed the key operating parameters considering the high risk of polymerisation of BAc and AAc assessed in their previous work [51]. In this way, several experiments were performed aiming to analyse different parameters, such as reflux ratio, distillate-to-feed mass ratio, feed molar ratio, top pressure and total liquid load. According to the results, the authors concluded that among the studied process parameters, the reflux ratio is the one with more influence in the RD process leading to the reduction of the conversion and product purity by increasing the reflux ratio and keeping the remaining parameters constant. A concentration profile can be observed in Figure 2.7, which was obtained in a RD pilot scale unit for a set of operating parameters.

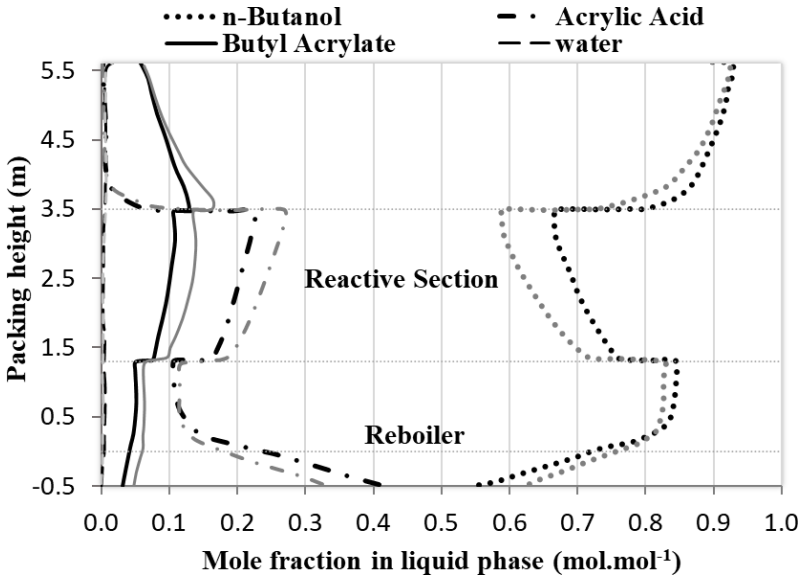

Figure 2.7. Concentration profile of a reactive distillation unit using a feed molar ratio of 3.1 (n-Butanol/AAc), a reflux ratio of 1.99 and a distillate-to-feed ratio of 0.5 at 0.30 bar. The grey lines represent the same simulation but with a distillate-to-feed ratio of 0.4. Adapted from Niesbach et al., 2012 [20].

In this case, the distillate-to-feed mass ratio was investigated concluding that decreasing this parameter (from 0.5 to 0.4), which is represented by the grey lines, leads to lower n-butanol concentrations in the reactive section and, consequently, higher concentrations of AAc and BAc are achieved. This way, the reaction conversion increases due to the faster reaction rate leading to a higher BAc overall concentration. Regarding the feed molar ratio (n-butanol/AAc) parameter, when it decreases the AAc concentration increases in the reactive section. However, the reaction rate remains nearly constant since it depends on the concentration of all components. On the other hand, the BAc purity in the bottom product is improved with the decreasing of the feed molar ratio due to the lower n-butanol concentration in that section. The pressure was also evaluated which directly influences the reactants conversion, increasing it due to a change in pressure from 0.3 to 0.4 bar, leading to a higher BAc purity in the bottom product. Moreover, this is a sensible parameter since it involves operating temperature changes. Therefore, the pressure value should be limited to avoid the system polymerisation and taking into account the catalyst specifications in terms of the maximum operating temperature. Additionally, the authors increased the total feed flow (about 21 %) and they observed

no significant effect, except on BAc profile that resulted from the conversion reduction, which shows that the RD column is a kinetically controlled process for the synthesis of BAc. In that work, a non-equilibrium-stage model was considered to predict all experimental results and the model was validated using their own experimental data. Nevertheless, experimentally, the maximum AAc conversion obtained over Amberlyst 46 was about of 39% using a reflux ratio of 1.014, a distillate-to-feed ratio of 0.494 and a feed molar ratio of 3.18 at 0.4 bar.

2.5.2. Sorption-enhanced reaction processes

Similarly to the RD technology, chromatographic reactors (CR) also comprise reaction and separation in the same equipment enabling to shift the equilibrium conversion in the forward direction and, consequently, achieving higher conversions by continuously removing one of the products. However, in CR a different separation technique is used, the chromatography separation, which is based on the selective adsorption of specific species in a solid stationary phase inducing different composition fronts along the reactor at different propagation velocities [52]. It means that, the compounds for which the solid/adsorbent has less affinity move faster along the reactor than the compounds for which the solid/adsorbent has more affinity, which are more retained leading, in this way, to the separation of the products. For this reason, this kind of reactors can operate at mild temperatures and, because of that, they are strongly recommended for the separation of complex molecules mixtures with similar volatilities and mixtures involving temperature sensitive compounds with high risk of polymerisation.

Commonly, the CR, like FBR, are packed with one solid material able to work as catalyst and adsorbent [53-58]. Some commercial ion exchange resins (as A-15 for instance) have shown to be a very effective material mainly for esterification reactions by playing this dual role in the process [59-62]. Nevertheless, there are few studies concerning CR for BAc synthesis. Actually, the work reported in Chapter 3 of this thesis represents the first approach to this strategy. Afterwards, Moraru and his co-workers published two studies [37, 38] based on FBR coupled with different distillation columns at industrial scale, which are discussed ahead (see Section 2.6).

2.5.2.1. New approach: Simulated Moving Bed Reactor

The Simulated Moving Bed Reactor (SMBR), which is a cyclic multi-column chromatographic process, allows a continuous production with high-purity even if low-selectivity adsorbents are available [63], unlike batch chromatography. In this case, a series of fixed-bed columns are interconnected in a closed system enabling to operate in a counter-current continuous mode. All chromatographic columns are, usually, packed with one solid material able to work as catalyst and adsorbent or packed with an adsorbent/catalyst homogeneous mixture, or other heterogeneous packing strategies [64]. It is a versatile equipment enabling to adopt different configurations (number of columns per section), which means that it is possible to increase or decrease the number of fixed-bed columns in the reaction/separation sections as required, depending on the system, for the respective process optimisation.

Regarding the operating principle of the SMBR, it is based on True Moving Bed (TMB) technology combined with reaction (commonly designated by TMBR, True Moving Bed Reactor), for which the underlying concept consists in promoting the contact between the liquid and solid (stationary) phases by using a counter-current mode in order to maximize the mass transfer driving force. In this manner, TMBR has the ability to convert and separate, continuously, a reactive feed mixture in two fractions, by carrying the reaction products in opposite directions, being the performance enhancement, over batch chromatography, linked with its counter-current nature. This operating mode leads to the reduction of the costs associated with the adsorbent and, consequently, the eluent consumptions [65]. However, according to the literature, there are drawbacks related to the solid motion, such as: equipment abrasion, mechanical erosion of the adsorbent and difficulty to keep the plug flow for the solid [63].

The Simulated Moving Bed (SMB) concept was developed in the 1960s by Universal Oil Products [66], and patented as *Sorbex*® process, with the purpose of overcoming the problems associated to TMB by interchanging inlet and outlet streams (without solid motion). Thus, at regular time intervals (commonly designated by switching time, t^*), all inlet and outlet streams move one fixed-bed column ahead in the fluid flow direction. In this way, the counter-current mode between the fluid and the stationary phases is performed by simulating the stationary solid phase movement. Hence, the same column

is in different sections during a cycle ($N_c\, t^*$, where N_c is the number of total columns in the equipment) passing through the different stages of the process:

(i) Regeneration of the solid (section I);

(ii) Desorption of the less adsorbed compound (section II);

(iii) Adsorption of the most adsorbed compound (section III) and,

(iv) Regeneration of the eluent/desorbent by the adsorption of the less adsorbed compound (section IV).

Over the years, the SMB technology has been investigated with focus on different applications of industrial interest, showing to be a very functional process for numerous large-scale separations, mainly on the petrochemical (purification of p-xylene, *"Parex®"* process, and separation of olefins from parafins, the *"Olex®"* process, for instance) and pharmaceutical industries (chiral separations). Alternative operating modes and technical design aspects have been developed depending on the system and the desired separation criteria. Focusing on PI concepts, chemical reaction was associated with the SMB technology in the same equipment which led to a new multifunctional reactor, the SMBR, where the reaction occurs in sections II and III while the desorption/adsorption of the less/most adsorbed compounds occurs, simultaneously, as represented in Figure 2.8.

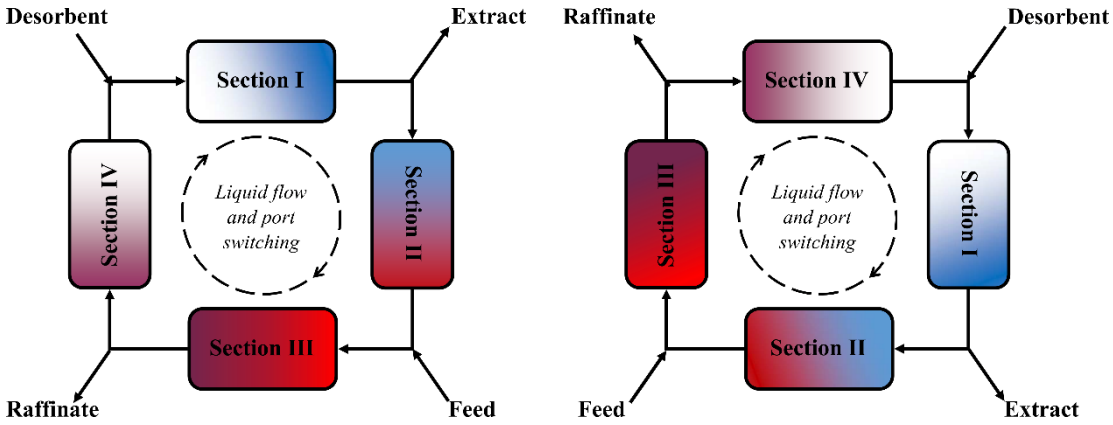

Figure 2.8. Schematic representation of a Simulated Moving Bed Reactor on: a) N^{th} step and b) $(N+1)^{th}$ step. White, red, purple and blue colours represent desorbent, feed mixture, the less and the most adsorbed product, respectively.

Nowadays, the SMBR is one of the most relevant technique for products purification from complex multicomponent reactive mixtures and it has been successfully applied for the production of different acetals and esters [67-73], showing to be an effective process for systems involving equilibrium-limited reactions [74] with almost 100 % of conversion and recovery of the desired products. Although the SMBR seems to be a very promising technology, its feasibility was never studied for the BAc production.

2.5.3. Pervaporation based hybrid processes

Membrane technology, where pervaporation process occurs, is strongly recommended for systems that involve heat-sensitive compounds since it enables operating at milder temperatures than RD processes. Furthermore, pervaporation has been recognized as a very efficient technique for azeotropic mixtures separation with low energy requirements and no additional species into the feed streams are needed [75]. A schematic representation of a pervaporation process is depicted in Figure 2.9.

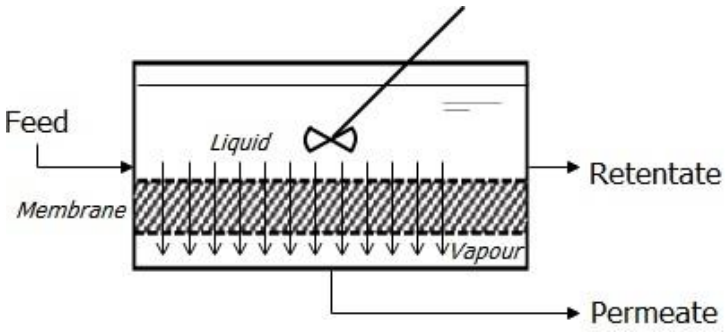

Figure 2.9. Schematic representation of a pervaporation process.

Basically, there are three streams which are the feed mixture, the permeate comprising, mainly, the compound for which the membrane has more selectivity and, the retentate stream composed by the remaining compounds. Typically, during this process three steps occur:

(i) Sorption of the permeable component into the separation layer of the membrane;

(ii) Diffusive transport of the substance across the membrane;

(iii) Desorption of the substance on the permeate side of the membrane and, for that, low pressures are used in order to keep the maximum driving force possible while the permeated vapours are condensed [76].

Regarding its industrial applications, pervaporation membranes are used, mostly, as downstream units in process integration strategies aiming to recycle a water free stream or even to purify the final desired product. One of the most relevant applications is the separation of water from organic solvents like alcohols dehydration, for instance, or from mixtures of solvents [76].

Like distillation and chromatography, membrane technology has been associated with chemical reaction, following the PI concepts, giving rise to another kind of multifunctional reactor, the pervaporation membrane reactor (PMR). This reactor was patented, for the first time, in 1960 [77] and, since then, many studies about pervaporation hybrid processes have been reported, mainly for esterification reactions [78, 79], as the esterification reaction of propionic acid with isobutyl alcohol to produce isobutyl propionate and water [80] or the esterification of butyric acid with n-propanol to produce propyl butyrate and water [81], among others [82]. Typically, for condensation reactions, which have water as by-product (as esterification reactions, for instance), hydrophilic membranes (water selective membranes) have shown very promising results, since water can be removed from the reaction media, continuously, overcoming the equilibrium conversion and improving the ester yield. Nevertheless, other kinds of membranes can be used according to the desired product and the required purity criteria, so, the membrane selection is a very important step for pervaporation aided esterification reaction studies and it should be performed taking into account the principal key performance indicators: selectivity, separation factor, permeate fluxes, driving force and chemical stability (reproducibility).

Sert and Atalay [39] investigated, for the first time, a pervaporation-esterification hybrid process to carry out simultaneously the esterification reaction of AAc and n-butanol and the separation of the water from BAc in order to increase the limiting reactant conversion. For that, the authors used a configuration that consists in a batch reactor (2 L) where a Pervap 2201 polymeric membrane was placed with an effective area of 179 cm^2 and the Amberlyst 131 ion exchange resin was used as catalyst using a pressure of 4 mbar at the permeate side for sampling collection. The pervaporation assisted esterification process was evaluated by changing different operating parameters including temperature, molar

ratio of n-butanol to AAc, catalyst loading and membrane area to reaction volume ratio (S/V), with temperature being pointed out as the principal parameter since it showed a dual effect increasing both the pervaporation and the reaction rate. In addition, the authors reported that the used membrane presented high selectivity to water in that system and they concluded that coupling pervaporation with esterification reaction showed to be an efficient strategy for the equilibrium shifting towards BAc production by continuous water removal from the reaction medium. The maximum conversion of AAc achieved was 96.3% at 358 K. However, that work was not complemented with a model able to predict the experimental results that would be interesting for future work in the design of different processes with integration of Pervap 2201 membrane for BAc production.

2.5.3.1. New approach: Simulated Moving Bed Membrane Reactor

Recently, a new technology based on Simulated Moving Bed Reactor combined with pervaporation membranes, also designated by Simulated Moving Bed Membrane Reactors (PermSMBR), has been successfully applied for the continuous synthesis of different products, including esters, acetals and green solvents [61, 83-86]. Its operating principle is very similar to the SMBR technology. The main difference is that PermSMBR comprises several membranes packed with catalyst/adsorbent, which allow removing an extra stream (permeate stream along the membranes), as can be observed in Figure 2.10, instead of the fixed-bed columns in SMBR.

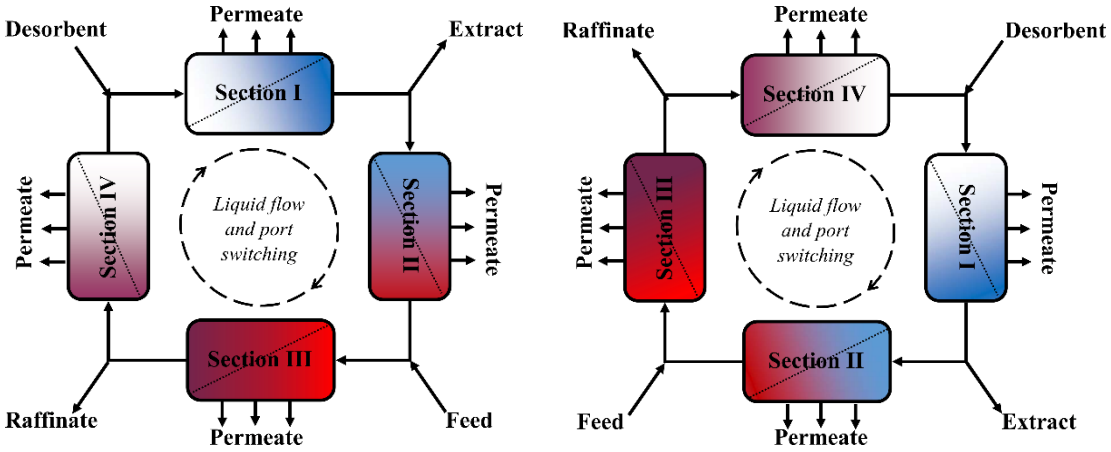

Figure 2.10. Schematic representation of a Simulated Moving Membrane Bed Reactor on: a) N^{th} step and b) $(N+1)^{th}$ step. White, red, purple and blue colours represent desorbent, feed mixture, the less and the most adsorbed product, respectively.

Among the reactive separation processes, PermSMBR has gained special attention due to its advantages in PI field, since it allows the reaction equilibrium displacement by continuous removing one of the products (water, typically) or more, by adsorption and pervaporation processes, simultaneously, from the reaction medium favouring the forward reaction. Indeed, it is also considered as Process Re-Intensification[86], because it is not a conventional multifunctional reactor but an enhanced multifunctional reactor since it combines different separation processes with the reaction step in the same equipment. [74] Notwithstanding, this technology was never tested for BAc production.

2.6. Process Integration Strategies at Industrial Scale

Alternative process designs at industrial scale for the BAc synthesis have emerged along the last years aiming to find a more feasible and competitive solution to answer to the fast market growth. A summary of all these strategies and the respective main output data can be found in Table 2.5.

Table 2.5. Review of the process integration strategies for butyl acrylate synthesis at industrial scale: processes, conditions and main results.

Source	Processes /Materials	Conditions	Remarks/ Results
Niesbach, A. et al., 2013 [22]	Single RD and RD coupled with Decanter (20,000 $t.year^{-1}$); Inhibitors: PTZ and HME; A-46.	T = 380 to 403 K; $r_{(A/B)}$ = 0.81; $r_{(A/B)}$ = 1.08 (with decanter); P = 0.58 - 0.59 bar; RR = 1.67; RR = 6.96 (with decanter).	X_{AAc} = 73.5 %; 99.9 % (with decanter); Reduction on the actual BAc market price (1350 €.t^{-1}) = 12 %; 37 % (with decanter).
Niesbach, A. et al., 2013 and 2015 [87, 88]	Semicontinuous Distillation coupled with a RD column and Decanter; Bio-n-butanol and bio-AAc as feed stream (containing impurities); A-46.	RD column: No change is required in the operating parameters in relation to the previous study [22]; Semicontinuous Distillation: Top P = 0.2, 0.4 and 0.576 bar; RR = 200, 300 and 600; Top/bottom mass flow = 5, 7.5 and 10; Initial AAc, n-butanol purity = 99.20, 9.44, 99.60 and 99.72 wt. %; Final AAc, n-butanol purity = 99.70, 99.80, 99.90 and 99.95 wt. %.	All impurities of bio-based sources were identified as well as the impurities that resulted from side reactions in a RD column; Semicontinuous distillation process is suggested for the purification of the final product and/or bio-based reactants; Cycle time is the critical parameter to reach the minimal purity desired.
Moraru M. D. et al., 2016 [38]	Two conventional reactive-separation-recycle processes (20,000 $t.year^{-1}$): FBR + 2 distillation columns (one recycle); FBR + 4 distillation columns (two recycles); A-131 (2000 kg).	$T_{Reactor\ 1}$ = 355.7 - 358.2 K; $T_{Reactor\ 2}$ = 353.2 - 358.2 K; $T_{dist.Colum\_RSR\ 1}$ = 373.2 - 493.2 K; $T_{dist.Column\_RSR\ 2}$ = 338.2 - 428.2 K.	X_{AAc} = 50 % (one recycle); X_{AAc} = 55 % (two recycles); Reduction on the actual BAc market price (1350 €.t^{-1}) = 38 %.
Moraru M. D. and Bildea C. S., 2017 [89]	Design and control of a RD with Decanter and Flash Vessel (20,600 $t.year^{-1}$); A-131 (2000 kg).	T = 338.2 - 403.2 K; P = 0.05 - 3.65 bar; Kinetic data from literature [35].	X = 99.9 % (both reactants); Water ≥ 99 wt. %; Recovery of unreacted alcohol; Reduction on the actual BAc market price (1350 €.t^{-1}) = 44 %.

Table 2.5-Continued. Review of the process integration strategies for butyl acrylate synthesis at industrial scale: processes, conditions and main results.

Source	Processes /Materials	Conditions	Remarks/ Results
Moraru M. D. and Bildea C. S., 2017 [37]	Design and plantwide control of two conventional reactive-separation-recycle processes (20,500 $t.year^{-1}$): FBR + 2 distillation columns (one recycle); FBR + 4 distillation columns (two recycles); A-131 (2000 kg).	T = 356.2 K; $r_{(A/B)}$ = 3.	Extractive distillation showed to be a better choice than conventional distillation; BAc ≥ 99.5 wt. %; Water ≤ 0.05 wt. %; AAc ≤ 0.01 wt. %.

According to the previous table (Table 2.5), the principal process integration strategies available at industrial scale focus on RD technology and FBR coupled with distillation columns. Niesbach and his co-workers performed a scale up of the RD process previously studied at pilot scale, which was optimised by coupling a decanter at the top of a RD column to allow the recycling of unused reactants. That new configuration and respective optimized operating parameters lead to a reduction on the actual product (BAc) cost of 37 % when compared with the conventional process (1350 €.t_{BAc}^{-1}) [22].

Moraru and Bildea [89] also investigated the design and control of a RD process with a decanter and a flash vessel at industrial scale allowing the recovery of 99 wt. % purity of waste water and leading to unreacted alcohol recovery. An economic evaluation was also performed and similar economic parameters to the values reported by Niesbach et al. [22] were reported, just reducing about 4 % of the product cost since a very similar process configuration is presented.

Afterwards, Niesbach et al. [87, 88] investigated a RD process making use of sustainable bio-based resources aiming to produce bio-BAc driven by the fossil fuels reserves decline as well as by the urge of achieving eco-friendly and sustainable processes through the implementation and design of "greener" processes. In this way, the authors suggested the use of n-butanol and AAc derived from biological processes, which involve the presence of impurities that can considerably affect the performance of the previously studied RD process. Aiming to understand the impact of those impurities in the global process, Niesbach et al. developed a four-step methodology, which comprises the design of the base-case process (step 1), the identification and clustering of impurities (step 2), process

simulation and process analysis (step 3) and, finally, the detailed design of bio-based process (step 4). Thereby, they started by analysing the biosynthetic routes for the synthesis of n-butanol and AAc as well as possible side-reactions of the main components and impurities in the RD column in order to identify which of the impurities present in each bio-reactant and the key components would have the biggest impact on the product purity. For that, the Acetone-Butanol-Ethanol (ABE) fermentation process using clostridium species to ferment sugars from biomass was considered for the synthesis of bio-butanol [90]. Regarding AAc, the most promising feedstock for its bio-based production is lactic acid either by a chemically catalysed dehydration reaction or by a fermentation process [91]. Nevertheless, according to the literature, there are other alternative routes to get bio-AAc [92-95]. The similarity of the boiling points of the impurities and the boiling point of the final product, possible azeotropes and the reliability of thermodynamic and physical properties were taken into account for the identification of the representative component in each cluster. Thus, in summary, among the several impurities that can be present in these bio-based raw materials, the four key components for the reactive distillation process towards bio-BAc production that were identified through the four-step methodology developed by the authors are: isobutanol, butyric acid, propionic acid and butyl butyrate. Afterwards, their impact on the RD process for the BAC synthesis was studied considering concentrations up to 3000 ppm according to the n-butanol and AAc suppliers material data sheets. The authors observed that additional purification steps are required since the critical impurities could not be removed just by changing the operating parameters of the RD process. So, they considered a semicontinuous distillation process to get the final product (BAc) with the desired commercial purity (≥ 99.5 wt.%), either by purifying the bio-reactants upstream before they enter the RD column or by purifying the final product after its production. According to the authors, the semicontinuous distillation is advantageous over batch distillation due to its flexibility to handle batch-to-batch variations in the initial concentrations of impurities (depending on the bio-sources) and in the final purity set point of the primary product. Moreover, the distillate and bottom products can be removed continuously at near steady state, which is a significant advantage over the continuous and batch distillation. A detailed study of ternary semi continuous distillation process is available in open literature for the BAc production from bio raw materials [87], where the purification of the final product and the bio-based reactants are considered, separately. The results obtained for the first approach

showed that this separation strategy allows keeping the final product purity just by changing the cycle times, and higher purities were attained with longer cycle times and without any change in the operating parameters (reflux ratio or column pressure). Concluding, it is an effective technology for the purification of the final product, as long as only small amounts of propionic acid are found in the bio-based feed streams leading to BAc with no significant concentrations of butyl propionate. Otherwise, butyl propionate is formed in the presence of propionic acid in the RD column, which is difficult to separate from BAc by semi continuous distillation process due to the similar vapour pressures. Regarding the upstream purification of the two bio reactants of the RD column, the semi continuous process demonstrated that it should only be feasible for n-butanol since in the AAc case, although all propionic acid is removed, a slight separation of AAc from acetic acid is observed. Moreover, it was concluded that this separation process is an attractive technology for other bio-based separations due to its high flexibility in respect to the chemical system treated and due to the fact that it is possible to perform different purification tasks using the same semi continuous distillation apparatus. Nevertheless, no economic evaluation study about this process is available to determine its economic viability for an industrial application.

Meanwhile, Moraru et al. [38] disclosed two alternative reactive-separation-recycle processes based on a FBR coupled with different distillation columns to split AAc and BAc. The first configuration encloses a conventional distillation and another one comprises an extractive distillation process using ethylene glycol. Later, the same authors provided a plant wide control study considering the previous configurations [37]. According to the authors, the control at the unit level was able to keep the mass inventory in the plant in dynamic simulations performed and achieve the required product purity when changes in throughput and reactor inlet temperature were made. The multiple possibilities to change the capacity, the ability for larger fresh feeds of AAc processing and the presence of only one steady state were factors pointed out as advantages of the process. They also concluded that employing extractive distillation is to some extent better, overcoming important drawbacks of the conventional distillation: the unit is smaller, less BAc is recycled, and the risk of polymerisation is lower due to lower temperatures. Though, slightly higher production cost, comparing with the values presented by Niesbach et al. [22], were reported.

2.7. Conclusions

Several studies have been developed to find more feasible and eco-friendly processes for butyl acrylate production. Hence, different process intensification strategies have emerged and have been proposed as alternative processes for the butyl acrylate synthesis with significant economic and environmental progress in relation to the conventional process. After a literature survey, the principal operating parameters used in the alternative processes studied, goals and respective results were summarized and gathered along this Chapter. Even though most of them focus on reactive distillation technology, new process intensification approaches, namely, adsorption/pervaporation processes integrated with reaction, have demonstrated to be very promising strategies to overcome the drawbacks associated with esterification reactions involving heat-sensitive compounds as the butyl acrylate case. Nevertheless, the feasibility of the continuous production of BAc in Simulated Moving Bed Reactors and Simulated Moving Bed Membrane Reactors was never studied before this work.

2.8. Notation

Abbreviations

A-15	Ion exchange resin Amberlyst-15
A-46	Ion exchange resin Amberlyst-46
A-131	Ion exchange resin Amberlyst-131
AAc	Acrylic Acid
BAc	Butyl Acrylate
Cat.	Catalyst
CR	Chromatographic Reactors
FBR	Fixed-Bed Adsorptive Reactor
HME	Hydroquinone Monomethyl Ether
LHHW	Langmuir-Hinshelwood-Hougen-Watson

PermSMBR	Simulated Moving Bed Membrane Reactor
PI	Process Intensification
PMR	Pervaporation Membrane Reactor
PTZ	Phenothiazine
RD	Reactive Distillation
RR	Reflux Ratio
RSR	Reactive-Separation-Recycle
SMBR	Simulating Moving Bed Reactor
t	tonnes
T	Temperature

Symbols

MM	Molecular Mass	$kg.mol^{-1}$
ΔH	Reaction enthalpy	$kJ.mol^{-1}$
ΔS	Reaction entropy	$J.mol^{-1}\cdot K^{-1}$
Ea	Activation energy	$kJ.mol^{-1}$
$k_{c,0}$	Arrhenius pre-exponential factor	$m^{4.5}\,mol^{-1.5}\,min^{-1}$
k_c	Kinetic constant	$mol.kg^{-1}.min^{-1}$
K_{eq}	Equilibrium reaction constant	-
$K_{s,water}$	Adsorption Constant for Water	-
R	Ideal gas constant	$J.K^{-1}.mol^{-1}$
$r_{(A/B)}$	Molar ratio (A= n-Butanol; B= AAc)	-
S/V	Membrane area to reaction volume ratio	m^{-1}
V_c	Critical volume	$m^3.mol^{-1}$
X	Reaction conversion	%
w	Acentric factor	-

2.9. References

1. Stankiewicz, A. I.; Moulijn, J. A., Process intensification: Transforming chemical engineering. *Chemical Engineering Progress* **2000,** 96, 22-33.

2. Stankiewicz, A., Reactive separations for process intensification: an industrial perspective. *Chem Eng Process* **2003,** 42, 137-144.

3. Brady, F. X.; Thomas F. Kauffman Hot melt adhesives based on ethylene-n-butyl acrylate. US 4874804, 1989.

4. Gower, M. D.; Shanks, R. A., Acrylic acid level and adhesive performance and peel master-curves of acrylic pressure-sensitive adhesives. *Journal of Polymer Science Part B: Polymer Physics* **2006,** 44, 1237-1252.

5. Gerst, M. M.; Auchter, G. B. D.; Beyers, C. P. A. PSA polymer of n-butyl acrylate, ethyl acrylate, vinyl acrylate, and acid monomer. US 0213992 A1, 2012.

6. Zeng, K.-L.; Kuo, C.-L.; Chien, I. L., Design and control of butyl acrylate reactive distillation column system. *Chemical Engineering Science* **2006,** 61, 4417-4431.

7. SIDS, O., N-Butyl Acrylate. http://www.inchem.org/documents/sids/sids/141322.pdf. (Accessed on May 2013).

8. Klaus Pfleger, W.; Wieland Zacher, W.; Klaus Boettcher, W.; Ronald Skorczyk, C.; Oskar Buechner, D.; Franz Georg Mietzner, L. Manufacture of ethylene/n-butyl acrylate copolymers. US 4087601, 1978.

9. Chernikova, E. V.; Yulusov, V. V.; Garina, E. S.; Kostina, Y. V.; Bondarenko, G. N.; Nikolaev, A. Y., Controlled synthesis of styrene-n-butyl acrylate copolymers with various chain microstructures mediated by dibenzyl trithiocarbonate. *Polymer Science Series B* **2013,** 55, 176-186.

10. Chernikova, E. V.; Yulusov, V. V.; Mineeva, K. O.; Garina, E. S.; Sivtsov, E. V., Controlled synthesis of copolymers of vinyl acetate and n-butyl acrylate mediated by trithiocarbonates as reversible addition-fragmentation chain-transfer agents. *Polymer Science Series B* **2012,** 54, 349-360.

11. Cooper, G.; Grieser, F.; Biggs, S., Butyl Acrylate/Vinyl Acetate Copolymer Latex Synthesis Using Ultrasound As an Initiator. *Journal of Colloid and Interface Science* **1996,** 184, 52-63.

12. Funt, B. L.; Ogryzlo, E. A., Copolymerization of butyl acrylate and vinylpyridine. *Journal of Polymer Science* **1957,** 25, 279-284.

13. TranTech Consultant, Chemical Profile: Butyl Acrylate. http://www.chemplan.ir/chemplan_demo/sample_reports/BA_PROFILE.pdf. (Accessed on November 2016).

14. Research, T. M., Global Butyl Acrylate Market:Transparency Market Research. https://globenewswire.com/news-release/2018/09/03/1564510/0/en/Global-Butyl-Acrylate-Market.html. (Accessed on September 2018).

15. Ostaniewicz-Cydzik, A. M.; Pereira, C. S. M.; Molga, E.; Rodrigues, A. E., Reaction Kinetics and Thermodynamic Equilibrium for Butyl Acrylate Synthesis from n-Butanol and Acrylic Acid. *Industrial & Engineering Chemistry Research* **2014,** 53, (16), 6647-6654.

16. Yaws, C. L., *Thermophysical Properties of Chemicals and Hydrocarbons (Electronic Edition)*. Knovel 2010.

17. Bhattacharyya, S. K.; Bhattacharyya, D. P., Catalytic synthesis of n-butyl acrylate from acetylene, carbon monoxide and n-butanol under high pressure. *Journal of Applied Chemistry* **1966,** 16, (7), 202-205.

18. Walter, R.; Robert, S. Acrylic acid ester production. US 2883418A, 1959.

19. DIPPR, Thermophysical Properties Database. In American Institute of Chemical Engineers- New York, 1998.

20. Niesbach, A.; Fuhrmeister, R.; Keller, T.; Lutze, P.; Górak, A., Esterification of Acrylic Acid and n-Butanol in a Pilot-Scale Reactive Distillation Column—Experimental Investigation, Model Validation, and Process Analysis. *Ind Eng Chem Res* **2012,** 51, 16444-16456.

21. Gmehling, J., *Azeotropic data*. Wiley-VCH: Weinheim, 2004.

22. Niesbach, A.; Kuhlmann, H.; Keller, T.; Lutze, P.; Górak, A., Optimisation of industrial-scale n-butyl acrylate production using reactive distillation. *Chem Eng Sci* **2013,** 100, 360-372.

23. W. Bauer, J.; Chapman, J. T.; Mirabelli, M. G. L.; Venter, J. J. Process for producing butyl acrylate. US 6180819 B1, 2001.

24. Erpenbach, H.; Gehrmann, K.; Joest, H. t.; Zerres, P. Continuous production of n-butylacrylate free from dibutylether. US 4012439 A, 1977.

25. Jawaid;, M. N. A.; Schepp, D. E. Process for the production and purification of n-butyl acrylate. US 6172258 B1, 2001.

26. Aichinger, H.; Fried, M.; Nestler, G. Method for producing (meth) acrylic acid esters. US 6320070 B1, 2001.

27. Deckert, P.; Herbst, H. Continuous preparation of alkyl esters of (meth) acrylic acid. US 6472554 B1, 2002.

28. Ho, F.; Julka, V. Processes for refining butyl acrylate. US 6605738 B1, 2003.

29. Riondel, A.; Bessalem, J. Process for preparing butyl acrylate by direct esterification. US 6846948 B2, 2005.

30. Cooper, C.; Zamarripa, R. Method for producing butyl acrylate. US 20050059837 A1, 2005.

31. Van Gerven, T.; Stankiewicz, A., Structure, Energy, Synergy, Time—The Fundamentals of Process Intensification. *Industrial & Engineering Chemistry Research* **2009,** 48, (5), 2465-2474.

32. Dupont, P.; Védrine, J. C.; Paumard, E.; Hecquet, G.; Lefebvre, F., Heteropolyacids supported on activated carbon as catalysts for the esterification of acrylic acid by butanol. *Applied Catalysis A: General* **1995,** 129, 217-227.

33. Jerzy, S.; Teresa, W.; Mirosław, G.; Mariusz, W., Kinetics of the synthesis of propyl and butyl acrylates in the presence of some heteropolyacids as catalysts. *International Journal of Chemical Kinetics* **2009,** 41, 12-17.

34. Sert, E.; Atalay, F. S., Esterification of Acrylic Acid with Different Alcohols Catalyzed by Zirconia Supported Tungstophosphoric Acid. *Industrial & Engineering Chemistry Research* **2012,** 51, 6666-6671.

35. Sert, E.; Buluklu, A. D.; Karakuş, S.; Atalay, F. S., Kinetic study of catalytic esterification of acrylic acid with butanol catalyzed by different ion exchange resins. *Chemical Engineering and Processing: Process Intensification* **2013**.

36. Schwarzer, S.; Hoffmann, U., Experimental Reaction Equilibrium and Kinetics of the Liquid-phase Butyl Acrylate Synthesis Applied to Reactive Distillation Simulations. *Chemical Engineering & Technology* **2002,** 25, 975-980.

37. Moraru, M. D.; Bildea, C. S., Design and plantwide control of n-butyl acrylate production process. *Journal of Process Control* **2017,** 58, 46-62.

38. Moraru, M. D.; Bildea, C. S.; Milea, A., Design and Economic Evaluation of a Process for n-Butyl Acrylate Production. *U.P.B. Sci. Bull, Series B* **2016,** 78, 113.

39. Sert, E.; Atalay, F. S., n-Butyl acrylate production by esterification of acrylic acid with n-butanol combined with pervaporation. *Chemical Engineering and Processing: Process Intensification* **2014,** 81, 41-47.

40. Chen, X.; Xu, Z.; Okuhara, T., Liquid phase esterification of acrylic acid with 1-butanol catalyzed by solid acid catalysts. *Applied Catalysis A: General* **1999,** 180, 261-269.

41. Lai, I. K.; Liu, Y.-C.; Yu, C.-C.; Lee, M.-J.; Huang, H.-P., Production of high-purity ethyl acetate using reactive distillation: Experimental and start-up procedure. *Chemical Engineering and Processing: Process Intensification* **2008,** 47, (9), 1831-1843.

42. Agreda, V. H.; Partin, L. R. Reactive distillation process for the production of methyl acetate. US 4435595 A, 1984.

43. Luyben, W. L.; Pszalgowski, K. M.; Schaefer, M. R.; Siddons, C., Design and Control of Conventional and Reactive Distillation Processes for the Production of Butyl Acetate. *Industrial & Engineering Chemistry Research* **2004,** 43, (25), 8014-8025.

44. Bakshi, A.; Jones Jr, E. M.; Strain, B. A. Process for the preparation of ETBE. US 5248836 A, 1993.

45. Adams, J. R.; Smith Jr, L. A.; Hearn, D.; Jones Jr, E. M.; Arganbright, R. P. Integrated Process for the Production of TAME. US 5792891 A, 1998.

46. Smith Jr, L. A. Process for the Preparation of MTBE. US 5118873 A, 1992.

47. Pathak, A. S.; Agarwal, S.; Gera, V.; Kaistha, N., Design and control of a vapor-phase conventional process and reactive distillation process for cumene production. *Industrial & Engineering Chemistry Research* **2011,** 50, (6), 3312-3326.

48. Kumar, A.; Daoutidis, P., Modeling, analysis and control of ethylene glycol reactive distillation column. *AIChE Journal* **1999,** 45, (1), 51-68.

49. Al-Arfaj, M. A.; Luyben, W. L., Design and control of an olefin metathesis reactive distillation column. *Chemical Engineering Science* **2002,** 57, (5), 715-733.

50. Hiwale R., S.; Bhate N., V.; Mahajan Y., S.; Mahajani S., M., Industrial Applications of Reactive Distillation: Recent Trends. In *International Journal of Chemical Reactor Engineering*, 2004; Vol. 2.

51. Niesbach, A.; Daniels, J.; Schröter, B.; Lutze, P.; Górak, A., The inhibition of acrylic acid and acrylate ester polymerisation in a heterogeneously catalysed pilot-scale reactive distillation column. *Chem Eng Sci* **2013,** 88, 95-107.

52. Mazzotti, M.; Neri, B.; Gelosa, D.; Morbidelli, M., Dynamics of a Chromatographic Reactor: Esterification Catalyzed by Acidic Resins. *Industrial and Engineering Chemistry Research* **1997,** 36, (8), 3163-3172.

53. Silva, V. M. T. M.; Rodrigues, A. E., Dynamics of a fixed-bed adsorptive reactor for synthesis of diethylacetal. *AIChE Journal* **2002,** 48, 625-634.

54. Gandi, G. K.; Silva, V. M.; Rodrigues, A. E., Synthesis of 1, 1-dimethoxyethane in a fixed bed adsorptive reactor. *Industrial & engineering chemistry research* **2006,** 45, (6), 2032-2039.

55. Graça, N. S.; Pais, L. S.; Silva, V. M.; Rodrigues, A. E., Dynamic study of the synthesis of 1, 1-dibutoxyethane in a fixed-bed adsorptive reactor. *Separation Science and Technology* **2011,** 46, (4), 631-640.

56. Regufe, M. J.; Faria, R. P. V.; Ribeiro, A. M.; Loureiro, J. M.; Rodrigues, A. E., Synthesis of the Biofuel Additive 1,1-Diethoxybutane in a Fixed-Bed Column with Amberlyst-15 Wet. *Chemical Engineering and Technology* **2016,** 39, (8), 1509-1518.

57. Faria, R. P. V.; Pereira, C. S. M.; Silva, V. M. T. M.; Loureiro, J. M.; Rodrigues, A. E., Sorption enhanced reactive process for the synthesis of glycerol ethyl acetal. *Chemical Engineering Journal* **2014,** 258, 229-239.

58. Graça, N. S.; Delgado, A. E.; Constantino, D. S. M.; Pereira, C. S. M.; Rodrigues, A. E., Synthesis of a Renewable Oxygenated Diesel Additive in an Adsorptive Reactor. *Energy Technology* **2014,** 2, (9-10), 839-850.

59. Kawase, M.; Suzuki, T. B.; Inoue, K.; Yoshimoto, K.; Hashimoto, K., Increased esterification conversion by application of the simulated moving-bed reactor. *Chemical Engineering Science* **1996,** 51, (11), 2971-2976.

60. Mazzotti, M.; Kruglov, A.; Neri, B.; Gelosa, D.; Morbidelli, M., A continuous chromatographic reactor: SMBR. *Chemical Engineering Science* **1996,** 51, 1827-1836.

61. Pereira, C. S. M.; Rodrigues, A. E., New sorption enhanced reaction technologies (SMBR and PermSMBR) for the production of diesel blends and green solvents. *Chimica Oggi* **2013,** 31, (3), 64-67.

62. Pereira, C. S. M.; Silva, V. M. T. M.; Rodrigues, A. E., Fixed Bed Adsorptive Reactor for Ethyl Lactate Synthesis: Experiments, Modelling, and Simulation. *Separation Science and Technology* **2009,** 44, 2721-2749.

63. Rodrigues, A.; Pereira, C.; Minceva, M.; Pais, L. S.; Ribeiro, A.; Ribeiro, A. M.; Silva, M.; Graça, N.; Santos, J. C., *Simulated Moving Bed Technology: Principles, Design and Process Applications*. Elsevier Science 2015.

64. Gonçalves, J. C.; Rodrigues, A. E., Simulated moving bed reactor for p-xylene production: Dual-bed column. *Chemical Engineering and Processing: Process Intensification* **2016,** 104, 75-83.

65. Nicoud, R.-M.; Fuchs, G.; Adam, P.; Bailly, M.; Küsters, E.; Antia, F. D.; Reuille, R.; Schmid, E., Preparative scale enantioseparation of a chiral epoxide: Comparison of liquid chromatography and simulated moving bed adsorption technology. *Chirality* **1993,** 5, (4), 267-271.

66. Broughton, D. B.; Gerhold, C. G. Continuous sorption process employing fixed bed of sorbent and moving inlets and outlets. US 66079057 A 1961.

67. Pereira, C. S. M.; Zabka, M.; Silva, V. M. T. M.; Rodrigues, A. E., A novel process for the ethyl lactate synthesis in a simulated moving bed reactor (SMBR). *Chem Eng Sci* **2009,** 64, (14), 3301-3310.

68. Pereira, C. S. M.; Gomes, P. S.; Gandi, G. K.; Silva, V. M. T. M.; Rodrigues, A. E., Multifunctional Reactor for the Synthesis of Dimethylacetal. *Industrial & Engineering Chemistry Research* **2007,** 47, (10), 3515-3524.

69. Graça, N. S.; Pais, L. S.; Silva, V. M. T. M.; Rodrigues, A. E., Analysis of the synthesis of 1,1-dibutoxyethane in a simulated moving-bed adsorptive reactor. *Chemical Engineering and Processing: Process Intensification* **2011,** 50, (11–12), 1214-1225.

70. Silva, V. M. T. M.; Rodrigues, A. E., Novel process for diethylacetal synthesis. *AIChE Journal* **2005,** 51, (10), 2752-2768.

71. Minceva, M.; Gomes, P. S.; Meshko, V.; Rodrigues, A. E., Simulated moving bed reactor for isomerization and separation of p-xylene. *Chemical Engineering Journal* **2008,** 140, (1–3), 305-323.

72. Kawase, M.; Inoue, Y.; Araki, T.; Hashimoto, K., The simulated moving-bed reactor for production of bisphenol A. *Catalysis Today* **1999,** 48, (1–4), 199-209.

73. Ströhlein, G.; Assunção, Y.; Dube, N.; Bardow, A.; Mazzotti, M.; Morbidelli, M., Esterification of acrylic acid with methanol by reactive chromatography: Experiments and simulations. *Chemical Engineering Science* **2006,** 61, 5296-5306.

74. Constantino, D. S. M.; Faria, R. P. V.; Rodrigues, A. E., Chapter Four - Sorption-Enhanced Reaction With Simulated Moving Bed Reactor and PermSMBR Technologies. In *Advances in Chemical Engineering*, Lemonidou, A. A., Ed. Academic Press 2017; Vol. 51, pp 261-330.

75. Shao, P.; Huang, R. Y. M., Polymeric membrane pervaporation. *Journal of Membrane Science* **2007,** 287, (2), 162-179.

76. Carbone-Lorraine, L., Industrial Applications of Pervaporation. In *Effective Industrial Membrane Processes: Benefits and Opportunities*, Turner, M. K., Ed. Springer Netherlands: Dordrecht, 1991; pp 281-293.

77. Jennings, J. F.; Binning, R. C. Organic chemical reactions involving liberation of water US 2956070 A, 1960.

78. Jyoti, G.; Keshav, A.; Anandkumar, J., Review on Pervaporation: Theory, Membrane Performance, and Application to Intensification of Esterification Reaction. *Journal of Engineering* **2015,** 2015, 24.

79. Genduso, G.; Luis, P.; Van der Bruggen, B., 19 - Pervaporation membrane reactors (PVMRs) for esterification. In *Membrane Reactors for Energy Applications and Basic Chemical Production*, Basile, A.; Di Paola, L.; Hai, F. l.; Piemonte, V., Eds. Woodhead Publishing: 2015; pp 565-603.

80. Chandane, V. S.; Rathod, A. P.; Wasewar, K. L., Enhancement of esterification conversion using pervaporation membrane reactor. *Resource-Efficient Technologies* **2016,** 2, S47-S52.

81. Khudsange, C. R.; Wasewar, K. L., Process intensification of esterification reaction for the production of propyl butyrate by pervaporation. *Resource-Efficient Technologies* **2017,** 3, (1), 88-93.

82. Rathod, A. P.; Wasewar, K. L.; Sonawane, S. S., Enhancement of Esterification Reaction by Pervaporation Reactor: An Intensifying Approach. *Procedia Engineering* **2013,** 51, 330-334.

83. Pereira, C. S. M.; Silva, V. M. T. M.; Rodrigues, A. E., Coupled PermSMBR – Process design and development for 1,1-dibutoxyethane production. *Chemical Engineering Research and Design* **2014,** 92, (11), 2017-2026.

84. Pereira, C. S.; Rodrigues, A. E., Process intensification: New technologies (SMBR and PermSMBR) for the synthesis of acetals. *Catalysis today* **2013,** 218, 148-152.

85. Pereira, C. S. M.; Silva, V. M. T. M.; Rodrigues, A. E., Green Fuel Production Using the PermSMBR Technology. *Industrial & Engineering Chemistry Research* **2012,** 51, (26), 8928-8938.

86. Silva, V. M. T. M.; Pereira, C. S. M.; Rodrigues, A. E., PermSMBR—A new hybrid technology: Application on green solvent and biofuel production. *AIChE Journal* **2011,** 57, (7), 1840-1851.

87. Niesbach, A.; Adams, T. A.; Lutze, P., Semicontinuous distillation of impurities for the production of butyl acrylate from bio-butanol and bio-acrylic acid. *Chemical Engineering and Processing: Process Intensification* **2013,** 74, 165-177.

88. Niesbach, A.; Fink, N.; Lutze, P.; Górak, A., Design of reactive distillation processes for the production of butyl acrylate: Impact of bio-based raw materials. *Chinese Journal of Chemical Engineering* **2015,** 23, (11), 1840-1850.

89. Moraru, M. D.; Bîldea, C. S., Process for n-butyl acrylate production using reactive distillation: Design, control and economic evaluation. *Chemical Engineering Research and Design* **2017,** 125, 130-145.

90. García, V.; Päkkilä, J.; Ojamo, H.; Muurinen, E.; Keiski, R. L., Challenges in biobutanol production: How to improve the efficiency? *Renewable and Sustainable Energy Reviews* **2011,** 15, (2), 964-980.

91. Haveren, J. V.; Scott, E. L.; Sanders, J., Bulk chemicals from biomass. *Biofuels, Bioproducts and Biorefining* **2008,** 2, (1), 41-57.

92. Dubois, J.-L.; Duquenne, C.; Hölderich, W. Method for producing acrylic acid from glycerol US 7910771 B2, 2011.

93. Ding, J.; Hua, W., Game Changers of the C3 Value Chain: Gas, Coal, and Biotechnologies. *Chemical Engineering & Technology* **2013,** 36, (1), 83-90.

94. Jong, E.; Higson, A.; Walsh, P.; Wellisch, M., *Bio-based Chemicals: Value Added Products from Biorefineries*. IEA Bioenergy Task 42 Biorefinery 2012.

95. Deleplanque, J.; Dubois, J. L.; Devaux, J. F.; Ueda, W., Production of acrolein and acrylic acid through dehydration and oxydehydration of glycerol with mixed oxide catalysts. *Catalysis Today* **2010,** 157, (1), 351-358.

3. Fixed-Bed Adsorptive Reactor

In this Chapter, the butyl acrylate synthesis through the esterification reaction of acrylic acid with n-butanol in a fixed-bed adsorptive reactor packed with Amberlyst-15 ion exchange resin was evaluated. Adsorption experiments were carried out with non-reactive pairs at two temperatures (323 and 363 K). The experimental results were used to obtain multicomponent adsorption equilibrium isotherms of Langmuir type. Reactive adsorption experiments, using different feed molar ratios and flow rates, were performed at 363 K and used to validate a mathematical model developed to describe the dynamic behaviour of the fixed-bed adsorptive reactor for the butyl acrylate synthesis.

This Chapter is adapted from Constantino, D. S. M.; Pereira, C. S. M.; Faria, R. P. V.; Ferreira, A. F. P.; Loureiro, J. M.; Rodrigues, A. E., Synthesis of butyl acrylate in a fixed-bed adsorptive reactor over Amberlyst 15. *AIChE Journal*. **2015,** 61 (4), 1263-1274. DOI 10.1002/aic.14701

3.1. Introduction

Among the different separation techniques used in chemical engineering processes, the Chromatography is considered one of the most relevant, which plays an essential role in the separation science mainly, due, to its versatility and simplicity. Basically, it is a method that allows separating the components of a mixture by their distribution between two phases: a solid stationary phase and a fluid mobile phase. This distribution is performed according to the different molecular interactions of the chemical compounds of the fluid phase towards the solid phase. As a result, the compounds with more affinity (stronger interactions) with the stationary phase are more retained by this phase and their movement through the system is slower than that of the compounds with weaker interactions [1] leading to different concentration profiles along the unit. In this manner, different concentration ranges of the products can be obtained at the outlet of the chromatographic column, at different time intervals. Various interactions can contribute to this kind of separation, involving, physical or weak chemical bonds like dipole-dipole, hydrogen bond formation, charge transfer, among others [2].

Fixed-bed adsorptive reactor (FBR) is the result of the combination of chromatography with chemical reaction. As the separation process is performed by adsorption while the reaction step occurs, FBR is more advantageous than reactive distillation (RD) for complex molecules that are difficult to separate by evaporation processes [3], since chromatographic reactors are able to operate at lower temperatures than RD being, in principle, preferable in order to prevent polymerisation reactions. This multifunctional reactor has gained special attention for equilibrium-limited reactions, since it allows overtaking the equilibrium conversion by continuously removing at least one of the products from the reaction medium using, typically, one of the reactants as eluent for the regeneration of the solid phase [4-8]. However, other solvents can be used as eluent for more complex mixtures [9] keeping the effectiveness of the process.

Many studies have been focused on heterogeneous catalysts for the esterification reaction between acrylic acid (AAc) and n-butanol [10-16] to overcome the environmental drawbacks associated with homogeneous catalysts as well as to facilitate their separation from the final product. It is known that ion exchange resins are active catalysts for esterification reactions. One example is the Amberlyst-15 (A-15) resin, which was,

recently, used in a kinetic study of the BAc system with good results in batch conditions [17]. Furthermore, A-15 was already successfully used, as solid phase, in simulated moving bed reactor (SMBR) based processes for other systems [6, 18, 19], showing high selectivity for water adsorption, leading to great reaction conversions and yields on the desired products. Because of this, A-15 seems to be a very attractive stationary phase for BAc synthesis in chromatographic reactors, acting as catalyst and adsorbent.

The present Chapter aims to study the production of BAc in a FBR using A-15, which is a very important step in order to determine the best conditions to implement in a future SMBR process for this system. Aiming to assess the performance of this type of reactors, the knowledge of basic data, as adsorption and reaction kinetics is crucial. The reaction kinetics was already investigated in a batch reactor over A-15 [17]. In this Chapter, an adsorption study with binary mixtures in the absence of reaction was performed, at 323 and 363 K, to obtain the multicomponent adsorption parameters. Then, BAc was successfully produced in a FBR under different conditions and all reactive adsorption experiments performed were used to validate the mathematical model developed, for which the kinetic and the adsorption data over A-15 were considered.

3.2. Experimental Data

3.2.1. Chemicals and materials

The chemicals used in the adsorption/reaction experiments were n-butanol (≥ 99.9 wt.%) from Fisher Scientific, AAc (≥ 99 wt.%) and BAc (≥ 99.5 wt.%) from Acros Organics. The last two chemicals were provided stabilized with inhibitor (about 200 ppm and 20 ppm of hydroquinone monomethyl ether (MeHQ) in AAc and in BAc, respectively). The additional inhibitor used in this study was phenothiazine (PTZ) (99 wt.%), also from Acros Organics. Isopropanol (≥ 99.9 wt.%) from Fisher Scientific was used as solvent in the chromatographic analysis (gas chromatography).

A-15 resin was used as catalyst and adsorbent. This is a highly cross-linked polystyrene-divinylbenzene ion exchange resin functionalized with sulfonic groups,

which swells selectively in contact with a liquid phase multicomponent mixture, especially with polar species [20]. This fact depends on the interactions between the fluid and the resin as well as on the amount of cross-links [21]. In this work, the swelling ratios were measured at 323 K for all compounds of the system under study. The values are 1.55, 1.54, 1.35, 1.08 for water, n-Butanol, AAc and BAc, respectively. Thereby, it is possible to conclude that A-15 has the following decreasing affinity order: water, n-Butanol, acrylic acid and butyl acrylate, which is in accordance with the species polarity. The concentration of active sites of this resin is 4.7 meq $H^+.g^{-1}$ (dry matter), its surface area is 53 $m^2.g^{-1}$, its average radius is 372.5 μm and its particle porosity is 0.36 [3]. The catalyst/adsorbent was firstly washed with deionized water and then with ethanol. Afterward, it was dried at 363 K and prior to packing, the resin was immersed in n-butanol.

3.2.2. Analytical method

All samples collected were analysed (at least two times) in a Shimadzu - GC 2010 Plus gas chromatograph equipped with flame ionization and thermal conductivity detectors (FID and TCD, respectively). The compounds were separated using a silica capillary column (CPWax57CB, 25 m x 0.53 mm ID, film thickness of 2.0 μm). Helium N50 was used as the carrier gas at a flow rate of 3.9 $mL.min^{-1}$. The linear velocity was set to 30 $cm.s^{-1}$ and the injection volume used was 0.8 μL with a split ratio of 15. The temperature of the injector and the TCD was set to 523 K while the temperature of the FID was set to 573 K. The initial column temperature was 393 K for 4.3 min, the temperature was then increased at 60 $K.min^{-1}$ up to 473 K, remaining constant for the following 17 min. Isopropyl alcohol (isopropanol) was used as solvent. The global associated uncertainty of the measured molar fractions was ≤ 0.05. More details about calibration curves are presented in *Appendix B.*

3.2.3. Experimental Setup and Procedure

The experiments at 323 K were carried out in a laboratory-scale jacketed glass column which was kept at the desired temperature by a thermostatic bath, while the experiments at 363 K were performed in a stainless steel column able to withstand higher temperatures placed inside an oven (see Figure 3.1). The main differences between the setups used,

besides the columns, are the sampling, which is performed manually at 323 K and automatically at 363 K, and the number of HPLC pumps used. On the left side setup, only one HPLC pump was used to feed the column while on the right side setup, one HPLC pump was used for the adsorption mixture and another for the regeneration step, avoiding the need to purge the system. Both columns were packed with the sulfonic acid ion exchange resin A-15 and their characteristics can be seen in Table 3.1.

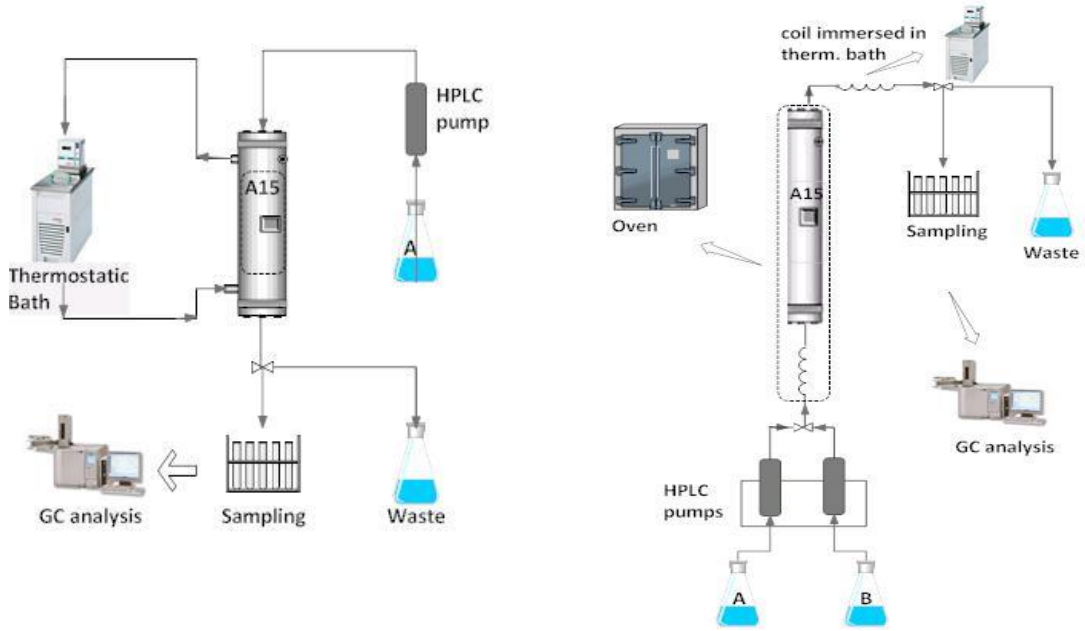

(a) (b)

Figure 3.1. Experimental setup: (a) jacket glass column used at 323 K (top-down flow direction); (b) stainless steel column used at 363 K (bottom-up flow direction).

Table 3.1. Characteristics of the Fixed-Bed Columns.

Characteristic/Column	Jacketed glass	Stainless steel
Length of the column , L_b (cm)	12.0	35.1
Internal diameter of the column, d_{int} (cm)	2.6	1.95
A-15 weight (g)	24.9	41.0
Bulk density, ρ_b (g.dm^{-3})	390.8	391.0

Tracer experiments were carried out by pulse injections of a Dextran solution (15 $kg.m^{-3}$) in water, since Dextran is insoluble in n-Butanol. Samples of 0.2 cm^3 were injected at different flow rates (5, 7.5 and 10 $mL.min^{-1}$) using water as eluent and the column outlet concentration was monitored using a UV-VIS detector (Gilson, Model 115) at 300 nm. At least, three runs were performed for each flow rate in order to check the stoichiometric time reproducibility of the experimental curves.

The adsorption experiments were performed by feeding to the fixed-bed column different binary mixtures of known composition of a reactant and a product of the esterification reaction, at constant temperature and feed flow rate. In order to obtain the breakthrough curves, small samples were collected at the column outlet, at periodic time intervals, and analysed by gas chromatography according to the analytical method described above. The reactive adsorption experiments were performed in a similar way, but now by feeding reactive mixtures comprising n-butanol and AAc, to the fixed-bed column. In both cases, the experiments proceeded until no changes were observed in the outlet stream composition.

Since BAc and AAc have high risk of polymerisation at high temperatures, preliminary tests were performed using binary mixtures of these compounds (AAc/Water and AAc/BAc) in batch conditions over A-15 resin at the same work temperatures during 8 hours. No by-products were formed at 323 K; however, at 363 K, two new peaks were observed in the corresponding chromatograms, which can be butyl 3-butoxypropanoate or butyl 3- acryloxypropanoate, according to the literature [10] (3-butoxypropionic acid and butyl hydroxypropanoate, also possible by-products, were tested and excluded as possibilities). Nevertheless, the area ratios observed were less than 5 % (A_i/A_{total}). Anyway, some adsorption experiments were repeated using PTZ as inhibitor to check its effect in the adsorption profile. The amount of PTZ used was 1000 ppm as suggested by Niesback and co-workers [22].

3.3. Mathematical Model

A mathematical model was developed to predict the internal concentration profiles or the concentration histories of a fixed-bed adsorptive reactor applied in the synthesis of

BAc using the A-15 resin as catalyst and water selective adsorbent, which takes into account the following assumptions:

(i) Isothermal operation;
(ii) Constant bed and packing porosities;
(iii) Plug flow model with axial dispersion but negligible radial dispersion;
(iv) Velocity variations due to changes in the bulk composition;
(v) Mass transfer described by the linear driving force model;
(vi) Multicomponent adsorption equilibrium described by extended Langmuir isotherm model.

The bulk fluid and pellet mass balances to component *i* are given by equations (3.1) and (3.2), respectively:

$$\frac{\partial C_i}{\partial t}+\frac{\partial (u\ C_i)}{\partial z}+\frac{(1-\varepsilon)}{\varepsilon}\frac{3}{r_p}k_{L,i}\left(C_i-\bar{C}_{p,i}\right)=D_{ax}\frac{\partial}{\partial z}\left(C_T\frac{\partial x_i}{\partial z}\right) \tag{3.1}$$

$$\frac{3}{r_p}k_{L,i}\left(C_i-\bar{C}_{p,i}\right)=\varepsilon_p\frac{\partial \bar{C}_{p,i}}{\partial t}+\left(1-\varepsilon_p\right)\frac{\partial \bar{q}_i}{\partial t}-\frac{\nu_i\rho_b}{1-\varepsilon}r\left(\bar{C}_{p,i}\right) \tag{3.2}$$

where u is the interstitial velocity, ε is the bed porosity and D_{ax} the axial dispersion coefficient , which was obtained from the Peclet number, according to equation (3.3); z is the axial dimension along the bed, r_p is the particle radius and t is time;

$$D_{ax}=\frac{uL_b}{P_e} \tag{3.3}$$

In equation (3.2), $k_{L,i}$, C_i and $\bar{C}_{p,i}$ represent the global mass transfer coefficient, the bulk concentration and the average concentration in the particle pores of component *i*, respectively; ρ_b is the bulk density, ε_p is the particle porosity, $\bar{q}_i$ is the average adsorbed phase concentration of species *i* in equilibrium with $\bar{C}_{p,i}$, ν_i is the stoichiometric coefficient of component *i* and r is the reaction rate; x_i represents the component molar fraction and C_T the total concentration in the liquid phase.

The interstitial fluid velocity variation is given by equation (3.4), which was obtained from the total mass balance.

$$\frac{du}{dz} = -\frac{(1-\varepsilon)}{\varepsilon}\frac{3}{r_p}\sum_{i=1}^{NC} k_{L,i} V_{M,i}\left(C_i - \bar{C}_{p,i}\right) \tag{3.4}$$

where $V_{M,i}$ is the molar volume of component *i* and *NC* is the number of compounds.

The adsorption equilibrium of component *i* is described by the multicomponent Langmuir adsorption equilibrium isotherm:

$$q_i = \frac{Q_i K_i \bar{C}_{p,i}}{1 + \sum_{j=1}^{NC} K_j \bar{C}_{p\,j}} \tag{3.5}$$

where Q_i is the monolayer capacity and K_i is the equilibrium constant for component *i*.

It is known that, for thermodynamic consistency, the maximum molar capacity of an adsorbent should be the same for all species in order to follow the Langmuir equilibrium model assumption. However, this assumption is not verified for molecules of very different sizes [8]. Therefore, in some scientific works it is assumed a constant monolayer capacity in terms of mass [23] or in terms of volumes [6]. In this work, it was considered a constant volumetric monolayer capacity for all species, Q_v, which is given by $Q_v = Q_i \times V_{M,i}$. This assumption allowed reducing the adjustable adsorption parameters from 8 (one molar monolayer capacity and one equilibrium constant for each species) to 5 (one volumetric monolayer capacity for all species and one equilibrium constant for each species), at each temperature.

The rate of chemical reaction is given by the following equation [24]:

$$r(mol.g^{-1}_{A15}.\min^{-1}) = k_c \frac{a_A a_B - \frac{a_c a_D}{K_{eq}}}{\left(1 + K_{s,D} a_D\right)^2} \tag{3.6}$$

wherein a_i are the species activities (calculated using the UNIFAC model), the subscripts A, B, C and D refer to n-butanol, AAc, BAc and water, respectively, and k_c, $K_{s,D}$ and

K_{eq} are the kinetic constant, the water adsorption constant, and the thermodynamic equilibrium constant, respectively, which are, according to the literature [24], equal to:

$$k_c(mol.(g_{A15}^{-1}.\min^{-1}) = 1.52\times10^7 \exp\left(-\frac{66988}{RT}\right) \quad (3.7)$$

where R is the ideal gas constant (J.mol^{-1}.K^{-1}),

$$K_{S,D} = 1.589 \pm 0.100 \quad (3.8)$$

$$K_{eq} = \exp\left(\frac{-1490 \pm 577}{T} + (7.21 \pm 1.67)\right) \quad (3.9)$$

Initial and Danckwerts boundary conditions are given by equations (3.10) to (3.13), where the subscripts *F* and *0* represent the feed and initial conditions, respectively.

$$t = 0 \quad C_i = \bar{C}_{p,i} = C_{i,0} \quad (3.10)$$

$$z = 0 \qquad uC_i - D_{ax}C_T \left.\frac{\partial x_i}{\partial z}\right|_{z=0} = uC_{i,F} \quad (3.11)$$

$$z = 0 \qquad u = u|_{z=0} \quad (3.12)$$

$$z = L_b \qquad \left.\frac{\partial C_i}{\partial z}\right|_{z=L_b} = 0 \quad (3.13)$$

3.3.1. Mass transfer parameters

In this model, a global mass-transfer coefficient was considered that combines external and internal mass transfer coefficients, k_e and k_i respectively, according to the resistances-in-series model given by the following equation:

$$\frac{1}{k_L} = \frac{1}{k_e} + \frac{1}{\varepsilon_p k_i} \quad (3.14)$$

The internal mass-transfer coefficient was estimated by Glueckauf equation (3.15) [25] while the external mass-transfer coefficient was estimated by the Wilson and Geankopolis correlation [26], expressed by equation (3.16).

$$k_i = \frac{5D_M / \tau}{r_p} \tag{3.15}$$

$$Sh_p = \frac{1.09}{\varepsilon}\left(Re_p S_c\right)^{0.33} \qquad 0.0015 < Re_p < 55 \tag{3.16}$$

where Sh_p and Re_p are the Sherwood and Reynolds numbers relative to the particle, respectively, described by equations (3.17) and (3.18). The Schmidt number, Sc , was determined according to equation (3.19).

$$Sh_p = \frac{k_e d_p}{D_M} \tag{3.17}$$

$$Re_p = \frac{\rho d_p u}{\eta} \tag{3.18}$$

$$Sc = \frac{\eta}{\rho D_M} \tag{3.19}$$

The infinite dilution diffusivities were estimated by the Scheibel correlation [27]:

$$D_{A,0}^{B} = \frac{8.2\times10^{-8}T}{\eta_B V_{M,A}^{1/3}}\left[1+\left(\frac{3V_{M,B}}{V_{M,A}}\right)^{2/3}\right] \tag{3.20}$$

where $D_{A,0}^{B}$ is the diffusion coefficient for a dilute solute A into a solvent B and η_B is the viscosity of pure solvent B.

Vignes equation [28], based on coefficients at infinite dilution, was used to predict the diffusion coefficient in concentrated solutions for binary systems:

$$D_{B,A} = D_{A,B} = (D_{A,B}^{0})^{x_2}(D_{B,A}^{0})^{x_1} \tag{3.21}$$

The diffusion coefficient for multicomponent concentrated solutions was determined by the Perkins and Geankoplis mixing rule [29]:

$$D_{A,m}\eta_m^{0.8} = \sum_{\substack{i=1 \\ i\neq A}}^{n} x_i D_{Aj}^0 \eta_i^{0.8} \tag{3.22}$$

where η_m is the viscosity of the mixture and η_i is the viscosity of the component *i*.

3.3.2. Numerical solution

The numerical solution of this problem was obtained by using the commercial software gPROMS (general PROcess Modelling System) version 3.5.3, using a method of orthogonal collocation in finite elements (OCFEM); to this end, the axial dimension of the bed was discretized in 21 finite elements with 2 interior collocation points in each finite element and the DASOLV integrated solver was used to solve the remaining system of ordinary differential equations in time. For all simulations a tolerance of 10^{-5} was used.

3.4. Results and Discussion

3.4.1. Fixed-bed column characterization

Tracer experiments were performed at 323 K to characterize the glass fixed-bed column in terms of *Peclet* number and bed porosity. These experiments were carried out by pulse injections of a Dextran solution, since its molecules are large enough to avoid entering in the resin particles pores. Figure 3.2 shows the tracer experimental and predicted results. The theoretical results were obtained using the proposed fixed-bed model without the reaction, adsorption and mass transfer terms, since these phenomena do not occur in the tracer experiments.

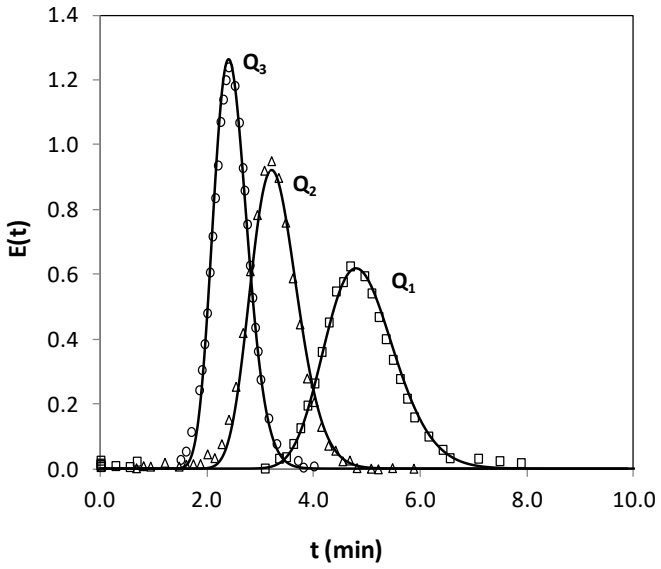

Figure 3.2. Tracer experiments with Dextran solution at different flow rates: 5 mL.min^{-1} (Q_1: □), 7.5 mL.min^{-1} (Q_2: Δ) and 10 mL.min^{-1} (Q_3: ○) at 323K. Points and lines represent the experimental and simulated results, respectively.

The bed porosity, ε, and the *Peclet* number, Pe, were calculated according to equations (3.24) and (3.25), respectively, where t_r is the mean residence time and σ^2 is the variance of the residence time distribution curve. The results obtained are presented in Table 3.2.

$$E(t) = \frac{C_{out}(t)}{\int_0^\infty C_{out}(t)dt} \tag{3.23}$$

$$\varepsilon = \frac{t_r}{V_b / Q} = \frac{\int_0^\infty tE(t)\,dt}{V_b / Q} \tag{3.24}$$

$$Pe = \frac{2t_r^{\,2}}{\sigma^2} = \frac{2t_r^{\,2}}{\int_0^\infty (t - t_r)^2 E(t)\,dt} \tag{3.25}$$

Table 3.2. Tracer experimental results at 323 K.

Run	Q (mL.min^{-1})	t_r (min)	ε	*Pe*	σ^2 (min^2)
1	5.0	4.87	0.42	107	0.446
2	7.5	3.27	0.41	109	0.215
3	10.0	2.45	0.41	116	0.199

Regarding the stainless steel column used for experiments performed at 363 K, despite its different dimensions (see Table 3.1), where the fixed-bed columns characteristics are presented), the bulk density is almost the same, which implies the same bed porosity (approximately 0.4). The *Pe* number was determined from the following empirical correlation valid for liquids in packed beds[30]: $\varepsilon Pe_p = 0.2 + 0.011 Re_p^{0.48}$ (subscript *p* corresponds to the particle), where $Pe_p = Ped_p / L_b$. The *Pe* number obtained from this correlation was 226. In order to validate the correlation, the same was applied to calculate the *Pe* number of the glass column. The correlation gives a *Pe* equal to 82, while from the tracer experiments an average value of 110 was determined (Table 3.2).

3.4.2. Adsorption isotherms

The multicomponent adsorption equilibrium was studied at two temperatures, 323 K and 363 K. The breakthrough curves of non-reactive pairs were measured in accordance to what was described in Section 3.2.3, in order to evaluate the A-15 performance in terms of adsorption capacity and selectivity for all compounds of the system under study. The possible binary mixtures to perform the breakthrough experiments in the absence of reaction are: n-Butanol/water, n-Butanol/BAc, AAc/water and AAc/BAc.

3.4.2.1. Preliminary studies

It has been referred in the literature [6, 8, 31] that it is extremely important to set the correct liquid flow direction, which should be based on the different species densities; bottom-

up or top-down direction must be used in order to ensure that the component above the front is less dense than the component below the front. This condition avoids a possible axial backmixing phenomenon driven by natural convection [8]. An example is shown in Figure 3.3, where the results of two adsorption experiments performed at the same conditions but using opposite feed flow directions are presented. According to the results, the use of the bottom-up configuration results in more dispersive curves than when the correct configuration (top-down direction since a less dense mixture is being fed) is used. In all the experiments, the correct feed flow direction was considered, taking into account the densities of the species, which, at 363 K, are 746 $kg.m^{-3}$, 823 $kg.m^{-3}$, 963 $kg.m^{-3}$ and 970 $kg.m^{-3}$, for n-Butanol, BAc, water and AAc, respectively.

The effect of the presence of inhibitor was also studied by performing the same breakthrough experiment with and without PTZ. According to the suggested by Niesbach et al.[22], in order to suppress the formation of by-products, it was ensured an amount of 1000 ppm of PTZ along the column bed during the experiment. The breakthrough curves obtained are shown in Figure 3.4, where it is visible that the inhibitor has no significant effect on the adsorption results.

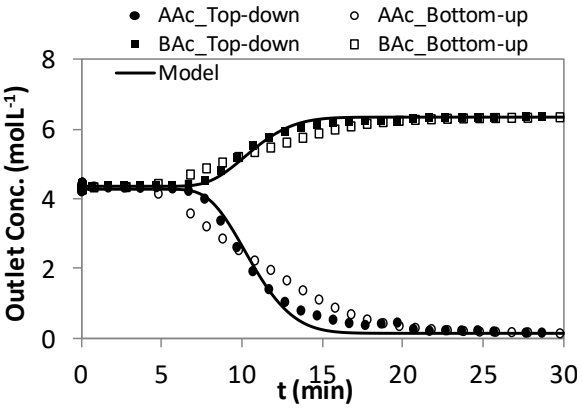

Figure 3.3. Breakthrough curves for BAc displacing a BAc/AAc mixture (50/50 mol %) using different feed configuration: Top-down (■/●) and Bottom-up (□/○).

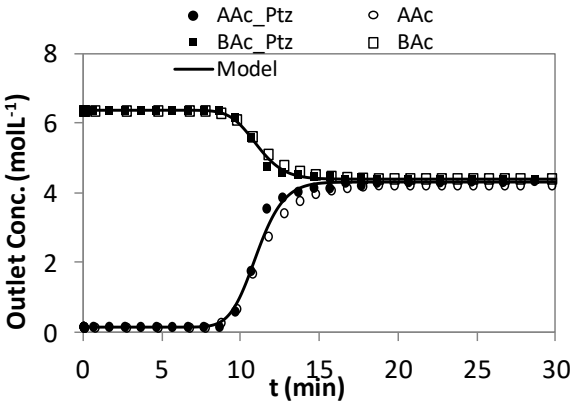

Figure 3.4. Breakthrough curves for a mixture BAc/AAc (50/50 mol %) displacing a BAc solution using or not inhibitor: with PTZ (■/●) and without PTZ (□/○).

3.4.2.2. Adsorption experiments

The adsorption results were used to calculate the experimental number of moles adsorbed/desorbed according to equation (3.26). Then, the parameters of the multicomponent Langmuir adsorption isotherms (equation (3.5) were determined by minimizing the difference between experimental and theoretical values (determined by equation (3.27), according to equation (3.28), and applying a Jackknife methodology [32]. The same procedure was applied for the results at 323 K.

$$n_{\exp} = \zeta Q \int_0^{\infty} \left[C_F - C_{out}(t) \right] dt \tag{3.26}$$

$$n_{the} = \zeta \left\{ \left(\left[\varepsilon + (1-\varepsilon)\varepsilon_p \right] (C_F - C_0) + (1-\varepsilon)(1-\varepsilon_p) \left[q(C_F) - q(C_0) \right] \right) / V \right\} \tag{3.27}$$

where $\zeta = 1$ for adsorption step and $\zeta = (-1)$ for desorption step.

$$F_{obj} = \sum_{k=1}^{NE} \left[\left(n_{\exp}^{ads} - n_{the}^{ads} \right)^2 + \left(n_{\exp}^{des} - n_{the}^{des} \right)^2 \right] \tag{3.28}$$

The final adsorption parameters for all species, as well as the respective molar volumes at 323 K and 363 K are summarized in Table 3.3.

Table 3.3. Adsorption parameters over A-15 resin and molar volume at 323 and 363 K.

Component	Q_V (mL.L$^{-1}_{solid}$)		K (L.mol^{-1})		V_M (mL.mol^{-1})	
	323 K	363 K	323 K	363 K	323 K	363 K
n-Butanol	462.0 ± 2.0	452.5 ± 10.8	6.90 ± 1.51	7.07 ± 2.59	94.71	99.38
Water			48.74 ± 7.39	22.74 ± 8.09	18.24	18.71
Butyl Acrylate			2.67 ± 0.30	1.94 ± 0.34	147.65	155.65
Acrylic Acid			3.51 ± 0.32	1.90 ± 0.45	70.85	74.31

From Figure 3.5 to Figure 3.8, the breakthrough curves at 363 K for all the possible binary mixtures obtained using the correct liquid flow direction and without inhibitor

(except the inhibitor already present in the AAc and BAc purchased), are shown, while the adsorption results at 323 K are shown in *Appendix C*.

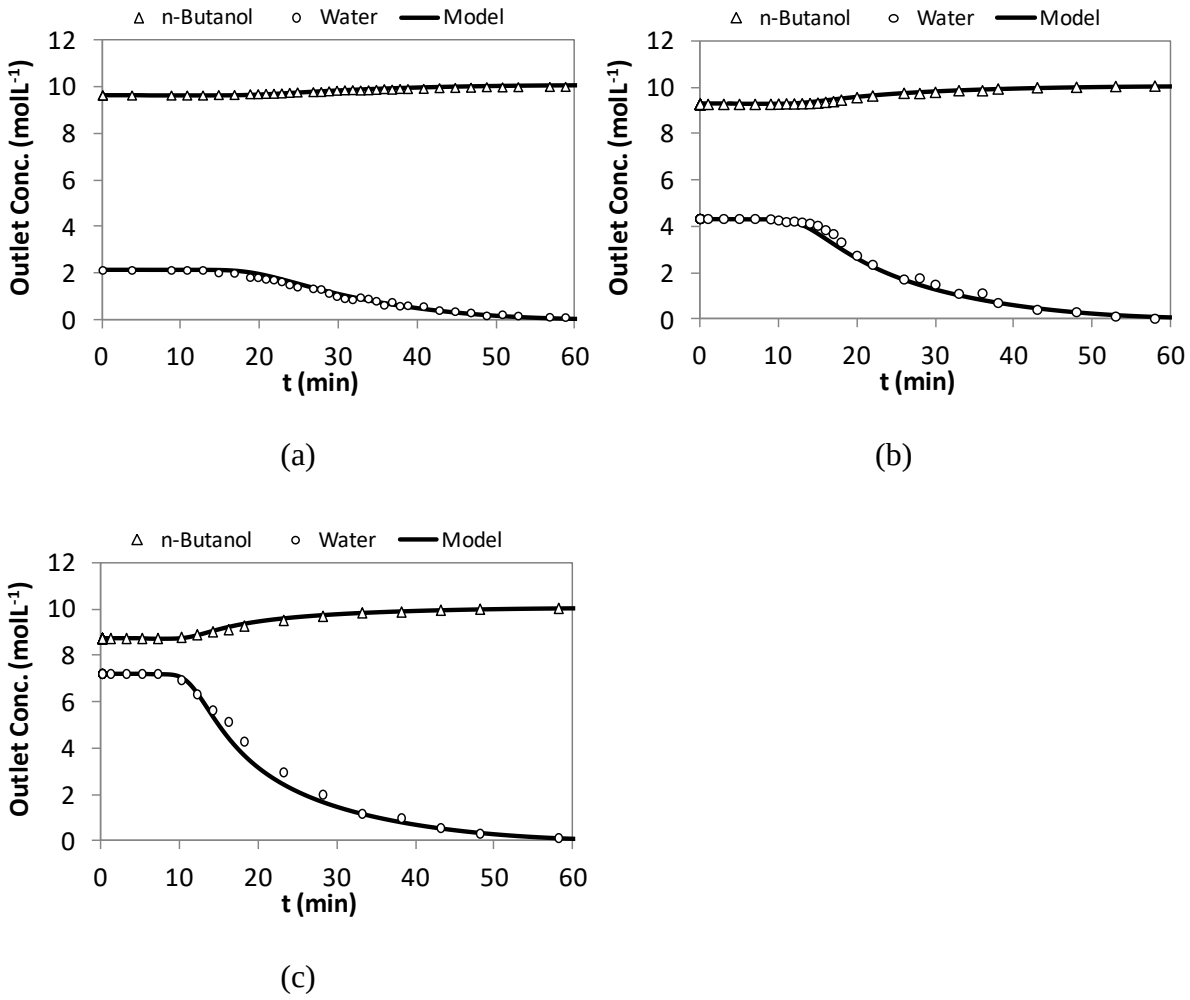

Figure 3.5. Breakthrough curves for n-butanol displacing n-Butanol/water mixtures (80/20 (a), 67/33 (b) and 55/45 (c) mol %) at 7.5 mL.min^{-1} and 363 K; Top-down direction.

The experimental results were, generally, well predicted by the mathematical model using the optimized adsorption parameters presented in Table 3.3. For the pair n-butanol/water, Figure 3.5, the mean deviations obtained between experimental and theoretical amounts of n-butanol adsorbed are 1.1, 1.7 and 0.2 % for the results presented in (a), (b) and (c), respectively. For water, deviations of 2.0 % (a) and 0.9 % ((b) and (c)) between the experimental and theoretical desorbed amounts were observed.

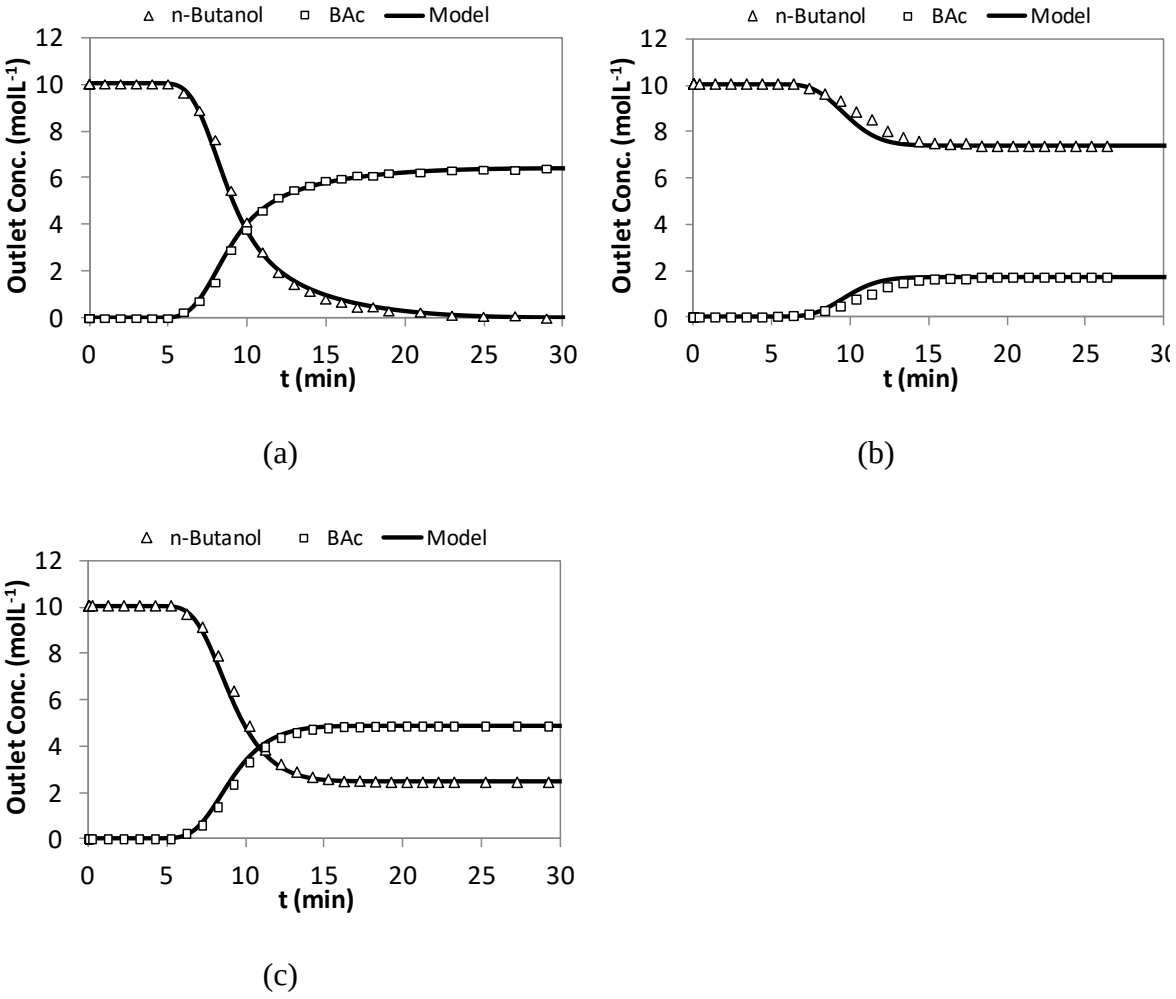

Figure 3.6. Breakthrough curves for n-butanol/BAc mixtures (0/100 (a), 80/20 (b) and 33/67 (c) mol %) displacing n-butanol at 7.5 mL.min^{-1} and 363 K; Bottom-up direction.

Regarding the n-Butanol/BAc pair (Figure 3.6), the differences obtained between the experimental amount adsorbed of BAc and the one predicted were 0.7, 7.9 and 1.5 % for the experiments shown in (a), (b) and (c), while for the amount desorbed of n-butanol the mean deviations obtained were 0.6, 8.0 and 0.8 %, respectively.

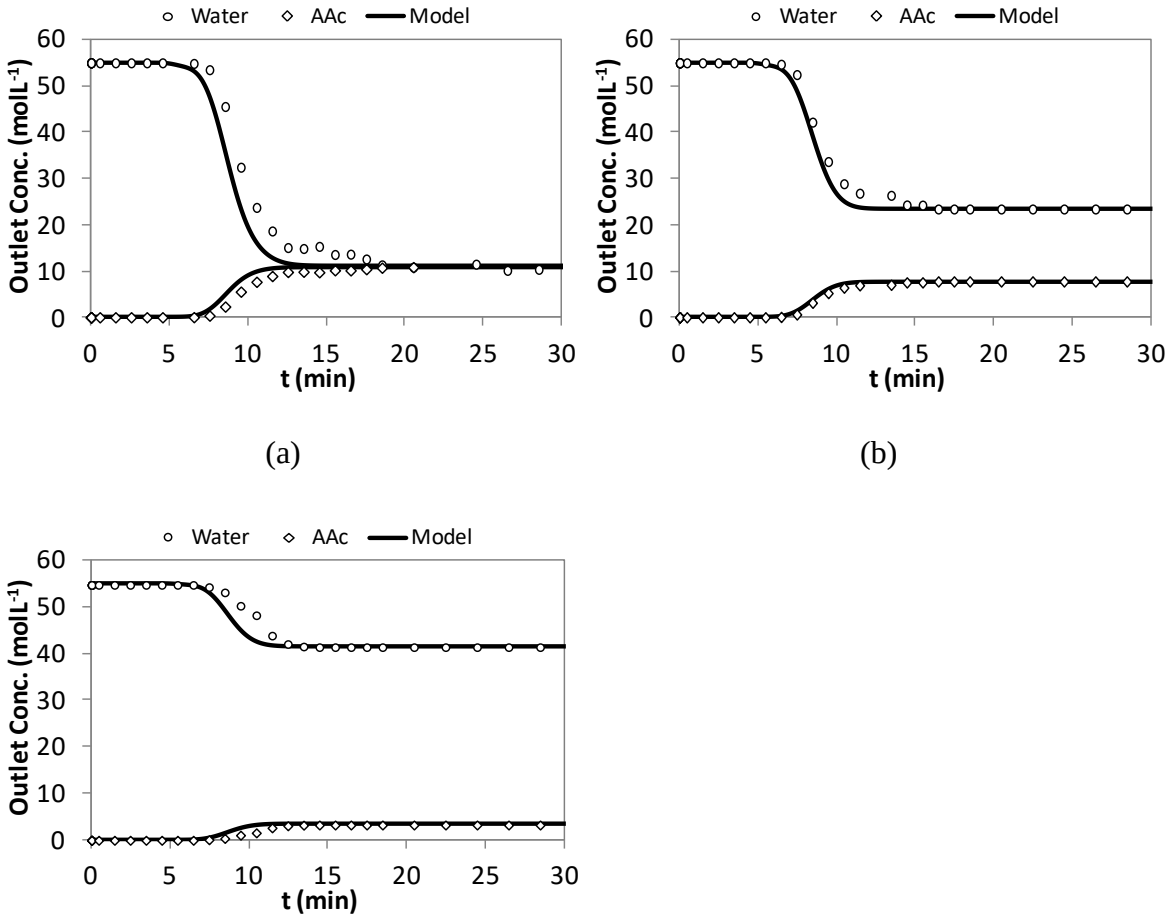

Figure 3.7. Breakthrough curves for AAc/Water mixtures (50/50 (a), 30/70 (b) and 10/90 (c) mol %) displacing Water at 7.5 mL.min^{-1} and 363 K; Bottom-up direction.

Higher deviations between the experimental results and the model predictions were observed for AAc/water mixture (Figure 3.7). A mean deviation of about 20 % for the amount adsorbed/desorbed of AAc/water were observed, except for the experiment (b) for which it was found a mean deviation of 6.4% between the experimental and theoretical number of moles for both species. This large deviation might be caused by some polymerisation of AAc in the column despite the fact that in the experiments performed using AAc, the concentration of this species was never higher than 50 mol %, because of the risk of polymerisation and also in order to avoid possible corrosion of the experimental setup components such as the HPLC pumps. Nevertheless, it is known that AAc tends to polymerise at high temperatures [22, 33, 34]. Indeed, after the adsorption

experiments performed with this binary mixture, the column was opened and it was observed the presence of an apparently viscous polymer like a colourless gel with elastic properties in the bulk. However, no significant amount of other species were detected in the liquid phase (less than 5% of A_i/A_{total}) as already reported by other authors [33].

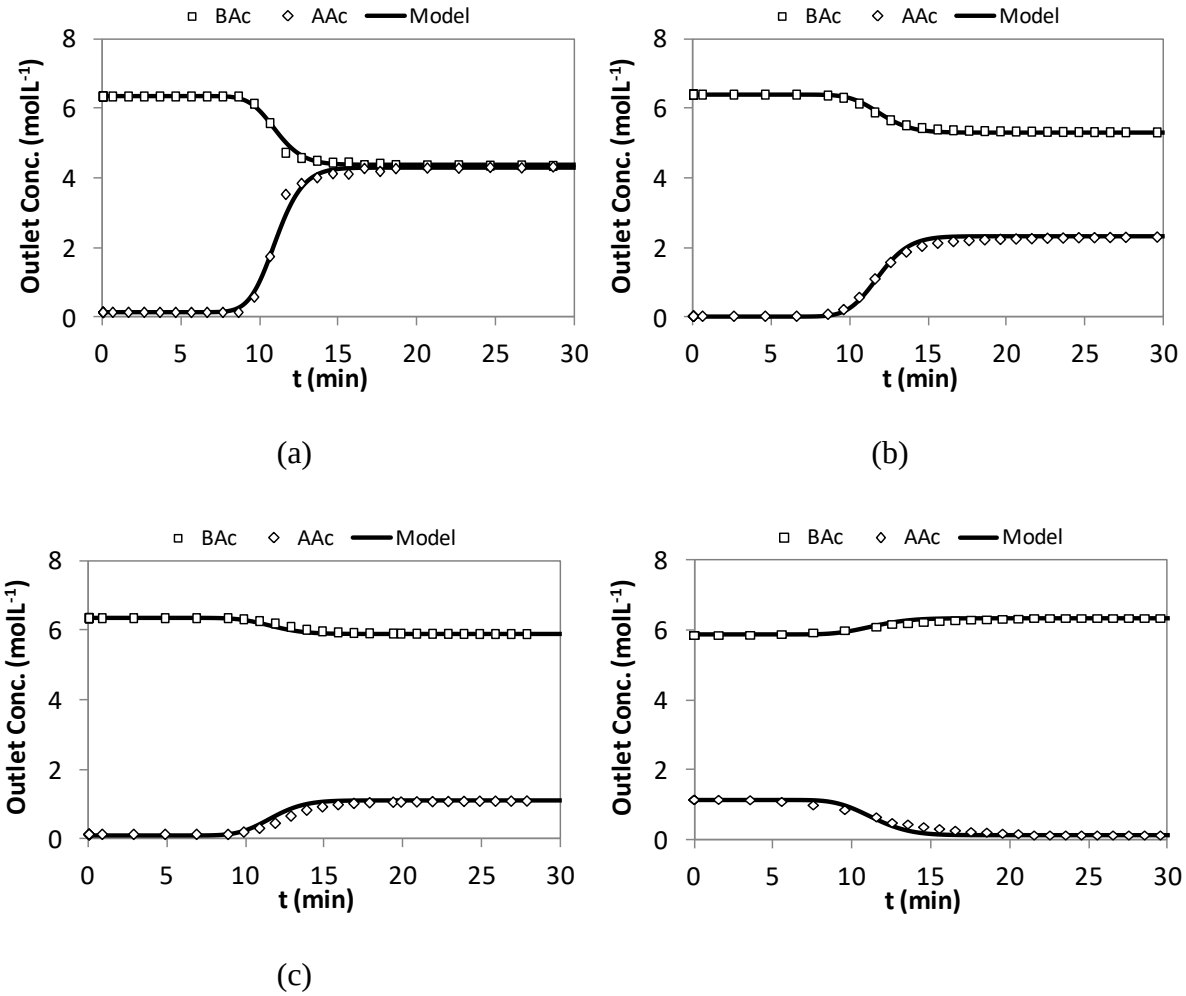

Figure 3.8. Breakthrough curves for AAc/BAc mixtures (50/50 (a), 35/65 (b), 10/90 (c), 0/100 mol %) displacing BAc at 7.5 mL.min^{-1} and 363 K; Bottom-up direction.

For the pair BAc/AAc, both species with high risk of polymerisation, good results were obtained as can be observed in Figure 3.8, resulting mean deviations of 0.2 (a), 3.0 (b), 12.3 (c) and 8.0 % (d) between experimental and predicted amounts desorbed of BAc and 0.9 (a), 1.9 (b), 11.2 (c) and 7.0 % (d) for the amounts adsorbed of AAc. Accordingly,

this fact leads to conclude that, besides the high temperature, water had the main role in the formation of the polymer observed in the experiments with AAc/water, like it happens in the hydrogel synthesis. This kind of polymers, as polyacrylic acid (PAA), are formed in the aqueous phase and they have water holding capacity and permeability as important characteristics, leading to the formation of a network that swells [35]. This process leads to believe that there was a change in the bulk conditions during these experiments (AAc/water), which can also explain the deviation of the breakthrough curves in relation to the predicted by the model. Nevertheless, the experimental adsorption results were overall well described by the considered mathematical model.

3.4.3. Fixed-bed adsorptive reactor

A simulation study was performed in order to predict the performance of the fixed-bed adsorptive reactor (FBR), at 323 and 363 K, when an equimolar mixture of reactants (AAc and n-Butanol) is fed at 1 $mL.min^{-1}$ to the fixed-bed column (stainless steel) saturated with n-Butanol. It was concluded that, at 323 K, the conversion achieved under these conditions is small due to the low reaction rate. At steady state, the conversion obtained is 17 %, which is significantly smaller than that attained in equlibrium conditions (56 %). Indeed, at this temperature, the reaction equilibrium conversion for an equimolar mixture of AAc and n-butanol can only be achieved for a FBR space-time of approximately 186 min.

In order to increase the reaction rate, attain higher conversions and, consequently, better performance in the BAc production, the reaction plus adsorption experiments were conducted at 363 K.

A first experiment (FBR_1) was performed by feeding a mixture comprising AAc and n-butanol in the stoichiometric amount, at a flow rate of 1.3 $mL.min^{-1}$, to the stainless steel column packed with A-15 saturated with n-butanol (Figure 3.9). As soon as the reactive mixture enters the column it is adsorbed by A-15 and starts to react producing BAc and water in stoichiometric amounts. As shown in Figure 3.9, BAc is the first eluted species, while water is the last, in accordance with the resin affinity towards these components (BAc is the less adsorbed component; water is the most adsorbed one). The concentration profiles evolution continues until the resin is completely saturated with

water. After this, the selective separation of BAc and water is no longer possible, the outlet stream composition remains constant and the FBR achieves the steady state. A maximum concentration of the desired product (BAc) equal to 5 $mol.L^{-1}$, at approximately 85 min, was achieved, which significantly overcomes the equilibrium concentration that is equal to about 3 $mol.L^{-1}$ (represented by a dashed line in Figure 3.9). This result demonstrates the potential of sorption enhanced reactor technologies, as the FBR and the SMBR, for the BAc production. After the FBR_1 experiment, a regeneration step was performed by feeding n-butanol at a flow rate of 7.5 $mL.min^{-1}$ to the column in order to displace all the adsorbed components. The concentration histories obtained at the fixed-bed column outlet during the regeneration step (FBR_1_R) are shown in Figure 3.10, where it can be observed that AAc and BAc are completely eluted after 12 min, while water requires about 60 min to be desorbed using therefore a significant larger amount of n-butanol than the other species. In both reactive and regeneration steps the model describes reasonably well the experimental results (see Figure 3.9 and Figure 3.10).

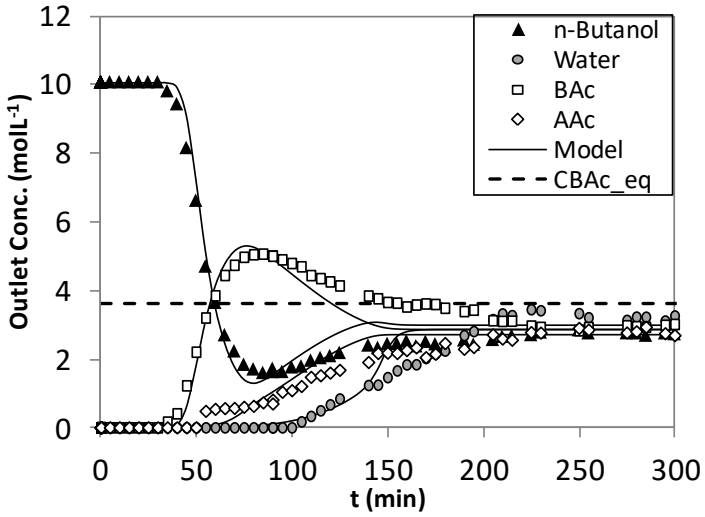

Figure 3.9. FBR_1 - Experimental and simulated concentration histories at the outlet of the fixed-bed adsorptive reactor initially saturated with n-butanol and fed with a mixture of AAc/n-butanol ($C_{n\text{-}butanol,F}$ = 5.88 $mol.L^{-1}$ and $C_{AAc,F}$ = 5.60 $mol.L^{-1}$); Bottom-up feed configuration; Q = 1.3 $mL.min^{-1}$ and T = 363 K. Dashed line represents the concentration of BAc in equilibrium, in batch conditions.

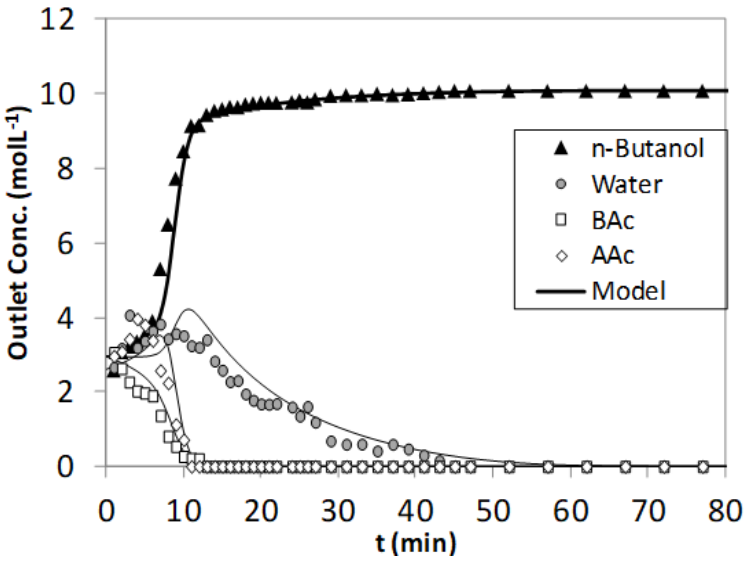

Figure 3.10. FBR_1_R - Experimental and simulated concentration histories at the outlet of the fixed-bed adsorptive reactor for the regeneration step with n-butanol; Top-down feed configuration; Q = 7.5 mL.min^{-1} and T = 363 K.

In order to validate the mathematical model, additional reactive adsorptive experiments were performed under different conditions: FBR_2 - an equimolar reactants ratio solution was fed at a flow rate of 0.9 mL.min^{-1} (Figure 3.11) and FBR_3 - a mixture with reactants molar ratio 3:1 (n-butanol: AAc) was fed at a flow rate of 1.0 mL.min^{-1} (Figure 3.12).

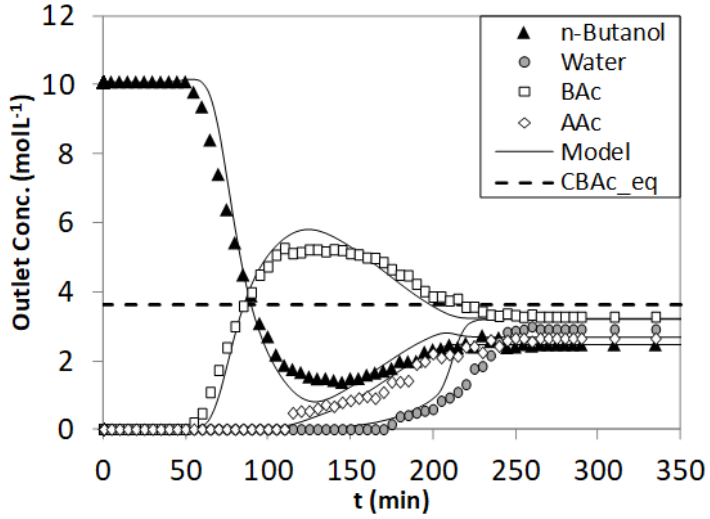

Figure 3.11. FBR_2 - Experimental and simulated concentration histories at the outlet of the fixed-bed adsorptive reactor initially saturated with n-butanol and fed with a mixture of AAc/n-butanol ($C_{n\text{-}butanol,F}$ = 5.91 $mol.L^{-1}$ and $C_{AAc,F}$ = 5.67 $mol.L^{-1}$); Bottom-up feed configuration; Q = 0.9 $mL.min^{-1}$ and T = 363 K. Dashed line represents the concentration of BAc in equilibrium, in batch conditions.

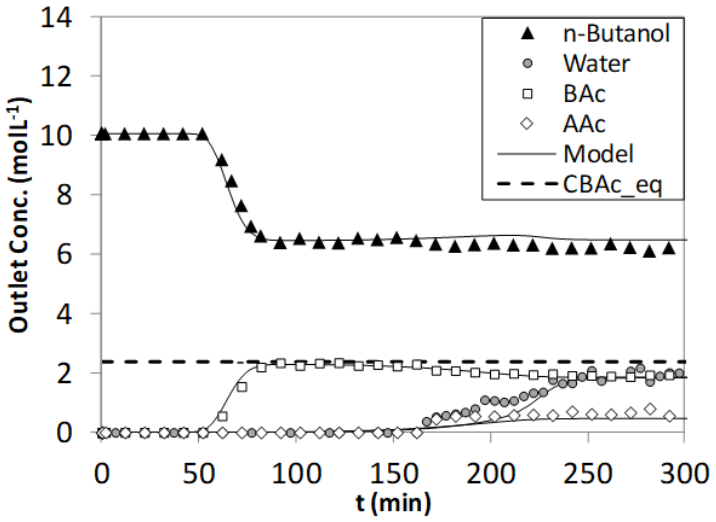

Figure 3.12. FBR_3 - Experimental and simulated concentration histories at the outlet of the fixed-bed adsorptive reactor initially saturated with n-butanol and fed with a mixture of AAc/n-butanol ($C_{n\text{-}butanol,F}$ = 8.35 $mol.L^{-1}$ and $C_{AAc,F}$ = 2.28 $mol.L^{-1}$); Bottom-up feed configuration; Q = 1.0 $mL.min^{-1}$ and T = 363 K. Dashed line represents the concentration of BAc in equilibrium, in batch conditions.

Once again, in both cases, the column was previously saturated with n-butanol. The behaviour observed in the species concentration histories at the column outlet shown in Figure 3.11 is similar to the one described above for the FBR_1. The outlet concentrations of both reactants and products at the steady state should be the same (as in experiment FBR_1); however, this is not observed in the case of the products (water presents a lower concentration than BAc), which might be due to errors associated with the analytical method. Due to the simultaneous reaction and separation steps, in the FBR_2 experiment, it was possible to obtain a BAc maximum concentration 38 % higher than the equilibrium concentration. The FBR_2 and FBR_3 experimental results are also reasonably well described by the considered mathematical model as can be seen in Figure 3.11 and Figure 3.12, respectively. Nevertheless, the quality of the fittings was determined quantitatively by computing the respective correlation coefficient, R^2_{corr}, according to the following equation:

$$R^2_{corr} = 1 - \frac{\sum_{i=1}^{NC}\sum_{j=1}^{NE}\sum_{k=1}^{NP}\left(C^{\exp}_{out,i,j,k} - C^{\mathrm{mod}}_{out,i,j,k}\right)^2}{\sum_{i=1}^{NC}\sum_{j=1}^{NE}\sum_{k=1}^{NP}\left(C^{\exp}_{out,i,j,k} - \overline{C}^{\mathrm{mod}}_{out,i}\right)^2} \tag{3.29}$$

where *NC*, *NE* and *NP* are the number of compounds, experiments and data points, respectively. The value obtained for this parameter was 0.975, confirming that the implemented mathematical model describes with good accuracy the concentration histories of all compounds in fixed-bed adsorptive reactor experiments.

3.5. Conclusions

The feasibility of the butyl acrylate production in a fixed-bed adsorptive reactor packed with Amberlyst-15 ion exchange resin was assessed.

An adsorption study using non-reactive binary mixtures was performed, at 323 and 363 K, in order to determine the adsorption parameters of the selected isotherm (multicomponent Langmuir isotherm) at these two temperatures. The resin affinity towards the species involved in butyl acrylate synthesis in descending order is: water, n-butanol, acrylic acid and butyl acrylate.

Reactive adsorption experiments were also performed under different conditions in order to validate the proposed mathematical model that considers: isothermal operation, axial dispersion, constant bed volume and packing (porosity), internal and external mass-transfer resistances and velocity variations due to changes in the bulk composition. This model is efficient in the prediction of adsorption, reaction and regeneration steps and it will be an important tool to implement and develop sorption enhanced reaction technologies. This type of reactors is very promising for the sustainable BAc synthesis as proved by the conversions significantly above the equilibrium attained in the fixed-bed adsorptive reactor.

3.6. Notation

Abbreviations

AAc	Acrylic Acid
A-15	Amberlyst-15
BAc	Butyl Acrylate
FID	Flame Ionization Detector
FBR	Fixed-Bed Adsorptive Reactor
gPROMS	General Process Modelling System
PTZ	Phenothiazine
RD	Reactive Distillation
SMBR	Simulated Moving Bed Reactor
TCD	Thermal Conductivity Detector

Symbols

a	Liquid phase activity	-
C	Liquid phase concentration	$mol.m^{-3}$
$\overline{C}_p$	Average liquid phase concentration inside the particle	$mol.m^{-3}$

C_t	Total liquid phase concentration	$mol.m^{-3}$
d_{int}	Internal diameter of the column	m
$D^0_{A,B}$	Diffusion coefficient for a dilute solute A into a solvent B	$m^2.s^{-1}$
$D_{A,B}$	Diffusion coefficient for binary concentrated solutions	$m^2.s^{-1}$
D_{ax}	Axial dispersion coefficient	$m^2.s^{-1}$
D_M	Molecular diffusivity	$m^2.s^{-1}$
d_p	Particle diameter	m
K	Langmuir equilibrium parameter	$m^3.mol^{-1}$
k_i	Internal mass transfer coefficient	$mm.s^{-1}$
k_e	External mass transfer coefficient	$m.s^{-1}$
k_c	Reaction kinetic constant	$mol.kg^{-1}.min^{-1}$
K_{eq}	Equilibrium constant	-
K_s	Adsorption constant (in the reaction rate law)	-
k_L	Global mass transfer coefficient	$m.s^{-1}$
L_b	Bed length	m
n	Number of moles	mol
Pe	*Peclet* number	-
$\overline{q}$	Average solid phase concentration in equilibrium with $\overline{C}_p$	$mol.m^{-3}_{solid}$
Q	Molar adsorption capacity ($Q_i = Q_v / V_{M,i}$)	$mol.m^{-3}_{solid}$
Q_v	Volumetric monolayer capacity	$m^3.m^{-3}_{solid}$
r	Reaction rate	$mol.kg^{-1}.min^{-1}$
r_p	Particle radius	m
Re_p	Reynolds number relative to the particle	-
Sc	Schmidt number	-
Sh_p	Sherwood number relative to the particle	-
T	Temperature	K

t_r	Mean residence time	min
u	Interstitial velocity	$m.s^{-1}$
V_M	Molar volume in the liquid phase	$m^3.mol^{-1}$
x	Liquid phase molar fraction	-
z	Fixed-bed adsorptive reactor axial coordinate	m

Greek Letters

ε	Bulk porosity	-
ε_p	Catalyst/adsorbent particle porosity	-
ζ	Correction factor	-
η	Fluid viscosity	$kg.m^{-1}.s^{-1}$
η_m	Mixture viscosity	$kg.m^{-1}.s^{-1}$
ρ	Fluid phase density	$kg.m^{-3}$
ρ_b	Bulk density	$kg.m^{-3}$
τ	Tortuosity	-

Subscripts

exp	Experimental
the	Theoretical
i	Relative to component *i* (n-butanol, water, BAc or AAc)
0	Relative to initial conditions
F	Relative to feed
out	At the outlet of the fixed-bed column
p	Relative to particle

3.7. References

1. Hage, D. S., 1 - Chromatography. In *Principles and Applications of Clinical Mass Spectrometry*, Rifai, N.; Horvath, A. R.; Wittwer, C. T., Eds. Elsevier: 2018; pp 1-32.

2. Poole, C. F., Chromatography. In *Encyclopedia of Separation Science*, Wilson, I. D., Ed. Academic Press: Oxford, 2000; pp 40-64.

3. Lode, F.; Mazzotti, M.; Morbidelli, M., A New Reaction-Separation Unit: The Simulated Moving Bed Reactor. *CHIMIA International Journal for Chemistry* **2001,** 55, 883-886.

4. Regufe, M. J.; Faria, R. P. V.; Ribeiro, A. M.; Loureiro, J. M.; Rodrigues, A. E., Synthesis of the Biofuel Additive 1,1-Diethoxybutane in a Fixed-Bed Column with Amberlyst-15 Wet. *Chemical Engineering and Technology* **2016,** 39, (8), 1509-1518.

5. Graça, N. S.; Pais, L. S.; Silva, V. M. T. M.; Rodrigues, A. E., Dynamic Study of the Synthesis of 1,1-Dibutoxyethane in a Fixed-Bed Adsorptive Reactor. *Separation Science and Technology* **2011,** 46, 631-640.

6. Pereira, C. S. M.; Silva, V. M. T. M.; Rodrigues, A. E., Fixed Bed Adsorptive Reactor for Ethyl Lactate Synthesis: Experiments, Modelling, and Simulation. *Separation Science and Technology* **2009,** 44, 2721-2749.

7. Gandi, G. K.; Silva, V. M.; Rodrigues, A. E., Synthesis of 1, 1-dimethoxyethane in a fixed bed adsorptive reactor. *Industrial & engineering chemistry research* **2006,** 45, (6), 2032-2039.

8. Silva, V. M. T. M.; Rodrigues, A. E., Dynamics of a fixed-bed adsorptive reactor for synthesis of diethylacetal. *AIChE Journal* **2002,** 48, 625-634.

9. Faria, R. P. V.; Pereira, C. S. M.; Silva, V. M. T. M.; Loureiro, J. M.; Rodrigues, A. E., Sorption enhanced reactive process for the synthesis of glycerol ethyl acetal. *Chemical Engineering Journal* **2014,** 258, 229-239.

10. Chen, X.; Xu, Z.; Okuhara, T., Liquid phase esterification of acrylic acid with 1-butanol catalyzed by solid acid catalysts. *Applied Catalysis A: General* **1999,** 180, 261-269.

11. Darge, O.; Thyrion, F. C., Kinetics of the liquid phase esterification of acrylic acid with butanol catalysed by cation exchange resin. *Journal of Chemical Technology & Biotechnology* **1993,** 58, 351-355.

12. Dupont, P.; Védrine, J. C.; Paumard, E.; Hecquet, G.; Lefebvre, F., Heteropolyacids supported on activated carbon as catalysts for the esterification of acrylic acid by butanol. *Applied Catalysis A: General* **1995,** 129, 217-227.

13. Jerzy, S.; Teresa, W.; Mirosław, G.; Mariusz, W., Kinetics of the synthesis of propyl and butyl acrylates in the presence of some heteropolyacids as catalysts. *International Journal of Chemical Kinetics* **2009,** 41, 12-17.

14. Sert, E.; Atalay, F. S., Esterification of Acrylic Acid with Different Alcohols Catalyzed by Zirconia Supported Tungstophosphoric Acid. *Industrial & Engineering Chemistry Research* **2012,** 51, 6666-6671.

15. Sert, E.; Buluklu, A. D.; Karakuş, S.; Atalay, F. S., Kinetic study of catalytic esterification of acrylic acid with butanol catalyzed by different ion exchange resins. *Chemical Engineering and Processing: Process Intensification* **2013**.

16. Schwarzer, S.; Hoffmann, U., Experimental Reaction Equilibrium and Kinetics of the Liquid-phase Butyl Acrylate Synthesis Applied to Reactive Distillation Simulations. *Chemical Engineering & Technology* **2002,** 25, 975-980.

17. Ostaniewicz-Cydzik, A. M.; Pereira, C. S. M.; Molga, E.; Rodrigues, A. E., Reaction Kinetics and Thermodynamic Equilibrium for Butyl Acrylate Synthesis from n-Butanol and Acrylic Acid. *Industrial & Engineering Chemistry Research* **2014,** 53, (16), 6647-6654.

18. Mazzotti, M.; Kruglov, A.; Neri, B.; Gelosa, D.; Morbidelli, M., A continuous chromatographic reactor: SMBR. *Chemical Engineering Science* **1996,** 51, 1827-1836.

19. Rodrigues, A. E.; Silva, V. M. T. M. Industrial process for acetals production in a simulated moving bed reactor. US 7488851, 2009.

20. Helfferich, F. G., *Ion exchange*. Courier Dover Publications: 1962.

21. Sainio, T.; Laatikainen, M.; Paatero, E., Phase equilibria in solvent mixture-ion exchange resin catalyst systems. *Fluid Phase Equilibria* **2004,** 218, 269-283.

22. Niesbach, A.; Daniels, J.; Schröter, B.; Lutze, P.; Górak, A., The inhibition of acrylic acid and acrylate ester polymerisation in a heterogeneously catalysed pilot-scale reactive distillation column. *Chem Eng Sci* **2013,** 88, 95-107.

23. Pöpken, T.; Götze, L.; Gmehling, J., Reaction Kinetics and Chemical Equilibrium of Homogeneously and Heterogeneously Catalyzed Acetic Acid Esterification with Methanol and Methyl Acetate Hydrolysis. *Industrial & Engineering Chemistry Research* **2000,** 39, (7), 2601-2611.

24. Ostaniewicz – Cydzik, A.; Pereira, C.; Molga, E.; Rodrigues, A. E., Reaction kinetics and thermodynamic equilibrium for butyl acrylate synthesis from n-butanol and acrylic acid. *Industrial & Engineering Chemistry Research* **2014**.

25. Glueckauf, E., Theory of chromatography. Part 10.-Formulae for diffusion into spheres and their application to chromatography. *Transactions of the Faraday Society* **1955,** 51, 1540-1551.

26. Ruthven, D. M., *Principles of Adsorption and Adsorption Processes*. Wiley & Sons: New York, 1984.

27. Scheibel, E. G., Correspondence. Liquid Diffusivities. Viscosity of Gases. *Industrial & Engineering Chemistry* **1954,** 46, 2007-2008.

28. Vignes, A., Diffusion in Binary Solutions. Variation of Diffusion Coefficient with Composition. *Industrial & Engineering Chemistry Fundamentals* **1966,** 5, 189-199.

29. Perkins, L. R.; Geankoplis, C. J., Molecular diffusion in a ternary liquid system with the diffusing component dilute. *Chemical Engineering Science* **1969,** 24, 1035-1042.

30. Butt, J. B., *Reaction kinetics and reactor design*. Prentice-Hall: Englewood Cliffs, NJ, 1980.

31. Ströhlein, G.; Assunção, Y.; Dube, N.; Bardow, A.; Mazzotti, M.; Morbidelli, M., Esterification of acrylic acid with methanol by reactive chromatography: Experiments and simulations. *Chemical Engineering Science* **2006,** 61, 5296-5306.

32. Miller, R. G., The jackknife-a review. *Biometrika* **1974,** 61, 1-15.

33. Mosnáček, J.; Nicolaÿ, R.; Kar, K. K.; Fruchey, S. O.; Cloeter, M. D.; Harner, R. S.; Matyjaszewski, K., Efficient Polymerization Inhibition Systems for Acrylic Acid Distillation: New Liquid-Phase Inhibitors. *Industrial & Engineering Chemistry Research* **2012,** 51, 3910-3915.

34. Ohara, T.; Sato, T.; Shimizu, N.; Prescher, G.; Schwind, H.; Weiberg, O.; Marten, K.; Greim, H., Acrylic Acid and Derivatives. In *Ullmann's Encyclopedia of Industrial Chemistry*, Wiley-VCH Verlag GmbH & Co. KGaA: 2000.

35. Onuki, Y.; Nishikawa, M.; Morishita, M.; Takayama, K., Development of photocrosslinked polyacrylic acid hydrogel as an adhesive for dermatological patches:

Involvement of formulation factors in physical properties and pharmacological effects. *International Journal of Pharmaceutics* **2008,** 349, 47-52.

4. Fixed-Bed Membrane Reactor

Experimental pervaporation data for multicomponent mixtures in absence of reaction were measured for the compounds involved in the esterification reaction of acrylic acid with n-butanol at different temperatures: 323 K, 353 K and 363 K. A commercial tubular microporous silica membrane from Pervatech was used which is highly selective to water and its performance was evaluated by studying several parameters like the selectivity, permeate fluxes, driving force of species and separation factor. The effect of temperature and feed composition were assessed for binary, ternary and quaternary mixtures. The permeance of each species was correlated with temperature according to Arrhenius equation and a mathematical model was proposed to develop an integrated reaction-separation process using the experimental data obtained.

This Chapter is adapted from Constantino, D.S.M., R.P.V. Faria, A.M. Ribeiro, J.M. Loureiro, A.E. Rodrigues, Performance Evaluation of Pervaporation Technology for Process Intensification of Butyl Acrylate Synthesis, *Ind. Eng. Chem. Res.* **2017,** 56 (45), pp 13064–13074. DOI: 10.1021/acs.iecr.7b0132.

4.1. Introduction

Membrane pervaporation process is a very interesting technology for organic-water [1-8] and organic-organic separations [9-11], being more advantageous than distillation which presents considerable thermodynamic limitations [12] and depends on the relative volatilities [13]. It is a very effective separation technique for systems that involve heat-sensitive products and azeotropic mixtures [13] since this process involves a transport mechanism based on physical-chemical interactions between the membrane material and the permeating molecules allowing to operate at lower temperatures than distillation process, for instance. Moreover, membrane pervaporation offers many other benefits such as high selectivity, low energy consumption, moderate cost to performance ratio, compact and modular design [14].

Typically, in industry its main applications are related to the dehydration of organic solvents or solvents mixtures. However, the pervaporation membrane benefits can be strengthened when combined with one or more separation techniques, usually known as pervaporation-based hybrid processes. Likewise, the pervaporation membrane may also appear linked with chemical reaction, extending its application field. As a result, a different type of reactors is generated, the pervaporation membrane reactors (PMR), which have a great potential to improve the reaction conversion of equilibrium limited reactions, as the esterification reactions case. Over the years, pervaporation-based hybrid processes have been investigated [14-20], mainly for intensification of esterification reactions [21], showing to be very advantageous from the process intensification (PI) point of view since they enable reducing the concentrations and the flow rates to be treated and, consequently, the energy requirement and associated costs [20]. Different configurations of PMR can be used: coupling a pervaporation unit to the reactor or integrating the pervaporation unit and the reactor in the same unit. Both configurations can be useful for the esterification reaction of acrylic acid (AAc) with n-butanol; however, the most promising comprises the process integration in the same unit where the reaction conversion can be favoured towards butyl acrylate (BAc) production by the continuous water removal (by permeation) from the reaction medium.

Although a pervaporation-based hybrid process has already been investigated for the esterification of acrylic acid with n-butanol [22], presenting a significantly enhanced reaction conversion (31% at 358 K, for instance, in the presence of pervaporation), experimental pervaporation data for the multicomponent mixture in absence of reaction were no reported. Nevertheless, these experimental data are required to understand the influence of the different compounds in the performance of the membrane for the global process (reaction combined with pervaporation). Moreover, in that work, where a batch reactor was coupled with a Pervap 2201 polymeric membrane considering Amberlyst 131 ion exchange resin as catalyst, the driving force was not studied.

In the present Chapter, a multicomponent pervaporation study for the compounds involved in the BAc production in the absence of reaction was performed, for the first time, at different temperatures, 323, 353 and 363 K and different parameters were evaluated, including the driving force. For that, a commercial tubular inorganic membrane was used since it presents better stability under acidic and high temperature conditions than polymeric membranes, being the best alternative for the dehydration of the reaction medium [16]. According to the literature [23], commercial microporous silica membrane from Pervatech showed better selectivity and water flux than the one from Pervap SMS from Sulzer Chemtech in dehydration of aqueous mixtures, so a Pervatech BV membrane was considered. The activation energies were also estimated by the dependence of permeance on temperature for each compound taking into account the driving force. A mathematical model was developed considering the mass transport under isothermal and non-isothermal conditions and it was applied for the study of enhanced esterification reaction of AAc with n-butanol by combining a fixed-bed reactor (FBR) with a pervaporation membrane. This configuration was already investigated for other esterification reactions as the esterification of oleic oil with ethanol [24], for which an increase of 3 % of the limiting reactant conversion was observed for the pervaporation-assisted reaction, and the esterification of lactic acid with ethanol [16], for which the integration of a pervaporation membrane increased more than twice the limiting reactant conversion of a conventional FBR process, considering isothermal conditions.

Moreover, it is important to refer that all experimental pervaporation data presented in this Chapter will be useful to design and optimise the Simulated Moving Bed Membrane

Reactor (PermSMBR) and other different configurations of pervaporation-based hybrid processes for BAc synthesis.

4.2. Experimental Data

4.2.1. Chemicals and materials

The chemicals used in the pervaporation experiments were n-butanol (≥ 99.9 wt.%) from Fisher Scientific, acrylic acid (≥ 99.0 wt.%) and butyl acrylate (≥ 99.5 wt.%) from Acros Organics. Acrylic acid and butyl acrylate were provided stabilized with inhibitor (about 200 ppm and 20 ppm of hydroquinone monomethyl ether, respectively). The additional inhibitor used in this study was phenothiazine (PTZ) (99.0 wt.%), also from Acros Organics. Isopropanol (≥ 99.9 wt.%) from Fisher Scientific was used as solvent in the chromatographic analysis.

A commercial Hybrid Silica AR membrane supplied by Pervatech BV (The Netherlands) was used, which presents hydrophilic characteristics. It consists of a modified silica selective layer coated onto gamma alumina and its separation layer is applied inside of an asymmetric ceramic tube that has an outer diameter of 10 mm, an inner diameter of 7 mm, and a length of 50 cm. This membrane has an effective area per tube of about 110 cm^2. It is able to be in contact with any solvent at any concentration; however, it is sensitive to extremely acidic and alkaline media being the limit pH range from 0.5 to 8.5.

4.2.2. Analytical method

All samples collected were analysed (at least two times) in a Shimadzu - GC 2010 Plus gas chromatograph equipped with a flame ionization detector (FID). The compounds were separated using a silica capillary column (CPWax57CB, 25 m x 0.53 mm ID, film thickness of 2.0 μm). The temperature of the injector was set to 523 K while the temperature of the FID was set to be 573 K. The initial column temperature was 353 K for 5 min, the temperature was then increased at 353 $K.min^{-1}$ up to 473 K and kept

constant for the following 7 min. Helium N50 was used as the carrier gas and the linear velocity was set to 30 $cm.s^{-1}$. Isopropyl alcohol was used as internal standard and acetone as cleaning solvent. The injection volume used was 1.0 µL with a split ratio of 30 for permeate samples, which are more diluted in water, and 90 for the retentate samples. Water content was determined from mass balances. The global associated uncertainty of the measured molar fractions was ≤ 0.05.

4.2.3. Experimental setup and procedure

The experimental data were measured in a pervaporation membrane unit at pilot scale which is represented in Figure 4.1. This unit can work either in batch or continuous mode at temperatures up to 373 K and it is equipped with a temperature sensor (TI) (type K thermocouple, with accuracy of about ± 2.2 K) and pressure sensors (PI). The absolute pressure is measured through two analogue dials, with accuracy of about ±0.5 bar, filled with glycerine and the permeate pressure is measured through one digital dial (ceraphant-T PTC31) with accuracy of about ±1 mbar. The temperature was controlled by a thermostatic bath (Lauda, Germany) with thermal M bath fluid (able to operate from 313 to 443 K) that flows through the feed vessel jacket; the pressure was set to 1.5 bar by applying an overpressure of helium to the system in order to prevent vaporisation of feed mixture over the whole temperature range.

Firstly, the feed vessel was charged with approximately 1.5 L of solution and the heating was switched on at the desired temperature. A positive displacement diaphragm pump (Hydra Cell G-03, Wanner International) was used to recirculate the feed solution over the entire system including the membrane in order to keep it at the same temperature in absence of vacuum on the permeate side. When the temperature is constant, the pervaporation experiment was started by applying vacuum to the permeate side with a vacuum pump (Boc Edwards, U.K.). Two parallel glass cold trap partially submerged in liquid nitrogen allowed the condensation of the permeate vapour. In the beginning, a cleaning procedure was performed by collecting the permeate sample during the first minute for a glass cold trap which was then rejected. After that, the permeate sample was collected in the other cold trap which was defrosted at the end of the experiment to be weighted and analysed by gas chromatography.

Along these measurements, it is important to keep the feed composition nearly constant, so the duration of each experiment was conditioned by the trade-off between ensuring a constant feed composition and a reasonable amount of permeate. Samples were collected before and after each experiment in order to verify the feed composition. The reproducibility was checked by collecting two or three permeate samples under steady state conditions at each temperature.

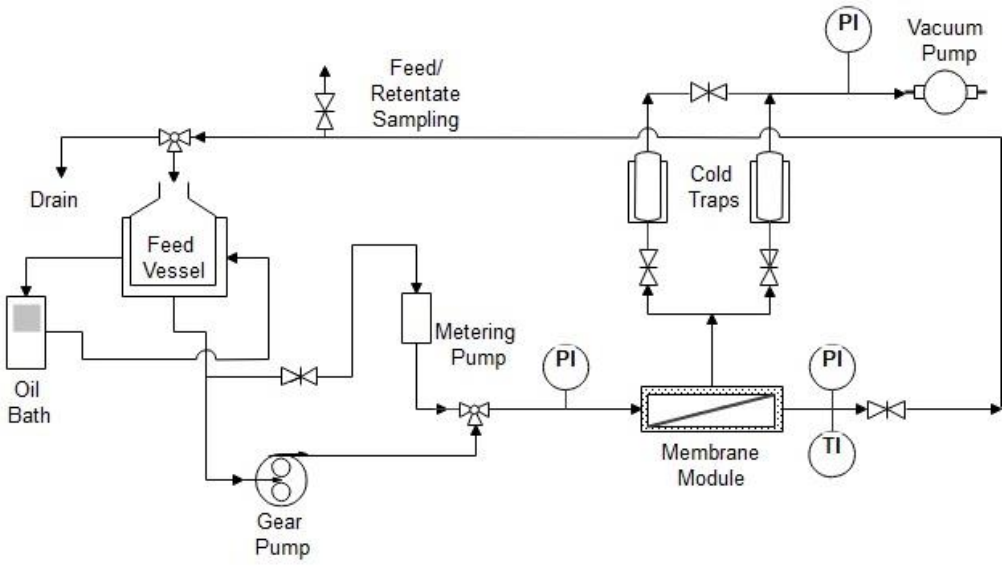

Figure 4.1. Setup of pervaporation membrane pilot scale unit.

4.3. Mathematical Model

The experimental pervaporation data measured for the silica membrane selected were used in mathematical model that was developed to predict the behaviour of the separation process, considering the following assumptions:

(i) Non-isothermal operation due to the heat consumption for species vaporisation;
(ii) Plug flow (retentate stream);
(iii) Retentate velocity variations inside the membrane due to the permeation of the components;
(iv) Concentration polarisation due to the global membrane resistance (diffusive transport in the boundary layer combined with the membrane resistance);
(v) Continuous process once it is a process integrated with the FBR unit.

Retentate mass balance to component i:

$$\frac{\partial C_{ret,i}}{\partial t} + \frac{\partial \left(u_s C_{ret,i} \right)}{\partial z} + A_m J_i = 0 \tag{4.1}$$

where z is the axial coordinate in the membrane modules, C_{ret} is the liquid phase concentration in the retentate side, u_s is the superficial velocity, $A_m$is the membrane area per unit membrane modules volume and J_i is the permeate molar flux of specie *i*, through the membrane, defined as:

$$J_i = k_{ov,i} \left(a_i P_i^0 - y_i P_{perm} \right) \tag{4.2}$$

where $k_{ov,i}$ is the global membrane mass transfer coefficient, that combines the resistance due to the diffusive transport in the boundary layer with the membrane [7] resistance:

$$\frac{1}{k_{ov,i}} = \frac{1}{Q_{m,i}} + \frac{a_i P_i^0 V_{M,i}}{x_{i,F} k_{bl}} \tag{4.3}$$

For laminar flow and Graetz number, $d_{int}^2 u_s / \left(D_m L_m \right)$, much greater that one, the mass transfer coefficient for transport in the boundary layer, k_{bl}, is determined by the Lévêque correlation [25] :

$$Sh = 1.62 Re^{0.33} Sc^{0.33} \left(\frac{d_{int}}{L_m} \right)^{0.33} \text{, (Re < 2300)} \tag{4.4}$$

where $Sh = k_{bl} d_{int} / D_M$, $Re = \rho d_{int} u_s / \eta$ and $Sc = \eta / (\rho D_M)$ are the Sherwood, Reynolds and Schmidt numbers, respectively, D_M is the solute diffusivity in the boundary layer, d_{int} is the internal diameter of the tubular membrane, L_m is the membrane length, ρ is the density and η is the viscosity.

The mole fraction of component *i* in the vapour phase (permeate side), y_i, is defined as:

$$y_i = \frac{J_i}{\sum_{i=1}^{n} J_i} \tag{4.5}$$

The fluid velocity variation in the membrane feed side is calculated from the total mass balance:

$$\frac{du_s}{dz} = u_s \sum_{i=1}^{n} C_i \frac{dV_{M,i}}{dz} - A_m \sum_{i=1}^{n} J_i V_{M,i} \tag{4.6}$$

where *n* is the total number of components and $V_{M,i}$ it is the molar volume of component *i*.

Retentate heat balance:

$$\sum_{i=1}^{n} \hat{C}_{p,i} C_{ret,i} \frac{\partial T}{\partial t} + \sum_{i=1}^{n} u_s \hat{C}_{p,i} C_{ret,i} \frac{\partial T}{\partial z} + A_m h_f \left(T - T_m\right) = 0 \tag{4.7}$$

where $\hat{C}_{p,i}$ is the liquid heat capacity of component *i*, *T* is the absolute temperature in the feed side of the membrane, T_m is the membrane absolute temperature, and h_f is the heat transfer coefficient in the liquid boundary layer.

Membrane heat balance:

$$\frac{d_{int}}{\left((d_{int}+\delta)/2\right)^2 - (d_{int}^2/4)} h_f \left(T - T_m\right) = \frac{d_{int}+\delta}{\left((d_{int}+\delta)/2\right)^2 - (d_{int}^2/4)} \sum_{i=1}^{n} \Delta H_i^v J_i \tag{4.8}$$

where δ is the membrane thickness, and ΔH_i^v is the heat of vaporisation of species *i*. The heat transport coefficient was estimated by the Sieder-Tate correlation, valid for laminar pipe flow [26]:

$$N_u = 1.86 \left(RePr \frac{d_{int}}{L_m} \right)^{0.33} \left(\frac{\eta}{\eta_m} \right)^{0.14} \tag{4.9}$$

where $N_u = h_f d_{int} / \lambda$ and $Pr = \eta \hat{C}_{p,i} / \lambda$ are the Nusselt and Prandtl numbers, respectively, η and η_m are the viscosity of the liquid in the feed and in the membrane, and λ is the thermal conductivity.

Initial and boundary conditions:

t = 0: $T = T_F$ (4.10)

$$C_{ret,i} = C_{0,i} \quad (4.11)$$

z = 0: $T = T_F$ (4.12)

$$C_{ret,i} = C_{F,i} \quad (4.13)$$

where subscripts *0* and *F* refer to initial state and membrane feed conditions, respectively.

The molar fractions of all the components at the outlet of the membrane (retentate side) were also calculated:

$$x_{out,i} = \frac{C_{out,i}}{\sum_{i=1}^{n} C_{out,i}} \quad (4.14)$$

where $C_{out,i} = C_{ret,i\,(z=1)}$.

The FBR was simulated according to the mathematical model described in Chapter 3 (Section 3.3).

4.3.1. Numerical solution

The numerical solution of this problem was obtained by using the commercial software gPROMS (general PROcess Modelling System) version 4.2.0, using orthogonal collocation in finite elements (OCFEM) with second order polynomials and one internal collocation point in each element; to this end, the axial dimension of the membrane was discretized in 100 finite elements. The DASOLV equation solver was used to solve the resulting system of ordinary differential equations in time. For all simulations, a tolerance of 10^{-5} was considered.

4.4. Results and Discussion

4.4.1. Preliminary study

A preliminary study was performed to find the minimal feed flow rate required to operate in absence of mass transfer resistance in the boundary layer due to concentration polarisation effects. This phenomenon is related to the accumulation of the retained species near the membrane surface and, consequently, their concentration will be higher in the boundary layer (adjacent to the membrane surface) than in the bulk [27]. Generally, concentration polarisation results from the depletion of the most permeable component in the vicinity of the feed/membrane interface and it is due to the slow diffusion of the solute from the bulk of the feed to the boundary layer [28]. The membrane flux and separation efficiency may be severely impaired due to polarisation [29].

The effect of mass transfer in the boundary layer was investigated with a binary mixture of n-butanol and 31 % of feed water mole fraction at constant temperature, 323 K, by varying the feed flow rate. According to Figure 4.2, this effect is negligible for flow rates higher than approximately 150 $L.h^{-1}$, since the total permeate flux remains constant from above this value. Therefore, all pervaporation experiments were carried out at 200 $L.h^{-1}$ ensuring the absence of mass transfer resistance.

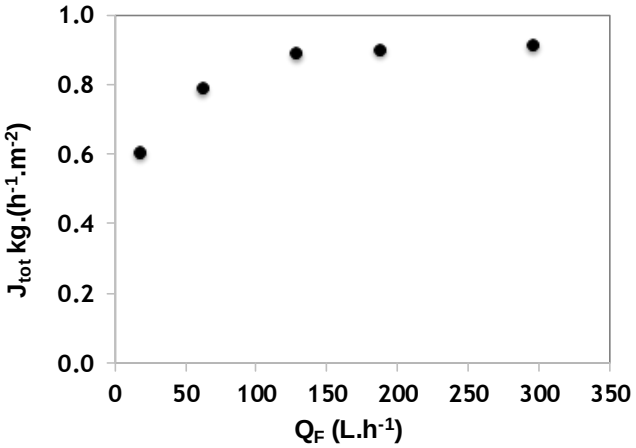

Figure 4.2. Total permeate flux as function of feed flow rate (P_{perm} = 35 mbar, T = 323 K, x_{water} = 0.309).

4.4.2. Pervaporation data

The performance of the membrane for the n-butanol/AAc/BAc/water system was evaluated by measuring pervaporation data for different mixture compositions in absence of reaction at three different temperatures: 323, 353 and 363 K. A pressure of 45 mbar was set in permeate side for all runs. The esterification reaction between AAc and n-butanol presents a very slow kinetics, according to the literature [30], which allows to measure pervaporation data for quaternary mixtures in absence of reaction even at high temperatures, since no catalyst was used. This fact was verified by collecting feed samples after each experiment and analysing them by gas chromatography. All experimental mixture compositions considered in this work are presented in Table 4.1.

Table 4.1. Feed molar compositions of the different mixtures studied.

Mixture	$x_{,n\text{-butanol}}$	$x_{,water}$	$x_{,BAc}$	$x_{,AAc}$
B1	0.741	0.259	-	-
B2	0.800	0.200	-	-
B3	0.911	0.089	-	-
B4	0.940	0.060	-	-
T1	0.652	0.159	0.189	-
T2	0.795	0.109	0.096	-
T3	0.526	0.061	0.413	-
Q1	0.708	0.095	0.097	0.100
Q2	0.587	0.175	0.176	0.062

The feed compositions reported are the average of the feed composition values at the beginning and at the end of the time interval of the permeate sample collection. However the molar fraction of each component did not change more than 1 % .These mixtures were prepared taking into account the miscibility ranges, which were studied by the UNIFAC-DMD model using the database available in the software Aspen Plus (version 8.6) and can be observed in the ternary diagram presented in Figure D.1 (see *Appendix D*). The pair n-butanol/water (mixtures B1 to B4 in Table 4.1) was initially studied since it

represents the extract stream of the SMBR process for the system in study. The AAc/Water binary was not considered due to the high risk of polymerisation described in the literature [31] apart from membrane safety issues. Regarding the pair BAc/water, there is a large area of immiscibility (Figure D.1, *Appendix D*), so this pair was also not studied. Three different ternary mixtures (T1 to T3) were selected taking into account the same feed water molar fraction studied in the binary mixtures for membrane performance comparison besides the miscibility range. One quaternary composition (Q1) was selected to have the same feed water molar composition of binary and ternary mixtures for performance comparison (± 10 % of water). The other mixture (Q2) represents the equilibrium composition of the esterification reaction between n-butanol and AAc with a molar feed ratio (3:1) since n-butanol is the eluent in SMBR based processes being always in excess in relation to the other components.

4.4.2.1. Dehydration of n-butanol: Effect of temperature and feed water composition

Temperature is a very important parameter in pervaporation processes as reported in the literature [13, 22, 32]. Therefore, the influence of the temperature on the total permeate flux was analysed, which can be observed in Figure 4.3. Moreover, the effect of the feed water molar fraction on this parameter (total permeate flux) can be analysed in the same figure (Figure 4.3) while the effect of the feed water molar fraction on the permeate composition is presented in Figure 4.4.

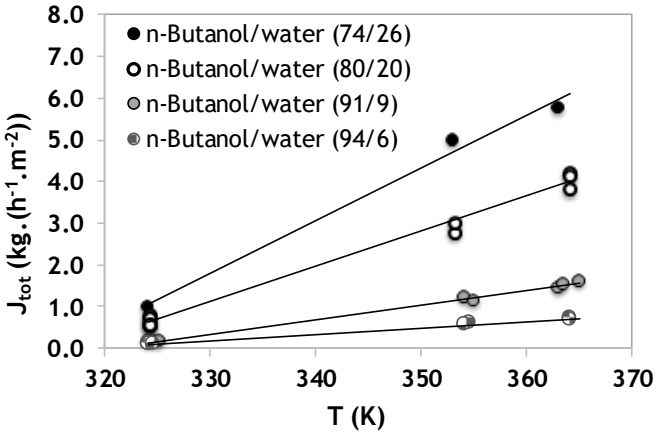

Figure 4.3. Total permeate flux as a function of temperature for different n-butanol/Water binary mixtures.

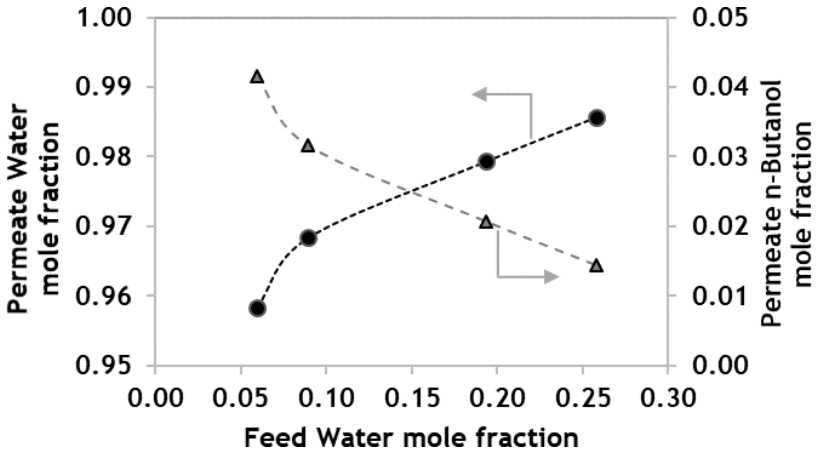

Figure 4.4. Permeate composition as a function of feed water molar composition for n-butanol/water binary mixtures (circles: water, triangles: n-butanol).

According to the experimental results presented in Figure 4.3, it is possible to observe that the total permeate flux increases with the operating temperature and the feed water mole fraction. The use of alumina as intermediate layer increases the hydrophilicity of the membrane, promoting adsorption and diffusion of water [33], leading to higher selectivity for this species. The experimental selectivity values obtained for the studied membrane were between 5 and 160 ($S = Q_{Water}/Q_{n-Butanol}$) which is within the range reported in the literature for microporous silica membranes [1]. Thus, the total permeate flux was mainly composed by water, as shown in Figure 4.4 ($y_w \geq 96$ %), which substantially increased with the feed water mole fraction due to the higher driving force in mixtures with large feed water content. The effect of the feed water mole fraction and temperature in the water driving force is presented in Figure 4.5.

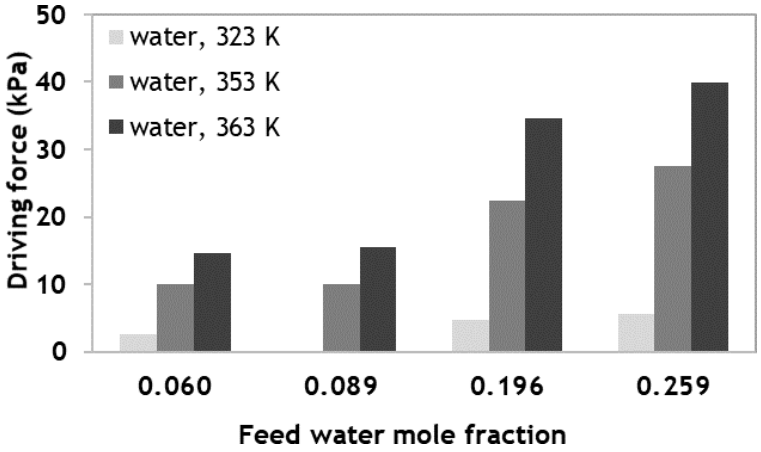

Figure 4.5. Influence of temperature and feed water mole fraction on the driving force of water.

On the other hand, the separation of liquid mixtures by partial vaporisation through a membrane is the principle behind pervaporation processes [21], so in this kind of processes the mass transfer is accompanied with heat transfer [13]. In this way, increasing the temperature also increases the driving force for water since the heat required for a phase change from the liquid to the vapour phase is lower for this compound than for n-butanol, presenting a higher vapour pressure for the same temperature (see Table 4.2), leading to higher permeate fluxes.

Table 4.2. Vapour pressure (bar) for water, n-butanol, Butyl Acrylate and Acrylic Acid at different temperatures [34].

Compound/ Temperature (K)	323	353	363
Water	0.124	0.473	0.701
n-Butanol	0.047	0.224	0.349
Butyl Acrylate	0.029	0.110	0.163
Acrylic Acid	0.024	0.105	0.162

4.4.2.2. Multicomponent pervaporation data for butyl acrylate system

Similarly, a multicomponent pervaporation study was performed for the compounds involved in the BAc production in absence of reaction and different parameters were evaluated. Several ternary and quaternary mixtures were considered according to Table 4.1. Regarding the feed water composition and temperature effects, both parameters increase the total permeate flux like happened in the binary mixture as is shown in Figure 4.6 (ternary mixtures) and Figure 4.7 (quaternary mixtures).

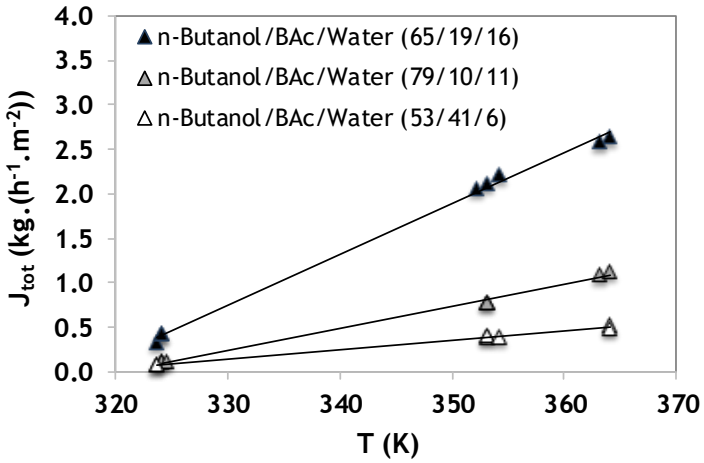

Figure 4.6. Total permeate flux as a function of temperature for different ternary mixtures: n-butanol/ water/BAc (black triangles: T1, grey triangles: T2, white triangles: T3).

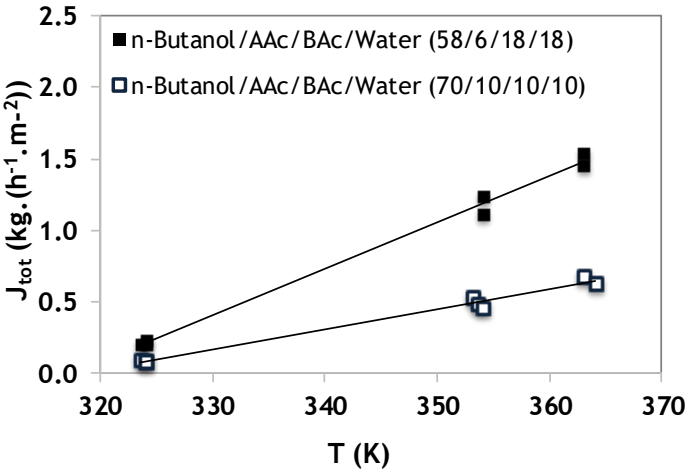

Figure 4.7. Total permeate flux as a function of temperature for different quaternary mixtures: n-butanol/AAc/BAc/water (black squares: Q1, white squares: Q2).

In order to understand the effect of the presence of the remaining compounds on the total permeate flux, different mixtures (binary, ternary and quaternary) with similar feed water molar composition are compared in Figure 4.8.

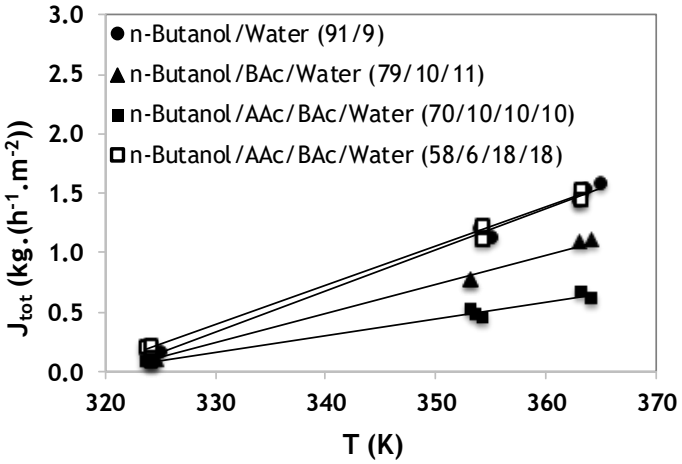

Figure 4.8. Total permeate flux as a function of temperature for the same feed water molar compositions (± 10 %): circles: binary mixture B3, triangles: ternary mixture T2, black squares: quaternary mixture Q1, white squares: quaternary mixture Q2).

The same conclusions reported previously for the binary system are valid for the multicomponent system. However, the total permeate flux decreases about 30 % when the BAc is present in the feed solution (ternary mixture T2) in relation to the binary mixture (B3) with the same feed water mole fraction. Regarding AAc, its presence together with BAc in the feed solution (Q1) leads to a loss of 56 % of the total permeate flux in relation to the binary with the same feed water mole fraction (B3). In the same way, if the quaternary (Q2) and the binary (B3) mixtures are compared, although the first has almost twice of the feed water content of the second, both show identical total permeate flux. These facts suggest that the presence of molecules like BAc and AAc induces higher mass transfer resistances in the boundary layer of the membrane significantly hindering the water flux. Nevertheless, their composition on the permeate stream is residual as it is shown in Figure D.2 (permeate stream compositions for ternary mixtures) and Figure D.3 (permeate compositions for quaternary mixtures), which are presented in *Appendix D* (see Section D.2).

The membrane selectivity towards the studied species follows the order: water > n-butanol > AAc > BAc. According to Table 4.2, n-butanol presents the second highest vapour pressure, so it is in according with the selectivity results (n-butanol presents the second highest flux through the membrane). Regarding the BAc, this compound presents the highest radius of gyration, which means that it has the biggest molecular size, hindering its passage through the membrane. Thus, AAc is slightly preferably permeated than BAc. The radius of gyration and the dipole moment parameters are shown in Table 4.3. Furthermore, the high boiling points of the BAc (421.0 K) and AAc (414.2 K) lead to smaller driving force comparing with n-butanol (390.8 K) and water (373.2 K).

Table 4.3. Radius of gyration and dipole moment for each compound [35].

Component/ Parameter	Radius of gyration (Å)	Dipole moment (Debye)
Water	0.615	1.850
n-Butanol	3.251	1.661
Butyl Acrylate	4.765	1.931[a]
Acrylic Acid	2.978	1.460

a) in benzene

The influence of temperature and feed water mole fraction on permeate compositions are summarized in Figure 4.9.

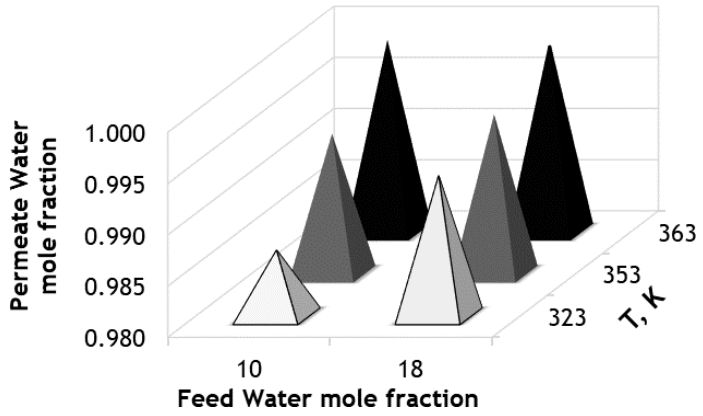

Figure 4.9. Water content on the permeate stream as a function of temperature and feed water mole fraction for quaternary mixtures.

Increasing the temperature, the water mole composition in permeate side increases whereas the n-butanol, BAc, and AAc decrease. Regarding the feed water mole composition, the same behaviour is observed. However, it seems this parameter does not influence the permeate water mole fraction anymore at 363 K since, at this temperature, the permeate composition is constant for the different molar feed water compositions.

Membrane productivity is usually characterized by permeate flux, which relates the product separation rate to the membrane area required to achieve the separation [13]. However, other important factors should be evaluated, particularly for multicomponent mixtures, such as the driving force and separation factor, which were also taken into account in this study. The driving force can be defined as the difference of partial pressures of the respective component at the feed and permeate side (see Section 4.4.2.3). Figure 4.10 provides information about the driving force for water in the different studied mixtures.

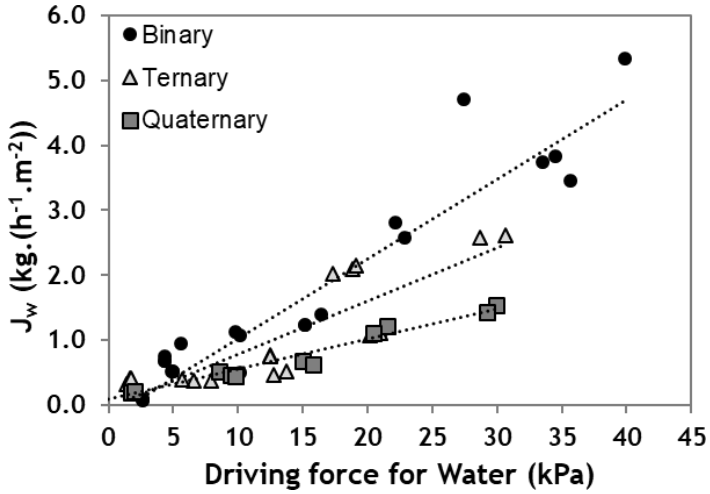

Figure 4.10. Total permeate flux as a function of the driving force for binary (circles), ternary (triangles) and quaternary mixtures (squares).

In order to have the same water permeate flux, the water requires higher driving force in the quaternary mixtures, like it was expected, due to the presence of the other compounds.

The process separation factor, which is described in the following section (see section 4.4.2.3), is represented as a function of temperature for binary, ternary and quaternary mixtures in Figure 4.11.

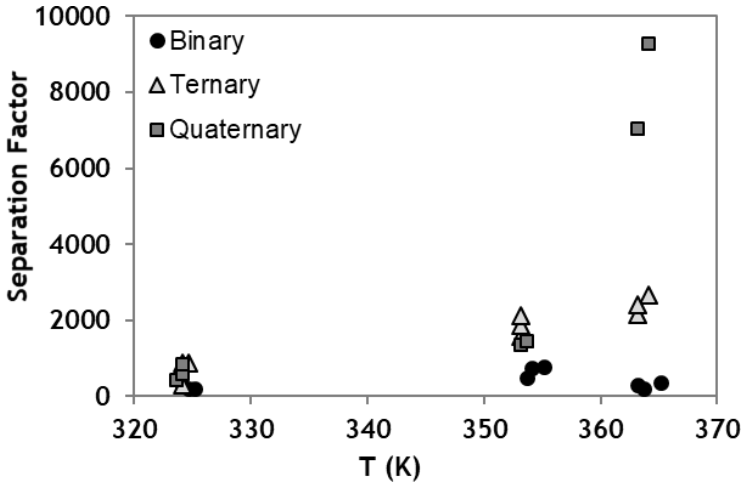

Figure 4.11. Separation factor as a function of temperature for binary (circles), ternary (triangles) and quaternary mixtures (squares).

Analysing the previous figure (Figure 4.11), it is possible to conclude that the separation factor is higher for quaternary mixtures and increases with the temperature. In order words, the membrane presents excellent selectivity for water mainly in ternary and quaternary mixtures at high temperatures (above 353 K), probably due to the lower vapour pressures of AAc and BAc, as mentioned previously (Table 4.2). Comparing the separation factor determined in this work for a feed water mole fraction of approximately 10 %, at 353 K and 45 mbar (α_{perv} = 665), with the values reported in the literature for the same type of membranes under similar conditions (α_{perv} = 340, at 348 K and 16 mbar) [4] it is possible to conclude that the Pervatech membrane used in this work has a separation factor almost two times higher. However, Boutikos et al.[1] reported a very similar value to the one found in this work (around 600).

It is important to mention that these experimental data can be very useful for future studies about process intensification for BAc synthesis, helping to understand what is the most sustainable way to produce it.

4.4.2.3. Pervaporation transport and parameters estimation

The solution-diffusion model [36] was applied to describe the mass transport through the membrane, which is given by the following equation (assuming that the mass transfer resistance in the boundary layer can be neglected):

$$J_i = Q_{m,i}\left(a_i P_{i,F}^0 - y_{i,perm} P_{perm}\right) \tag{4.15}$$

where $Q_{m,i}$ is the permeance of the membrane in relation to component i, a_i is the activity coefficient (determined using the UNIFAC method), $P_{i,F}^0$, is the saturation pressure in the feed (Table 4.2), $y_{i,perm}$ and P_{perm} are the vapour molar fraction and the total pressure in the permeate side. The term that is inside the brackets, $a_i p_{i,F}^0 - y_{i,perm} P_{perm}$, gives the driving force of component i.

The separation factor, α, is given by:

$$\alpha_{perv} = \frac{y_{w,perm}\left(1 - x_{w,F}\right)}{x_{w,F}\left(1 - y_{w,perm}\right)} \tag{4.16}$$

where the subscripts *F* and *w* correspond to the feed and water, respectively.

In this work, the activation energy required for the phase change of the permeate species were obtained by fitting the experimental results to the Arrhenius equation to describe the permeance dependence on temperature:

$$Q_{m,i} = Q_{m0,i} \exp\left(\frac{-E_{Perm,i}}{RT}\right) \tag{4.17}$$

where $Q_{m,0}$ is the pre-exponential factor , *T* is the absolute temperature, *R* is the ideal gas constant and E_{Perm} is the activation energy of permeation which is a combination of the activation energy of diffusion (E_D) and the heat of adsorption of the permeate in the membrane (ΔH):

$$E_{Perm} = E_D + \Delta H \tag{4.18}$$

Since temperature influences, both membrane permeability and the driving force for mass transport [13], the activation energy of permeation should be evaluated from the slope $\ln(Q_{m,i})$ vs $1/T$. This way, an average of all permeance values for each species and temperature were calculated and the activation energies of permeation as well as the pre-exponential factors were determined from the corresponding linear regressions. The Arrhenius adjustments are shown in Figure 4.12 for all species and the values of the respective parameters are presented in Table 4.4.

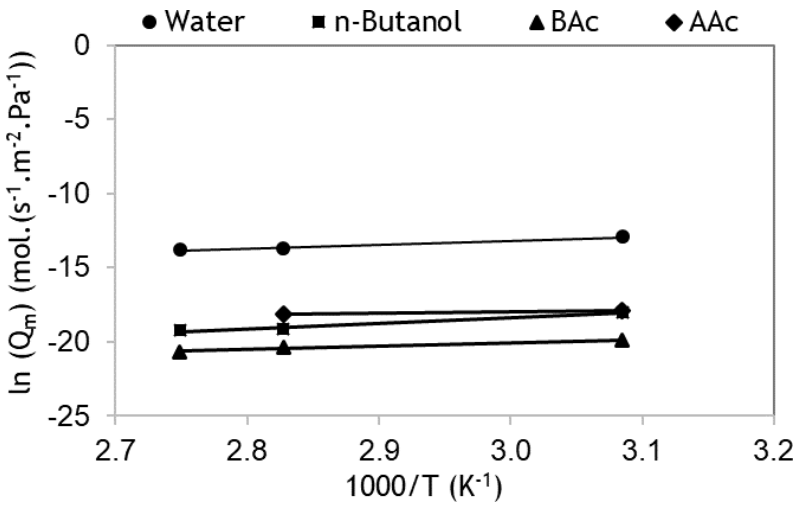

Figure 4.12. Linearized Arrhenius plot for permeance as a function of temperature.

Table 4.4. Overall activation energies and pre-exponential factors for each compound.

Compound	$E_{perm,\,i}$ (kJ.mol^{-1})	$Q_{m0,\,i}$ (mol.s^{-1}.m^{-2}.Pa^{-1})
Water	-30.53	3.90×10^{-11}
n-Butanol	-26.62	5.66×10^{-13}
Butyl Acrylate	-20.85	1.72×10^{-12}
Acrylic Acid	-9.37	5.17×10^{-10}

The water presents the lowest activation energy followed by n-butanol, BAc and AAc is the compound that requires more activation energy to be permeated through the membrane. The negative value of the activation energy reveals that the permeation of all species investigated is governed by the adsorption, according to equation (4.18).

The effect of the introduction of additional species to form ternary and quaternary mixtures was also evaluated by comparing the permeation results obtained for water and n-butanol in binary mixtures. The respective activation energies and pre-exponential factors for each compound in the different systems studied (binary, ternary and quaternary) are presented in Table D.1 and Table D.2 (see Appendix D), respectively. From that, it is possible to determine the respective permeance of each compound for different temperatures, which are displayed at 363 K, as an example, in Table D.3.

According to the results (Table D.3), the multicomponent system has more influence in the butanol permeance than in the water permeance when compared with the binary system. The water permeance decreases almost twice while the butanol permeance decreases about 30 times in the quaternary system comparing with the binary one. Even though water permeance decreases it is still the species with higher permeation values in the multicomponent system.

4.4.3. Pervaporation membrane-assisted esterification reaction

In order to predict the behaviour of the continuous reaction-separation process by combining a fixed-bed reactor with a membrane, the experimental data obtained (permeance of each species according to the respective driving force and temperature) were used with the mathematical model described in section 4.3 (at the steady state). The fixed-bed results were obtained from the model reported in Chapter 3 (Section 3.3).

The performance of a fixed-bed membrane reactor (FBMR) consisting of a Pervatech tubular membrane packed (inside) with A-15 was assessed. For that, beside the reaction kinetic and thermodynamic equilibrium constants reported in the literature [30], the multicomponent adsorption parameters (presented in Chapter 3) and the permeation data (presented in this Chapter, Section 4.4.2.3), all measured over A-15, were considered. Table 4.5 displays the reactor parameters used in the simulations.

Table 4.5. Reactor parameters used in the simulation runs.

Parameters	Value
Feed concentration ($mol.L^{-1}$)	$C_{n\text{-butanol}} = 6.39$; $C_{AAc} = 4.91$
Feed temperature (K)	363
Feed flow rate ($mL.min^{-1}$)	1.0
Permeate pressure (mbar)	45 (used in FBMR)
Bed porosity	0.41
Bed length (cm)	34.0
Internal diameter (cm)	1.95

Accordingly, the feed reactants molar ratio considered was 1.3 ($n_{n\text{-butanol}}/n_{AAc}$) and the dimensions of the FBR used experimentally in Chapter 3 were kept. Initially, it was considered that the A-15 was saturated with n-butanol at 363 K and that the n-butanol/AAc mixture was fed at 1 mL.min^{-1}. The performance of a conventional FBR (without membrane), considering isothermal conditions, is presented in Figure 4.13 (a). After that, a FBMR was simulated with the same operating and design parameters, and the respective concentration profiles are given in Figure 4.13 (b). Figure 4.13 (c) shows the concentration profiles of the FBMR at steady state considering non-isothermal operation as well as the temperature profile.

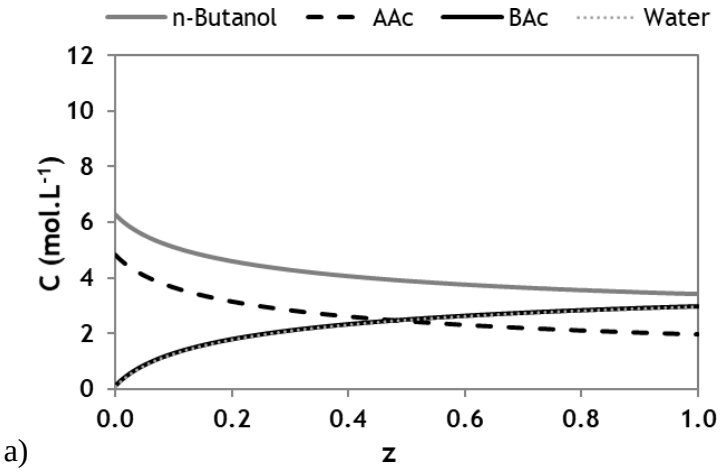

a)

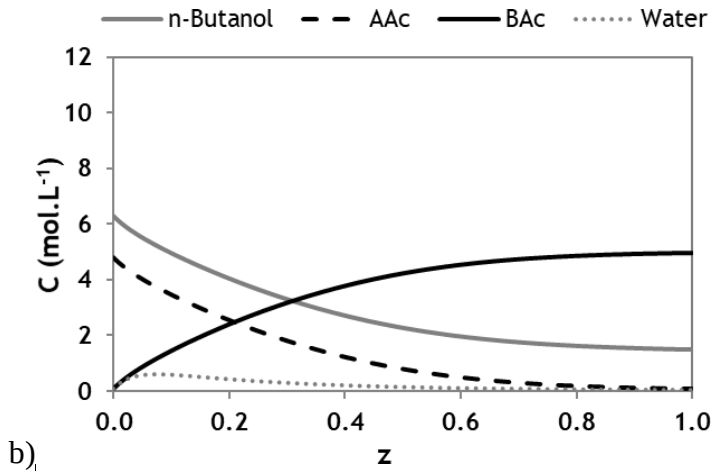

b)

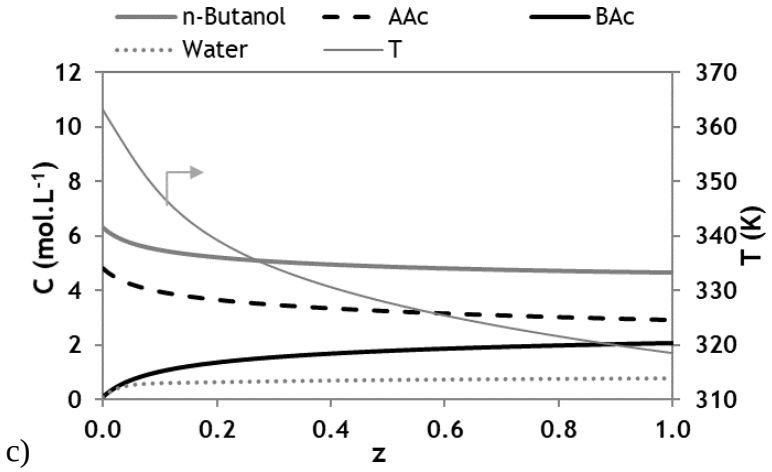

c)

Figure 4.13. Concentration profiles at steady state of the: a) FBR at isothermal conditions; b) FBMR at isothermal conditions; c) FBMR at non-isothermal conditions.

Comparing the concentration profiles in the FBR and the FBMR at isothermal conditions, a considerable improvement is observed in the performance of the FBMR since at steady state AAc is almost fully converted achieving a reaction conversion of 98.7 % while the FBR reached 59.4 % at the same conditions. This result is a direct consequence of the continuous removal of water from the reaction media by pervaporation (in the FMBR) which displaces the chemical reaction equilibrium, extending the conversion beyond the values predicted by the thermodynamics. According to the simulation results, just one membrane (with an effective area of 110 cm^2) is required to obtain this excellent performance producing BAc with a purity of 97.8 % (in solvent free basis).

According to the results (Figure 4.13 (c)), if non-isothermal operation was considered, the performance is clearly impaired by the temperature drop of about 45 K along the membrane due to the heat required for species vaporisation. This leads to lower water permeation fluxes and mainly lower reaction rates, decreasing the conversion about 28 % in relation to the FBR at the same operating conditions. The same behaviour was reported by Pereira et al.[16] for the esterification reaction of lactic acid with ethanol to produce ethyl lactate. Nevertheless, the good performance attained under isothermal conditions can be ensured by using a heat source to the pervaporation membrane in order to offset the temperature required for species vaporisation, depending on where the

selective layer coating is placed. According to the literature, a heated sweep gas source is the most suitable way to provide heat to the retentate liquid stream when the selective coated layer is placed inside the membrane tube, like it was assumed in this case. On the other hand, if the selective layer is coated on the external (shell) side of the membrane tube, an appropriate heated solution can be used as heat source by re-circulating it through jacketed modules. In this way, the heat can be efficiently transferred to the retentate stream [16]. Like this, the energy required to heat the membrane adsorptive reactor in order to keep the operation closer to isothermal conditions was determined according to the heat of vaporisation of water and taking into account the average molar flux of water (8.16×10^{-04} mol.(dm^{-2}.min^{-1})) attained at isothermal conditions (363 K) leading to a value of 33.2 J.(dm^{-2}.min^{-1}). Despite this, the energy saving potential of the FBMR comparing with the conventional process is evident since at the end of the FBMR a reaction mixture with approximately 75.7 % of BAc and 22.6 % of n-butanol (using a feed ratio of 1.3) is obtained having the remain compounds residual compositions (1.0 % of AAc and 0.7 % of water). Therefore, just one distillation column shall be required to purify BAc instead of the three distillations columns required by the conventional process. Moreover, the two reactors used in the conventional process can be reduced to one making use of the adsorption and pervaporation technologies as suggested in this work.

4.5. Conclusions

Pervaporation data for multicomponent mixtures were measured for the compounds involved in butyl acrylate synthesis in absence of reaction for the first time. The performance of commercial tubular silica membrane supplied by Pervatech BV (The Netherlands) was evaluated by studying different parameters. Selectivity and separation factor were determined and presented similar values to the literature.

Besides the selectivity towards water induced by the alumina used as intermediate layer on the membrane, the driving force of this species is enhanced by increasing the temperature, since water presents the highest vapour pressure. These conditions lead to higher permeate water mole fraction and, consequently, higher total flux since it is composed mainly by water. The feed water mole fraction also increases the driving force

of this compound leading to higher permeate fluxes, however, above 363 K, this parameter no longer has a significant influence.

The presence of butyl acrylate and acrylic acid impairs severely the total permeate flux, inducing to higher mass transfer resistances in the boundary layer of the membrane, hindering the water flux. The compounds are preferably permeated by the following order: water > n-butanol > acrylic acid > butyl acrylate mainly due to lower vapour pressures of butyl acrylate and acrylic acid.

The performance of a pervaporation-based hybrid process by combining a fixed-bed adsorptive reactor with a membrane was studied for the first time for the butyl acrylate synthesis. For that, a mathematical model was developed, taking into account the experimental data obtained in this Chapter, to predict the concentrations profiles of a FBMR at steady state. Considering isothermal operation, the fixed-bed membrane reactor presented a limiting reactant conversion 66 % higher when compared with a fixed-bed reactor at the same conditions due to the continuous water permeate fluxes that allow removing practically all water produced through the reaction.

4.6. Notation

Abbreviations

AAc	Acrylic Acid	-
A-15	Amberlyst-15 ion exchange resin	-
BAc	Butyl Acrylate	-
FBR	Fixed-Bed Adsorptive Reactor	
FBMR	Fixed-Bed Membrane Reactor	
FID	Flame Ionization Detector	
gPROMS	General Process Modelling System	-
RD	Reactive Distillation	
RSR	Reactor Separation Recycle	-
SMBR	Simulated Moving Bed Reactor	-

Symbols

A_m	Membrane area per unit module volume	$m^2_{membrane}.m^{-3}_{bulk}$
a	Liquid phase activity (= $\gamma_i x_i$)	-
C	Liquid phase concentration	$mol.m^{-3}$
$\hat{C}_p$	Liquid heat capacity	$J.mol^{-1}.K^{-1}$
d_{int}	Internal diameter of the membrane	m
D_M	Solute diffusivity in the boundary layer	$m^2.s^{-1}$
E_D	Activation energy of diffusion	$J.mol^{-1}$
E_{perm}	Activation energy of permeation	$J.mol^{-1}$
h_f	Heat transfer coefficient in the liquid boundary	$W.K^{-1}$
ΔH	Heat of adsorption	$J.mol^{-1}$
ΔH^v	Heat of vaporisation	$J.mol^{-1}$
J	Total permeate flux	$mol.m^{-2}.s^{-1}$
k_{bl}	Mass transfer coefficient	$m.s^{-1}$
$k_{ov,i}$	Global membrane mass transfer coefficient	$mol.s^{-1}.m^{-2}.Pa^{-1-1}$
L_m	Membrane length	m
n	Number of compounds	-
Nu	Nusselt number	-
P^0	Vapour pressure	bar
P_R	Prandtl number	-
Q_m	Membrane permeance	$mol.s^{-1}.m^{-2}.Pa^{-1}$
$Q_{m,0}$	Pre-exponential factor in Arrhenius equation	$mol.s^{-1}.m^{-2}.Pa^{-1}$
R	Ideal gas constant	$kJ.mol^{-1}.K^{-1}$
R_e	Reynolds number	-
S	Selectivity of the membrane	
S_c	Schmidt number	-
Sh	Sherwood number	-
t	Time variable	s
T	Temperature	K

u_s	Superficial velocity	$m.s^{-1}$
V_M	Molar volume	$m^3.mol^{-1}$
x	Liquid phase molar fraction	-
y	Vapour phase molar fraction	-
z	Axial coordinate in the membrane module	m

Greek Letters

α	Relative volatility	-
α_{perv}	Separation factor	-
δ	Membrane thickness	m
η	Fluid viscosity in the feed	$kg.m^{-1}.s^{-1}$
η_m	Fluid viscosity in the membrane	$kg.m^{-1}.s^{-1}$
λ	Thermal conductivity	$(W.m^{-1}.K^{-1})$
ρ	Density	$kg.m^{-3}$

Subcripts

0	Relative to initial conditions
F	Relative to feed
i	Component *i* (n-butanol, water, AAc and BAc)
m	Membrane
out	At the outlet
ret	Retentate
perm	Permeate
w	Water

4.7. References

1. Boutikos, P.; Pereira, C. S. M.; Silva, V. M. T. M.; Rodrigues, A. E., Performance evaluation of silica membrane for water–n-butanol binary mixture. *Separation and Purification Technology* **2014,** 127, (0), 18-28.

2. Hyder, M. N.; Huang, R. Y. M.; Chen, P., Pervaporation dehydration of alcohol–water mixtures: Optimization for permeate flux and selectivity by central composite rotatable design. *Journal of Membrane Science* **2009,** 326, (2), 343-353.

3. Jiang, L. Y.; Chung, T.-S.; Rajagopalan, R., Dehydration of alcohols by pervaporation through polyimide asymmetric hollow fibers with various modifications. *Chemical Engineering Science* **2008,** 63, (1), 204-216.

4. Sommer, S.; Melin, T., Performance evaluation of microporous inorganic membranes in the dehydration of industrial solvents. *Chemical Engineering and Processing: Process Intensification* **2005,** 44, (10), 1138-1156.

5. Sommer, S.; Melin, T., Influence of operation parameters on the separation of mixtures by pervaporation and vapor permeation with inorganic membranes. Part 1: Dehydration of solvents. *Chemical Engineering Science* **2005,** 60, (16), 4509-4523.

6. Guo, W. F.; Chung, T.-S.; Matsuura, T., Pervaporation study on the dehydration of aqueous butanol solutions: a comparison of flux vs. permeance, separation factor vs. selectivity. *Journal of Membrane Science* **2004,** 245, (1–2), 199-210.

7. Wijmans, J. G.; Athayde, A. L.; Daniels, R.; Ly, J. H.; Kamaruddin, H. D.; Pinnau, I., The role of boundary layers in the removal of volatile organic compounds from water by pervaporation. *Journal of Membrane Science* **1996,** 109, (1), 135-146.

8. Zhang, S.; Zou, Y.; Wei, T.; Mu, C.; Liu, X.; Tong, Z., Pervaporation dehydration of binary and ternary mixtures of n-butyl acetate, n-butanol and water using PVA-CS blended membranes. *Separation and Purification Technology* **2017,** 173, 314-322.

9. Smitha, B.; Suhanya, D.; Sridhar, S.; Ramakrishna, M., Separation of organic–organic mixtures by pervaporation—a review. *Journal of Membrane Science* **2004,** 241, (1), 1-21.

10. Kopeć, R.; Meller, M.; Kujawski, W.; Kujawa, J., Polyamide-6 based pervaporation membranes for organic–organic separation. *Separation and Purification Technology* **2013,** 110, 63-73.

11. Ray, S.; Ray, S. K., Synthesis of highly methanol selective membranes for separation of methyl tertiary butyl ether (MTBE)–methanol mixtures by pervaporation. *Journal of Membrane Science* **2006,** 278, (1), 279-289.

12. Luis, P.; Van der Bruggen, B., The driving force as key element to evaluate the pervaporation performance of multicomponent mixtures. *Separation and Purification Technology* **2015,** 148, 94-102.

13. Feng, X.; Huang, R. Y. M., Liquid Separation by Membrane Pervaporation: A Review. *Industrial & Engineering Chemistry Research* **1997,** 36, (4), 1048-1066.

14. Lipnizki, F.; Field, R. W.; Ten, P.-K., Pervaporation-based hybrid process: a review of process design, applications and economics. *Journal of Membrane Science* **1999,** 153, (2), 183-210.

15. Sanz, M. T.; Gmehling, J., Study of the Dehydration of Isopropanol by a Pervaporation-Based Hybrid Process. *Chemical Engineering & Technology* **2006,** 29, (4), 473-480.

16. Pereira, C. S. M.; Silva, V. M. T. M.; Pinho, S. P.; Rodrigues, A. E., Batch and continuous studies for ethyl lactate synthesis in a pervaporation membrane reactor. *Journal of Membrane Science* **2010,** 361, (1–2), 43-55.

17. Pereira, C. Process Intensification for the Green Solvent Ethyl Lactate Production based on Simulated Moving Bed and Pervaporation Membrane Reactors. PhD Thesis, Porto, 2009.

18. Van Hoof, V.; Van den Abeele, L.; Buekenhoudt, A.; Dotremont, C.; Leysen, R., Economic comparison between azeotropic distillation and different hybrid systems combining

distillation with pervaporation for the dehydration of isopropanol. *Separation and Purification Technology* **2004,** 37, (1), 33-49.

19. Chandane, V. S.; Rathod, A. P.; Wasewar, K. L., Enhancement of esterification conversion using pervaporation membrane reactor. *Resource-Efficient Technologies* **2016,** 2, Supplement 1, S47-S52.

20. Ahmad, S. A.; Lone, S. R., Hybrid process (pervaporation–distillation): a review. *Int. J. Sci. Eng. Res.* **2012,** 3, 1-5.

21. Jyoti, G.; Keshav, A.; Anandkumar, J., Review on Pervaporation: Theory, Membrane Performance, and Application to Intensification of Esterification Reaction. *Journal of Engineering* **2015,** 2015, 24.

22. Sert, E.; Atalay, F. S., n-Butyl acrylate production by esterification of acrylic acid with n-butanol combined with pervaporation. *Chemical Engineering and Processing: Process Intensification* **2014,** 81, 41-47.

23. Casado, C.; Urtiaga, A.; Gorri, D.; Ortiz, I., Pervaporative dehydration of organic mixtures using a commercial silica membrane: Determination of kinetic parameters. *Separation and Purification Technology* **2005,** 42, (1), 39-45.

24. Han, Y.; Lv, E.; Ma, L.; Lu, J.; Chen, K.; Ding, J., Coupling membrane pervaporation with a fixed-bed reactor for enhanced esterification of oleic acid with ethanol. *Energy Conversion and Management* **2015,** 106, 1379-1386.

25. Lévêque, A., *Les Lois de la transmission de chaleur par convection*. Dunod: 1928.

26. Welty, J.; Wicks, C.; Wilson, R.; Rorrer, G., *Fundamentals of Momentum, Heat, and Mass Transfer*. John Wiley & Sons: New York, 2008.

27. Mulder, M. H. V., Chapter 2 Polarization phenomena and membrane fouling. *Membrane Science and Technology* **1995,** 2, 45-84.

28. Noble, R. D.; Stern, S. A., *Membrane Separations Technology: Principles and Applications*. Elsevier Science: 1995.

29. Strathmann, H., Membrane Separation Processes, 4. Concentration Polarization and Membrane Fouling. In *Ullmann's Encyclopedia of Industrial Chemistry*, Wiley-VCH Verlag GmbH & Co. KGaA: 2000.

30. Ostaniewicz-Cydzik, A. M.; Pereira, C. S. M.; Molga, E.; Rodrigues, A. E., Reaction Kinetics and Thermodynamic Equilibrium for Butyl Acrylate Synthesis from n-Butanol and Acrylic Acid. *Industrial & Engineering Chemistry Research* **2014,** 53, (16), 6647-6654.

31. Constantino, D. S. M.; Pereira, C. S. M.; Faria, R. P. V.; Ferreira, A. F. P.; Loureiro, J. M.; Rodrigues, A. E., Synthesis of butyl acrylate in a fixed-bed adsorptive reactor over Amberlyst 15. *AIChE Journal* **2015,** 61, (4), 1263-1274.

32. Qunhui, G.; Ohya, H.; Negishi, Y., Investigation of the permselectivity of chitosan membrane used in pervaporation separation II. Influences of temperature and membrane thickness. *Journal of Membrane Science* **1995,** 98, (3), 223-232.

33. Sekulić, J.; Ten Elshof, J.; Blank, D., Separation mechanism in dehydration of water/organic binary liquids by pervaporation through microporous silica. *Journal of membrane science* **2005,** 254, (1), 267-274.

34. Yaws, C. L.; Narasimhan, P. K.; Gabbula, C., Yaws' Handbook of Antoine Coefficients for Vapor Pressure (2nd Electronic Edition). In Knovel.

35. Yaws, C. L., *Thermophysical properties of chemicals and hydrocarbons*. William Andrew: 2008.

36. Wijmans, J. G.; Baker, R. W., The solution-diffusion model: a review. *Journal of Membrane Science* **1995,** 107, (1), 1-21.

5. Simulated Moving Bed Reactor

The feasibility of butyl acrylate synthesis in a simulated moving bed reactor packed with Amberlyst-15 ion exchange resin was studied at different temperatures (323 and 363 K). For that, a mathematical model was developed to describe the dynamic behaviour of the simulated moving bed reactor considering internal and external mass-transfer resistances and velocity variations due to changes in the bulk composition. The effect of operating conditions, as the simulated moving bed reactor configuration (columns arrangement) and switching time, on the performance parameters was studied at isothermal operation. As a first approach, the reactive separation region was determined for the following set of parameters: equimolar feed composition, switching time equal to 3.1 minutes and configuration 2-4-4-2. The influence of the feed molar ratio (n-butanol/acrylic acid) was also evaluated and the optimal operating conditions were found (through the determination of new reactive separation regions) in order to get the best performance parameters: minimum butyl acrylate purity in the raffinate of 99.5 mol. % ensuring the minimum desorbent (n-butanol) consumption and maximum productivity. Finally, a simulated moving bed reactor unit was designed at industrial scale as well as pervaporation and distillation units to treat the extract (n-butanol and water) and the raffinate (n-butanol and butyl acrylate) streams, respectively. A global process was simulated disclosing very promising results with nearly complete n-butanol recovery and a competitive production capacity (51,500 $t_{BAc}.year^{-1}$).

This Chapter is adapted from Constantino, D. S. M.; Pereira, C. S. M.; Faria, R. P. V.; Loureiro, J. M.; Rodrigues, A. E.,, Simulated Moving Bed Reactor for Butyl Acrylate Synthesis: From Pilot to Industrial Scale, *Chem. Eng. Process*. **2015,** 97, pp 153-168. DOI: 10.1016/j.cep.2015.08.003.

5.1. Introduction

Liquid phase sorption-enhanced reaction processes (SERP) in continuous operation provide great advantages for the production of oxygenated compounds and green solvents, which are obtained from equilibrium-limited reactions. These processes result from the association of chromatographic separation with chemical reaction, which are able to extend the equilibrium conversion towards a specific product by continuous removal one or more products simultaneously. Simulated Moving Bed Reactor (SMBR), which arose from the integration of the chemical reaction with the Simulated Moving Bed (SMB) technology, is one of the chromatographic reactors (CR) most studied over the last decades. It plays an important role in Reaction Engineering since significant productivity improvements are reached with substantial energy savings by reducing the equipment and the operating temperature required.

The SMBR consists in several fixed-bed columns interconnected in series, packed, usually, with a material that acts as adsorbent and catalyst at the same time. However, other packing configurations are also possible, as mixtures of different materials, for instance [1, 2]. This counter-current cyclic process, based on the True Moving Bed Reactor (TMBR) concept, maximizes the mass transfer driving force by promoting the counter-current contact between the fluid and the solid (adsorbent/catalyst) phases without the solid motion, taking advantage over TMBR. Thus, all streams shift, periodically, one column ahead at regular time intervals (switching time), in the fluid movement direction simulating, in this manner, the solid phase movement in the opposite direction. This procedure is repeated as required in a continuous operation allowing an effective use of the stationary and mobile phases and leading to the decrease of the desorbent required and the improvement of the productivity per unit time and unit mass of stationary phase [3]. Usually, there are four streams distributed by four sections: two inlet streams (feed and desorbent) and two outlet streams (extract and raffinate), according to the Figure 5.1, where a reaction $A + B \leftrightarrow C + D$ is taking place. The extract stream is composed mainly by the desorbent (A) and the most retained compound (D) and the raffinate is composed mostly by the less retained compound (C) with the desorbent. In section 1 (between desorbent and extract nodes), the adsorbent is regenerated by desorption of the most retained product from the solid, while in section 2 (between extract and feed nodes) and

in section 3 (between feed and raffinate nodes) the reaction occurs, together with the products separation. The most adsorbed product is strongly adsorbed in sections 2 and 3 and it is transported with the solid phase to the extract port. The less adsorbed product is desorbed in sections 2 and 3 and is transported with the liquid in the direction of the raffinate port. In section 4 (between raffinate and desorbent nodes), the less retained product is adsorbed allowing the regeneration of the desorbent before being recycled to the next section (1) [4]. A cycle is finished when a number of switches equal to the total number of columns is accomplished. The cyclic steady state is achieved when no significant differences (deviations less or equal to 1%) are observed in the compounds concentration comparing with the previous cycle.

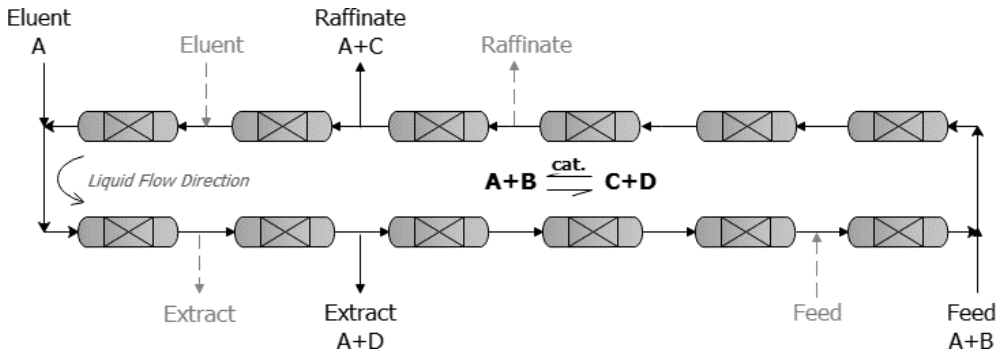

Figure 5.1. Schematic representation of a Simulated Moving Bed Reactor with a configuration of 2-4-4-2. Grey and dashed lines represent the preceding position of the streams in the previous period (step (n - 1)) of that cycle.

Although the SMBR was already successfully applied to different systems involving equilibrium-limited reactions [4-9], with promising performances, this approach was never assessed for the butyl acrylate (BAc) synthesis. Moreover, the previous study (presented in Chapter 3), which concerns the adsorption of all compounds of this system in the absence and in the presence of reaction in a fixed-bed adsorptive reactor (FBR) packed with Amberlyst-15 ion exchange resin (A-15), showed that sorption enhanced reaction processes are a very promising strategy for BAc production.

In this Chapter, the feasibility of a SMBR process for the production of BAc was studied. For that, a mathematical model able to describe the dynamic behaviour of the SMBR was developed, taking into account the multicomponent adsorption study

previously performed (see Chapter 3) and the kinetic results obtained for this system in batch conditions over A-15 available in open literature [10]. The limiting operating conditions were found based on the Equilibrium Theory and several concentration profiles were simulated changing the design parameters (arrangement of the columns and switching time) in order to evaluate the influence of each factor in the performance parameters. After determining the ideal design parameters, the optimal operating conditions (temperature, flow rates and feed ratio) were found based on the reactive separation region (RSR) at pilot scale, ensuring the best performance, i.e., maximum raffinate purity (≥ 99.5 mol. %) with the minimum desorbent (n-butanol) consumption and maximum productivity. The proof-of-concept was attained by performing experiments under different operating conditions, in the SMBR unit at pilot scale over A-15. Finally, a new SMBR unit was designed at industrial scale and a global process was simulated considering different configurations for the desorbent recovery using suitable downstream units and the respective outlet streams.

5.2. Experimental Data

5.2.1. Chemical and materials

The chemicals used in the SMBR experiments were n-butanol (≥ 99.9 wt.%) from Fisher Scientific, acrylic acid (≥ 99 wt.%) and butyl acrylate (≥ 99.5 wt.%) from Acros Organics. Acrylic acid and butyl acrylate were provided stabilized with inhibitor (about 200 ppm and 20 ppm of hydroquinone monomethyl ether, respectively). The additional inhibitor used in this study was phenothiazine (PTZ) (99.0 wt.%), also from Acros Organics. Isopropanol (≥ 99.9 wt.%) from Fisher Scientific was used as solvent in the chromatographic analysis. A-15 resin was used as catalyst and adsorbent, which is a highly cross-linked polystyrene-divinylbenzene ion exchange resin functionalized with sulfonic groups. More details were previously described in Chapter 3 (Section 3.2.1). The catalyst/adsorbent was firstly washed with deionized water and then with ethanol. Then, it was dried at 363 K in order to have its dry weight and, after that, it was immersed in the solvent (n-butanol) prior to the packing of each column.

5.2.2. Analytical method

All samples collected were analysed (at least two times) in a DANI - Master Fast Gas Chromatograph equipped with flame ionization and thermal conductivity detectors (FID and TCD, respectively). The compounds were separated using a silica capillary column (Stabilwax, 60 m x 0.25 mm ID, film thickness of 0.25 μm). Helium N50 was used as the carrier gas at a flow rate of 8.0 $mL.min^{-1}$. The linear velocity was set to 35 $cm.s^{-1}$ and the injection volume used was 1.0 μL with a split ratio of 30. The temperature of the injector was set to 523 K while the temperature of the FID and TCD was set to 573 K. The initial column temperature was 353 K for 6.0 min, the temperature was then increased at 10 $K.min^{-1}$ up to 453 K remaining constant for the following 2 min. Isopropyl alcohol (isopropanol) was used as clean solvent. The global associated uncertainty of the measured molar fractions was ≤ 0.05. More details about calibration curves are presented in *Appendix B.*

5.2.3. Experimental setup and procedure

All SMBR runs were performed in a pilot scale LICOSEP® 12-26 unit by Novasep (France), which is presented in Figure 5.2. This unit comprises 12 columns Superformance SP 230 x 26 (length x internal diameter, mm) by Götec Labortechnik (Germany), which are connected in series and can withstand up to 333 K and 60 bar. Each column is connected to four lines: feed and eluent (inlet streams), extract and raffinate (outlet streams) being each line connected to a HPLC pump (MERCK-HITACHI), resulting in 12 lines of each type. Only one line of each type can open at a given time which is shifted to the next one in the flow direction after a given time interval (switching time) making one period of a cycle. A whole cycle is composed of successive periods until all lines come back to its initial positions. There are four on-off pneumatic valves between every two columns, which are actuated by the control system. This configuration allows pumping of the feed or eluent into the system or removing the extract or raffinate streams according to the defined operating parameters. A positive displacement three-head membrane pump (Milton Roy, France with a flow rate range of 20 to 120 $mL.min^{-1}$ and 100 bar of pressure) provides the eluent recirculation flow. The recycling flow rate

is controlled through the indications given by a flowmeter. During a cycle, the recycling pump set-point changes according to the SMBR section it is in, therefore the actual recycling flow rate is controlled through a flowmeter. The feed, eluent and raffinate flow rates are fixed while the extract flow rate is controlled through the pressure measured at the recycling pump inlet (usually around 1.5 bar as set by the user). For the internal concentration profiles measurement, a six-port valve (located between the twelfth and the first columns) was used for collecting samples.

Regarding the procedure, firstly, all columns were packed with A-15 in water, which was previously weight in dry condition, and a pulse of blue dextran solution (15 $kg.m^{-3}$) was injected in each column in order to characterize the respective packing in terms of Peclet number and bed porosity (tracer). For that, samples of 0.2 cm^3 were injected at 10 $mL.min^{-1}$ using water as eluent, since blue dextran is insoluble in n-butanol. The outlet concentration of each column was monitored using a UV-VIS detector (Gilson, Model 115) at 300 nm. At least, three runs were performed for each column in order to check the space time of the experimental curves and the bulk parameters reproducibility (Peclet number and bed porosity). The average values of those parameters were considered in the mathematical model for all simulation runs. The characteristics of the SMBR columns are shown in Table 5.1.

Figure 5.2. SMBR LICOSEP pilot scale unit with 12 columns (a side view with 6 columns).

Table 5.1. Characteristics of the pilot scale SMBR columns.

Parameter (symbol, unit)	Value
Column length (L_b, cm)	23
Column internal diameter (d_{int}, cm)	2.6
Solid dry weight (A-15, g)	48.9
Bulk density (ρ_b, kg.m^{-3})	400
Average particle radius (r_p, μm)	375
Particle porosity (ε_p)	0.36 [11]
Bulk porosity (ε)	0.41
Peclet number	143

5.3. Mathematical Model

A mathematical model was developed to assess the variations in concentration profiles all over the setup as well as the extract and raffinate streams compositions within a set period. A constant bed volume and packing porosity was assumed together with plug flow and axial dispersion, linear driving force (LDF) approximation for the inter and intra-particle mass transfer rates, velocity variations due to changes in the bulk compositions and isothermal operation. Therefore, the dynamic behaviour of the SMBR is described by the following equations:

Bulk fluid mass balance to component *i* in column *k*:

$$\frac{\partial C_{ik}}{\partial t}+\frac{\partial (u_k C_{ik})}{\partial z}+\frac{(1-\varepsilon)}{\varepsilon}\frac{3}{r_p}k_{L,ik}\left(C_{ik}-\bar{C}_{p,ik}\right)=D_{ax,k}\frac{\partial}{\partial z}\left(C_T\frac{\partial x_{ik}}{\partial z}\right) \qquad (5.1)$$

Particle mass balance to component *i* in column *k*:

$$\frac{3}{r_p}k_{L,ik}\left(C_{ik}-\bar{C}_{p,ik}\right)=\varepsilon_p\frac{\partial \bar{C}_{p,ik}}{\partial t}+(1-\varepsilon_p)\frac{\partial q_{ik}}{\partial t}-\frac{\nu_i\rho_b}{1-\varepsilon}r\left(\bar{C}_{p,ik}\right) \qquad (5.2)$$

The total mass balance, which allows to determine the interstitial fluid velocity variation, is given by:

$$\frac{du_k}{dz} = -\frac{(1-\varepsilon)}{\varepsilon}\frac{3}{r_p}\sum_{i=1}^{NC} k_{L,ik} V_{M,i}\left(C_{ik} - \bar{C}_{p,ik}\right) \tag{5.3}$$

Rate of the chemical reaction:

$$r(mol.(g_{A15}^{-1}.min^{-1})) = k_c \frac{a_A a_B - \frac{a_C a_D}{K_{eq}}}{\left(1 + K_{S,D} a_D\right)^2} \tag{5.4}$$

The activities (a_i) of the components (A = n-butanol, B = AAc, C = BAc and D = water), are calculated based on the average concentration in the particle pores using UNIFAC method. The necessary parameters for the determination of the activity coefficients, the equilibrium constant and the kinetic parameters measured over A-15 for this system are available in the literature [10]:

The equilibrium constant is given by:

$$K_{eq} = \exp\left(\frac{-1490 \pm 577}{T} + (7.21 \pm 1.67)\right) \tag{5.5}$$

The adsorption constant for water, $K_{S,D,}$ is 1.589 ± 0.100 and the kinetic constant is given by:

$$k_c(mol.(g_{A15}^{-1}.\min^{-1}) = 1.52 \times 10^7 \exp\left(-\frac{66988}{RT}\right) \tag{5.6}$$

The global mass-transfer coefficient was defined as:

$$\frac{1}{k_L} = \frac{1}{k_e} + \frac{1}{\varepsilon_p k_i} \tag{5.7}$$

The internal mass-transfer coefficient was estimated by the following expression:

$$k_i = \frac{5 D_M / \tau}{r_p} \tag{5.8}$$

The external mass-transfer coefficient was estimated by the Wilson and Geankoplis correlation [12]:

$$Sh_p = \frac{1.09}{\varepsilon}\left(Re_p Sc\right)^{0.33} \qquad 0.0015 < Re_p < 55 \tag{5.9}$$

where $Sh = k_{bl,ik} d_{int} / D_M$ (Sherwood number), $Re_p = \rho d_p u / \eta$ (Reynolds number) and $Sc = \eta / (\rho D_M)$ (Schmidt number).

The infinite dilution diffusivities as well as the diffusion coefficient in concentrated solutions were estimated according to the equations described in Chapter 3 (see Section 3.3.1). The adsorption equilibrium of component *i* in column *k*, is described by the multicomponent Langmuir isotherm equation*:*

$$q_{ik} = \frac{Q_i K_i \overline{C}_{p,ik}}{1 + \sum_{j=1}^{NC} K_j \overline{C}_{p,jk}} \tag{5.10}$$

where Q_i is the monolayer capacity and K_i is the equilibrium constant for component *i*..

Initial and Danckwerts boundary conditions:

$$t = 0: \; C_{ik} = \overline{C}_{p,ik} = C_{ik,0} \tag{5.11}$$

$$z = 0: \qquad u_j C_{ik} - D_{axj} C_T \frac{\partial x_{ik}}{\partial z}\Big|_{z=0} = u_j C_{ik,F} \tag{5.12}$$

$$z = L_b: \qquad \frac{\partial C_{ik}}{\partial z}\Big|_{z=L_b} = 0 \tag{5.13}$$

where the indices *F* and *0* refer to the feed and initial states, respectively and the subscript *j* corresponds to a section/zone of the SMBR.

Mass balances at the nodes of the inlet and outlet lines of the SMBR:

Eluent node:

$$C_{i(j=4,z=L_b)} = \frac{u_1}{u_4} C_{i(j=1,z=0)} \tag{5.14}$$

Extract (j = 2) and raffinate (j = 4) nodes:

$$C_{i(j-1,z=L_b)} = C_{i(j,z=0)} \tag{5.15}$$

Feed node:

$$C_{i(j=2,z=L_b)} = \frac{u_3}{u_2} C_{i(j=3,z=0)} - \frac{u_F}{u_2} C_i^F \tag{5.16}$$

where:

$u_1 = u_4 + u_{EL}$ (Eluent node, where the subscript EL is the eluent); (5.17)

$u_2 = u_1 - u_{Ext}$ (Extract node, where the subscript Ext is the extract); (5.18)

$u_3 = u_2 + u_F$ (Feed node); (5.19)

$u_4 = u_3 - u_{Raff}$ (Raffinate node, where the subscript Raff is the raffinate); (5.20)

The ratio between the fluid interstitial velocity, u_j, and the simulated solid velocity can be defined for each section using the following parameter:

$$\gamma_j = \frac{u_j}{U_s} \tag{5.21}$$

The cyclic behaviour of the SMBR can be predicted from the steady state model of the TMBR, by considering the relation between the interstitial solid velocity, U_s, and the switching time, t^*, in SMBR operation,

$$U_s = L_b / t^* \tag{5.22}$$

where L_b is the column bed length.

5.3.1. Performance parameters

The SMBR process performance is calculated over a complete cycle according to the following equations:

$$P_{Raff}(\%) = 100 \int_{t}^{t+N_c t^*} C_{Raff,C}\,dt \Big/ \left(\int_{t}^{t+N_c t^*} \left(C_{Raff,B} + C_{Raff,C} + C_{Raff,D} \right) dt \right) \tag{5.23}$$

$$P_{Ext}(\%) = 100 \int_{t}^{t+N_c t^*} C_{Ext,D}\,dt \Big/ \left(\int_{t}^{t+N_c t^*} \left(C_{Ext,B} + C_{Ext,C} + C_{Ext,D} \right) dt \right) \tag{5.24}$$

$$Conv(\%) = 100 \left[1 - \left(Q_{Ext} \int_{t}^{t+N_c t^*} C_{Ext,B}\,dt + Q_{Raff} \int_{t}^{t+N_c t^*} C_{Raff,B}\,dt \right) \Big/ \left(Q_F C_{F,B} N_c t^* \right) \right] \tag{5.25}$$

$$Prod\left(kg_{BAc}.(L_{ads}^{-1}.day^{-1})\right) = Q_{Raff} \int_{t}^{t+N_c t^*} MM_C C_{Raff,C}\,dt \Big/ \left((1-\varepsilon) V_{unit} t^* N_c \right) \tag{5.26}$$

$$DesC(L_{n-Butanol} / kg_{BAc}) = N_c t^* V_{M,A} \left(Q_{EL} C_{EL,A} + Q_F (C_{F,A} - X C_{F,B}) \right) \Big/ \left(MM_C Q_{Raff} \int_{t}^{t+N_c t^*} C_{Raff,C}\,dt \right) \tag{5.27}$$

where N_c represents the total number of columns, t^*represents the switching time and X is the conversion of AAc (component B). The productivity is defined considering the BAc (component C, desired product) produced which is gathered in the raffinate stream. The desorbent/eluent (component A) consumed in the reaction is not taken into account to calculate the eluent consumption, being only considered the amount of n-butanol used as eluent.

5.3.2. Numerical solution

The numerical solution of this problem was obtained by using the commercial software gPROMS (general PROcess Modelling System) version 3.5.3, using orthogonal collocation in finite elements (OCFEM) with third order polynomials; to this end, the axial dimension of the bed was discretized in 10 and 41 finite elements for pilot and industrial scales, respectively, with 2 interior collocation points in each finite element. The DASOLV system solver was used to solve the resulting system of ordinary differential equations in time. For all simulations, a tolerance of 10^{-5} was used. It was

assumed that an SMBR simulation reached the cyclic steady state when the columns' profiles in two consecutive cycles had less than 1.0%.

5.4. Results and Discussion

5.4.1. Design parameters

The design and optimization of SMBR units to carry out simultaneous continuous reaction and separation are challenging and essential tasks to define the feasibility of the process at industrial scale. Thereby, relevant design variables ought to be determined such as: inlet and outlet flow rates, fixed bed columns arrangement by section (configuration) and switching time. For that, an approach followed for SMB separations was applied to the present system in order to estimate a suitable set of SMBR operating flow rates that would potentially lead to complete separation of the two reaction products. This approach makes use of the concept of the TMB, considering the Equilibrium Theory. The following constraints (equations (5.28) and (5.29)) should be defined and fulfilled for the ratio between the fluid and the solid interstitial velocities, γ_j, for each section, *j*, of the TMB:

$$\gamma_1 > \frac{(1-\varepsilon)}{\varepsilon}\left(\varepsilon_p + (1-\varepsilon_p)\frac{q_{D_1}}{C_{p,D_1}}\right) \tag{5.28}$$

$$\gamma_4 < \frac{(1-\varepsilon)}{\varepsilon}\left(\varepsilon_p + (1-\varepsilon_p)\frac{q_{C_4}}{C_{p,C_4}}\right) \tag{5.29}$$

Meeting the above constraints guarantees that water (D) is preferentially carried by the liquid phase in section 1 and by the solid phase in the other sections and BAc (C) is preferentially carried by the solid phase in section 4 and by the liquid phase in the other sections. Both sections, 1 and 4, have an important role in SMBR operation. In section 1, the solid phase is regenerated by removing the adsorbed water, while in section 4, the desorbent is cleaned by adsorption of BAc and the desorbent is returned to the system by the recycle stream. Thereby, according to the Equilibrium Theory, the limit flow rates in

section 1 and section 4 are determined by calculating the ratios between the liquid and solid interstitial velocities (equations (5.28) and (5.29)). The equivalence between the SMBR and TMBR systems is made by keeping constant the net-flow of the liquid relative to the solid:

$$u_j^{SMB} = u_j^{TMB} + U_s \tag{5.30}$$

where u_j is the interstitial fluid velocity in the section *j* of the moving bed. Combining the equation (5.21) with the equation (5.30), it is possible to obtain equation (5.31), which allows to determine the limiting ratio values for the critical sections (1 and 4) during a SMB/SMBR process and to find the ideal operating flow rates from that.

$$\gamma_j^{SMB} = \gamma_j^{TMB} + 1 \tag{5.31}$$

The values obtained for the system in study, at 323 K and 363 K, are shown in Table 5.2. A security factor (SF) of 5 % is applied to ensure that there is no contamination in the critical zones.

Table 5.2. Ratios between the liquid and solid interstitial velocities for TMB and SMB systems.

323 K		363 K	
TMB		TMB	
γ_1 > 16.19	γ_4 < 0.63	γ_1 > 7.66	γ_4 < 0.60
SMB		SMB	
γ_1 > 17.19	γ_4 < 1.63	γ_1 > 8.66	γ_4 < 1.60
SMB (SF = 5%)		SMB (SF = 5%)	
γ_1 > 18.05	γ_4 < 1.55	γ_1 > 9.10	γ_4 < 1.52

For a switching time (t^*), the solid velocity is determined according to equation (5.22). Afterwards, the interstitial velocity of each zone can be determined from equation (5.21) which is then used to determine the respective flow rates in section 1 (minimum) and 4 (maximum). However, the effect of the switching time on the performance parameters must be studied in order to know what is the optimal value to achieve the optimal operating conditions: minimal desorbent consumption (*DesC*) and maximum productivity (*Prod*) ensuring significant conversion (Conv ≥ 95 %) with, at least, the minimal raffinate purity (P_{Raff}) required (99.5 %) [13]. The configuration was initially assumed to be 2-4-4-2 in order to have a reasonable reaction zone length once this system presents a very slow kinetics, $k_{c,363K} = 3.51\times10^{-3} mol.g^{-1}_{A15}.\min^{-1}$, according to the literature [10]. The effects of these parameters (switching time and configuration) on the performance parameters will be presented and discussed ahead (see sections 5.4.3.1 and 5.4.3.2, respectively).

5.4.2. Separation region vs reactive separation region

The successful design and operation of counter-current chromatographic separation units depends on the correct selection of the operating conditions, particularly of the flow rates in each section [14]. Separation (SR) and reactive separation regions (RSR) were obtained numerically with the mathematical model described above (Section 5.3). The SR were obtained by simulating a SMB unit that separated the products, BAc and water, in absence of reaction, while the RSR were obtained by considering a SMBR unit where an equimolar ratio of the reactants, n-butanol and AAc, is fed, taking into account the reaction kinetics besides the adsorption data. The procedure used to define the SR/RSR consists on keeping constant simultaneously the values of the switching time (3.1 minutes) and of the flow rates in sections 1 and 4, which are determined from the Equilibrium Theory as described in the previous section (Section 5.4.1). For example, a RSR at 363 K is defined in a γ_2-γ_3 plane by setting $\gamma_1 = 9.10$ and $\gamma_4 = 1.52$ (according to Table 5.2), for the set of pairs of net-flows in sections 2 and 3 that accomplish the desired separation with the required raffinate purity, which is 99.5% [13] (minimum value in a solvent-free basis). It means that, keeping the flow rates in sections 1 and 4 constant leads to constant desorbent and recycle flow rates. So, beginning with a low feed flow rate, the SMBR operation is simulated for different extract flow rates and the range, for which the

required separation is obtained, is drawn[15, 16]. The SR/RSR are defined for several feed flow rates until the feed flow rate reaches a value for which no extract flow rate can fulfil the desired separation, being the previous value, the maximum feed flow rate allowed to get the desired separation; usually, this point corresponds to the maximum performance that can be achieved: maximum productivity and minimum desorbent consumption. At this stage, the extract purity (P_{Ext}) is not an important parameter since water is a secondary product, so it was defined to be 95%. However, in a more detailed study for industrial application it will be an important factor in order to reduce the equipment size and the energy costs for the treatment of the respective extract stream, as it will be discussed in Section 5.4.7.

It is important to refer that BAc and water in equimolar composition are completely immiscible, as can be seen in Figure D.1 (see *Appendix D*), so actual SMB operation under these conditions is not possible. Nevertheless, the SR was also determined at 363 K to compare its dimension with that of the RSR and to understand the influence of the reaction on the SMBR process. In Figure 5.3, it is possible to compare the SR with the RSR, which correspond to SMB and SMBR processes, respectively. It can be readily noticed that the reaction is the limiting step leading to the contamination of the raffinate stream with the limiting reactant (AAc), explaining the large difference between the separation regions of the SMB and SMBR units.

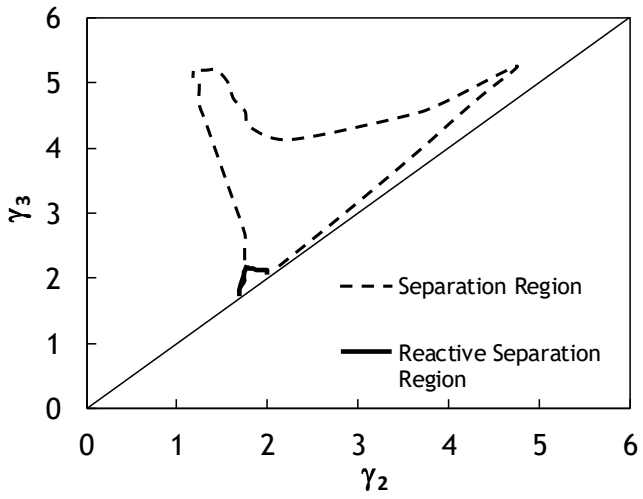

Figure 5.3. Reactive Separation Region for an equimolar ratio of AAc and n-butanol in the feed (SMBR) vs Separation Region for an equimolar ratio of butyl acrylate and water in the feed (SMB) at 363 K. Both regions were determined for a raffinate purity criteria ≥ 99.5 % (solvent-free basis).

5.4.2.1. Effect of temperature

The same procedure was performed at 323 K; however, it was not possible to achieve the required purity criterion of BAc (≥ 99.5 %) whatever the set of flow rates used at this temperature. The reaction kinetics is slower at lower temperatures, so a lower feed flow rate is required to have a residence time long enough and, consequently, to further consume the limiting reactant (AAc), decreasing the contamination with this compound by increasing the reaction conversion. Accordingly, the temperature decrease leads to contamination with AAc like it was previously mentioned. The maximum raffinate purity (in a solvent-free basis) achieved was 99.47 % with the following flow rates: Q_{EL} = 264 mL.min^{-1}, Q_{Rec} = 24 mL.min^{-1}, Q_{Ext} = 261 mL.min^{-1} and Q_F = 0.8 mL.min^{-1}. Nevertheless, the SR was drawn to compare it with the SR at 363 K. Figure 5.4 provides this comparison where it is clear that the temperature increase benefits the products separation process (BAc and water). According to the literature [17], this behaviour was expected because although there is no reaction, the solid phase regeneration is improved by the temperature increase. Thereby, the same behaviour would be expected for RSR (SMBR process) because the temperature increase promotes the reaction kinetics.

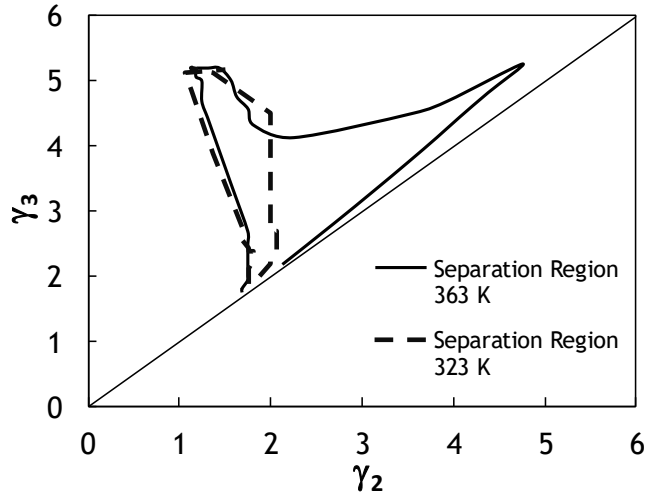

Figure 5.4. Influence of the temperature in Separation Region for equimolar feed ratio of BAc and water (SMB process). Both regions were determined for a raffinate purity criteria ≥ 99.5 % (solvent-free basis).

5.4.2.2. Effect of feed composition

The effect of feed composition on RSR at 363 K was studied as shown in Figure 5.5 for different feed molar ratios (n-butanol/AAc). The results show that increasing the feed molar ratio (from 1 to 3) the vertex of the region (i.e. the optimal point) moves slightly downwards and to the left resulting in more eluent/desorbent consumption (about twice as much) and the productivity is halved. Therefore, the optimal operating conditions at 363 K, which fulfil the required performance criteria with the largest productivity and the lowest desorbent consumption, are the following: Q_F = 6.5 mL.min^{-1}, Q_{Ext} = 117.6 mL.min^{-1}, Q_{EL} = 122 mL.min^{-1} and Q_{Rec} = 24 mL.min^{-1}, using an equimolar feed ratio. Meanwhile, since the BAc system presents a very slow reaction rate, a different feed molar ratio was simulated in order to understand its impact on the performance parameters of a SMBR during the BAc synthesis. Thus, a mixture comprising n-butanol/AAc/BAc/water (4.8/37.8/28.7/28.7 (%), respectively) in equilibrium conditions at 363 K, was used as feed solution of a SMBR operating at the same temperature with the aim of making better use of the equipment. Indeed, according to the respective RSR represented as a dotted line in Figure 5.5, for which the same γ_1 (9.10) and γ_4 (1.52) were used, it is possible to extend the reaction beyond the values reached when an equimolar

mixture of n-butanol and AAc is fed. This fact is due to the eluent (n-butanol) present along the SMBR, which is also one of the reactants and it will consume the remaining limiting reactant still present in the feed stream. Additionally, the reactive front will be confined to the surroundings of the feed port, and a larger portion of the SMBR will be almost exclusively dedicated to the products separation. Since the feed stream already contains a reasonable amount of BAc and the remainder AAc is being converted into this ester as well, the SMBR is able to produce and separate a higher amount of BAc in this scenario. Hence, this configuration leads to the improvement of the performance parameters, increasing the productivity (20 %) and also reducing the eluent consumption (18 %) when compared with the results for an equimolar ratio feed. In this case, the optimal operating conditions at 363 K are Q_F = 5.6 mL.min^{-1}, Q_{Ext} = 115.4 mL.min^{-1}, Q_{EL} = 122 mL.min^{-1} and Q_{Rec} = 24 mL.min^{-1}.

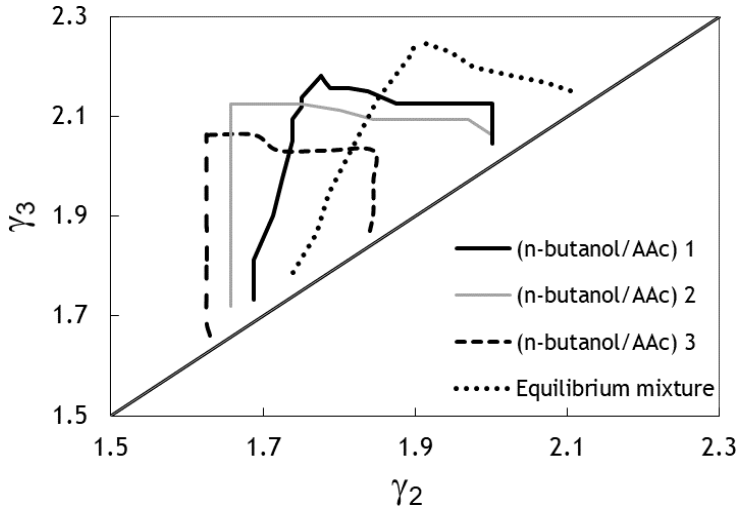

Figure 5.5. Reactive Separation Regions for different feed compositions using a switching time of 3.1 min and the configuration 2-4-4-2 at 363 K. Equilibrium mixture comprises n-butanol/AAc/BAc/water with the following molar compositions 4.8/37.8/28.7/28.7 (%), respectively. Raffinate purity criteria of 99.5 % (solvent-free basis).

5.4.3. Proof-of-concept

Experimental runs were performed in the SMBR LICOSEP pilot scale unit under different operating conditions aiming to validate the mathematical model previously developed using the respective kinetic data and adsorption parameters. All runs were carried out at 323 K over A-15, which was used as catalyst and adsorbent. The operating conditions that correspond to each experimental run are displayed in Table 5.3, while the respective concentration profiles obtained under the different operating conditions can be observed in Figure 5.6 to Figure 5.8.

Table 5.3. Experimental conditions and performance parameters of the different runs performed in SMBR LICOSEP pilot scale unit at 323 K with configuration 2-4-4-2 and a switching time of 3.1 min. The predicted values are presented between the brackets.

Parameter/Experiment	SMBR01	SMBR02	SMBR03
$C_{n\text{-butanol, F}}$ ($mol.L^{-1}$)	6.04	0.60	0.60
$C_{AAc, F}$ ($mol.L^{-1}$)	6.04	4.78	4.78
$C_{BAc, F}$ ($mol.L^{-1}$)	-	3.64	3.64
$C_{water, F}$ ($mol.L^{-1}$)	-	3.64	3.64
Q_F ($mL.min^{-1}$)	0.86	2.10	2.10
Q_{Ext} ($mL.min^{-1}$)	24.3	25.6	25.0
Q_{El} ($mL.min^{-1}$)	29.7	29.2	29.2
Q_{Rec} ($mL.min^{-1}$)	29.0	20.0	23.0
P_{Ext} (%)	57.1 (48.7)	32.7 (27.2)	54.4 (54.5)
P_{Raff} (%)	26.1 (31.0)	33.7 (33.4)	65.0 (79.6)
Conv (%)	29.1 (39.3)	21.8 (13.5)	32.8 (43.2)
Prod ($kg_{BAc}.(L_{ads}^{-1}.day^{-1})$)	0.223 (0.274)	0.210 (0.289)	1.67 (2.04)
DesC ($L_{n\text{-butanol}}.kg_{BAc}^{-1}$)	213 (174)	233 (169)	29.3 (23.9)

The LICOSEP pilot scale unit presents considerable limitations for the implementation of a SMBR process for the production of BAc. First of all, the maximum operating temperature is 323 K, which is below the desired value for this system (363 K). Moreover, the maximum allowed flow rate in section 1 is much lower than the predicted by the Equilibrium Theory (288 $mL.min^{-1}$) since the maximum eluent flow rate is limited to 30 $mL.min^{-1}$. These technical constraints were the main reason why it was not possible to reach the BAc purity, productivity and conversion values presented in the previous sections in any of the experiments performed.

Thus, an equimolar ratio of n-butanol/AAc was fed in the first run and, according to the results presented in Figure 5.6, there was not separation of BAc from AAc in the raffinate port, which is at the outlet of column 10. Indeed, the maximum operating temperature is a limitation for the BAc synthesis in the LICOSEP unit, since the reaction rate of this system is very slow [10] and, for this reason, the reaction conversion is low at this temperature (323 K). As the result, the unreacted AAc is carried by the liquid, preferentially, since the resin selectivity between AAc and BAc is smaller than between AAc and water, leading to raffinate contamination. Therefore, the results could eventually be improved by reducing the recycling flow rate. Besides that, according to the results obtained in Section 5.4.2.1, higher eluent (264 $mL.min^{-1}$) and extract (261 $mL.min^{-1}$) flow rates are required to achieve the maximum raffinate purity (99.47 mol. %) at 323 K; however, the maximum operating flow rate of the eluent and extract pumps is 30 $mL.min^{-1}$.

A better separation between AAc and BAc is possible by feeding an equilibrium mixture obtained at 363 K (from an equimolar amount of the reactants fed to a FBR), as concluded in RSR study (Section 5.4.2.2). Therefore, this equilibrium mixture was considered as feed solution for the SMBR in the second experimental run (Figure 5.7) with the purpose of overcoming the temperature and flow rates limitations of the LICOSEP pilot scale unit. Although higher raffinate purity was achieved when compared with the previous experimental run, it is clear that BAc was carried with AAc by the solid, in the opposite direction of the fluid flow. These results suggest that higher recycle flow rate is required to move all concentration fronts to the right towards higher raffinate purity.

Afterwards, a third experimental run (SMBR03) was carried out increasing slightly the recycling flow rate in relation to the previous run (from 20 to 23 $mL.min^{-1}$). As a

result, which is displayed in Figure 5.8, a raffinate purity of 65 %, approximately, was obtained with a productivity of 1.7 $kg_{BAc}.(L_{ads}^{-1}.day^{-1})$ and an eluent consumption of 29.3 $L_{n\text{-}butanol}.kg_{BAc}^{-1}$. Additionally, the raffinate and extract streams were collected and the average concentration history of each compound was determined by gas chromatography.

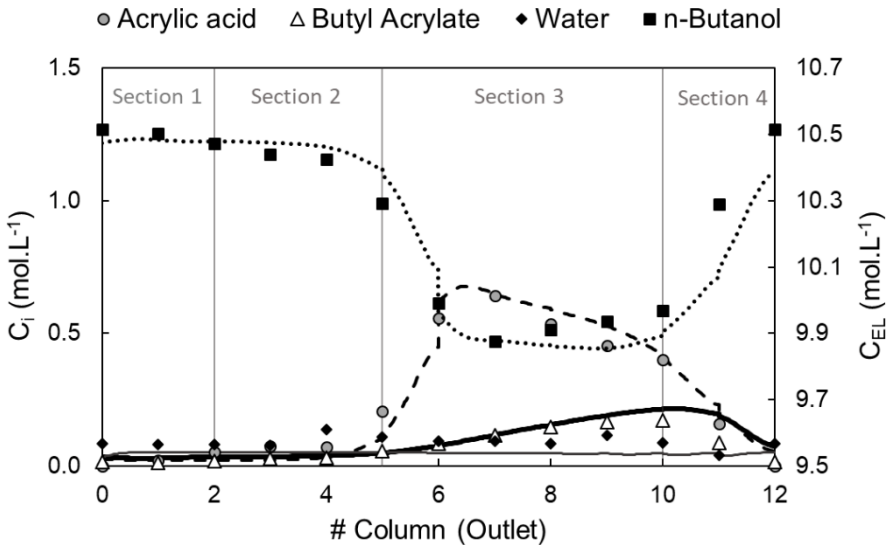

Figure 5.6. Experimental and simulated concentration profiles in SMBR LICOSEP unit at the middle of the switching time (3.1 min) and the cyclic steady state (13th cycle) at 323 K: run SMBR01.

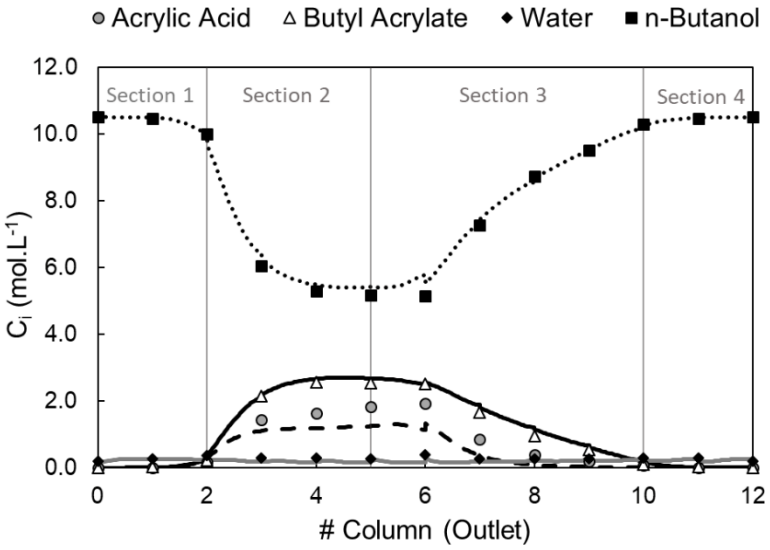

Figure 5.7 .Experimental and simulated concentration profiles in SMBR LICOSEP unit at the middle of the switching time (3.1 min) and the cyclic steady state (13th cycle) at 323 K: run SMBR02.

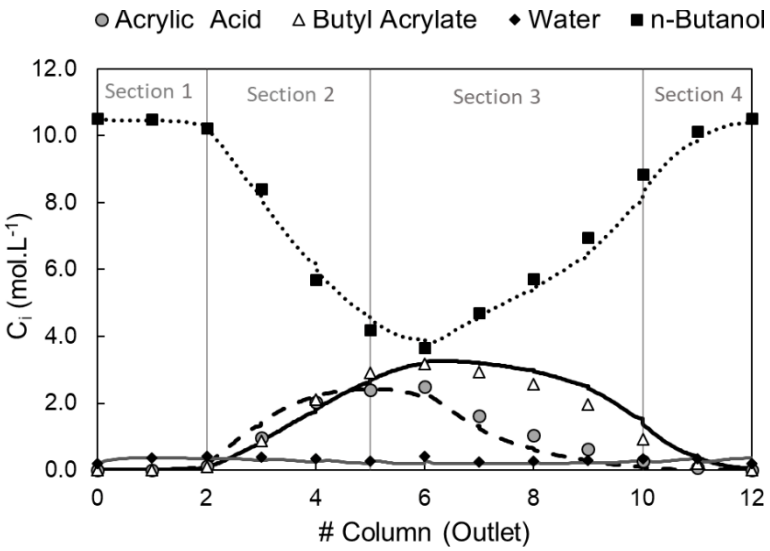

Figure 5.8. Experimental and simulated concentration profiles in SMBR LICOSEP unit at the middle of the switching time (3.1 min) and the cyclic steady state (13th cycle) at 323 K: run SMBR03.

In Figure 5.9, it is possible to observe the experimental and the predicted concentration values for each outlet stream. The theoretical values were calculated with the SMBR mathematical model. As expected, BAc is the main compound in the raffinate stream (Figure 5.9 a)) while the water is the predominant compound in the extract stream (Figure 5.9 b)), both in eluent free basis. Some oscillations in the experimental concentration histories are observed, which can be induced either by operating flow rates fluctuations occurred during the experimental runs or by errors associated with gas chromatography analysis; however, the steady state was achieved.

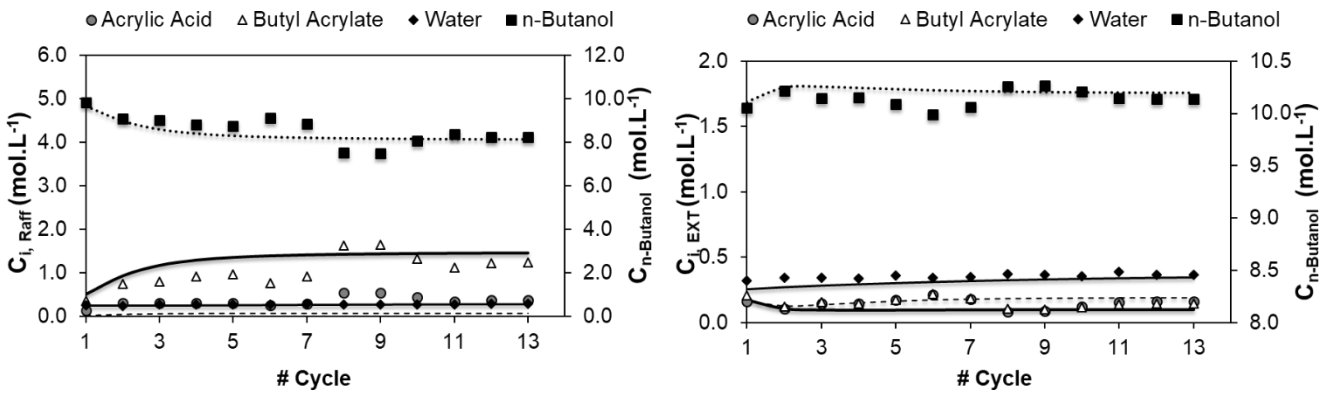

a) b)

Figure 5.9. Experimental and simulated average concentrations histories obtained during the last experimental run (run SMBR03) in the raffinate (a) and extract (b) streams at 323 K.

Regarding the mathematical model, in a general way, it predicts reasonably the SMBR performance for the BAc synthesis by using the experimental multicomponent adsorption parameters described in Chapter 3 (see Section 3.4.2.2) and the kinetic data available in open literature [10] (also described in Section 5.3). Nevertheless, it is important to refer that more dispersed concentration fronts were obtained experimentally comparing with the curves predicted by the mathematical model using the parameters described in Table 5.1. However, a better fit of these experimental curves was possible considering a lower Peclet number (10) instead of the value obtained from the tracer experiments (143), as shown in Figure E.3, in *Appendix E*. Several factors can contribute to this phenomenon. One of the reasons can be associated with the shrinking on the A-15 when pure n-butanol is displaced either by AAc or BAc (initially, all columns are filled with pure n-butanol). This leads to higher dead volumes (apart from the dead volume of the recycling pump which is about 21 cm^3) and unstable bulk conditions (see Figure E.1, *Appendix E*) comparing with the initial conditions previously characterized through tracer experiments. Depending on the feed flux direction, top-down or bottom-up, the bulk conditions inside of the fixed-bed columns change (Figure E.1). Furthermore, this instability can be induced by the high section flow rates used in the pilot scale LICOSEP unit, which are significantly higher (approximately, 54 mLmin^{-1} in section 1 of the SMBR) than the flow rates used in the tracer experiments (10 mL.min^{-1}). Besides that,

while the A-15 resin shrinks it gives rise to a significant void inside of the columns creating favourable conditions to preferred pathways formation, mainly, in case of not compressed bulks or ineffective packing. Thus, additional tracer experiments were performed, with a similar void (approximately 1 cm) observed in the experimental SMBR runs, with the purpose of understanding its effect in terms of dispersion. As a result, a lower Peclet number (80) was obtained comparing with the previous one (143, without void), indicating that the void, effectively, leads to higher dispersion than the initially expected. However, this new Peclet number (80) is still not low enough to predict well the experimental curves. It suggests that, probably, there is an additional factor contributing to the dispersion, like the liquid mixture density and other physical-chemical properties, for example, which were not taken into account during the tracer experiments since water is had to be used as solvent (blue dextran solution is not soluble in the remaining compounds).

Moreover, previously in Chapter 3, it was noticed that the feed configuration was an important issue in the dynamic study of the FBR. So, since the fluid flow is performed in both directions (top-down and bottom-up) in the LICOSEP pilot scale unit, alternately, to have the minimal dead volume from a column outlet to the inlet of the next one, it is also important to analyse the feed configuration effect on the reactor performance. For that, two additional FBR experiments were performed using two columns of the pilot scale LICOSEP unit connected in series using different feed flow configurations: one in which both columns were fed from the top and another in which they were fed from bottom. More details can be found in *Appendix E*. As can be observed in Figure E.2 (*Appendix E*), although both configurations lead to different changes in the bulk conditions, there was reproducibility between the FBR experiments performed with the different feed flow configurations, showing that the feed flow configuration is not determinant on the SMBR performance.

In summary, concentration profiles with higher dispersion were obtained comparing with the expected concentration curves and one parameter was considered to be changed in order to predict this effect with the mathematical model proposed. Nevertheless, dispersed concentration fronts can be avoided during the BAc synthesis in a SMBR using a different recycle line configuration and/or recycle pump that reduces the dead volume in this specific part of the unit. Other possibility is the use of fixed-bed special columns with dynamic adjustable pistons during the reaction allowing to get similar bulk

conditions in all SMBR sections and reducing the void (dead volume) inside each fixed-bed column while shrinking occurs. For this reason, the dispersion effect will not be considered in the numerical SMBR study at 363 K at pilot and industrial scales.

5.4.4. Reference case

The ideal operating parameters to achieve the desired separation with the maximum performance were found through the RSR study like previously described (Section 5.4.2). However, aiming to extend the SMBR study to industrial scale based on safer operating conditions, a reference case corresponding to a slightly inner point of the RSR should be selected to study the design and influence of the operating parameters on the reactor performance. This fact ensures a more reliable study since this system is very sensitive to small flow rates deviations, namely in recycling flow rate as shown with the experimental results. For this reason, working on the RSR limit (which corresponds to the maximum performance) can lack robustness since any flow rate fluctuation may be enough to leave the respective RSR and not achieve the desired separation. Therefore, a reference case at 363 K was selected, slightly different from the ideal parameters found through the RSR. The respective operating conditions, as well as, the performance parameters determined with SMBR model are presented in Table 5.4, where it is possible to observe an excellent performance with a reaction conversion of 99.7 % achieving a raffinate purity of 99.9 %. Figure 5.10 shows the concentration profiles obtained at these conditions.

Table 5.4. Reference case at pilot scale: operating conditions and performance parameters at 363 K.

Operating Parameters		Performance Parameters	
Configuration	2-4-4-2	P_{Ext} (%)	99.2
t* (min)	3.1	P_{Raff} (%)	99.9
Q_{EL} ($mLmin^{-1}$)	122	Conv (%)	99.7
Q_F ($mLmin^{-1}$)	5.0	DesC ($L_{n\text{-}butanol}.kg_{BAc}^{-1}$)	33.3
Q_{Rec} ($mLmin^{-1}$)	24.0	Prod ($kg_{BAc}.(L_{ads}^{-1}.day^{-1})$)	6.0
Q_{Ext} ($mLmin^{-1}$)	118.0		
$C_{n\text{-}butanol,F}$ ($mol.L^{-1}$)	5.76		
$C_{AAc,F}$ ($mol.L^{-1}$)	5.76		

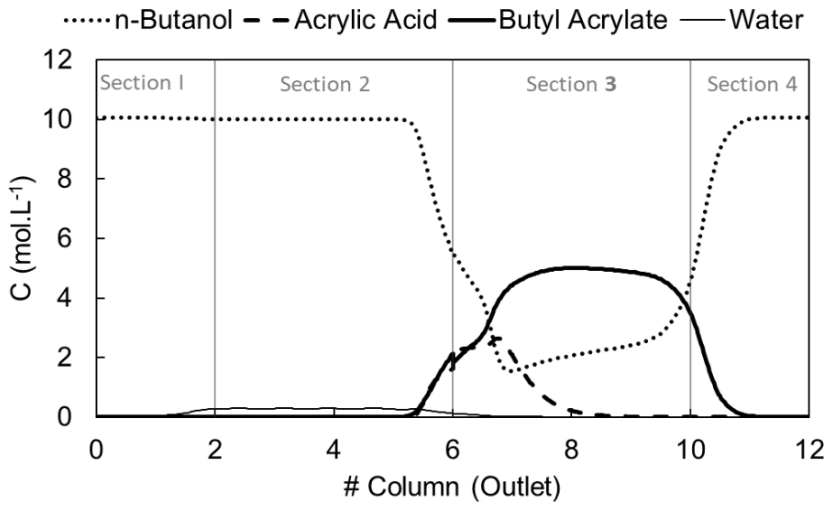

Figure 5.10.Concentration profiles simulated in SMBR pilot scale unit at cyclic steady state (21th cycle) and 363 K using t=3.1 min and configuration 2-4-4-2 (reference case). The respective operating parameters are presented in Table 5.4.*

5.4.4.1. Effect of configuration

The effect of the configuration was evaluated at 363 K, using 2-4-4-2, 3-3-3-3 and 2-3-5-2 columns arrangement per section. So, the contact time between the reactants/products and the catalyst/adsorbent in each section was changed. In practice, the configuration 2-4-4-2 means that the extract stream is collected right away after column 2, then the feed stream is introduced after 4 columns (after column 6), the

raffinate stream is collected after 4 more columns (after column 10) and finally the eluent or desorbent stream is continuously fed in the inlet of the first column (after column 12). These results allow to evaluate the most suitable configuration for BAc synthesis leading to the best performance parameters in the SMBR. According to the simulated results given in Table 5.5, the best configurations are 2-4-4-2 and 2-3-5-2, which can be explained by the highest residence time in the reaction section (total of 8 columns in the sections 2 and 3) leading to higher reaction conversion and, consequently, improving the raffinate purity since there is no contamination with AAc (which is substantially converted). However, the first arrangement (2-4-4-2) presents slightly higher productivity and lower desorbent consumption.

Table 5.5. Effect of configuration using a t= 3.1 min.*

Parameter/ Configuration	2-4-4-2	3-3-3-3	2-3-5-2
P_{Ext} (%)	99.18	99.18	99.18
P_{Raff} (%)	99.94	99.77	99.94
Conv. (%)	99.66	99.50	99.67
Prod. ($kg_{BAc}.(L_{ads}^{-1}.day^{-1})$)	6.00	5.96	5.99
DesC ($L_{n\text{-}butanol}.kg_{BAc}^{-1}$)	33.30	33.55	33.35

5.4.4.2. Effect of switching time

The switching time sensitivity analysis was also conducted at 363 K for two different situations: a) keeping constant Q_{EL} and Q_{Rec} (Table 5.6) and b) keeping constant $\gamma_1 = 9.10$ and $\gamma_4 = 1.52$ (Table 5.7), by changing the respective eluent and recycle flow rates. For both cases, the run #2 that corresponds to the switching time of 3.1 min, presents the best results in terms of performance parameters and taking into account the required separation criteria.

Table 5.6. Effect of t keeping constant Q_{EL} and Q_{Rec} and using the configuration 2-4-4-2.*

Parameter/ Run	#1	#2	#3
*t** (min)	3.0	3.1	3.2
P_{Ext} (%)	85.56	99.18	98.91
P_{Raff} (%)	99.87	99.94	99.74
Conv. (%)	98.17	99.66	99.45
Prod. ($kg_{BAc}.(L_{ads}^{-1}.day^{-1})$)	5.07	6.00	6.03
DesC ($L_{n\text{-}butanol}.kg_{BAc}^{-1}$)	39.40	33.30	33.13

Table 5.7. Effect of t keeping constant $\gamma_1 = 9.10$ and $\gamma_4 = 1.52$ and using the configuration 2-4-4-2.*

Parameter/ Run	#4	#2	#5
*t** (min)	3.0	3.1	3.2
P_{Ext} (%)	99.16	99.18	59.11
P_{Raff} (%)	97.38	99.94	99.87
Conv. (%)	97.17	99.66	96.23
Prod. ($kg_{BAc}.(L_{ads}^{-1}.day^{-1})$)	5.91	6.00	2.03
DesC ($L_{n\text{-}butanol}.kg_{BAc}^{-1}$)	34.94	33.30	95.39

5.4.5. From pilot scale to industrial scale

5.4.5.1. SMBR scaling up to industrial scale

In this section, the procedure followed for a SMBR scaling up to an industrial scale is described. For that, an algorithm was developed and it is displayed in Figure 5.11. Basically, the procedure was based on the pilot scale reference case studied in the previous section (Section 5.4.4), by keeping the residence times and flow ratios constant in each section. According to the Equilibrium Theory, the limiting ratios between the fluid and the solid interstitial velocities are determined for sections 1 and 4 as described previously in Section 5.4.1. In the following step, guessing the length of each column and using the same *t** (3.1 minutes) of the pilot scale unit, the solid velocity (U_s) is

determined. After that, the interstitial fluid velocities in sections 1 and 4 are found from which it is possible to obtain the desorbent and recycle flow rates, respectively. The bed porosity was kept at 0.41 like in the SMBR at pilot scale. The feed and extract flow rates were found by keeping the respective flow rates and the desorbent flow rate ratio of the pilot scale unit. Afterwards, the raffinate flow rate (Q_{Raff}) can be determined from the flow rates balance presented in the algorithm (Figure 5.11). Finally, the global process productivity is simulated using the raffinate flow rate (Q_{Raff}) of the SMBR as the feed flow rate of the downstream unit (described in Section 5.4.6.1). As a reference for the global process productivity, the information described in a market report about global market share for BAc in 2013 [18] was used. In order to get a competitive production, the SMBR unit at industrial scale of this work was designed to have a similar production to that of the BASF company located in Freeport, TX, USA, which produced in that year about 50,000 tonnes of BAc, according to the same report. As a result, the dimensions found for each column of the SMBR at industrial scale were 2.23 m diameter and 0.62 m length, resulting in a total volume of 29 m^3 (corresponding to 12 columns). The ratio between the diameter and the length of each column was assumed to be within the range presented by industrial SMBR units, such as the Parex unit that presents a value of 3.6 [19].

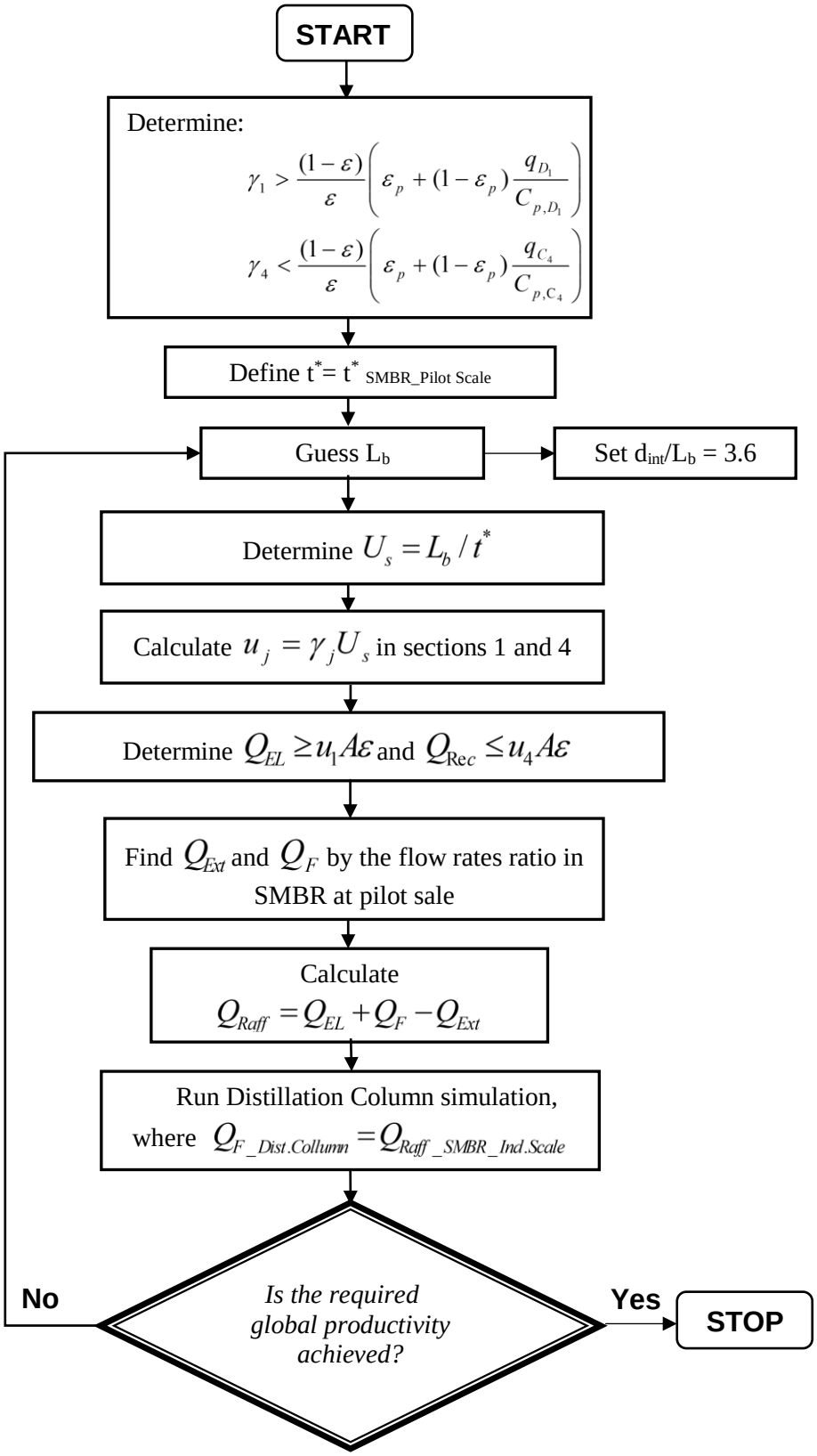

Figure 5.11. Design algorithm to scale up a SMBR unit according to the desired global productivity.

5.4.5.2. Concentration profile and performance parameters

After sizing a SMBR unit at industrial scale and finding the correspondent operating parameters according to the procedure described in the previous Section (5.4.4), the respective concentration profiles were simulated at 363 K using the operating conditions presented in Table 5.8 and taking into account the new dimensions (V_{SMBR_IS} = 29 m^3). The performance parameters obtained are shown in the same table and the resulting concentration profiles are presented in Figure 5.12.

Table 5.8. Reference case at industrial scale: operating conditions and performance parameters at 363 K.

Operating Parameters		Performance Parameters	
Configuration	2-4-4-2	P_{Ext} (%)	99.3
t* (min)	3.10	P_{Raff} (%)	99.8
Q_{EL} ($L.min^{-1}$)	2397	Conv. (%)	99.5
Q_F ($L.min^{-1}$)	118	DesC ($L_{n\text{-}butanol}.kg_{BAc}^{-1}$)	27.6
Q_{Rec} ($L.min^{-1}$)	475	Prod ($kg_{BAc}.(L_{ads}^{-1}.day^{-1})$)	7.20
Q_{Ext} ($L.min^{-1}$)	2315		
$C_{n\text{-}butanol,F}$ ($mol.L^{-1}$)	5.76		
$C_{AAc,F}$ ($mol.L^{-1}$)	5.76		

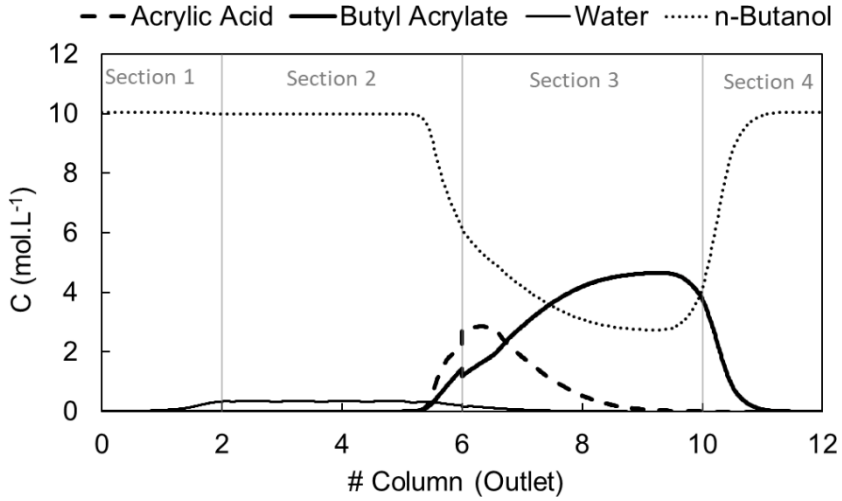

Figure 5.12. Concentration profiles simulated in the SMBR at industrial scale unit at cyclic steady state (21st cycle) and 363 K using t=3.1 min and configuration 2-4-4-2.*

As a result, an attractive performance was attained with a great raffinate purity (99.8 %, in solvent free basis). These operating conditions lead to a raffinate flow rate of 200 $L.min^{-1}$, which requires treatment in a downstream unit in order to get pure BAc (see Section 5.4.6.1). Comparing the performance parameters obtained at pilot scale (Table 5.4) and industrial scale (Table 5.8) it is noticed that there are no significant differences in terms of P_{Ext}, P_{Raff} and Conv.; however, at industrial scale the DesC is lower and the Prod. is higher. This better performance achieved at industrial scale can be related with the SMBR dimensions in terms of d_{int}/L_b ratio that is much bigger than the d_{int}/L_b ratio at pilot scale (approximately thirty times larger), which leads to changes in the hydrodynamics leading to a decrease of the mass transfer resistance.

5.4.6. Downstream units

In order to assess the process sustainability, downstream units were studied to treat the extract and raffinate streams from the SMBR unit. These units will allow separating the water from the eluent (n-butanol) as well as the BAc from the eluent, respectively and, besides that, to recover the eluent and to re-use it in the initial unit (SMBR) depending on its purity. The scheme of the global process plant is shown in Figure 5.13, where it is proposed to recycle n-butanol from both downstream units to the eluent stream of the SMBR unit. However, this situation will be discussed ahead (see Section 5.4.7).

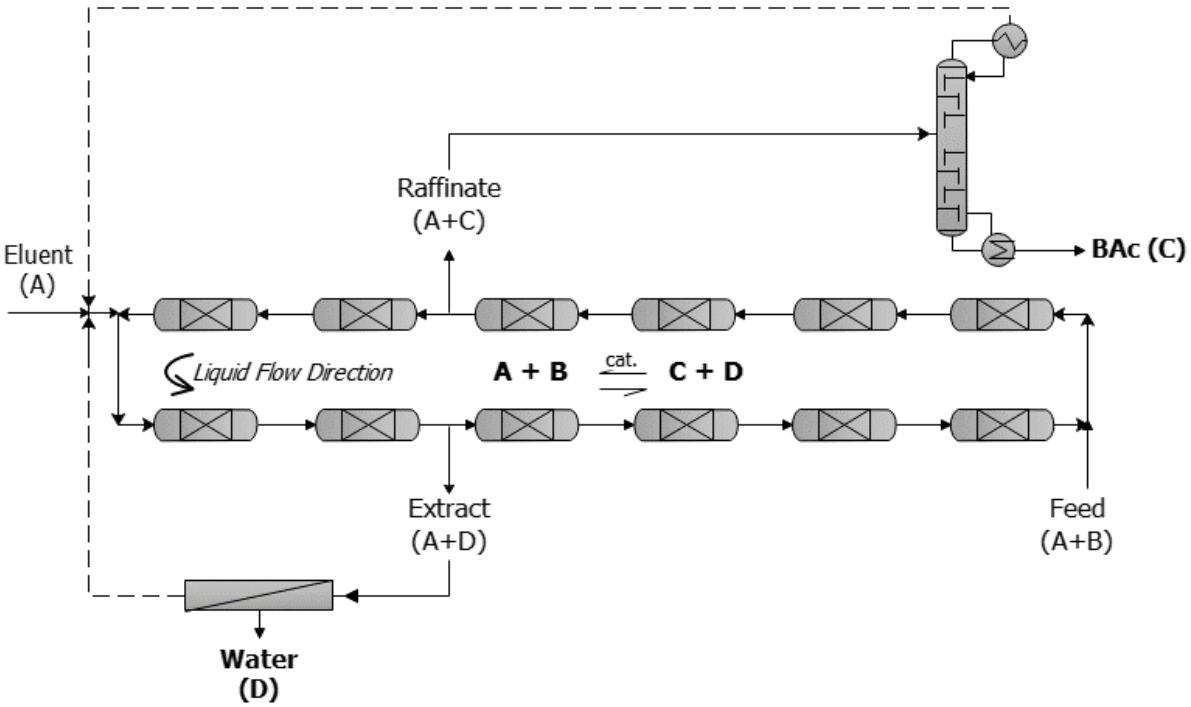

Figure 5.13. Global process plant for a SMBR operation for butyl acrylate synthesis using a configuration of 2-4-4-2 (columns per section). A = n-Butanol, B = Acrylic Acid, C = Butyl Acrylate and D = Water.

5.4.6.1. Distillation column

Analysing the outlet streams obtained from a SMBR unit at industrial scale, it is possible to determine the molar composition of the extract and raffinate streams. The last one is composed of 0.52 molar fraction of n-butanol and 0.48 molar fraction of BAc. For the raffinate stream treatment, a distillation column was simulated in ASPEN PLUS (Version 8.6). A distillation column was selected because it is the most common, even in the industry and, besides that it is easier to apply to this separation; however, if relative volatilities of components is less than 1.1, distillation becomes very expensive [20]. So, the first step is to determine the relative volatility of the mixture, which is 2.13 according to the following equation:

$$\alpha_{BC} = \frac{K_B}{K_C} = \frac{y_B / x_B}{y_C / x_C} = \frac{\frac{P_B^{sat}}{P}}{\frac{P_C^{sat}}{P}} = \frac{P_B^{sat}}{P_C^{sat}} \tag{5.32}$$

where P_B^{sat} corresponds to the saturation pressure of n-butanol and P_C^{sat} corresponds to the saturation pressure of BAc, both at 363 K that is the operating temperature of the SMBR unit. NRTL Hayden-O'Connell model was used to estimate the respective saturation pressures. Furthermore, the operating pressure selected was atmospheric pressure, in order to attain an economical operation. Nevertheless, operation under vacuum can be considered for heat-sensitive compounds or polymerisable materials. In this case, vacuum operation was not considered because the number of stages required is low, as it will be shown ahead, so that the residence time required is not too long and it was assumed that there was no danger of polymerisation. Despite this, experimentally it may be necessary to implement vacuum operation once BAc is a heat-sensitive compound at high temperatures. The vapour-liquid equilibrium data at the operating pressure are also important. According to the literature [21, 22] and the thermodynamic UNIFAC, UNIQUAC and NRTL models, all available in ASPEN software, there are no azeotropes for this binary system (BAc/n-butanol) at the operating conditions selected.

Some operating parameters might be set like the feed flow rate of the input stream, *F*, the composition of the light compound in the feed (n-butanol, in this case), Z_F, as well as the purity of the light compound in distillate (x_D) and bottom (x_B) streams. The total amount of distillate and bottom can be calculated based on equations (5.33) and (5.34). All these values are shown in Table 5.9.

$$z_F F = x_D D + x_B B \tag{5.33}$$

$$F = D + B \tag{5.34}$$

Table 5.9. Process operating parameters of the distillation column for the raffinate treatment in the conventional SMBR process.

F (L.min^{-1})	Z_F	X_D	X_B	D	B (L.min^{-1})
200	0.521	0.990	0.005	105	95.5

After assigning the operating conditions and determining the relative volatility as well as the vapour-liquid equilibrium data, it is possible to simulate a distillation column using one of the simplified distillation methods, as the shortcut distillation design method, DSTWU (the single diameter trayed tower), which is available in ASPEN PLUS software (version 8.6). The DSTWU method provides a very good starting point for distillation column design and it uses the Gilliland's, Winn's and Underwood's methods [23] for calculation of stage and reflux ratio. The calculations are completed based on two assumptions, constant molar overflow and constant relative volatilities. For a specific product recovery (light and heavy) and a minimum number of stages or reflux ratio, the DSTWU estimates the required minimum number of theoretical stages, the feed stage number and the minimum reflux ratio based on the user input. Besides that, it estimates the optimum feed stage location and the condenser and reboiler duties. Therefore, it is possible to get an idea about the process and use its output as an input to a more detailed method, like RadFrac (rigorous fractionation) that is more rigorous and requires more input data being also available in ASPEN PLUS software (version 8.6). Firstly, the recovery of light $\left(L_{Rec}\right)$ and heavy $\left(H_{Rec}\right)$ compounds was calculated as well as the minimum and the actual reflux ratio to use as input in DSTWU and RadFrac methods, according to the following equations, respectively:

$$L_{Rec} = \frac{D\,x_D}{F\,z_F} \tag{5.35}$$

$$H_{Rec} = \frac{D\left(1-x_D\right)}{F\,\left(1-z_F\right)} \tag{5.36}$$

$$\frac{R_{min}}{R_{min}+1} = \frac{x_D - y}{x_D - z_F} \tag{5.37}$$

$$y = \alpha \frac{x}{1+x\left(\alpha-1\right)} \tag{5.38}$$

$$R_{actual} = 1.2 \times R_{min} \tag{5.39}$$

where, R_{min} represents the minimum reflux ratio, R_{actual} is the operating reflux ratio, and the equilibrium curve can be obtained by relating the relative volatility to the composition of the liquid, according to equation (5.38). Table 5.10 gives all the required

values to determine the minimum reflux ratio while the input and output data of the DSTWU and RadFrac methods are presented in Table 5.11 and Table 5.12, respectively.

Table 5.10. Parameters involved in R_{min} calculation.

Parameter	x_D	α	x	y	R_{min}
Value	0.99	2.13	0.52	0.70	1.63

Table 5.11. Input and output data of the distillation column simulation using DSTWU method.

Parameter	Input value	Parameter	Output value
L_{Rec}	0.995	N	170
H_{Rec}	0.011	N_F	136
R_{actual}	1.96	BAc purity (bottom), %	99.5
Condenser	total	N-butanol purity (top), %	99.0
		Reboiler duty, $J.s^{-1}$	2.25×10^6

Table 5.12. Input and output data of the distillation column simulation using RadFrac method.

Parameter	Input value	Parameter	Output value
N	170	BAc purity (bottom), %	100
N_F	136	n-butanol purity (top), %	96.5
R_{actual}	1.96	Reboiler duty, $J.s^{-1}$	2.25×10^6
Condenser	total		
Bottom to feed ratio	0.96		

According to Table 5.11, it would be possible to get 99.5 % of BAc purity on the bottom stream and 99.0 % of n-butanol on the top stream. However, by using a more rigorous method (RadFrac) it can be observed that, for the same parameters of the DSTWU method, it is possible to get 100 % of BAc purity while in the top stream the n-butanol purity is just about 96.5 % (Table 5.12). To have an idea, 514 stages would be necessary to get a n-butanol purity of 97.0%. Indeed, the most important parameter is the BAc purity which should be ≥ 99.5 %; nevertheless, the purity of n-butanol must be taken

into account to recover this compound and recycle it to the SMBR unit, towards a more efficient process. Thus, a study about the eluent recovery with different downstream units is presented in the following section (5.4.7), where the influence of the n-butanol purity in the global process performance is assessed and the respective saved amount in relation to the open SMBR process (without n-butanol recovery from the downstream units) is determined.

The distillation column was optimised by determining the minimal stage number for a minimal reflux ratio to get the same purities of BAc and n-butanol reached in the RadFrac simulation. The respective results can be observed in Table 5.13 leading to conclude that it is possible to reduce significantly the number of stages achieving similar purities to the previous ones. A sensitivity analysis was also performed by changing the feed stage and analysing the reboiler duty in order to find the best position for the feed stream, being it the 25th stage. The characteristics of the distillation column required to purify the raffinate stream are shown in Table 5.14, which were calculated according to the following equations [20].

$$N_{actual} = N / Eff \tag{5.40}$$

$$H_{tower} = H_{tray} \times N_{actual} \tag{5.41}$$

$$L_{tower} = 1.2 \times H_{tower} \tag{5.42}$$

where N and N_{actual} represent the theoretical and actual number of trays, respectively. Typical values for tray efficiency (Eff) range from 0.5 to 0.7 according to the literature [20]. In this study, it was considered 0.7. The variables H_{tower}, L_{tower} and H_{tray} represent the tower height, the required length of the column (estimated to be 20 % higher than the required just for trays) and the height of each tray (assumed to be 0.7 m), respectively, according to the same source [20].

Finally, it is important to mention that feeding the total raffinate stream (200 L.min$^{-1)}$ to the distillation column unit, a production capacity of 51,500 t_{BAc}.year^{-1} is obtained, very similar to the production capacity of the BASF Company in TX, USA, as previously stated.

Table 5.13. Final parameters optimised with RadFrac method simulation.

Parameter	Input value	Parameter	Output value
N	33	BAc purity (bottom), %	99.9
N_F	25	n-butanol purity (top), %	96.4
R_{actual}	1.83	Reboiler duty, $J.s^{-1}$	2.12×10^6
Condenser	total		
Bottoms to feed ratio	0.96		

Table 5.14. Sizing of distillation column.

N_{actual}	H_{tower} (m)	L_{tower} (m)	D_{tower} (m)	H_{tray} (m)
47.1	33.05	39.66	1.92	0.70

5.4.6.2. Pervaporation unit

According to the simulation results of the SMBR unit at industrial scale, the extract stream is composed of 0.967 molar fraction of n-butanol and 0.033 molar fraction of water. Since it presents such a low amount of water, a distillation column would become an expensive choice. Accordingly, in this case the separation unit selected to n-butanol dehydration was a membrane selective to water. Pervaporation is a very effective and economical technique for the separation of water from organic solvents and solvent mixtures [24]. Besides that, this process presents several advantages as high selectivity, low energy consumption, moderate operation cost and compact and modular design [25, 26]. The dehydration of solvents, including n-butanol, has been intensively investigated, by using different kinds of membranes [27-32] and the cost of different techniques has been compared concluding that pervaporation is the most economic to remove low water contents (10 wt. % and less) [33]. As in this case, the amount of water present in the extract stream is about 1 wt.%, the pervaporation process is proposed for this step (n-butanol/water separation). However, the performance of this process depends on several variables, such as temperature, permeate pressure, feed composition, permeate flux (J_i) and some membrane characteristics as the permeance of the membrane ($Q_{m,i}$) for each species.

5.4.6.2.1. Membrane Mathematical Model

A mathematical model was developed for pervaporation membrane processes to simulate different membranes at this work conditions considering:

(i) non-isothermal operation due to the heat consumption for species vaporisation and temperature polarisation;
(ii) plug flow (retentate stream);
(iii) retentate velocity variations inside the membrane due to permeation of components;
(iv) concentration polarisation due to the global membrane resistance (diffusive transport in the boundary layer combined with the membrane resistance);
(v) continuous process once it is a process subsequent to the SMBR unit and both units should be operating continuously. The pervaporation membrane model equations are described following all previous assumptions:

Retentate mass balance to component i:

$$\frac{\partial C_{ret,i}}{\partial t} + \frac{\partial \left(u_s C_{ret,i} \right)}{\partial z} + A_m J_i = 0 \tag{5.43}$$

where z is the axial coordinate in the membrane modules, C_{ret} is the liquid phase concentration in the retentate membrane side, u_s is the superficial velocity, $A_m$is the membrane area per unit membrane modules volume and J_i is the permeate molar flux of species *i*, through the membrane, defined as:

$$J_i = k_{ov,i} \left(a_i p_i^0 - y_i P_{perm} \right) \tag{5.44}$$

where $k_{ov,i}$is the global membrane mass transfer coefficient, that combines the resistance due to the diffusive transport in the boundary layer with the membrane resistance [34]:

$$\frac{1}{k_{ov,i}} = \frac{1}{Q_{m,i}} + \frac{a_i p_i^0 V_{M,i}}{x_{i,F} k_{bl}} \tag{5.45}$$

where $x_{i,F}$ is the liquid molar fraction in the feed.

For laminar flow and Graetz number, $d_{int}^2 u_s / \left(D_M L_m \right)$, much greater that one, the mass transfer coefficient for transport in the boundary layer, k_{bl}, is determined by the Lévêque correlation [35]:

$$Sh = 1.62 Re^{0.33} Sc^{0.33} \left(\frac{d_{int}}{L_m} \right)^{0.33}, (Re < 2300) \tag{5.46}$$

where $Sh = k_{bl} d_{int} / D_M$, $Re = \rho d_{int} u_s / \eta$ and $Sc = \eta / (\rho D_M)$ are the Sherwood, Reynolds and Schmidt numbers, respectively, D_m is the solute diffusivity in the boundary layer, d_{int} is the internal diameter of the tubular membrane, L_m is the membrane length, ρ is the density and η is the viscosity.

The mole fraction of component *i* in the vapour phase (permeate side), y_i, is defined as:

$$y_i = \frac{J_i}{\sum_{i=1}^{n} J_i} \tag{5.47}$$

Fluid velocity variation in the membrane feed side is calculated from the total mass balance:

$$\frac{du_s}{dz} = -A_m \sum_{i=1}^{n} J_i V_{M,i} \tag{5.48}$$

where n is the total number of components.

Retentate heat balance:

$$\sum_{i=1}^{n} \hat{C}_{p,i} C_{ret,i} \frac{\partial T}{\partial t} + \sum_{i=1}^{n} u_s \hat{C}_{p,i} C_{ret,i} \frac{\partial T}{\partial z} + A_m h_f \left(T - T_m \right) = 0 \tag{5.49}$$

where $\hat{C}_{p,i}$ is the liquid heat capacity of component *i*, *T* is the absolute temperature in the feed side of the membrane, T_m is the membrane absolute temperature, and h_f is the heat transfer coefficient in the liquid boundary layer.

Membrane heat balance:

$$\frac{d_{int}}{\left((d_{int} + \delta)/2 \right)^2 - (d_{int}^2 / 4)} h_f \left(T - T_m \right) = \frac{d_{int} + \delta}{\left((d_{int} + \delta)/2 \right)^2 - (d_{int}^2 / 4)} \sum_{i=1}^{n} \Delta H_i^v J_i \tag{5.50}$$

where d_{int} is the internal radius of the membrane, δ is the membrane thickness, and ΔH_i^v is the heat of vaporisation of species *i*. The heat transport coefficient was estimated by the Sieder-Tate correlation, valid for laminar pipe flow [36]:

$$N_u = 1.86\left(RePr\frac{d_{int}}{L}\right)^{0.33}\left(\frac{\eta_b}{\eta_w}\right)^{0.14} \tag{5.51}$$

where $N_u = h_f d_{int}/\lambda$ and $Pr = \eta\hat{C}_{p,i}/\lambda$ are the Nusselt and Prandtl numbers, respectively, η_b and η_w are the viscosity of the liquid in the feed and in the membrane wall, and λ is the thermal conductivity.

Initial and boundary conditions:

t = 0: $T = T_m$ (5.52)

$$C_{ret,i} = C_{0,i} \tag{5.53}$$

z = 0: $T = T_m$ (5.54)

$$C_{ret,i} = C_{F,i} \tag{5.55}$$

where subscripts *0* and *F* refer to initial state and membrane feed conditions, respectively.

In order to evaluate the performance of the process, the following variable was monitored:

$$x_{out} = \frac{C_{out,i}}{\sum_{i=1}^{n} C_{out,i}} \tag{5.56}$$

where $C_{out,i} = C_{ret,i\,(z=1)}$. (5.57)

The outlet flow rate was also analysed $Q_{out,i} = Q_{ret,i\,(z=1)}$, in order to take into account the real flow rate in the recycle study (see Section 5.4.7).

5.4.6.2.2. Numerical solution

The numerical solution of this problem was obtained by using the commercial software gPROMS (general PROcess Modelling System) version 3.5.3, using orthogonal collocation in finite elements (OCFEM) with second order polynomials and one internal collocation point in each element; to this end, the axial dimension of the membrane at industrial scale was discretized in 100 finite elements. The DASOLV equation solver was used to solve the resulting system of ordinary differential equations in time. For all simulations a tolerance of 10^{-5} was used.

5.4.6.2.3. Membrane Results

Several simulations were performed using pervaporation data from the literature for n-butanol dehydration. The best performance was obtained using data from Sommer's and Melin's work [27] relative to a commercial tubular amorphous silica membrane which is distributed by ECN, Petten (The Netherlands) and by Sulzer Chemtech GmbH Membrane Technology, Neunkirchen (Germany), as Pervap® SMS. In that work, the authors present the following equations, relative to permeance and molar flux permeate, respectively:

Permeance is described as follows:

$$Q_{m,i} = Q_{m,i,ref}\, exp\left[\frac{E_i}{R}\left(\frac{1}{T_{ref}} - \frac{1}{T}\right)\right] \tag{5.58}$$

where $Q_{m,i}$ and $Q_{m,i,ref}$ are the permeance of the membrane in relation to component *i* and the permeance of the membrane at $T_{ref} = 353.25\,\mathrm{K}$,respectively, E_i is the activation energy and T is the feed temperature of the membrane;

Molar flux permeate is given by:

$$J_i = Q_{m,i}\left(a_i P_{i,F}^0 - y_{i,perm} P_{perm}\right) \tag{5.59}$$

where a_i is the activity of species ($a_i = \gamma_i x_i$) which is determined using the UNIFAC method, $P_{i,F}^0$, is the saturation pressure of the feed stream, $y_{i,perm}$ and P_{perm} are the molar vapour fraction and the total pressure in the permeate side. The parameters necessary to determine the permeance and the permeate molar flux for each compound are presented in Table 5.15.

The process selectivity is given by:

$$\alpha_m = \frac{y_{i,perm}\left(1-x_{i,F}\right)}{x_{i,F}\left(1-y_{i,perm}\right)} \tag{5.60}$$

Table 5.15. Parameters necessary to determine the permeance and permeate molar flux of the membrane.

Parameter/Compound	n-butanol	water
$Q_{m,i,ref}$ (kg.(m^{-2} h^{-1} bar^{-1}))	0.207[a]	16.4[a]
E_i (J.mol^{-1})	20.2[a]	6.90[a]
$x_{i,F}$	0.968	0.032
$y_{i,perm}$	0.160	0.840
$p_{i,F}^0$ (bar)	0.342	0.700
P_{perm} (bar)	0.016	
T (K)	363	
α_m	160[b]	

[a,b] *data from Sommer's and Melin's work [27, 30].*

The permeance values obtained were 0.207 kg.(m^{-2}.h^{-1}.bar^{-1}) and 16.4 kg.(m^{-2}.h^{-1}.bar^{-1}) for n-butanol and water, respectively. The permeate molar flux for n-butanol was 0.068 kg.(m^{-2}.h^{-1}) and for water was 1.25 kg.(m^{-2}.h^{-1}). After the determination of these parameters, the simulation of the pervaporation unit was carried out. The feed flow rate used was the extract flow rate from SMBR unit, which is 2315 L.min^{-1}, and the internal diameter of each membrane was 7×10^{-3} m (commercial value).

The required module dimensions were 2950 membranes with 10 m of length, resulting in a total membrane area of 649 m^2. This value is acceptable taking into account that the largest application of pervaporation presents 2400 m^2 of membrane area [37] and, besides that, the present mixture contains a very small amount of water, which hinders the separation. Furthermore, according to the literature, pervaporation in a continuous process requires more area than in a batch process, but in return it requires less energy [37], offsetting the investment costs. This separation unit allows reducing 97.3 % of water, resulting in 99.98 wt % of n-butanol purity. The simulation results are shown in Figure 5.14, from which it is possible to conclude that there was no significant temperature variation. The final outlet flow rate is slightly lower than the feed flow rate, 2309 $L.min^{-1}$.

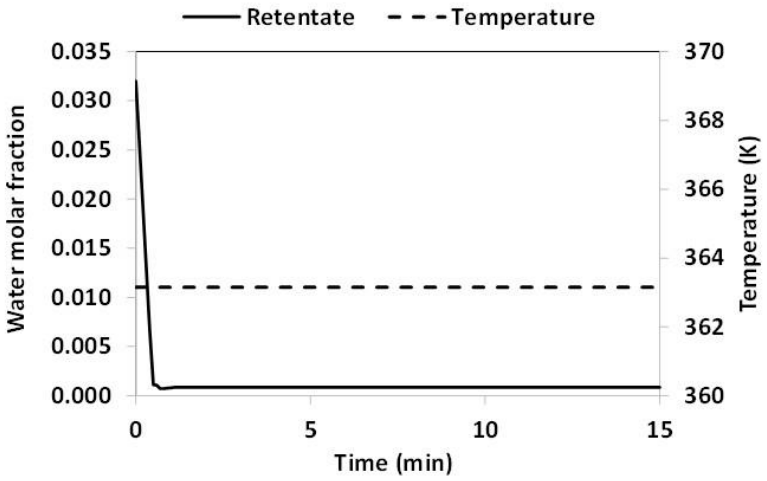

Figure 5.14. Composition and temperature history for n-butanol dehydration process in the pervaporation unit at 363 K (feed temperature).

5.4.7. Process integration: eluent recovery

Aiming a more sustainable global process, a study about n-butanol recovery was performed, as this compound represents the largest operating cost due to its use as reactant and mainly as eluent of the SMBR unit. Hereafter, there will be presented two different configurations that allow n-butanol recovery and which will be studied in detail.

5.4.7.1. Configurations

One of the configurations studied is presented in Figure 5.15 where the n-butanol from each separation unit (pervaporation and distillation column) is sent to the eluent stream of the SMBR unit (ER1) and, the other one is presented in Figure 5.16, where the n-butanol from pervaporation unit is sent to the eluent stream and the n-butanol from the distillation column to the feed stream (ER2).

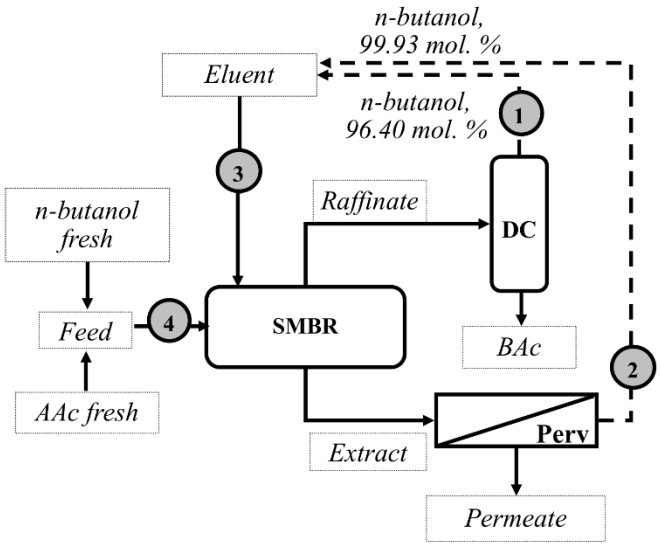

Figure 5.15. Configuration ER1 for n-butanol recycle (eluent recovery).

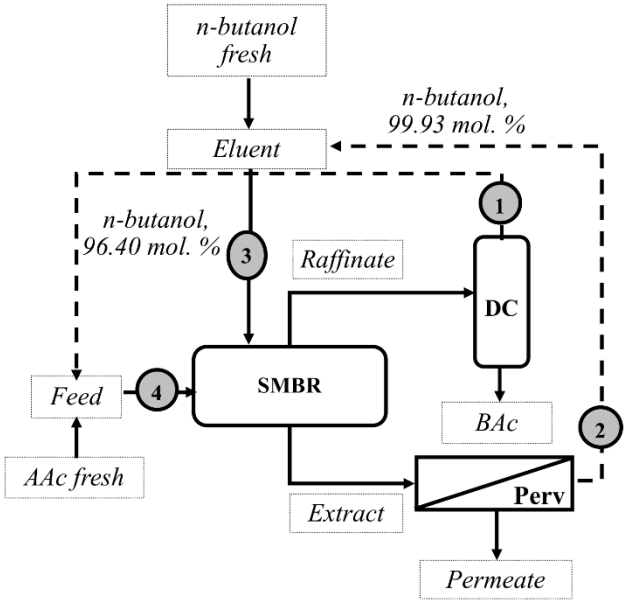

Figure 5.16. Configuration ER2 for n-butanol recycle (eluent recovery).

Regarding the first situation, each stream was also studied separately: (i) recovering the n-butanol from the distillation column to the eluent stream and discarding the stream from the pervaporation unit (ER1.1); (ii) recovering the n-butanol from the pervaporation unit to the eluent stream and discarding the stream from the distillation column (ER1.2). This study allows understanding the influence of the recycling of each outlet stream from the downstream separation units in the global process, in terms of savings and in the final BAc purity obtained.

5.4.7.2. Material balances and simulation results

In order to study each scenario of n-butanol recovery, all balances were performed for each situation (equation (5.63) until equation (5.70)). The different streams flow rates and the respective concentrations are presented in Table 5.16 for each stream (#1 to #4) while the different situations studied for the n-butanol recovery are summarized in Table 5.17.

Table 5.16. Concentrations and flow rates of the different streams.

Stream	Designation	Flow rate ($L.min^{-1}$)	$C_{n\text{-butanol}}$ ($mol.L^{-1}$)	C_{AAc} ($mol.L^{-1}$)	C_{BAc} ($mol.L^{-1}$)	C_{water} ($mol.L^{-1}$)
#1	Top_distillation column	91.31	9.51×10^{0}	-	3.55×10^{-1}	-
#2	Retentate_Pervaporation	2310	1.01×10^{-1}	-	-	6.90×10^{-3}
#3	Eluent_SMBR	2397	1.01×10^{-1}	-	-	-
#4	Feed_SMBR	117.9	5.76×10^{0}	5.76×10^{0}	-	-

Table 5.17. Summary of eluent recovery streams.

Scenario	n-Butanol recycling from
ER1	(#1 + #2) to Eluent
ER1.1	#1 to Eluent
ER1.2	#2 to Eluent
ER2	#1 to Feed and #2 to Eluent

SCENARIO ER1

$$\left(Q_{retentate}\right)_{Pervaporation}+\left(Q^{*}_{top-stream}\right)_{DC}+Q_{n\text{-}butanol,\,fresh}=\left(Q_{EL}\right)_{SMBR} \tag{5.61}$$

where EL is the eluent stream in the SMBR unit and $Q^{*}_{top\_stream}$ means that just a part of the total flow rate from the top stream was used.

$$\left(Q_{retentate}C_i\right)_{Pervaporation}+\left(Q^{*}_{top\_stream}C_{i,}\right)_{DC}+ \tag{5.62}$$
$$+\left(QC_i\right)_{n\text{-}butanol,\,fresh}=\left(Q_{EL}C_i\right)_{SMBR}$$

SCENARIO ER1.1

$$\left(Q_{top\_stream}\right)_{DC}+Q_{n-butanol,\,fresh}=\left(Q_{EL}\right)_{SMBR} \tag{5.63}$$

$$\left(Q_{top\_stream}C_i\right)_{DC}+\left(QC_i\right)_{n\text{-}butanol,\,fresh}=\left(Q_{EL}C_i\right)_{SMBR} \tag{5.64}$$

SCENARIO ER1.2

$$\left(Q_{retentate}\right)_{Pervaporation}+Q_{n\text{-}butanol,\,fresh}=\left(Q_{EL}\right)_{SMBR} \tag{5.65}$$

$$\left(Q_{retentate}C_i\right)_{Pervaporation}+\left(QC_i\right)_{n\text{-}butanol,\,fresh}=\left(Q_{EL}C_i\right)_{SMBR} \tag{5.66}$$

SCENARIO ER2

$$\left(Q_{retentate}\right)_{Pervaporation}+Q_{n\text{-}butanol,\,fresh}=\left(Q_{EL}\right)_{SMBR} \tag{5.67}$$

$$\left(Q_{retentate}C_i\right)_{Pervaporation}+\left(QC_i\right)_{n\text{-}butanol,\,fresh}=\left(Q_{EL}C_i\right)_{SMBR} \tag{5.68}$$

$$\left(Q^{*}_{top\_stream}\right)_{DC}+Q_{AAc,\,fresh}=\left(Q_{F}\right)_{SMBR} \tag{5.69}$$

$$\left(Q^{*}_{top\_stream}C_i\right)_{DC}+\left(QC_i\right)_{AAc,\,fresh}=\left(Q_{F}C_i\right)_{SMBR} \tag{5.70}$$

where F represents the feed stream.

The first equation of scenario ER1.1, for example, enables to find the fresh n-butanol flow rate required to feed as eluent stream in the SMBR unit together with the stream #1 (top stream of the distillation column). The second equation of this scenario (ER1.1) allows determining the n-butanol concentration in the final eluent stream (distillation column + fresh) and the respective contamination of BAc in that stream. The molar compositions resulting from this mixture and from the mixtures of the remaining scenarios are shown in Table 5.18.

Table 5.18. Input molar composition data in SMBR simulations according to the different n-butanol recycling scenarios.

Scenario	Ref. Case (IS)	ER1	ER1.1	ER1.2	ER2	
STREAM INPUT	Eluent	Eluent	Eluent	Eluent	Eluent	Feed
$x_{n\text{-butanol}}$	1.000	0.998	0.999	0.999	0.999	0.491
x_{AAc}	0.000	0.000	0.000	0.000	0.000	0.491
x_{BAc}	0.000	0.001	0.001	0.000	0.000	0.018
x_{water}	0.000	0.001	0.000	0.001	0.001	0.000

Analysing the results, the contamination in the final eluent stream is about 0.1 % of BAc. The influence of this contamination in the final SMBR process, in terms of performance parameters, and the savings achieved with this procedure are presented in Table 5.19.

Table 5.19. Final performance parameters resulting from SMBR simulations according to the different n-butanol recycling scenarios.

Performance Parameters	Ref. Case (Industrial Scale)	ER1	ER1.1	ER1.2	ER2
P_{Ext} (%)	99.32	95.86	95.42	99.99	99.99
P_{Raff} (%)	99.75	99.71	99.85	99.63	99.66
Conv (%)	99.53	99.84	99.86	99.77	99.80
Prod ($kg_{BAc}.(L_{ads}^{1}.day^{-1})$)	7.220	7.240	7.240	7.220	7.250
DesC_open ($L_{n\text{-}butanol}.kg_{BAc}^{-1}$)	27.58	-	-	-	-
DesC_closed ($L_{n\text{-}butanol}.kg_{BAc}^{-1}$)	-	0.000	26.66	1.010	1.000

Comparing all scenarios with the reference case (without n-butanol recycling) leads to conclude that there are no significant differences in the performance parameters with the exception of the extract purity. In the scenarios ER1 and ER1.1 it is possible to observe that the extract purity decreased. This fact is due to the contamination in section 1 of the SMBR unit with stream #1 (from the distillation column) which presents 0.07 mol % of BAc in n-butanol.

The n-butanol saving with the scenario ER1.1 in relation to reference case is about 3%. This fact is due to the low flow rate of the stream #1 which is 91.31 $L.min^{-1}$ while the eluent required is 2397 $L.min^{-1}$, so 2306 $L.min^{-1}$ of fresh n-butanol must be added.

Regarding scenario ER1.2, the same procedure was performed to find the purity of the final eluent stream (#3) and the results are also shown in Table 5.18. According to the results, the same purity of eluent is achieved, however, the contaminant is water. Discarding the stream #1 and recycling the stream #2 (2310 $L.min^{-1}$), it is possible to save about 96 % of n-butanol, once it is only necessary to add 87.4 $L.min^{-1}$ of fresh n-butanol. It is important to refer that 4 % of stream #1 (top distillation column) must be discarded when the outlet streams from both separation units are used as eluent to the SMBR unit (scenario ER1), in order to use the required eluent stream in the SMBR, since the stream #1 presents contamination with BAc (Table 5.16). *Q** means that just a part of the total top stream flow rate was used. In this way, the purity of the final eluent stream is lower

than in the other scenarios (ER1.1 and ER1.2) and the extract purity decreased like in scenario ER1.1, due to the contamination of the eluent in section 1 with BAc coming from stream #1. Nevertheless, comparing all results from Table 5.19, scenario ER1 allows the maximum of n-butanol saving (approximately 100%).

The last scenario (ER2) was thought in order to avoid contaminations in section 1 of the SMBR unit, so the outlet streams from the different separation units were used in different sections of the SMBR unit. Like this, the stream #1 was added to the feed stream of the SMBR while the stream #2, provided by the pervaporation unit, water free was added to the eluent stream (#3). Comparing this scenario with the others, this seems to be the best choice for this process, since it presents good reaction conversion and excellent extract purity for the maximum productivity and saving a significant amount of n-butanol (96.0 %).

In order to provide a more objective analysis regarding the energy requirements associated with the separation units included in the studied processes, a simple estimation of the energy demand per kg of BAc produced was carried out. For this purpose, the SMBR was considered to operate under isothermal conditions, the reboiler duty was obtained from ASPEN PLUS simulations (Version 8.6), the non-isothermal model used to describe the pervaporation unit allowed to determine its energy requirements and all the thermophysical data necessary were obtained from the open literature [38] (see *Appendix E*). As expected, scenario ER2 presented the lowest energy demand, consuming 1.8×10^3 $kJ.kg_{BAc}^{-1}$. In contrast, the worst performance was achieved with the configuration of scenario ER1.1 with a total energy consumption 2.5 times larger than scenario ER2. These results reveal, once again, the relevance of recycling stream #2, which not only allows to save a significant amount of desorbent, as it reduces the energy necessary to increase the temperature of the desorbent stream, since the outlet stream of the membranes module presents a high flow rate and its temperature is close to 363 K, the operating temperature of the SMBR. Furthermore, scenario ER1 and scenario ER1.1 present lower extract purities implying larger and more expensive pervaporation membrane modules, which also increases n-butanol recovery costs.

As previously stated, reactive distillation has been reported as an efficient alternative to the conventional process for the production of BAc (which comprises two homogeneously catalysed reactors and three distillation columns), reducing in more than 10% its production costs. Moreover, by coupling reactive distillation with a liquid-liquid

phase separator the costs reduction can reach 37 % [39]. Following the strategy previously described for the estimation of the process energy consumption it was possible to determine that these two alternatives would require approximately 2.0 x 10^3 and 1.7 x 10^3 $kJ.kg_{BAc}^{-1}$, respectively. Hence, the industrial process proposed in this Chapter for the production of BAc, particularly the configuration that corresponds to the scenario ER2, demonstrated to be a competitive and environmental friendly alternative process for the BAc synthesis.

5.5. Conclusions

A new process intensification based approach for butyl acrylate synthesis was studied and butyl acrylate was produced by Simulated Moving Bed Reactor technology over Amberlyst-15 ion exchange resin for the first time. The process was assessed numerically at pilot and industrial scales through a proposed mathematical model, which was validated with different experimental runs at 323 K (maximum operating temperature of the pilot scale unit).

A SMBR unit was sized at industrial scale and the ideal design and operating parameters were found. Reference cases were selected ensuring complete regeneration of the resin (in section 1) and eluent/desorbent (in section 4) with Q_{EL} = 122 $mL.min^{-1}$, Q_{Rec} = 24 $mL.min^{-1}$, Q_F = 5 $mL.min^{-1}$ and Q_{Ext} = 118 $mL.min^{-1}$ at pilot scale and 363 K, while at industrial scale the reference case is the following: Q_{EL} = 2397 $L.min^{-1}$, Q_{Rec} = 475 $L.min^{-1}$, Q_F = 118 $L.min^{-1}$ and Q_{Ext} = 2315 $L.min^{-1}$, at the same temperature.

The reactive separation region was determined at 363 K based on the equilibrium theory and the effect of the temperature and the feed molar ratio were studied. Increasing the feed molar ratio increased the desorbent consumption and decreased the productivity, while increasing the temperature improved the separation process.

The composition profiles were analysed showing great performance parameters, a reaction conversion of 99.5 % was obtained with extract and raffinate purities of 99.3 % and 99.8 %, respectively. The effects of configuration and switching time on the

performance parameters were studied, concluding that the ideal parameters are 3.1 min as switching time and 2-4-4-2 as configuration of the Simulated Moving Bed Reactor.

In addition, downstream units were also sized: a distillation column, to treat the raffinate stream, with approximately 40 m of length and 1.9 m of diameter, which allows to obtain a bottom-stream with 99.9 mol % of butyl acrylate purity and a top-stream rich in n-butanol (96.4 mol %); and a pervaporation membrane unit, to treat the extract stream, with a required area of 649 m^2 to get a retentate stream with 99.9 mol % of n-butanol purity.

Finally, the global process was simulated at industrial scale with n-butanol recovery taking into account several possible scenarios, from which ER2 showed to be the best eluent recovery strategy: adding the top stream from the distillation column to the SMBR feed and the retentate stream from the pervaporation unit to the eluent SMBR stream. The final global process showed a very competitive production capacity of 51,500 $t_{BAc}.year^{-1}$ recycling almost all the n-butanol used as eluent.

In summary, in this Chapter an alternative process for the butyl acrylate synthesis was proposed, in which the number of units required was reduced comparing to the conventional process. Moreover, a more environmental friendly catalyst was used (Amberlyst-15 ion exchange resin), which is easier to separate, leading to a reduction of the energy required to purify the target product (butyl acrylate).

5.6. Notation

Abbreviations

AAc	Acrylic Acid	-
A-15	Amberlyst-15 ion exchange resin	-
BAc	Butyl Acrylate	-
DC	Distillation Column	-
EL	Eluent	-
ER	Eluent Recovery	-
FBR	Fixed-Bed Adsorptive Reactor	-

gPROMS	General Process Modelling System	-
Rec	Recycle	-
RSR	Reactive Separation Region	-
SMB	Simulated Moving Bed	-
SMBR	Simulated Moving Bed Reactor	-
SR	Separation Region	-

Symbols

a	Liquid phase activity	-
B	Flow rate relative to bottom	-
C	Liquid phase concentration	$mol.m^{-3}$
$Conv$	Reaction Conversion	%
$\overline{C}_p$	Average liquid phase concentration inside the particle	$mol.m^{-3}$
C_T	Total liquid phase concentration	$mol.\ m^{-3}$
C_{ret}	Liquid phase concentration in the retentate membrane	$mol.\ m^{-3}$
D_{ax}	Axial dispersion coefficient	$m^2.s^{-1}$
$DesC$	Desorbent Consumption	$m_{n\text{-}butanol}^3.kg_{BAc}^{-1}$
d_{int}	Column/Membrane internal diameter	m
D_M	Molecular diffusivity	$m^2.s^{-1}$
d_p	Particle diameter	m
F	Feed flow rate (relative to distillation unit)	$m^3.min^{-1}$
Eff	Tray efficiency	-
H_{tower}	Tower height	m
H_{tray}	Height of each tray	m
K_i	Langmuir equilibrium parameter	$m^3.mol^{-1}$
k_i	Internal mass transfer coefficient	$m.s^{-1}$
k_e	External mass transfer coefficient	$m.s^{-1}$
k_c	Reaction kinetic constant	$mol.kg^{-1}.min^{-1}$
K_{eq}	Equilibrium constant	-

$K_{s,D}$	Adsorption constant relative to compound D	-
k_L	Global mass transfer coefficient	$m.s^{-1}$
$k_{ov,i}$	Global membrane mass transfer coefficient	$kg.(m^{-2}.h^{-1}.bar^{-1})$
L_{tower}	Tower length	m
L_b	Bed length	m
MM	Molecular mass	$kg.mol^{-1}$
n	Number of compounds	-
N	Theoretical number of trays	-
N_{actual}	Actual number of trays	-
N_F	Feed tray	-
P_e	Peclet number	-
P_{Ext}	Extract Purity	%
P_{Raff}	Raffinate Purity	%
$Prod$	Productivity	$kg_{BAc}.(m_{ads}^{-3}.day^{-1})$
$\overline{q}$	Average solid phase concentration in equilibrium with $\overline{C}_p$	$mol.m_{res}^{-3}$
Q	Volumetric flow rate	$m^3.min^{-1}$
Q^*	A fraction of the volumetric flow rate	$m^3.min^{-1}$
Q_i	Molar adsorption capacity ($Q_i = Q_v / V_{M,i}$)	$mol.m_{res}^{-3}$
Q_m	Membrane permeance	$kg.(m^{-2}.h^{-1}.bar^{-1})$
Q_v	Volumetric monolayer capacity	$m^3.m_{res}^{-3}$
R	Ideal Gas constant	$J.mol^{-1}.K^{-1}$
r	Reaction rate	$mol.kg^{-1}.min^{-1}$
r_p	Particle radius	m
Re_p	Reynolds number relative to the particle	-
Sc	Schmidt number	-
Sh_p	Sherwood number relative to the particle	-
T	Temperature	K
u	Interstitial liquid velocity	$m.s^{-1}$
u_s	Superficial velocity	$m.s^{-1}$

U_s	Solid velocity	$m.s^{-1}$
V_M	Molar volume in the liquid phase	$m^3.mol^{-1}$
x	Liquid phase molar fraction	-
x_B	Composition of the light compound in bottom	-
x_D	Composition of the light compound in distillate	-
y	Vapour phase molar fraction	-
z_F	Composition of the light compound in the feed	-

Greek Letters

α	Relative volatility	-
α_m	Selectivity relative to pervaporation process	-
γ	Interstitial velocities ratio	-
δ	Membrane thickness	m
ε	Bulk porosity	-
ε_p	Catalyst/adsorbent particle porosity	-
η	Fluid viscosity	$kg.m^{-1}.s^{-1}$
η_m	Mixture viscosity	$kg.m^{-1}.s^{-1}$
ρ	Fluid phase density	$kg.m^{-3}$
ρ_b	Bulk density	$kg.m^{-3}$

Subcripts

0	Relative to initial conditions	-
EL	Relative to eluent	-
Ext	Relative to extract	-
F	Relative to feed	-
j	Relative to a section of SMBR unit	-
m	Membrane	-
out	At the outlet of the fixed-bed column	-
p	Relative to particle	-
perm	Permeate	-

perv	Pervaporation	-
Raff	Relative to raffinate	-
Rec	Relative to recycle	-
ret	Relative to retentate	-

5.7. References

1. Gonçalves, J. C.; Rodrigues, A. E., Simulated moving bed reactor for p-xylene production: Dual-bed column. *Chemical Engineering and Processing: Process Intensification* **2016,** 104, 75-83.

2. Hashimoto, K.; Adachi, S.; Noujima, H.; Ueda, Y., A new process combining adsorption and enzyme reaction for producing higher-fructose syrup. *Biotechnology and Bioengineering* **1983,** 25, (10), 2371-2393.

3. Mazzotti, M.; Storti, G.; Morbidelli, M., Optimal operation of simulated moving bed units for nonlinear chromatographic separations. *Journal of Chromatography A* **1997,** 769, (1), 3-24.

4. Pereira, C. S. M.; Zabka, M.; Silva, V. M. T. M.; Rodrigues, A. E., A novel process for the ethyl lactate synthesis in a simulated moving bed reactor (SMBR). *Chem Eng Sci* **2009,** 64, (14), 3301-3310.

5. Pereira, C. S. M.; Gomes, P. S.; Gandi, G. K.; Silva, V. M. T. M.; Rodrigues, A. E., Multifunctional Reactor for the Synthesis of Dimethylacetal. *Industrial & Engineering Chemistry Research* **2007,** 47, (10), 3515-3524.

6. Graça, N. S.; Pais, L. S.; Silva, V. M. T. M.; Rodrigues, A. E., Analysis of the synthesis of 1,1-dibutoxyethane in a simulated moving-bed adsorptive reactor. *Chemical Engineering and Processing: Process Intensification* **2011,** 50, (11–12), 1214-1225.

7. Silva, V. M. T. M.; Rodrigues, A. E., Novel process for diethylacetal synthesis. *AIChE Journal* **2005,** 51, (10), 2752-2768.

8. Minceva, M.; Gomes, P. S.; Meshko, V.; Rodrigues, A. E., Simulated moving bed reactor for isomerization and separation of p-xylene. *Chemical Engineering Journal* **2008,** 140, (1–3), 305-323.

9. Kawase, M.; Inoue, Y.; Araki, T.; Hashimoto, K., The simulated moving-bed reactor for production of bisphenol A. *Catalysis Today* **1999,** 48, (1–4), 199-209.

10. Ostaniewicz-Cydzik, A. M.; Pereira, C. S. M.; Molga, E.; Rodrigues, A. E., Reaction Kinetics and Thermodynamic Equilibrium for Butyl Acrylate Synthesis from n-Butanol and Acrylic Acid. *Industrial & Engineering Chemistry Research* **2014,** 53, (16), 6647-6654.

11. Lode, F.; Houmard, M.; Migliorini, C.; Mazzotti, M.; Morbidelli, M., Continuous reactive chromatography. *Chemical Engineering Science* **2001,** 56, (2), 269-291.

12. Ruthven, D. M., *Principles of Adsorption and Adsorption Processes*. Wiley & Sons: New York, 1984.

13. Arkema, http://www.arkema.com/export/shared/.content/media/downloads/products-documentations/acrylicmonomers/tds-butyl-acrylate.pdf (Accessed on June 2014).

14. Storti, G.; Mazzotti, M.; Morbidelli, M.; Carrà, S., Robust design of binary countercurrent adsorption separation processes. *AIChE Journal* **1993,** 39, (3), 471-492.

15. Rodrigues, A.; Pereira, C.; Minceva, M.; Pais, L. S.; Ribeiro, A.; Ribeiro, A. M.; Silva, M.; Graça, N.; Santos, J. C., *Simulated Moving Bed Technology: Principles, Design and Process Applications*. Elsevier Science 2015.

16. Minceva, M.; Rodrigues, A. E., Simulated moving-bed reactor: Reactive–separation regions. *AIChE journal* **2005,** 51, (10), 2737-2751.

17. Graça, N. S.; Pais, L. S.; Silva, V. M. T. M.; Rodrigues, A. E., Thermal effects on the synthesis of acetals in a simulated moving bed adsorptive reactor. *Chemical Engineering Journal* **2012,** 207–208, (0), 504-513.

18. Research, T. M., Global Butyl Acrylate Market:Transparency Market Research. https://globenewswire.com/news-release/2018/09/03/1564510/0/en/Global-Butyl-Acrylate-Market.html. (Accessed on September 2018).

19. Minceva, M.; Rodrigues, A. E., Two-level optimization of an existing SMB for p-xylene separation. *Computers & Chemical Engineering* **2005,** 29, (10), 2215-2228.

20. Douglas, J. M., *Conceptual design of chemical processes*. McGraw-Hill: 1988.

21. Zeng, K.-L.; Kuo, C.-L.; Chien, I. L., Design and control of butyl acrylate reactive distillation column system. *Chemical Engineering Science* **2006,** 61, 4417-4431.

22. Ho, F.; Julka, V. Processes for refining butyl acrylate. US 6605738 B1, 2003.

23. Jana, A. K., *Process Simulation And Control Using Aspen*. Prentice-Hall Of India Pvt. Limited: 2009.

24. Turner, K., *Effective Industrial Membrane Processes: Benefits and Opportunities*. Springer Netherlands: 2012.

25. Baker, R. W., *Membrane Technology and Applications*. Wiley: 2004.

26. Huang, R. Y. M., *Pervaporation membrane separation processes*. Elsevier: 1991.

27. Sommer, S.; Melin, T., Influence of operation parameters on the separation of mixtures by pervaporation and vapor permeation with inorganic membranes. Part 1: Dehydration of solvents. *Chemical Engineering Science* **2005,** 60, (16), 4509-4523.

28. Guo, W. F.; Chung, T.-S.; Matsuura, T., Pervaporation study on the dehydration of aqueous butanol solutions: a comparison of flux vs. permeance, separation factor vs. selectivity. *Journal of Membrane Science* **2004,** 245, (1–2), 199-210.

29. Boutikos, P.; Pereira, C. S. M.; Silva, V. M. T. M.; Rodrigues, A. E., Performance evaluation of silica membrane for water–n-butanol binary mixture. *Separation and Purification Technology* **2014,** 127, (0), 18-28.

30. Sommer, S.; Melin, T., Performance evaluation of microporous inorganic membranes in the dehydration of industrial solvents. *Chemical Engineering and Processing: Process Intensification* **2005,** 44, (10), 1138-1156.

31. Pereira, C. S. M.; Silva, V. M. T. M.; Rodrigues, A. E., Green Fuel Production Using the PermSMBR Technology. *Industrial & Engineering Chemistry Research* **2012,** 51, (26), 8928-8938.

32. Genduso, G.; Luis, P.; Van der Bruggen, B., 19 - Pervaporation membrane reactors (PVMRs) for esterification. In *Membrane Reactors for Energy Applications and Basic Chemical Production*, Basile, A.; Di Paola, L.; Hai, F. I.; Piemonte, V., Eds. Woodhead Publishing: 2015; pp 565-603.

33. Kujawski, W., Application of Pervaporation and Vapor Permeation in Environmental Protection. *Polish Journal of Environmental Studies* **2000,** 9, (1), 13-26.

34. Wijmans, J. G.; Athayde, A. L.; Daniels, R.; Ly, J. H.; Kamaruddin, H. D.; Pinnau, I., The role of boundary layers in the removal of volatile organic compounds from water by pervaporation. *Journal of Membrane Science* **1996,** 109, (1), 135-146.

35. Lévêque, A., *Les Lois de la transmission de chaleur par convection*. Dunod: 1928.

36. Welty, J.; Wicks, C.; Wilson, R.; Rorrer, G., *Fundamentals of Momentum, Heat, and Mass Transfer*. John Wiley & Sons: New York, 2008.

37. Noble, R. D.; Stern, S. A., *Membrane Separations Technology: Principles and Applications*. Elsevier Science: 1995.

38. Yaws, C. L., *Thermophysical Properties of Chemicals and Hydrocarbons (Electronic Edition)*. Knovel 2010.

39. Niesbach, A.; Kuhlmann, H.; Keller, T.; Lutze, P.; Górak, A., Optimisation of industrial-scale n-butyl acrylate production using reactive distillation. *Chem Eng Sci* **2013,** 100, 360-372.

6. Enhanced Simulated Moving Bed Reactor

A novel process design based on the simulated moving bed technology for the synthesis of butyl acrylate was investigated in order to get a more competitive industrial process. For that, a fixed-bed adsorptive reactor was coupled with a simulated moving bed reactor. Reactive separation regions were determined for different conditions of process configurations and feed compositions allowing to find the optimal operating parameters for the respective process. Besides that, the process integration was analysed with different configurations for the desorbent (n-butanol) recovery and ensuring the minimal butyl acrylate purity commercially required (99.5 wt. %).

This Chapter is adapted from Constantino, D. S. M.; Pereira, R. P. V.; C. S. M.; Faria; Loureiro, J. M.; Rodrigues, A. E., Enhanced Simulated Moving Bed Reactor Process for Butyl Acrylate Synthesis: Process Analysis and Optimization. *Ind. Eng. Chem. Res.* 2016, 55 (40), pp 10735-10743. DOI: 10.1021/acs.iecr.6b02474.

6.1. Introduction

A detailed study of butyl acrylate (BAc) synthesis over Amberlyst-15 ion exchange resin in simulated moving bed reactor (SMBR) was reported in the previous Chapter, where promising results were presented revealing a competitive production capacity at industrial scale (51,500 $t_{BAc}.year^{-1}$). For that, the ideal operating parameters to achieve high separation performance with reduced costs were found according to the reactive-separation region (RSR) determined. The data showed that the separation region (SR) is much larger than the respective RSR allowing to conclude that the process is severely limited by the chemical reaction due to the slow kinetics of this system, as mentioned in literature [1]. Accordingly, the reactants, n-butanol and acrylic acid (AAc), require long residence time in sections 2 and 3 of the SMBR (between the extract and raffinate streams) in order to completely convert the limiting reactant (AAc). Otherwise, this compound will preferentially contaminate the raffinate stream, since the resin selectivity between AAc and BAc is smaller than the one between AAc and water. This fact implies that the process can only operate under low feed flow rates leading to a negligible or not competitive production capacity.

Recently, Seidel-Morgenstern and his group reported a system for the continuous synthesis and purification of complex reaction mixtures using the SMB technology. A layout based on a tubular reactor with a multi-column chromatographic separation process was successfully studied for the nucleophilic aromatic substitution reaction of 2,4-difluoronitrobenzene with morpholine under continuous flow conditions [2]. However, up to now, no esterification reaction has been investigated with this methodology.

In this Chapter, the study of a similar configuration is performed for the first time in an attempt to overcome the limitations imposed by the slow reaction kinetics of the esterification reaction between n-butanol and AAc, instead of the nucleophilic aromatic substitution reaction studied by Seidel-Morgenstern et al. [2]. The main objective is to attain a better performance (less desorbent consumption and higher productivity with the same target product purity, $\geq$ 99.5%) than the obtained with the previously studied technologies, including the conventional SMBR process. This novel concept consists in coupling a fixed-bed adsorptive reactor (FBR) with a SMBR unit. Thus, the reaction takes

place firstly in the FBR and after the reaction equilibrium is reached, the outlet stream of the FBR is introduced in the SMBR unit, which works, essentially, as separation unit turning it into a more efficient process (with higher purity and lower costs) according to the SR determined in advance for this system (Chapter 5). This design strategy tends to be even more efficient since it is possible to achieve the complete conversion of unreacted AAc from the FBR, by extending the reaction with the eluent/reactant (n-butanol) that is inside of the SMBR, while the separation occurs, simultaneously. Another advantage of this configuration is that it allows operate under higher feed flow rates than in the previous process (conventional SMBR) leading to higher production capacities and lower desorbent consumptions. Finally, the process optimization was performed considering the energy consumption for different eluent recovery strategies.

6.2. Results and Discussion

6.2.1. Process design

Despite the promising results of the conventional SMBR process at industrial scale reported in the previous Chapter, a better performance can be achieved taking advantage of the SMB technology integrated with other coupled reaction process. Indeed, when the RSR of a SMBR unit fed with an equimolar mixture of AAc and n-butanol (the reactants for producing BAc) is compared with a hypothetical SR of a purely separative SMB unit fed with an equimolar of BAc and water (the products of this esterification reaction) it is clear that the performance of the unit was severely conditioned by the equilibrium-limited reaction. According to the literature [1], this system presents a very slow kinetics, $k_{c,363K} = 3.51\times10^{-3} mol.g_{A15}^{-1}.\min^{-1}$, so long residence times in the reaction zone of the SMBR (sections 2 and 3) are required which implies working under low feed flow rates in order to achieve reasonable reactants conversions, leading to a lower production capacity. Therefore, an SMB process coupled with another sorption enhanced reaction process can be more advantageous than the conventional SMBR. It has a much higher productivity and it needs less desorbent to reach the same final product purity. In this

context, a new process design was considered and the SMBR process was revaluated in order to take full advantage of that technology potential for the synthesis of BAc. The new process design proposal consists in adding a FBR before the SMBR, as shown in Figure 6.1, keeping the remaining units as suggested in the previous process design studied (see Chapter 5). Thus, the esterification reaction between AAc and n-butanol takes place, firstly, in the FBR and, according to Figure 6.1, the outlet stream of the FBR at equilibrium conditions is directly connected to the SMBR where the separation of the extract and raffinate streams occurs. Furthermore, practically all unreacted AAc from the first reactor (FBR) is then consumed in the second one (SMBR), where there is n-butanol in excess, since this reactant is also used as eluent/desorbent. Afterwards, a pervaporation unit (PERV) and a distillation column are used as separation units for the outlet streams treatment, extract and raffinate, respectively. Then, the operating parameters of each unit were optimised to assess if it would be possible to achieve a better performance than the one obtained previously with the conventional SMBR process (Chapter 5): same raffinate purity ($P_{Raff} \geq 99.5$ %) with higher productivity and less desorbent consumption. Each unit was optimised in terms of dimensions and operating parameters, considering different scenarios for eluent recovery, which will be discussed in Section 6.2.3.2. However, the dimensions of SMBR at industrial scale obtained in the previous Chapter were kept in order to set a reference for performance data comparison (12 columns with a length of 0.615 m and a diameter of 2.23 m).

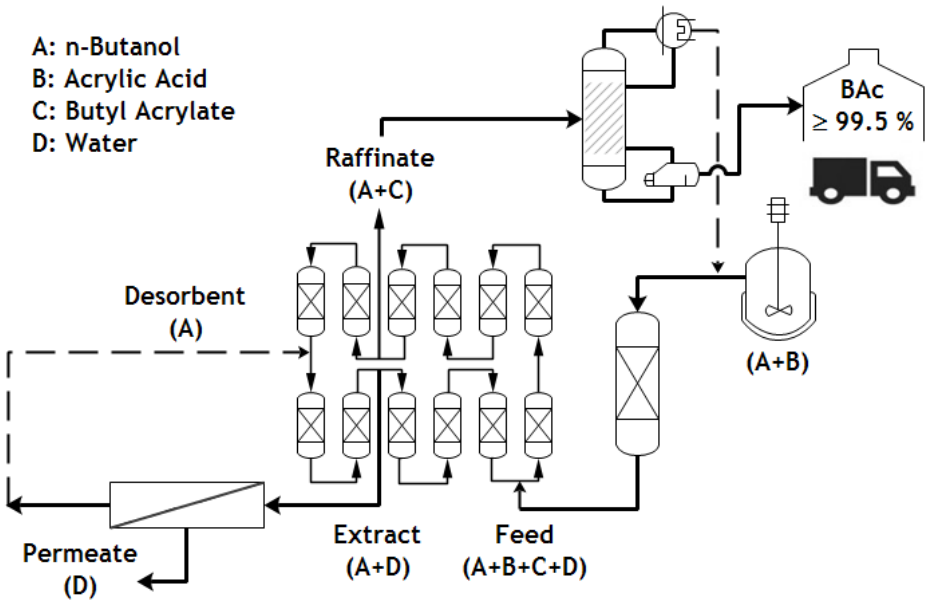

Figure 6.1. New process plant design (enhanced SMBR) for BAc synthesis.

6.2.2. SMBR optimisation

For the evaluation of the process feasibility, the determination of the design parameters is mandatory. Therefore, firstly, it is essential to know its design and configuration. As previously mentioned, in order to compare the production capacity of the conventional SMBR and actual process designs, equivalent SMBR dimensions were considered in both studies. In the previous case (conventional reactor), the optimisation was performed by determining the RSR at different conditions. The best performance was achieved by using a configuration 2-4-4-2, two columns for section 1, four columns for section 2 and 3 and, two columns for section 4, respectively, and a switching time of 3.1 minutes at 363 K, reaching a limiting reactant conversion of 99.5 % and a raffinate purity of 99.9 %. The annual production capacity reached with that process was about of 51,500 $t_{BAc}.year^{-1}$, consuming 1.0 $L_{n\text{-}Butanol}.kg_{BAc}^{-1}$ (after recycling all possible eluent from the raffinate and the extract streams). In this case (enhanced SMBR), the same procedure was followed for the process optimisation. The RSRs were determined for different SMBR configurations, considering that the feed stream is composed by a reaction mixture in equilibrium conditions coming from FBR (which was previously feed with a mixture of n-butanol/AAc with the molar ratio of (1:2)) instead of an equimolar composition of the reactants as considered in conventional SMBR. For each configuration, the operating optimal point of the respective RSR was determined by changing γ_2 and γ_3 (ratio of interstitial liquid and simulated solid velocities in the section 2 and 3 of the SMBR, respectively), in order to find the maximum feed flow rate that allows to obtain the desired separation (BAc purity ≥ 99.5 %, free eluent basis), which corresponds to the vertex of the region [3]. This procedure is performed for a fixed values of γ_1 = 9.10 and γ_4 =1.52, as determined by the equilibrium theory applying a safety factor of 5 %. The RSRs determined for the proposed process strategy (FBR coupled with SMBR) are presented in Figure 6.2, as well as the RSR obtained for the conventional SMBR in order to allow a direct comparison between the two process designs.

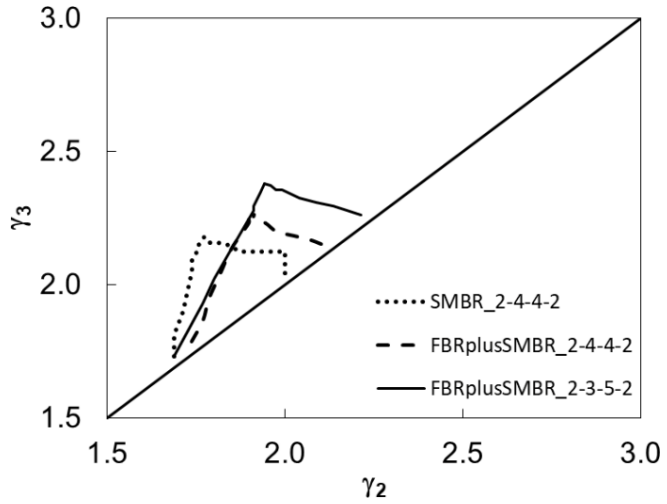

Figure 6.2. Reactive Separation Region for Enhanced SMBR process (FBR coupled with SMBR) using two different configurations (2-4-4-2 and 2-3-5-2) and optimal RSR for the conventional SMBR process. Raffinate purity criteria ≥ 99.5 % (solvent-free basis).

Analysing the Figure 6.2, it is possible to conclude that coupling the FBR with the SMBR can enhance the BAc production. Comparing the different configurations studied for the FBR plus SMBR process design, it is noticeable that the most efficient performance is achieved when the configuration 2-3-5-2 is used. Due to the relatively low selectivity of the resin between BAc and AAc, it is necessary to increase the number of columns in section 3 in order to avoid the contamination of the raffinate stream with AAc. That way, this configuration is more suitable for this system allowing to work with higher feed flow rate ensuring the required purity specifications leading to higher productivity and less desorbent consumption.

A sensitivity analysis to the flow rate ratios between the liquid and the solid phases of sections 1 and 4 (the critical sections for the SMBR operation), was made aiming to maximize the process performance. As described in Chapter 5 (Section 5.4.1), through the Equilibrium Theory, the most widely used methodology for the determination of these parameters, a value of 9.10 is determined for the flow rate ratio in section 1 (γ_1) and 1.52 in section 4 (γ_4), respectively, assuming that no chemical reaction takes place in those sections. The sensitivity analysis was carried out by varying γ_1 from -6 % to 4 % and γ_4 from -2 % to 2 %. Since the SMBR dimensions and the switching time (t^*) were kept

constant, consequently and according to equation (6.1), the solid velocity (U_s) remains constant. Therefore, the flow rate ratios in each section were changed varying the liquid flow rate in that section, according to the equations from (6.2) to (6.6). The solid velocity is determined by equation (6.1):

$$U_s = \frac{L_b}{t^*} \tag{6.1}$$

where L_b is the column length, and the relation between the liquid and solid velocity in each section is given by:

$$\gamma_j = \frac{u_j}{U_s} = \frac{Q_j}{A\varepsilon U_s} \tag{6.2}$$

where u_j and Q_j represent the liquid velocity and the volumetric flow rate in the section *j* (1 to 4), respectively.

In turn, the flow rate of each section is given by the following equations:

$$Q_1 = Q_{EL} + Q_{Rec} \tag{6.3}$$

$$Q_2 = Q_1 - Q_{Ext} \tag{6.4}$$

$$Q_3 = Q_2 + Q_F \tag{6.5}$$

$$Q_4 = Q_3 - Q_{Raff} = Q_{Rec} \tag{6.6}$$

For each pair of γ_1 and γ_4 a new RSR was determined. The respective optimal points in terms of productivity and desorbent consumption are represented in Figure 6.3 (a) and b), respectively, which show that the effect on the process productivity (on the left) promoted by changing γ_1 in the range of -4% to 4% relative to the equilibrium theory value (keeping γ_4) is almost negligible. Nevertheless, looking at the desorbent consumption (on the right), there is an evident minimum consumption when γ_1 is decreased by 4 % and the Equilibrium Theory value is kept for γ_4 (1.52).

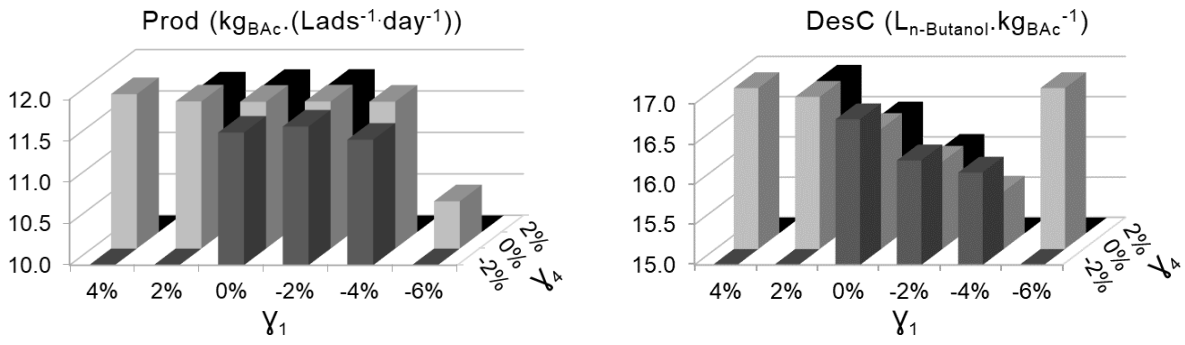

a) b)

Figure 6.3. Sensitivity analysis to γ_1 and γ_4 using a 2-3-5-2 configuration: a) Productivity data ($k_{BAc}.(L_{Ads}^{-1}.day^{-1})$) and b) Desorbent consumption ($L_{n\text{-}butanol}.kg_{BAc}^{-1}$). 0% corresponds to the original values obtained from the Equilibrium Theory (γ_1 = 9.10 and γ_4 =1.52).

The operating and performance parameters obtained along this study are summarized in Table 6.1 together with the values previously determined for the conventional SMBR (first column).

Table 6.1. Operating and performance parameters optimised for Enhanced SMBR vs Conventional SMBR at 363 K.

Process	Conventional SMBR	Enhanced SMBR			
Parameters/Configuration	2-4-4-2	2-4-4-2	2-3-5-2	2-3-5-2 sensitivity analysis	2-3-5-2 sensitivity analysis with S.F.
Q_F ($L.min^{-1}$)	118	110	138	138	130
Q_{Ext} ($L.min^{-1}$)	2315	2265	2256	2145	2148
Q_{EL} ($L.min^{-1}$)	2397	2390	2390	2280	2280
Q_{Rec} ($L.min^{-1}$)	475	478	478	478	478
$C_{n\text{-}butanol,F}$ ($mol.L^{-1}$)	5.76	0.57	0.57	0.57	0.57
$C_{AAc,F}$ ($mol.L^{-1}$)	5.76	4.56	4.56	4.56	4.56
$C_{BAc,F}$ ($mol.L^{-1}$)	-	3.47	3.47	3.47	3.47
$C_{Water,F}$ ($mol.L^{-1}$)	-	3.47	3.47	3.47	3.47
P_{Ext} (%)	99.3	99.5	99.6	99.6	99.6
P_{Raff} (%)	99.8	99.6	99.6	99.5	99.7
Conv. (%)	99.5	98.9	99.0	99.0	99.3
Prod ($kg_{BAc}.(L_{ads}^{-1}.day^{-1})$)	7.22	9.39	11.8	11.8	11.1
DesC ($L_{n\text{-}Butanol}.kg_{BAc}^{-1}$)	27.6	20.8	16.5	15.7	16.7

The second and third columns of Table 6.1 correspond to the vertex of the RSR (optimal point) for the enhanced SMBR process (FBR plus SMBR) using the configurations 2-4-4-2 and 2-3-5-2, respectively. It is possible to increase the productivity by 25% with the 2-3-5-2 configuration and to decrease the desorbent consumption by approximately 20%. After the sensitivity analysis performed to γ_1 and γ_4, it was possible to decrease the desorbent consumption even further (5% less n-butanol is required). On the other hand, if these operating parameters were implemented at real industrial scale, this process would be working under a very sensitive set of conditions with respect to the raffinate purity. Any disturbance on the optimal operating parameters (such as slight variations of the feed stream composition or fluctuations on the flow rate of the inlet and outlet streams of the SMBR, for instance) might lead to the contamination of the raffinate, making it impossible to obtain BAc with the required specifications (minimum purity of 99.5%). Therefore, a security factor (S.F.) must be applied to some of the most relevant

operating parameters (feed and extract flow rates) in order to get a reliable set of operating conditions, which can be observed on the right column in Table 6.1 (2-3-5-2 after sensitivity analysis with S.F.). Accordingly, in this case, a S.F. of (-0.5) % and (-1.5) % were applied to γ_2 and γ_3, respectively.

Afterwards, the optimal operating conditions found for the enhanced SMBR (on the right column of Table 6.1) were used to obtain the respective concentration profiles, which are shown in Figure 6.4 together with the concentration profile obtained with the conventional SMBR process.

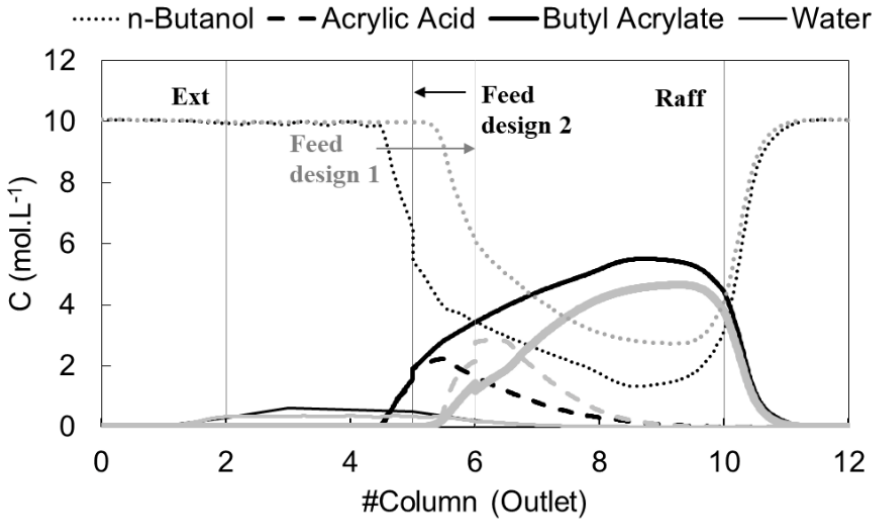

Figure 6.4. Concentration profiles in the conventional SMBR and enhanced SMBR at cyclic steady state (21st cycle) and 363 K using $t^* = 3.1$ min (all operating conditions are presented in Table 6.1). Grey profile corresponds to the conventional SMBR study (Feed design 1 = 2-4-4-2) and the black one corresponds to the enhanced SMBR (Feed design 2 = 2-3-5-2).

Comparing both profiles, it can be concluded that there was an evident extension of the reaction in the enhanced SMBR strategy (FBR plus SMBR), as intended. In section 3, it is possible to observe a sudden decrease in n-butanol concentration, since this is the section where the reaction between the AAc and n-butanol occurs yielding BAc and water. Furthermore, according to the adsorption data measured over Amberlyst-15 (see *Chapter 3*), this resin is more selective to water than to BAc and, because of that, this

compound is present inside the unit at higher concentrations. Indeed, this is one of the advantages of SMBR since the reaction and adsorption occur simultaneously.

6.2.3. Process integration and optimisation

The process integration was studied in order to assess the feasibility of the global process design suggested in this Chapter. For that, all remaining units presented in Figure 6.1 were dimensioned: the FBR and the downstream units to treat the outlet streams of SMBR. All data are presented below.

6.2.3.1. Dimensioning of FBR

A FBR operating at 363 K was simulated according to the mathematical model described in Chapter 3 (see Section 3.3). For that, a feed solution comprising a n-butanol/AAc mixture with the molar ratio of (1:2) was considered as previously, at the same optimal feed flow rate (130 $L.min^{-1}$) found for the enhanced SMBR with a 2-3-5-2 configuration after the sensitivity analysis and the application of S.F. in γ_2 and γ_3.

The respective dimensions needed to reach the equilibrium conversion were determined and they are presented in Table 6.2, together with the characteristics of the adsorbent/catalyst used. The ratio between the diameter and the length (d_{int}/L_b = 3.6) of each column of the industrial SMBR configuration was kept for FBR unit to avoid differences on the bed properties.

Table 6.2. Characteristics of the FBR and resin (Amberlyst-15) used in simulation runs.

Parameter	Value
Column length (L_b), m	2.00
Column internal diameter (d_{int}), m	7.25
Resin particle porosity (ε_p)	0.360
Bed porosity (ε)	0.410
Resin Particle radius (r_p), µm	375
Bulk density (ρ_b), kg m^{-3}	400

Then, a simulation run was performed considering the reaction data measured for BAc system over the ion exchange resin Amberlyst-15 that is available in the open literature [1] and the multicomponent adsorption data determined in Chapter 3 (Table 3.3). The concentration histories are shown in Figure 6.5.

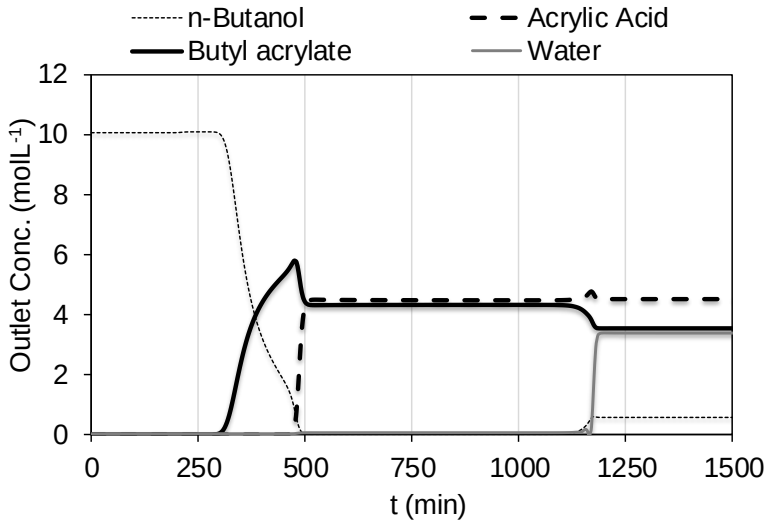

Figure 6.5. Concentration histories at the outlet of the FBR initially saturated with n-butanol and fed with a mixture of n-butanol/AAc ($C_{n\text{-}butanol,F}$ = 4.06 mol.L^{-1} and $C_{AAc,F}$ = 8.06 mol.L^{-1}); Q_F = 130 L.min^{-1} and T = 363 K.

Contrarily to the conventional SMBR process, in this case it is possible to use AAc in excess in the feed stream, since it enters diluted in SMBR (outlet stream of FBR) avoiding raffinate contamination with AAc, as shown in the concentration histories presented in Figure 6.5. Initially, the reactor is saturated with the eluent (n-butanol) that acts also as reactant. As the feed mixture enters the reactor, the AAc is consumed producing BAc and water. When the steady state is achieved, a mixture almost at equilibrium conditions is obtained, composed by 4.8 % of n-butanol, 37.8 % of AAc and 28.7 % of BAc and water. This outlet stream is, then, fed to the SMBR unit.

6.2.3.2. Eluent recovery

Additional separation units were studied to treat the outlet streams of the SMBR, the raffinate and extract streams, composed by n-butanol and BAc and n-butanol and water, respectively. After analysing the concentration profiles of the SMBR and determining its outlet streams compositions it is possible to design the complementary separation units in order to get the desired product purity (BAc, ≥ 99.5 %). Furthermore, through the process integration it is possible to study the eluent recovery enabling to evaluate the process sustainability. So, the raffinate stream of the SMBR comprises 50.7 mol.% of n-butanol and 49.1 mol.% of BAc while the remaining composition corresponds to impurities of AAc and water (0.02 %). Thus, a distillation column was considered to treat this stream and a similar procedure to the previous study (Chapter 5) was followed aiming to determine the optimised parameters required to perform the desired separation. Accordingly, ASPEN PLUS (Version 8.6) was used to simulate this unit using the RadFrac method (after a first estimation with the DSTWU method, as previously done in Chapter 5). In summary, the inputs for this simulation method are the feed volumetric flow rate (F), temperature (T), number of trays (N), feed stage (N_F), reflux ratio (R_{actual}) and the bottom to feed ratio besides the molar feed composition. The main process operating parameters of the distillation column are displayed in Table 6.3 while the input and final parameters obtained with Radfrac method are presented in Table 6.4, respectively.

Table 6.3. Process operating parameters of the distillation column for the raffinate treatment in the enhanced SMBR process.

F (L.min^{-1})	Z_F	X_D	X_B	D (L.min^{-1})	B (L.min^{-1})
262	0.491	0.990	0.005	98.9	101.5

Table 6.4. Input and output data of the distillation column simulation using RadFrac method.

Parameter	Input value	Parameter	Output value
N	29	BAc purity (bottom), mol. %	99.7
N_F	19	n-butanol purity (top), mol. %	95.6
R_{actual}	1.70	Reboiler duty, J.s^{-1}	2.10×10^6
Condenser	total		
bottoms to feed ratio	0.96		

The final parameters were calculated based on equations (5.40) to (5.42), which are described in Chapter 5 (see Section 5.4.6.1) and, they are presented in Table 6.5.

Table 6.5. Final parameters required for the distillation unit to treat the raffinate stream from enhanced SMBR.

N_{actual}	H_{tower} (m)	L_{tower} (m)	D_{tower} (m)	H_{tray} (m)
41.4	29.0	34.9	1.55	0.70

Analysing the results, the dimensions of the distillation column required for this process (enhanced SMBR) are smaller than the dimensions of the distillation column determined for conventional SMBR (34.9 x 1.55) m instead of (39.7 x 1.92) m, reducing also the required energy consumption. These facts are due to the differences in the molar compositions of the raffinate stream obtained in SMBR of the different design processes, since BAc is more concentrated in raffinate stream coming from the enhanced SMBR (FBR plus SMBR).

Under optimum conditions, the BAc purity obtained on the bottom stream of the distillation column reached 99.7 % while the n-butanol obtained on top stream presented a purity of 95.6 %. Furthermore, it is possible to conclude that the process design strategy studied in this Chapter is able to produce 67,000 $t_{BAc}.year^{-1}$ by feeding 262 $L.min^{-1}$ (total raffinate flow rate) to this distillation column. This represents a production capacity 30 % higher than the production capacity of the previous process design configuration (conventional SMBR).

It is important to note that despite the high temperatures verified in the reboiler, the risk of polymerisation is low or negligible since the polymerisation reaction of AAc and BAc is initiated by radicals present in the mixture [4]. So, it is unlikely to occur in the present distillation column, because its function is limited to the separation of n-butanol and BAc in the presence of only trace amounts of AAc.

As in the previous Chapter, the length of the column was estimated to be 20 % higher than the required just for trays and the height of each tray was assumed to be 0.7 m, as mentioned in the open literature [5].

Regarding the extract stream from the enhanced SMBR unit, it presents a molar composition of 95.4 % of n-butanol and 4.6 % of water. Since the amount of water is less than 10 % [6], a pervaporation unit was considered for the n-butanol dehydration with hydrophilic membanes. This unit was investigated according to the mathematical model described in the previous Chapter (see Section 5.4.6.2). The parameters required to determine the permeance as well as the molar flux permeate, J_i, for each compound, which are essential to carry out the pervaporation process simulation, are summarized in Table 6.6.

Table 6.6. Parameters required to determine the permeance and the permeate molar flux of the pervaporation unit to treat the extract stream of the enhanced SMBR at 363 K.

Parameter/Compound	n-Butanol	Water
$Q_{memb,i,ref}$ (kg.(m^{-2} h^{-1} bar^{-1}))	0.207[a]	16.4[a]
E_i (J.mol^{-1})	20.2[a]	6.90[a]
$x_{i,F}$	0.954	0.046
$y_{i,perm}$	0.115	0.885
$P^0_{i,F}$ (bar)	0.342	0.700
P_{perm} (bar)	0.016	
T (K)	363.2	
α_m	160[b]	

[a,b] *data from Sommer's and Melin's work [7, 8].*

From Table 6.6, the permeance values, $Q_{m,i}$, can be determined at 363 K being 0.207 kg.(m^{-2} h^{-1} bar^{-1}) for n-butanol and 16.4 kg.(m^{2}·h^{-1}.bar^{-1}) for water [6]. After that, a simulation of the pervaporation process was performed considering a feed flow rate of 2148 L.min^{-1} that corresponds to the extract flow rate from SMBR unit. As a result, a module of 785 m^2 is needed, allowing to remove 97.70 % of water and to reach 99.97 wt. % of n-butanol purity (retentate).

Finally, the eluent recovery (ER) can be studied taking into account the recycling of the outlet streams obtained from the downstream units. For that, two different scenarios were investigated, ER1 and ER2, which are presented in Figure 6.6 and Figure 6.7, respectively.

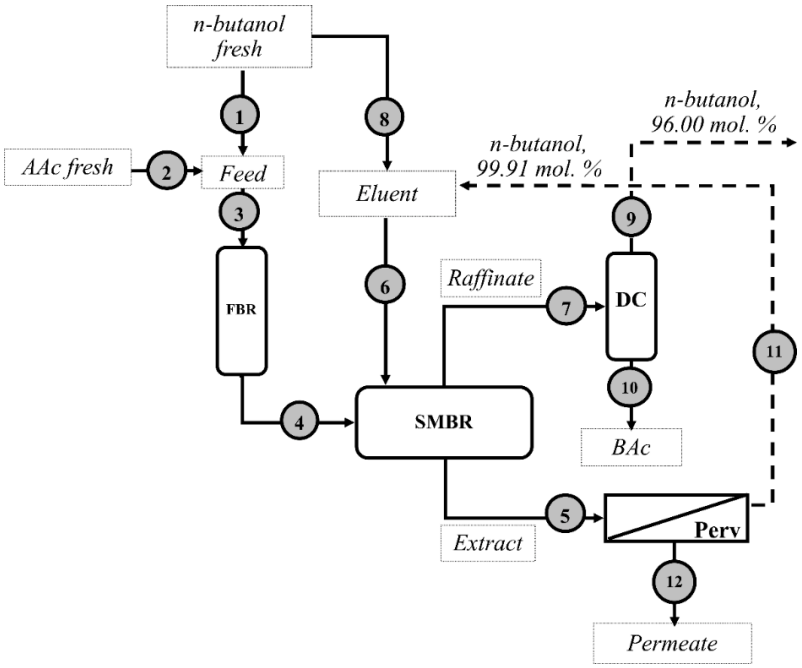

Figure 6.6. Configuration for n-butanol recycle using the outlet stream of the pervaporation unit (Scenario ER1). Feed and Eluent represent the feed and eluent nodes, respectively.

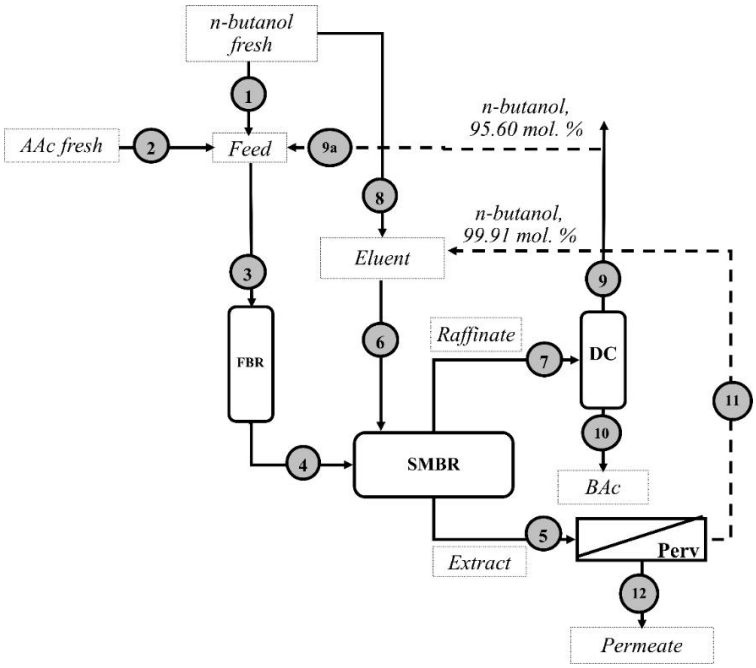

Figure 6.7. Configuration for n-butanol recycle using the outlet stream of the pervaporation unit and 48.5 % of the top stream of the distillation column (Scenario ER2).

The most relevant stream for the recovery of the eluent is the outlet stream from the pervaporation unit, representing the highest saving in eluent and energy consumption. Basically, the scenario ER1 consists of n-butanol recycle from the membrane (stream 11) to the eluent stream of SMBR (stream 6). In the second scenario (ER2), besides the eluent recovery strategy adopted in scenario ER1, 48.5 % of the top stream of the distillation column is reintroduced in the process through the feed stream of the FBR. The remaining is discarded to ensure the required molar feed ratio of n-butanol/AAc (1:2), in order to get the same molar feed composition for the SMBR. That way, the total amount of fresh n-butanol required in the process (which is introduced through streams 1 and 8) can be significantly reduced. The different flow rates and the respective concentrations for each stream, according to the different scenarios ER1 and ER2, are shown in Table 6.7 and Table 6.8, respectively.

Table 6.7. Concentrations and flow rates of the streams according to the scenario ER1.

Stream	Q ($L.min^{-1}$)	$C_{n\text{-butanol}}$ ($mol.L^{-1}$)	C_{AAc} ($mol.L^{-1}$)	C_{Bac} ($mol.L^{-1}$)	C_{Water} ($mol.L^{-1}$)
#3	130	4.06×10^{0}	8.06×10^{0}	-	-
#4	130	5.75×10^{-1}	4.56×10^{0}	3.47×10^{0}	3.47×10^{0}
#9	112	9.44×10^{0}	-	4.24×10^{-1}	1.98×10^{-2}
#11	2141	10.0×10^{0}	-	-	1.07×10^{-2}

Table 6.8. Concentrations and flow rates of the streams according to the scenario ER2.

Stream	Q ($L.min^{-1}$)	$C_{n\text{-butanol}}$ ($mol.L^{-1}$)	C_{AAc} ($mol.L^{-1}$)	C_{Bac} ($mol.L^{-1}$)	C_{Water} ($mol.L^{-1}$)
#3	130	3.95×10^{0}	7.83×10^{0}	1.78×10^{-1}	8.00×10^{-3}
#4	130	5.74×10^{-1}	4.50×10^{0}	3.53×10^{0}	3.36×10^{0}
#9a	54.4	9.44×10^{0}	-	4.25×10^{-1}	1.98×10^{-2}
#11	2141	10.0×10^{0}	-	-	1.07×10^{-2}

In Table 6.9 are displayed the global performance parameters, including the energy and desorbent consumption, according to each scenario studied for the eluent recovery in the enhanced SMBR process design, as well as the best performance obtained in the conventional SMBR process (ER2).

Table 6.9. Final performance parameters of the enhanced SMBR integrated according to the different eluent recovery scenarios (ER1 and ER2) and comparison with the conventional SMBR process (scenario ER2).

Performance Parameters	Coventional SMBR (ER2)	Enhanced SMBR (Open)	Enhanced SMBR (ER1)	Enhanced SMBR (ER2)
BAc purity (%)	99.7	99.7	99.5	99.5
Production capacity ($\times 10^3$) ($t_{BAc}.year^{-1}$)	51.5	67.3	67.2	67.0
DesC ($L_{n\text{-}Butanol}.kg_{BAc}^{-1}$)	1.00	16.9	1.49	1.11
Energy consumption ($kJ.kg_{BAc}^{-1}$) ($\times 10^3$)	1.80	3.77	1.93	1.87

The results show that it is possible to save about 91.1 % of the eluent (with the scenario ER1) in relation to the open process (without n-butanol recycle) while the scenario ER2 allows to recover 93.4 %, approximately. Accordingly, the energy demand per kg of the product was estimated for each scenario, considering the enthalpies of each stream. The reactors were considered to operate under isothermal conditions, the reboiler duty was obtained from the simulations results in ASPEN PLUS (Version 8.6) and the energy required for the pervaporation unit was determined by using the non-isothermal model described in Chapter 5. All thermophysical data necessary were found in the open literature [9] (see *Appendix E*). As expected, the ER2 showed to be the most economic choice, requiring 1.85×10^3 $kJ.kg_{BAc}^{-1}$ against 1.93×10^3 $kJ.kg_{BAc}^{-1}$ for the ER1 and 3.77×10^3 $kJ.kg_{BAc}^{-1}$ for the open process. Comparing with the conventional SMBR (1.80×10^3 $kJ.kg_{BAc}^{-1}$), both present similar energy demand for a similar eluent recovery strategy, although this actual process design (enhanced SMBR) affords a higher production capacity (around 30 %).

6.3. Conclusions

An enhanced SMBR process for butyl acrylate synthesis over Amberlyst-15 was studied by coupling a FBR with a SMBR unit operating at 363 K. The viability of this novel process design was investigated at industrial scale, by modelling the process according to the flow diagram proposed.

The design and operating parameters were found ensuring the desired separation and complete regeneration of the resin and eluent in sections 1 and 4, respectively. Reactive separation regions were determined for different SMBR configurations (columns arrangement per section) and further optimisation was performed with sensitivity analysis to the flow rates ratios determined from the Equilibrium Theory.

The best performance was achieved with a molar feed ratio (n-butanol/AAc) of 1:2 in the FBR and a configuration of 2-3-5-2 (columns per section) in the SMBR, achieving the maximum productivity with the minimum desorbent/eluent (n-butanol) consumption for the BAc purity required. The most suitable operating flow rates for the new process design are: Q_{EL} = 2280 L.min^{-1}, Q_{Rec} = 478 L.min^{-1}, Q_F = 130 L.min^{-1} and Q_{Ext} = 2148 L.min^{-1}.

A distillation column and a membrane pervaporation unit were dimensioned and optimised to treat the SMBR raffinate and the extract streams, respectively. In this case, a pervaporation unit of 785 m^2 and a distillation column with 34.9 m of length (42 trays) and 1.55 m of diameter are enough to accomplish the purity specifications. Smaller downstream units are required for this new process design, since the extract flow rate to be treated by the pervaporation unit is lower and the BAc concentration in the raffinate stream is higher when the FBR is used before the SMBR, which simplifies the purification step and increases the process productivity.

Additionally, the global process was studied considering different eluent recovery scenarios. The most attractive process was found by recycling the n-butanol from the pervaporation unit to the eluent stream of the SMBR and using 48.5 % of the top stream of distillation column as feed of the FBR (scenario ER2). As a result, it is possible to reach an eluent recovery of 93 % with a productivity of 67,000 t_{BAc}.year^{-1}.

Finally, energy balances were performed and analysed which showed the viability of this process design and its competitiveness, since it presented the highest production

capacity (30 % higher than the conventional SMBR) for a similar energy demand (1.87×10^3 $kJ.kg_{BAc}^{-1}$) comparing with other state-of-the-art processes for the BAc synthesis, presented so far.

6.4. Notation

Abbreviations

AAc	Acrylic Acid	-
BAc	Butyl Acrylate	-
ER	Eluent Recovery	-
FBR	Fixed-Bed Adsorptive Reactor	-
RSR	Reactive Separation Region	-
SMB	Simulated Moving Bed	-
SMBR	Simulated Moving Bed Reactor	-
SR	Separation Region	-

Symbols

A	Area	m^2
Conv.	Reaction Conversion	%
DesC	Desorbent Consumption	$m_{n\text{-}Butanol}^3.kg_{BAc}^{-1}$
d_{int}	Column internal diameter	m
C_p	Liquid phase concentration inside the particle	$mol.\ m^{-3}$
E_i	Activation energy	$J.mol^{-1}$
Eff	Tray efficiency	-
F	Feed flow rate (relative to distillation unit)	$m^3.min^{-1}$
H_{tower}	Tower height	m
H_{tray}	Height of each tray	m
J	Permeate molar flux	$kg.(m^{-2}.h^{-1})$

L_b	Column bed length of reactors	m
L_{tower}	Tower length	m
N	Number of trays	-
N_F	Feed tray	-
P_{Ext}	Extract Purity	%
P_{Perm}	Permeate pressure	bar
P_{Raff}	Raffinate Purity	%
$Prod$	Productivity	$kg_{BAc}.(m_{ads}^{-3}.day^{-1})$
Q	Volumetric flow rate	$m^3.min^{-1}$
Q_m	Membrane permeance	$kg.(m^{-2}.h^{-1}.bar^{-1})$
R_{actual}	Reflux ratio	-
r_p	Particle radius	m
t^*	Switching time	min
T	Temperature	K
U_s	Solid velocity	$m.s^{-1}$
u_s	Superficial velocity	$m.s^{-1}$
u_j	Liquid velocity	$m.s^{-1}$
x	Liquid phase molar fraction	-
x_B	Composition of the light compound in bottom	-
x_D	Composition of the light compound in distillate	-
y	Vapour phase molar fraction	-
z_F	Composition of the light compound in the feed	-

Greek Letters

α_m	Selectivity relative to pervaporation process	-
γ	Interstitial velocities ratio	-
ε	Bulk porosity	-
ε_p	Catalyst/adsorbent particle porosity	-
ρ_b	Bulk density	$kg.m^{-3}$

Subcripts

0	Relative to initial conditions	-
EL	Eluent	-
Ext	Extract	-
F	Feed	
i	Relative to a species	
j	Relative to a section of SMBR unit	
out	At the outlet of the fixed-bed column	
p	Particle	
perm	Permeate	
Raff	Raffinate	
Rec	Recycle	
ret	Retentate	

6.5. References

1. Ostaniewicz-Cydzik, A. M.; Pereira, C. S. M.; Molga, E.; Rodrigues, A. E., Reaction Kinetics and Thermodynamic Equilibrium for Butyl Acrylate Synthesis from n-Butanol and Acrylic Acid. *Industrial & Engineering Chemistry Research* **2014,** 53, (16), 6647-6654.

2. Lee, J. W.; Horváth, Z.; O'Brien, A. G.; Seeberger, P. H.; Seidel-Morgenstern, A., Design and optimization of coupling a continuously operated reactor with simulated moving bed chromatography. *Chemical Engineering Journal* **2014,** 251, 355-370.

3. Rodrigues, A.; Pereira, C.; Minceva, M.; Pais, L. S.; Ribeiro, A.; Ribeiro, A. M.; Silva, M.; Graça, N.; Santos, J. C., *Simulated Moving Bed Technology: Principles, Design and Process Applications*. Elsevier Science 2015.

4. Niesbach, A.; Daniels, J.; Schröter, B.; Lutze, P.; Górak, A., The inhibition of acrylic acid and acrylate ester polymerisation in a heterogeneously catalysed pilot-scale reactive distillation column. *Chem Eng Sci* **2013,** 88, 95-107.

5. Douglas, J. M., *Conceptual design of chemical processes*. McGraw-Hill: 1988.

6. Kujawski, W., Application of Pervaporation and Vapor Permeation in Environmental Protection. *Polish Journal of Environmental Studies* **2000,** 9, (1), 13-26.

7. Sommer, S.; Melin, T., Influence of operation parameters on the separation of mixtures by pervaporation and vapor permeation with inorganic membranes. Part 1: Dehydration of solvents. *Chemical Engineering Science* **2005,** 60, (16), 4509-4523.

8. Sommer, S.; Melin, T., Performance evaluation of microporous inorganic membranes in the dehydration of industrial solvents. *Chemical Engineering and Processing: Process Intensification* **2005,** 44, (10), 1138-1156.

9. Yaws, C. L., *Thermophysical Properties of Chemicals and Hydrocarbons (Electronic Edition)*. Knovel 2010.

7. Simulated Moving Bed Membrane Reactors

In this Chapter, a novel approach to the study of the butyl acrylate synthesis is detailed focusing on Simulated Moving Bed Reactor based process re-intensification, which comprises a membrane reactor combined with Simulated Moving Bed technology (PermSMBR). This new hybrid technology includes two different separation processes, adsorption and pervaporation, with chemical reaction for butyl acrylate production by continuous water removal with hydrophilic membranes. In order to find the ideal conditions to reach the best PermSMBR performance, the process was investigated numerically for different operating and design parameters and an optimisation study was performed. For that, a mathematical model was proposed considering linear driving force (LDF) approximation for the mass-transfer resistances, membrane concentration polarisation and the solution-diffusion model to describe the membrane permeation.

Promising results were obtained for 3-sections integrated PermSMBR with a configuration 4-6-2 (hydrophilic membranes per section packed with Amberlyst-15 ion exchange resin) and using a switching time of 4.0 min at 363 K. Comparing with the conventional Simulated Moving Bed Reactor, the productivity increased 36 % reducing significantly the desorbent consumption in 98 %. After the scaling up of the unit at industrial scale, the process integration was studied considering a distillation column for the eluent recovery (n-butanol) from the raffinate output stream. In this way, 100 % of the n-butanol was recovered from the top stream of the distillation column and it was used as a part of the feed solution of the integrated PermSMBR with 3 sections, which led to a n-butanol saving of 52 % in the respective fresh stream.

7.1. Introduction

Integrating chemical reaction with a separation process in the same equipment brings significant benefits for any continuous process. Usually, milder temperatures are enough to achieve good performance with higher reaction conversions and productivities comparing with the conventional processes (reaction followed by a separation step). Furthermore, savings on energy and other operating costs are expected [1, 2].

In order to improve the performance of Simulated Moving Bed Reactor (SMBR) based processes previously studied, in this Chapter a new paradigm of the chemical engineering was taken into account, the process re-intensification[3]. In this framework, a multifunctional reactor (SMBR) is combined with an additional separation technique (membrane pervaporation) towards a new hybrid process, the simulated moving bed membrane reactor, also known by PermSMBR [3]. This new approach consists of several pervaporation membrane/chromatographic reactors working based on the simulated moving bed (SMB) technology operating principle and which can be implemented according to two different configurations, as follows:

(i) Coupled configuration, which comprises a set of chromatographic reactors, packed with a catalyst/adsorbent, intercalated with tubular pervaporation membrane modules being all connected in series, as can be observed in Figure 7.1;

(ii) Integrated configuration, which comprises a set of tubular pervaporation membrane modules packed with a catalyst/adsorbent inside or outside of the membrane depending on where its active layer is placed, as represented in Figure 7.2.

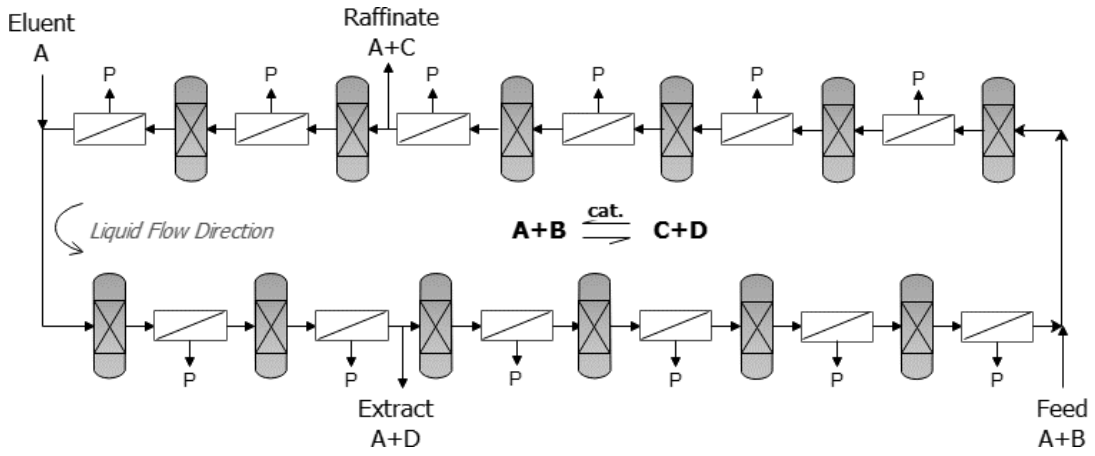

Figure 7.1. Schematic diagram of a Simulated Moving Bed Membrane Reactor (PermSMBR) with four sections and a coupled configuration with 2-4-4-2 packed chromatographic columns per section with 2-4-4-2 membranes intercalated. P represents the permeate stream trough the membranes which is composed majority by water (considering hydrophilic membranes).

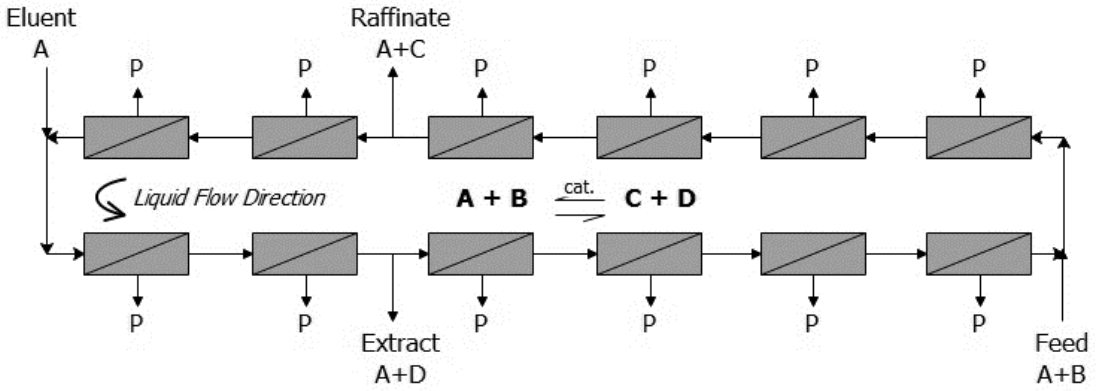

Figure 7.2. Schematic representation of a Simulated Moving Bed Membrane Reactor (PermSMBR) with four sections and an integrated configuration with 2-4-4-2 packed membrane per section. P represents the permeate stream trough the membranes which is composed majority by water (considering hydrophilic membranes).

Both configurations allow the combination of chromatography and pervaporation with chemical reaction in the same unit leading to a more effective secondary product removal (water in this case) from the system. Moreover, this continuous removal by

different ways allows a reaction conversion enhancement and a reduction on the desorbent/eluent consumption for the adsorbent regeneration since the most adsorbed compound is, simultaneously, the most permeated through the membranes.

PermSMBR technology was already applied in the synthesis of different oxygenated compounds like esters and acetals [4-6] showing to be a very effective process able to reduce significantly the desorbent consumption and leading to productivity enhancement when compared with the SMBR. One of the first applications was the synthesis of 1,1-dietoxyethane (1,1-DEE) [3], which is a blending agent for biofuels that can be included in diesel fuel up to 10 % allowing a reduction of 34.6 % on the emissions of particulate mass and 3.3 % on the NOx emissions from fuel combustion. Comparing with SMBR, the synthesis of 1,1-DEE was improved using PermSMBR technology with a reduction of 40 % on the eluent consumption and increasing the productivity about 53 %. A green solvent, the ethyl lactate [3], was also produced using this novel technology with very promising results. In this case, the productivity was improved 33.9 % and the eluent consumption was reduced 28.2% relatively to the results obtained with the SMBR. Afterwards, the application of this new hybrid technology was extended to the synthesis of 1,1-dibutoxyethane (1,1-DBE) [7], for which a productivity of 72.1 $kg_{DBE}.(L_{ads}^{-1}.day^{-1})$ was attained with a desorbent consumption of 1.84 $L_{n\text{-}butanol}.kg_{DBE}^{-1}$. This performance corresponds to a productivity enhancement of 33 % and a desorbent consumption reduction of 30 % showing to be a more effective process than SMBR. Moreover, further improvement on the PermSMBR performance is even possible by eliminating the extract outlet stream that leads to a reduction on the sections number of the unit (from 4 to 3) requiring less desorbent consumption for the adsorbent regeneration. With this process configuration strategy, it is possible to produce 1,1-DBE with significantly reduced amount of eluent, less 88 % than in SMBR process and a similar productivity.

In summary, the promising results obtained with PermSMBR technology for the production of the different oxygenated compounds show that it is a very effective process for butyl acrylate synthesis. So, in this Chapter the performance of this new hybrid technology was investigated numerically at industrial scale and compared with the other SMBR based processes studied previously.

7.2. Mathematical Model

A mathematical model similar to that described for the SMBR (Chapter 5, equations (5.1) – (5.22)) was considered to predict the concentrations profiles and the outlet streams compositions (extract and raffinate) obtained with a PermSMBR for a set period. Thus, similar assumptions considered on the SMBR study were taken into account, such as:

i) plug flow with axial dispersion for the bulk fluid phase;
ii) constant bed volume and packing porosity;
iii) linear driving force (LDF) approximation for the inter and intra-particle mass transfer rates;
iv) velocity variations due to changes in the bulk compositions (resulting from reaction, adsorption/desorption and species permeation, in this case);
v) multicomponent adsorption equilibrium (at the adsorbent phase);
vi) isothermal operation.

However, besides that, the model also considers:

vii) membrane concentration polarisation;
viii) solution-diffusion model to describe the membrane permeation.

The UNIFAC method was used to determine the activity coefficients, as previously. Therefore, for the integrated PermSMBR configuration, the particle mass balance is the same of the SMBR model described by equation 5.2 (Chapter 5) while the equations (5.1) and (5.3) must be replaced by the equations (7.1) and (7.2) for the PermSMBR model, respectively:

Bulk fluid mass balance to component *i* in membrane *k:*

$$\frac{\partial C_{ik}}{\partial t}+\frac{\partial (u_k C_{ik})}{\partial z}+\frac{(1-\varepsilon)}{\varepsilon}\frac{3}{r_p}k_{L,ik}\left(C_{ik}-\bar{C}_{p,ik}\right)=D_{ax,k}\frac{\partial}{\partial z}\left(C_T\frac{\partial x_{ik}}{\partial z}\right)-\frac{A_m}{\varepsilon}J_{ik} \qquad (7.1)$$

The total mass balance, which allows determining the interstitial fluid velocity variation, is given by*:*

$$\frac{du_k}{dz}=-\frac{(1-\varepsilon)}{\varepsilon}\frac{3}{r_p}\sum_{i=1}^{NC}k_{L,ik}V_{M,i}\left(C_{ik}-\bar{C}_{p,ik}\right)-\frac{A_m}{\varepsilon}\sum_{i=1}^{n}J_{ik}V_{M,i} \qquad (7.2)$$

where A_m is the membrane specific area (membrane area per volume) and the permeate flux through each membrane, J_{ik}, should be taken into account according to the following equation (considering a pervaporation membrane in this case):

$$J_{ik} = k_{ov,ik}\left(a_{ik}P_i^0 - y_{ik}P_{perm}\right) \tag{7.3}$$

where P_i^0 and P_{perm} are the saturation and permeate pressures, respectively, while a_{ik} and y_{ik} are the liquid phase activity of each compound and the molar composition in the vapour phase (permeate side). The mole fraction of component *i* in the vapour phase of the column *k*, y_{ik}, can be calculated as follows:

$$y_{ik} = \frac{J_{ik}}{\sum_{i=1}^{NC} J_{ik}} \tag{7.4}$$

Regarding the global membrane mass transfer coefficient, $k_{ov,ik}$, it combines the membrane resistance (that corresponds to the inverse of the membrane permeance, $Q_{m,ik}$) with the resistance due to the diffusive transport in the boundary layer [8]:

$$\frac{1}{k_{ov,ik}} = \frac{1}{Q_{m,ik}} + \frac{a_{ik}P_{ik}^0 V_{M,i}}{x_{i,F}k_{bl,ik}} \tag{7.5}$$

where $k_{bl,ik}$ is the membrane boundary layer mass transfer coefficient that can be determined through the Lévêque correlation [9] (valid for laminar flow and Graetz number, $d_{int}^2 u_s / \left(D_M L_m\right)$, much greater that one):

$$Sh = 1.62 Re^{0.33} Sc^{0.33}\left(\frac{d_{int}}{L_m}\right)^{0.33}, \text{(Re < 2300)} \tag{7.6}$$

where $Sh = k_{bl,ik}d_{int}/D_M$, $Re = \rho d_{int}u_s/\eta$ and $Sc = \eta/(\rho D_M)$ are the Sherwood, Reynolds and Schmidt numbers, respectively, D_M is the molecular diffusivity in the boundary layer, d_{int} is the internal diameter of the tubular membrane, L_m is the membrane length, ρ is the fluid density and η is the fluid viscosity.

The infinite dilution diffusivities as well as the diffusion coefficient in concentrated solutions were estimated according to the equations (3.20)-(3.22), which are described in Section 3.3.1.

Concerning a PermSMBR with a coupled configuration, other changes are required since a membrane module follows each chromatographic reactor, sequentially. Therefore, the mass balance equations are independent for each unit being the equations (5.1) and (5.3) described for the chromatographic reactors in the SMBR mathematical model also considered in this case. However, the membrane mass balance and the fluid velocity variation must be included in the present model:

Mass balance to component i in the retentate side of the membrane *m:*

$$\frac{\partial C_{i,m}}{\partial t}+\frac{\partial (u_m C_{i,m})}{\partial z}=D_{ax,m}\frac{\partial}{\partial z}\left(C_T\frac{\partial x_{i,m}}{\partial z}\right)-A_m J_{i,m} \tag{7.7}$$

where $J_{i,m}$ is obtained by equation (7.3).

Fluid velocity variation in membrane *m*:

$$\frac{du_m}{dz}=-A_m\sum_{i=1}^{NC}J_{i,m}V_{M,i} \tag{7.8}$$

Initial and Danckwerts boundary conditions are given by:

$$t=0:\ C_{i,m}=C_{ik}=\bar{C}_{p,ik}=C_{ik,0}\ \text{and}\ q_{ik}=q_{ik,0} \tag{7.9}$$

$$z=0:\ u_k C_{ik}\,|_{z=0}-D_{ax,k}\frac{\partial C_{ik}}{\partial z}|_{z=0}=u_k C_{ik,F} \tag{7.10}$$

$$u_m C_{i,m}\,|_{z=0}-D_{ax,m}\frac{\partial C_{i,m}}{\partial z}|_{z=0}=u_m C_{i,m}\,|_{z=L_m} \tag{7.11}$$

$$z=L_{b,m}:\quad \frac{\partial C_{ik}}{\partial z}|_{z=L_b}=0 \tag{7.12}$$

$$\frac{\partial C_{i,m}}{\partial z}|_{z=L_m}=0 \tag{7.13}$$

where the subscripts *F* and *0* refers to the feed and initial states, respectively.

The mass balance to the nodes (eluent, extract, raffinate and feed) can be described by equations (5.14) – (5.20); however, each section must consider also the following equations:

$$C_{b,i,k|z=L_{b,m}} = C_{i,m|z=0} \tag{7.14}$$

$$C_{i,m|z=L_{b,m}} = C_{b,i,k+1|z=0} \tag{7.15}$$

$$Q_{k|z=L_{b,m}} = Q_{m|z=0} \tag{7.16}$$

$$Q_{m|z=L_{b,m}} = Q_{k+1|z=0} \tag{7.17}$$

Similarly to the SMBR, the ratio between the fluid interstitial velocity, u_j, and the simulated solid velocity for each section is given by $\gamma_j = u_j / U_s$ while the switching time is defined by $t^*_{Integrated} = L_m / U_s$, where U_s is the solid interstitial velocity and L_m is the membrane module length in the PermSMBR integrated configuration. For the coupled configuration, the switching time was determined based on the average residence time required for the flow to go through each membrane module plus the switching time used in SMBR unit, as described in Section 7.3.1.

For both configurations, the axial dispersion coefficient (D_{ax}) is estimated from the following empirical correlation, which is valid for liquids in packed beds [10] .

$$\varepsilon Pe_p = 0.2 + 0.011 Re_p^{0.48} \tag{7.18}$$

where $Pe_p = ud_p / D_{ax}$ and $Re_p = \rho d_p u / \eta$ are the Peclet and the Reynolds number relative to the particle, respectively.

Finally, to complete the PermSMBR mathematical model, fundamental data are required, including the kinetic parameters and equilibrium constant which are described in Chapter 5 (equations (5.4)-(5.6)) and the multicomponent adsorption data that are presented in Table 3.3. The adsorption equilibrium of component *i* in column/membrane *k*, is described by the multicomponent Langmuir isotherm equation, which is described in Chapter 3 (equation (3.5)).

All those data were measured over Amberlyst-15 ion exchange resin, which is considered in PermSMBR model as catalyst and adsorbent material like in the other SMBR based processes studied. Besides that, the pervaporation data measured with hydrophilic membranes and presented in Chapter 4 (Table 4.4) must also be taken into account. In both PermSMBR configurations, commercial hybrid silica membranes from Pervatech with hydrophilic characteristics were considered, which present a maximum operating temperature and pressure of 423 K and 10 bar, respectively (more details are given in Chapter 4, Section 4.2.1). The difference is that, on the integrated configuration the membrane modules were considered to be packed (inside of each membrane, as represented in Figure 7.3) with A-15, acting as catalyst and adsorbent, while in the coupled configuration just the fixed-bed columns are considered to be packed with A-15 and each membrane that follows each FBR just works as pervaporation unit.

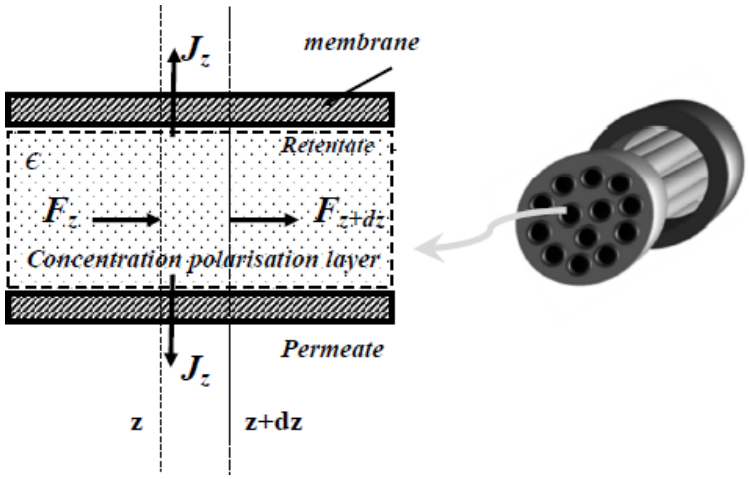

Figure 7.3. Schematic representation of the fluxes in a membrane of the PermSMBR process. F corresponds to the flux and ε represents the bed porosity in the integrated configuration case where each membrane is packed with Amberlyst-15.

Regarding the PermSMBR process performance, independently of the configuration, it can be assessed for different operating conditions over a complete cycle according to the performance parameters described by equations (5.23)-(5.27) in SMBR mathematical model (Chapter 5, *Section 5.3.1*).

7.2.1. Numerical Solution

The numerical solution of this problem was obtained by using the commercial software gPROMS (general PROcess Modelling System) version 4.2.0, using orthogonal collocation in finite elements (OCFEM) with third order polynomials; to this end, the axial dimension of the bed was discretized in 30 finite elements with 2 interior collocation points in each finite element. The DASOLV system solver was used to solve the resulting system of ordinary differential equations in time. For all simulations, a tolerance of 10^{-5} was used. It was assumed that a PermSMBR simulation reached the cyclic steady state when the columns profiles in two consecutive cycles had less than 1.0 % of relative deviation.

7.3. Results and Discussion

7.3.1. Process Design

An equivalence between PermSMBR and SMBR was performed in order to compare both technologies in a fair way. For that, the same solid velocity used in SMBR was considered, 7.42 (cm.min^{-1}), in the PermSMBR integrated configuration. So, since the length (L_m) of the commercial membranes is higher than the fixed-bed columns considered in the SMBR pilot scale unit (LICOSEP), a new switching time was determined according to equation (5.22). Furthermore, the ratio between the fluid interstitial velocity and the simulated solid interstitial velocity (γ_j) of each section (from 1 to 4) of the SMBR were also kept according to the Equilibrium Theory by changing the respective section flow rates. In order to have the same specific area of each column, 13 membranes per module were considered. Regarding the coupled configuration, a new switching time ($t^*_{Coupled}$) was determined based on the average of the residence time required for the flow to go through each membrane module ($\overline{t}_{r,\mathrm{mod}}$ = 3.74 min) plus the switching time used in SMBR unit (3.1 min), according to equations (7.19-7.20), from

which was obtained a value of 6.84 min. In Table 7.1 the main parameters used in the PermSMBR and SMBR simulations are summarized.

$$t^*_{Coupled} = t^*_{SMBR} + \overline{t}_{r,\mathrm{mod}} \tag{7.19}$$

$$\overline{t}_{r,\mathrm{mod}} = \sum_{j=1}^{4}\left(\frac{V_{\mathrm{mod}}}{Q_{j,SMBR}} \times N_{\mathrm{mod},j} \right) \tag{7.20}$$

where V_{mod} is the volume of a membrane module that is 127.3 cm^3 (considering 13 membranes per module), $N_{\mathrm{mod},j}$ corresponds to the number of membrane modules per section (j) and $Q_{j,SMBR}$ is the section flow rate in SMBR process. Design parameters considered in the different processes are summarised in Table 7.1.

Table 7.1. Parameters considered in the simulations of the SMBR and the PermSMBR.

Parameters	SMBR	Integrated PermSMBR	Coupled PermSMBR
Number of fixed-bed columns/ membranes per module, N	12 packed fixed-bed columns	12 modules of 13 packed membranes (per module)	12 packed fixed bed columns + 12 modules of 13 membranes
Length, L_b (cm)	23	-	23
Length, L_m (cm)	-	25.45	25.45
Internal diameter, d_{int} (cm)	2.6	0.7/ membrane	2.6/column and 0.7/membrane
A-15 solid weight (g)	48.9	51.0	48.9
Switching time, t^* (min)	3.1	3.43	6.84
Bed porosity, ε	0.41	0.41	0.41
Solid Velocity, U_s ($cm.min^{-1}$)	7.42	7.42	7.08
γ_1; γ_4 ($=u_j/U_s; 1\leq j \leq 4$))	9.27;1.52	9.27;1.52	9.27;1.52
Pressure, P (mbar)	-	5.00	5.00

After the PermSMBR mathematical model implementation and before studying its performance for the BAc synthesis, the first step was to validate the mathematical model to compare it with the SMBR results. For that, it was considered that no flux crosses the membrane (total flux, $J_t = 0$). In this way, a similar concentration profile to the one obtained with SMBR mathematical model is expected using the PermSMBR mathematical model with the parameters presented in Table 7.2 and the respective section flow rates determined (Table 7.2) with base on the equivalence of the two technologies described previously.

Table 7.2. Operating and performance parameters of SMBR and integrated PermSMBR without flux (J=0).

Parameters	SMBR	Integrated PermSMBR (J=0)
Configuration	2-4-4-2	
T, K	363	
t^* (min)	3.10	3.43
Q_F (mL.min^{-1})	6.50	6.10
Q_{Ext} (mL.min^{-1})	117.6	111
Q_{EL} (mL.min^{-1})	122	115.2
Q_{Rec} (mL.min^{-1})	24.0	22.5
P_{Ext} (%)	99.4	99.4
P_{Raff} (%)	99.5	99.6
Conv. (%)	99.3	99.5
Prod. ($kg_{BAc}.(L_{ads}^{-1}.day^{-1})$)	7.83	7.33
Des.C ($L_{n\text{-}Butanol}.kg_{BAc}^{-1}$)	25.5	24.7

As a result, the concentration profiles obtained in both reactors, SMBR and PermSMBR (without flux through of the membranes), using the different mathematical models are presented in Figure 7.4.

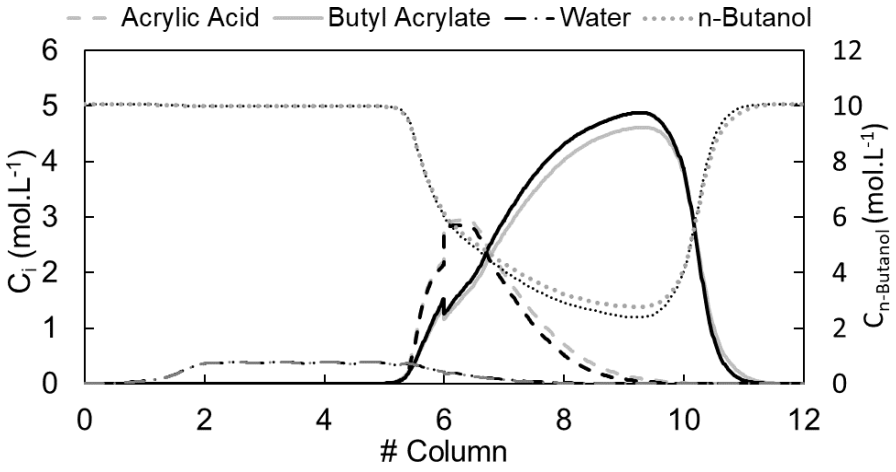

Figure 7.4. Concentration profiles in SMBR (grey profile) and PermSMBR without flux through the membranes (black profile) at the middle of the switching time (3.10 min and 3.43 min, respectively) at cyclic steady state (21st and 41th cycle, respectively) at 363 K.

Comparing both concentration profiles, it is possible to observe that they are very similar confirming that the mathematical model described in this Chapter and the respective assumptions considered are suitable for the comparison of the two reactors.

Afterwards, it is possible to evaluate the integrated PermSMBR performance for the synthesis of BAc considering the total flux that crosses the membranes by including the pervaporation data and performing an optimisation study, which is presented in the following sections.

7.3.2. Reactive Separation Region

7.3.2.1. Coupled and integrated PermSMBR configurations

Reactive separation regions (RSR) were determined numerically with the PermSMBR mathematical model considering two different configurations of the reactor: i) integrated PermSMBR, where the SMBR columns are replaced by packed pervaporation membranes and, ii) coupled PermSMBR, where each fixed-bed column is followed by a pervaporation membrane (not packed, in this case). Thus, the esterification reaction

between AAc and n-butanol was simulated at 363 K using different PermSMBR configurations. For a fair comparison with SMBR technology, the RSR of the different configurations were determined by keeping constant the recycle and eluent flow rates (γ_1 and γ_4). The respective RSR are presented in Figure 7.5 for which a configuration 2-4-4-2 was used, like in the conventional SMBR study (Chapter 5).

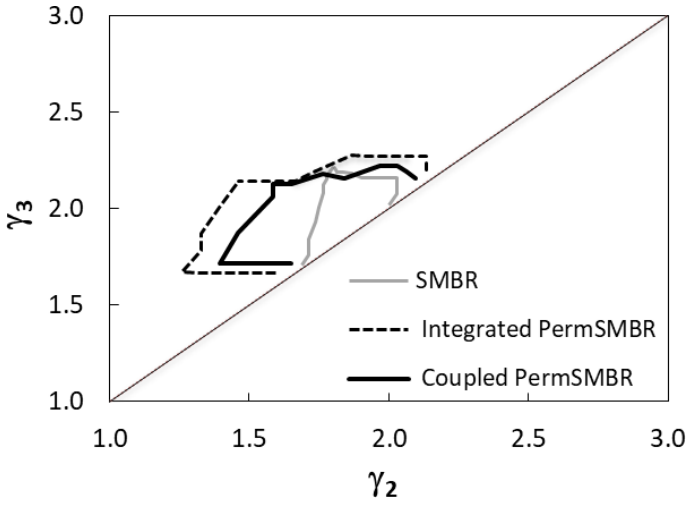

Figure 7.5. Reactive Separation Region for the integrated PermSMBR, coupled PermSMBR and SMBR processes (Configuration: 2-4-4-2; feed solution with equimolar reactants composition; t^*_{SMBR}= 3.10 min, $t^*_{Integrated}$ = 3.43 min and $t^*_{Coupled.}$ = 6.84 min) at 363 K. Raffinate purity criteria ≥ 99.5 % (solvent-free basis).

According to the results, the RSR for both PermSMBR configurations are bigger than for SMBR due to better water separation efficiency, being the integrated PermSMBR the most effective process, which allows having a larger RSR. In both cases, the raffinate purity increased as expected since water is now removed from the reaction medium by adsorption and pervaporation processes.

However, regarding the maximum productivity and desorbent consumption, the two PermSMBR processes are very similar to the SMBR. Although water is more efficiently removed, the BAc contamination with AAc is still high since the adsorption parameters are very similar for both components, so the purity criteria required for BAc (≥ 99.5 %) is not fulfilled for much higher feed flow rates than the one used in the conventional

SMBR. Nevertheless, the productivity improved 2.1 % (8.00 $kg_{BAc}.(Lads^{-1}.day^{-1})$) and the desorbent consumption was reduced 11 % (22.6 $L_{n\text{-}butanol}.kg_{BAc}^{-1}$) with the integrated PermSMBR configuration comparatively to the conventional SMBR technology.

7.3.2.2. Integrated PermSMBR with 3 sections

Since the PermSMBR technology allows removing the water continuously by adsorption and by pervaporation process along the reactor, as mentioned previously, the extract stream is not required. Thus, a new columns arrangement was considered for the integrated PermSMBR process optimisation, namely, a configuration of 4-6-2 (membranes per section) in which the extract stream is removed reducing the unit to 3 sections (PermSMBR-3s), as can be observed in Figure 7.6. Afterwards, another RSR was determined and compared with the remaining RSR (Figure 7.7).

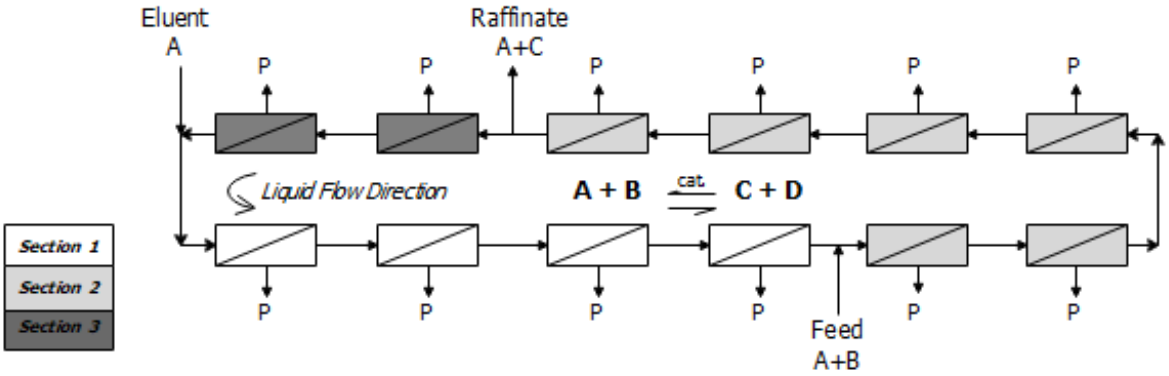

Figure 7.6. Schematic representation of an integrated PermSMBR with 3 sections, using a 4-6-2 configuration. P represents the permeate stream trough the membranes which is mainly composed by water (considering hydrophilic membranes). A = n-Butanol, B = Acrylic Acid, C = Butyl Acrylate, D = Water.

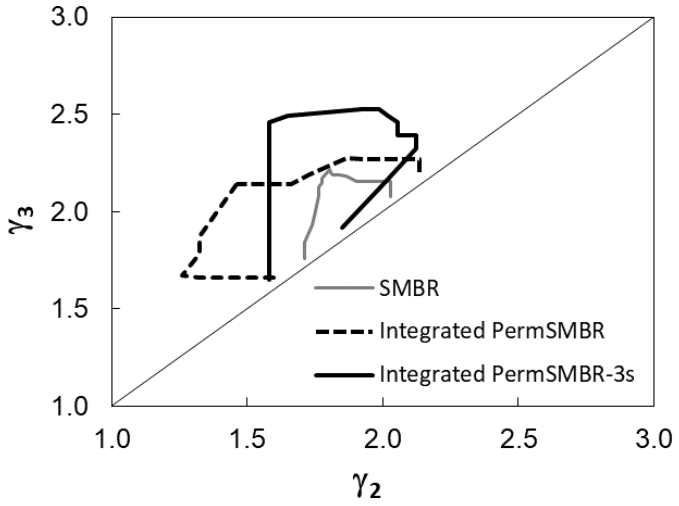

Figure 7.7. Reactive Separation Regions for integrated PermSMBR and SMBR processes (Configuration: 2-4-4-2) and integrated PermSMBR with 3 sections (Configuration: 4-6-2); t^*_{SMBR}= 3.10 min and $t^*_{PermSMBR}$ = 3.43 min; feed solution with equimolar reactants composition at 363 K. All regions were determined for a raffinate purity criteria ≥ 99.5 % (solvent-free basis).

In order to compare all RSR in a fair way, in the PermSMBR-3s it was considered that $\gamma_2 = \gamma_1$ due to the elimination of the extract stream, so the flow rate ratios are kept constant from section 1 to section 2. The results show that a more effective process was achieved allowing to use higher feed flow rates than the previous configuration (2-4-4-2) and leading to higher productivity (more 26 %) and lower desorbent consumption (less 96 %).

7.3.2.3. Effect of switching time

Additionally, other RSR were determined using different switching times for both configurations, 4 sections (integrated PermSMBR, 2-4-4-2) and 3 sections (3-sections integrated PermSMBR, 4-6-2) and the maximum operating points of each one are represented in Figure 7.8 and Figure 7.9, respectively.

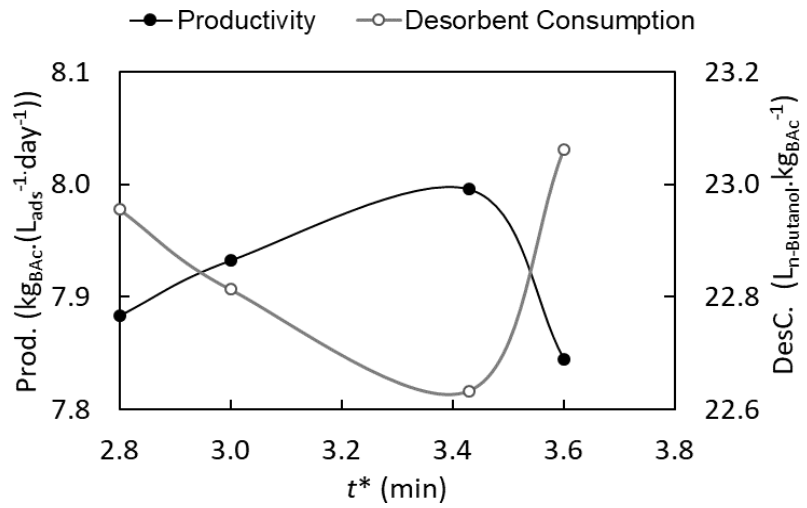

Figure 7.8. Optimal operating points as a function of switching time for the integrated PermSMBR process.

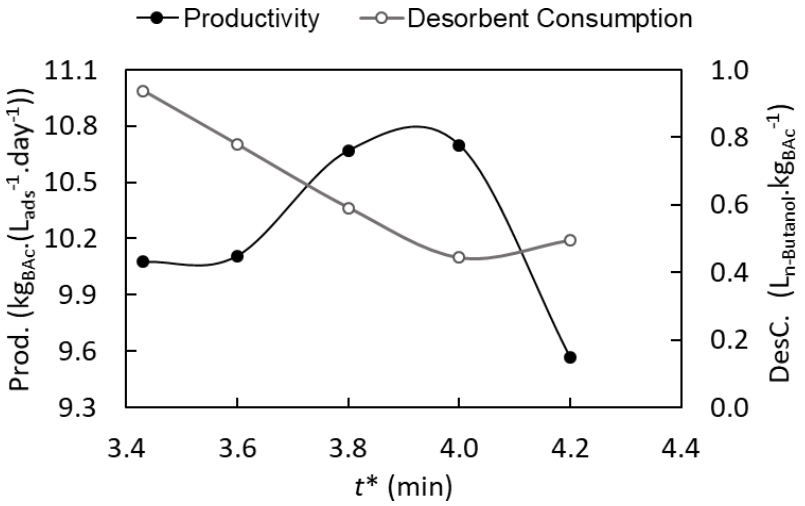

Figure 7.9. Optimal operating points as a function of switching time for the integrated PermSMBR with 3 sections.

In integrated configuration case (4 sections) the maximum performance (maximum productivity and minimum eluent consumption) is obtained with the switching time of 3.43 min that was obtained previously by equation (5.22) considering the membrane module length (25.45 cm) and for which the RSR presented in Figure 7.7 (dashed lines) was determined. The concentration profiles obtained at those operating conditions are

presented in Figure 7.10, which shows that both sections 1 and 4 are totally regenerated (solid and eluent, respectively).

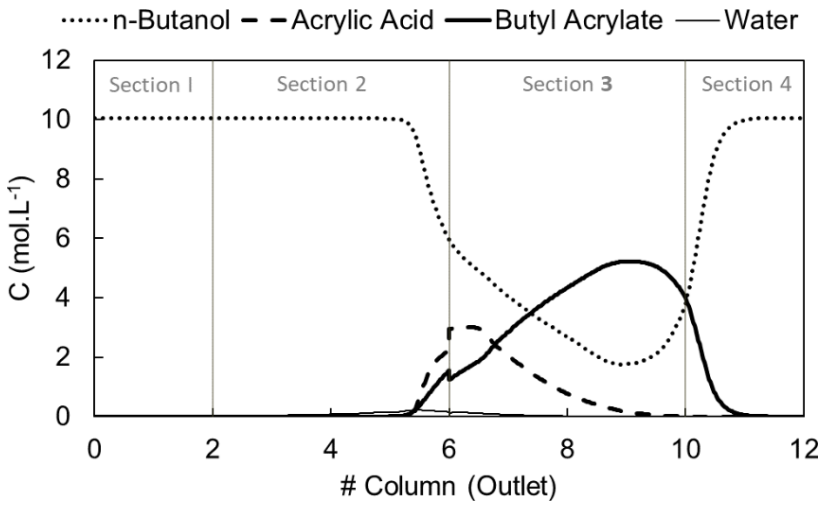

Figure 7.10. Concentration profiles in the integrated PermSMBR configuration for BAc synthesis at the middle of the switching time (3.43 min) at cyclic steady state (41th cycle); T = 363 K and configuration 2-4-4-2 (feed solution with an equimolar reactants composition).

The ideal operating parameters found for this configuration allow a great BAc purity (99.7 mol. %) on raffinate stream (outlet of the column 10) since the unreacted AAc is dragged with solid to the left and the permeate streams through of the integrated hydrophilic membranes lead to a significant water removal from inside the reactor.

On the other hand, according to the Figure 7.9, the maximum performance in the 3 sections configuration case is attained with a switching time of 4.0 min (maximum productivity and minimum eluent consumption). The respective concentration profiles can be observed in Figure 7.11, where the enhanced BAc production along the reactor is clear. Comparing with the SMBR performance, the productivity was improved by 36 % (10.7 $kg_{BAc}.(L_{ads}^{-1}.day^{-1})$) and the eluent consumption was significantly reduced, about 98 % (0.44 $L_{n\text{-}Butanol}.kg_{BAc}^{-1}$). Besides that, the results show that the ideal section flow rates found are not enough to regenerate the solid (section 1) and eluent (section 4). However, the contamination of those sections is made with the target product and increases the overall concentration of BAc throughout the unit.

A summary of all operating and performance parameters for the most effective PermSMBR configurations, namely, integrated, integrated with 3-sections and optimised integrated with 3-sections, can be observed and compared in Table 7.3.

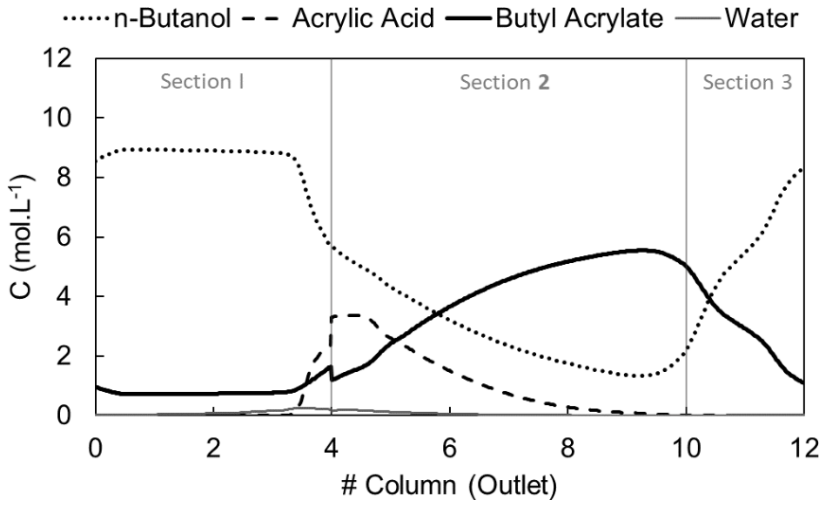

Figure 7.11. Concentration profiles in the optimised PermSMBR with 3 sections for BAc synthesis at the middle of the switching time (4.0 min) at cyclic steady state (41th cycle); T = 363 K and Configuration 4-6-2 (feed solution with an equimolar reactants composition).

Table 7.3. Operating and performance parameters of integrated PermSMBR and integrated PermSMBR-3s at 363 K.

Parameters	Integrated PermSMBR	Integrated PermSMBR-3s	Optimised Integrated PermSMBR-3s
Configuration	2-4-4-2	4-6-2	4-6-2
t^* (min)	3.43	3.43	4.00
Q_F (mL.min^{-1})	7.10	9.00	9.5
Q_{Ext} (mL.min^{-1})	109.8	-	-
Q_{EL} (mL.min^{-1})	115.2	6.00	3.00
Q_{Rec} (mL.min^{-1})	22.5	22.5	22.1
P_{Ext} (%)	90.5	-	-
P_{Raff} (%)	99.7	99.6	99.5
Conv. (%)	99.5	99.8	99.6
Prod. ($kg_{BAc}.(L_{ads}^{-1}.day^{-1})$)	8.00	10.1	10.7
Des.C ($L_{n\text{-}Butanol}.kg_{BAc}^{-1}$)	22.6	0.93	0.44

7.3.2.1. Sensitivity Analysis

Finally, a sensitivity analysis to γ_1 and γ_4 (the ratio between the liquid and solid velocity in sections 1 and 4, respectively) was performed by varying each one by 2 and 4 %, above and below the values determined by the Equilibrium Theory and the results are presented in Figure 7.12 and Figure 7.13, for the integrated PermSMBR with 4 and 3 sections, respectively.

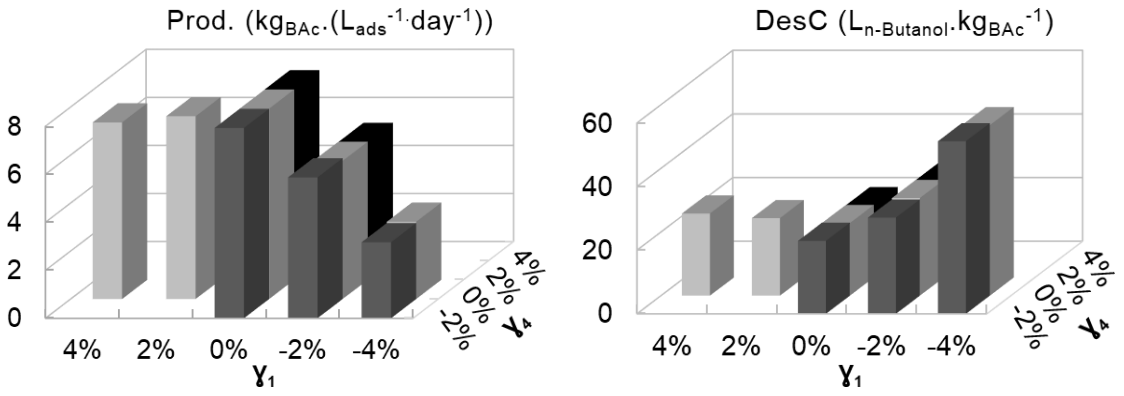

a) *b)*

Figure 7.12. Sensitivity analysis to the RSR of the integrated PermSMBR process: a) Productivity; b) Desorbent Consumption; 0% corresponds to the original values obtained from the Equilibrium Theory (γ_1 = 9.10 and γ_4 =1.52).

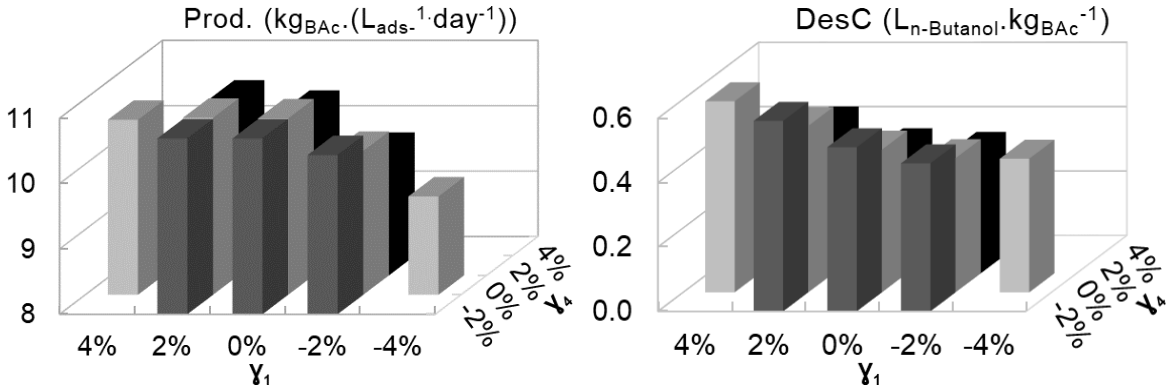

a) *b)*

Figure 7.13. Sensitivity analysis to the RSR of the 3-sections integrated PermSMBR: a) Productivity; b) Desorbent Consumption; 0% corresponds to the original values obtained for a switching time of 4.0 min (γ_1 = 1.94 and γ_4 =1.71).

Looking at the maximum productivity of the first case (Figure 7.12 **(**a)) and minimum desorbent consumption (Figure 7.12 **(**b)), the maximum performance is attained when γ_4 is between -2 and 2 % of the original value (1.55) and γ_1 is kept constant (9.27).

Regarding the 3 sections configuration, it is important to mention that, contrary to the previous case, although several points are displayed in the Figure 7.13, the values of (γ_1 , γ_4) that fulfill the purity criteria (BAc ≥ 99.5 %) are (0,0) % and (0,-2) %. So, between them, the maximum performance is attained with the original values determined from Equilibrium Theory (1.97 and 1.74), remembering that $\gamma_1 = \gamma_2$ in this case.

7.3.3. From pilot to industrial scale

7.3.3.1. PermSMBR scaling up to industrial scale

A scaling-up study of PermSMBR was carried out. For that, the same production capacity that was set in the SMBR study at industrial scale was also set as the target of the PermSMBR-3s, 50,000 $t_{BAc}.year^{-1}$. Initially, the volume of the unit required to achieve the desired production capacity is calculated based on the volume of the pilot scale unit and the respective production capacity, according to equation (7.21):

$$V_{PermSMBR,IndustrialScale} = ScaleFactor \times V_{PermSMBR,PilotScale} \tag{7.21}$$

$$ScaleFactor = \frac{Prod.Capacity_{Ind.Scale}}{Prod.Capacity_{PilotScale}} \tag{7.22}$$

The total area of membranes inside of each module is given by equation (7.23):

$$A_{t,m} = \pi r_m^{\,2} N_m \tag{7.23}$$

where r_m and N_m are the radius of a membrane and the number of membranes considered inside of each module, respectively. Considering that a membrane module has a tubular design, the total radius of membranes ($r_{t,m}$) can be obtained from equation (7.24). For a fair comparison of the reactors' performance, SMBR and PermSMBR, the ratio between the total diameter of membranes and the respective length $(d_{t,m} / L_m)$ was kept constant (3.6).

$$A_{t,m} = \pi r_{t,m}^{\,2} \tag{7.24}$$

Moreover, the diameter of each membrane module was calculated considering a shell and tube heat exchanger design, according to the equation (7.25) [11].

$$D_{s,\mathrm{mod}} = 0.637\left(\frac{CL}{CTP}\right)^{1/2}\left[\frac{A_{\mathrm{mod}}\left(\frac{P_T}{d_{out}}\right)^2 d_{out}}{L_m}\right]^{1/2} \tag{7.25}$$

where $P_T = d_{out} + C$ and $C = 0.25 d_{out}$. The tube outside diameter, d_{out}, was considered to be the commercial value of the membranes,0.3937 in. L_m is the membrane length, CL is the tube layout constant (0.87 for equilateral triangular pitch) and CTP is the tube pass constant (0.93 for one tube pass). The heat exchange area is given by:

$$A_{\mathrm{mod}} = \pi d_{out} N_m L_m \tag{7.26}$$

where N_m is the number of membranes inside of each module.

A triangular pitch (tubes arrangement inside of each module) was considered, since it ensures a more compact arrangement and a smaller shell. Besides that, this arrangement facilitates a higher heat transfer rate [12]. In Figure 7.14 a schematic representation of the selected arrangement is represented where P_T and C correspond to the tube pitch (the shortest centre to centre distance between the adjacent tubes) and clearance, respectively.

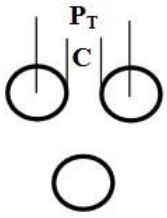

Figure 7.14. Schematic representation of triangular pitch (tubes arrangement inside a membrane module).

In Table 7.4 are presented the respective design parameters determined to simulated the concentration profiles at industrial scale, according to the design algorithm presented in Figure 7.15. All ratios between liquid and solid velocities optimised in PermSMBR-3s

at pilot scale were kept constant in all sections of the industrial scale unit in order to determine the respective ideal operating flow rates.

Table 7.4. Design parameters of membrane modules at pilot and industrial scale.

Parameter/ Scale	Pilot	Industrial
N_m; N_{mod}	13; 12	83,000; 12
d_{out}; $Ds_{,mod}$ (dm)	0.100; 0.332	0.100; 39.33
$d_{t,m}$ (dm)	0.252	20.17
A_{t_m} (dm^2)	0.050	319.4
A_{mod} (dm^2)	10.39	146,070
L_m (dm)	2.550	5.600
$V_{PermSMBR}$ (dm^3)	19.86	21,470
Production Capacity ($kg_{BAc}.day^{-1}$)	127.5	136,986

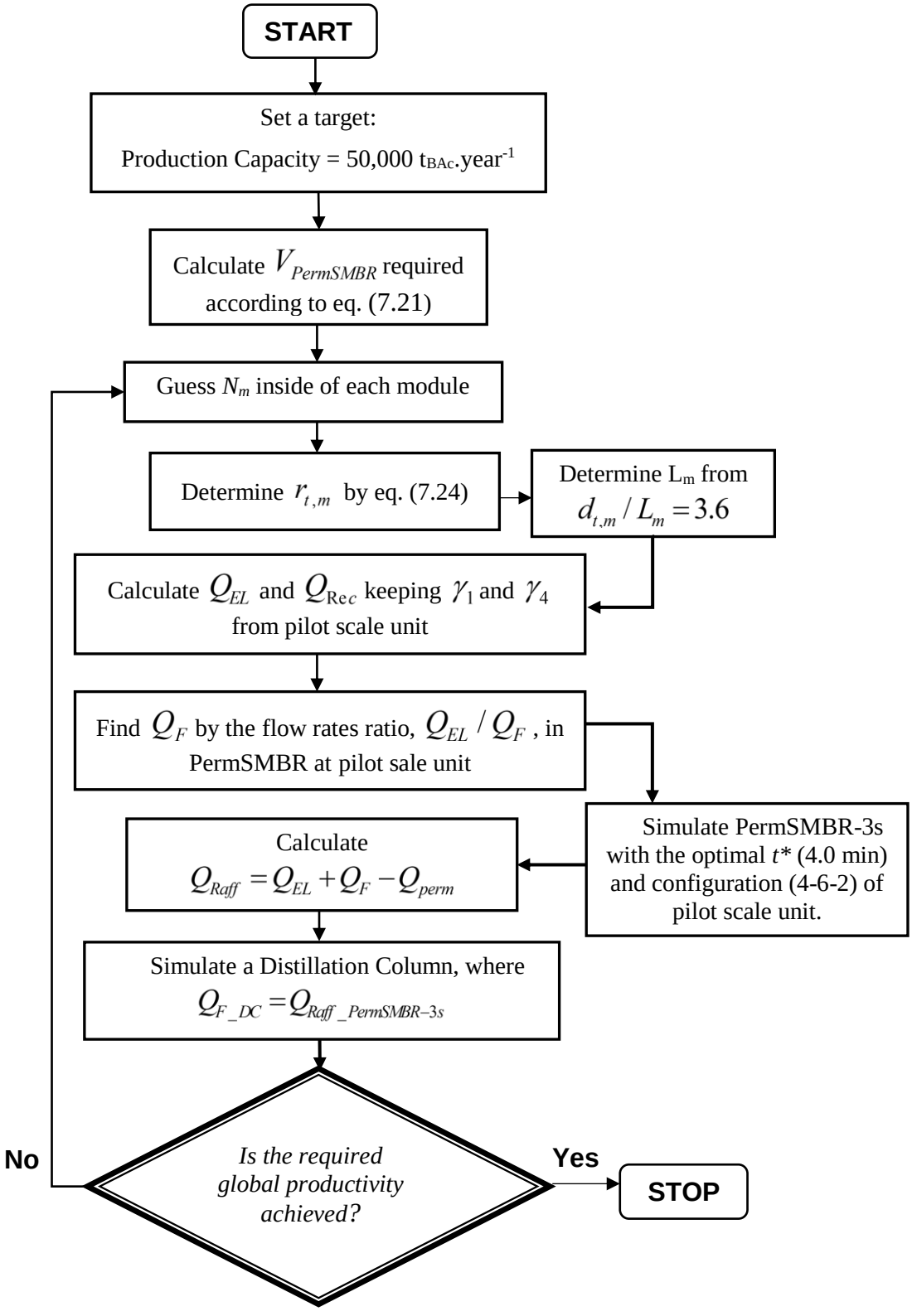

Figure 7.15. Design algorithm to scale up a PermSMBR-3s unit according to the desired global productivity.

The concentration profiles were simulated according to the mathematical model described in section 7.2 and the respective operating and performance parameters obtained for PermSMBR-3s at industrial scale are shown in Table 7.5. Comparing the values obtained with the conventional SMBR performance at the same scale, higher productivity (48 %) and lower desorbent consumption (98 %) were achieved when membrane modules were integrated with SMBR technology and the extract stream is removed, PermSMBR-3s, which led to a significant reduction on the required eluent for the adsorbent regeneration. Similar results had been observed at pilot scale study.

Table 7.5. Operating parameters of SMBR and PermSMBR-3s at Industrial Scale.

Parameter/ Process	SMBR	PermSMBR-3s
Temperature (K)	363	363
Configuration	2-4-4-2	4-6-2
t^* (min)	3.40	4.00
Q_{EL} ($L.min^{-1}$)	2397	42.2
Q_{Rec} ($L.min^{-1}$)	475	310.6
Q_{Ext} ($L.min^{-1}$)	2314.5	-
Q_F ($L.min^{-1}$)	118.0	133.5
Q_{Raff} ($L.min^{-1}$)	200.5	175.7
P_{Ext} (%)	99.32	-
P_{Raff} (%)	99.75	99.53
Conv. (%)	99.53	99.64
Prod. ($kg_{BAc}.(L_{ads}^{-1}.day^{-1})$)	7.22	10.69
Des.C ($L_{n\text{-}Butanol}.kg_{BAc}^{-1}$)	22.7	0.44

7.3.3.2. Process integration: eluent recovery

Since the extract stream is not considered in PermSMBR-3s, the global process just requires one downstream unit. Thus, a distillation column unit was considered for the raffinate stream treatment and the process integration was investigated. The distillation column was dimensioned considering the raffinate stream, provided by PermSMBR-3s,

as the feed stream and then it was optimised. As the result, 99.5 mol. % of BAc is obtained at the bottom considering a reflux ratio of 2.71 and 13 theoretical plates being the column fed in the seventh tray. Like in the previously studied processes, the required dimensions were determined being the length (L_{tower}) and the diameter tower (D_{tower}) 15 m and 1.2 m, respectively. Other process parameters are displayed in Table 7.6 while the input and final parameters obtained with Radfrac method are presented in Table 7.7.

Table 7.6. Process operating parameters of the distillation column for the raffinate treatment in the integrated PermSMBR process with 3 sections.

F (L.min^{-1})	Z_F	X_D	X_B	D (L.min^{-1})	B (L.min^{-1})
152.95	0.328	0.990	0.005	50.2	102.7

Table 7.7. Input and output data of the distillation column simulation using RadFrac method.

Parameter	Input value	Parameter	Output value
N	13	BAc purity (bottom), mol. %	99.5
N_F	7	n-butanol purity (top), mol. %	91.4
R_{actual}	2.71	Reboiler duty, J.s^{-1}	1.56×10^6
Condenser	total		
Bottoms to feed ratio	0.96		

The different scenarios considered for the eluent recovery are represented in Figure 7.16 and Figure 7.17, scenarios ER1 and ER2, respectively.

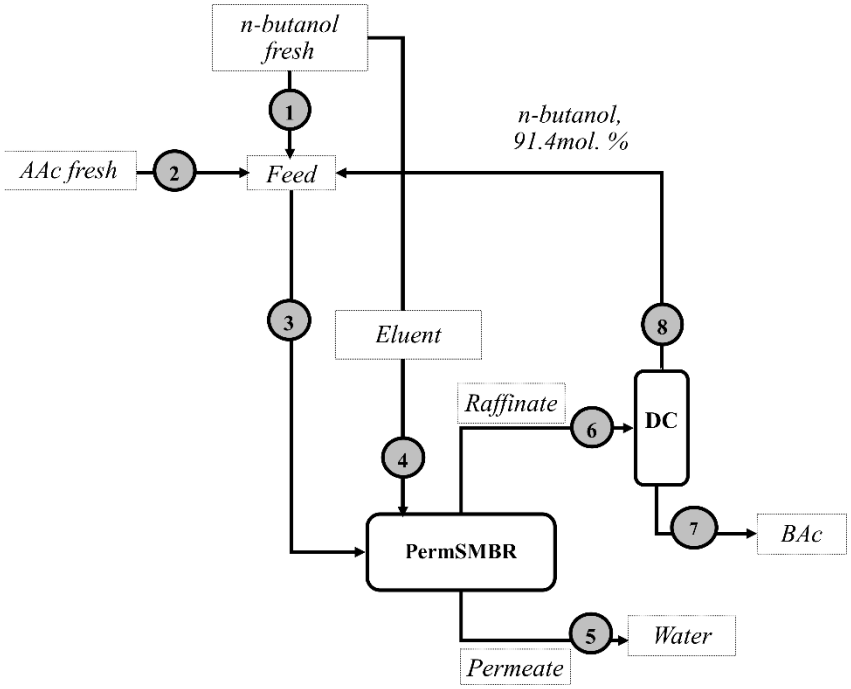

Figure 7.16. Configuration for eluent recycle using the top stream of the distillation column as part of the feed solution to the PermSMBR-3s unit (ER1).

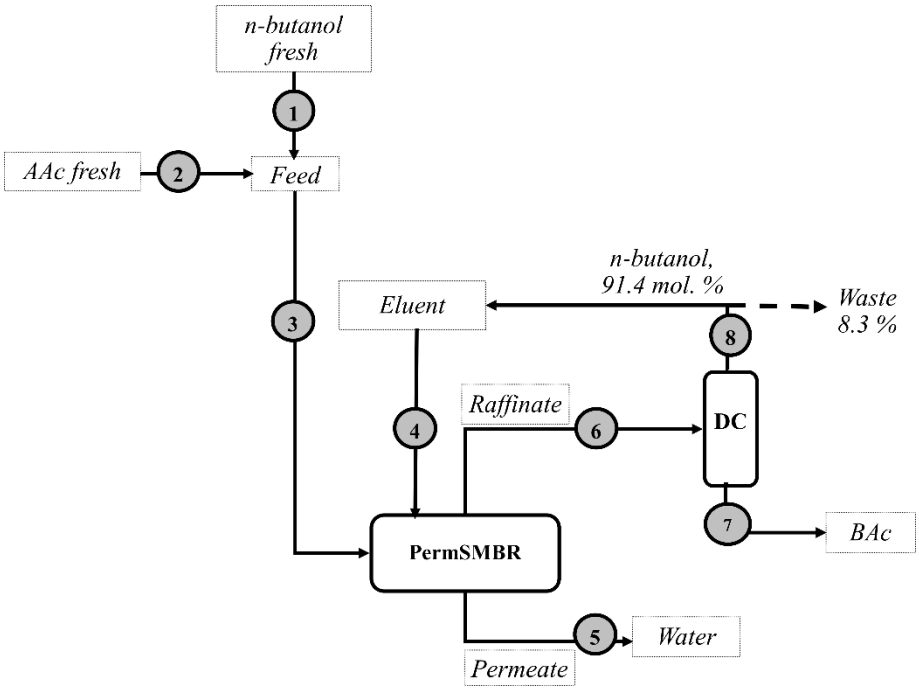

Figure 7.17. Configuration for eluent recycle using the top stream of the distillation column unit to the eluent stream of the PermSMBR-3s unit (ER2).

The first one considers that the eluent recovery is provided by the distillation column top stream as part of the feed stream to the PermSMBR-3s unit and the second one considers the eluent recovery from the distillation column top stream to the eluent stream of the PermSMBR-3s. After an energy balance to both scenarios, similar energy is required for the respective global processes, 1137 $kJ.kg_{BAc}^{-1}$, leading to a reduction of 5.2 % when compared with the energy required for the open process (without eluent recovery), 1200 $kJ.kg_{BAc}^{-1}$. However, the second scenario does not allow achieving the desired BAc purity (99.5 %), so the most suitable choice is the eluent recovery from the distillation column top stream as a part (42 $L.min^{-1}$) of the total feed solution (133.5 $L.min^{-1}$) to the PermSMBR-3s unit. Fresh streams of n-butanol and AAc are required at 36 $L.min^{-1}$ and 55 $L.min^{-1}$, respectively, representing a n-butanol saving of 52 % in the feed solution by recovering 100% of the condenser output stream. As the result, a new feed composition is obtained which is presented in Table 7.8 as well as all new input molar compositions according to the different scenarios. Regarding the final performance parameters, they can be observed in Figure 7.9.

Table 7.8. Input molar composition data in PermSMBR-3s simulations at industrial scale according to the different eluent recycling scenarios.

Scenario	Open Process		ER1		ER2	
STREAM INPUT	Feed	Eluent	Feed	Eluent	Feed	Eluent
$x_{n\text{-butanol}}$	0.5000	1.0000	0.4884	1.0000	0.5000	0.9141
x_{AAc}	0.5000	0.0000	0.4886	0.0000	0.5000	0.0000
x_{BAc}	0.0000	0.0000	0.0223	0.0000	0.0000	0.0831
x_{water}	0.0000	0.0000	0.0007	0.0000	0.0000	0.0028

Table 7.9. Final performance parameters resulting from PermSMBR-3s simulations at industrial scale according to the different eluent recycling scenarios.

Performance Parameters	Open Process	ER1	ER2
P_{Raff} (%)	99.53	99.55	96.98
Conv. (%)	99.64	99.65	97.06
Prod. ($kg_{BAc}.(L_{ads}^{-1}.day^{-1})$)	10.69	10.74	10.83
DesC ($L_{n\text{-}butanol}.kg_{BAc}^{-1}$)	0.44	0.44	0.40
Energy consumption ($kJ.kg_{BAc}^{-1}$) ($\times 10^3$)	1.24	1.18	1.18

From the results in Figure 7.9, ER1 is the best choice for a sustainable PermSMBR process integration at industrial scale fulfilling the BAc purity criteria with great conversion and productivity values achieving a production capacity of 50,220 $t_{BAc}.year^{-1}$. Moreover, this scenario leds to an energy saving of 5.2 % comparing with the open process (without eluent recovery).

7.4. Conclusions

PermSMBR technology was studied for the first time for butyl acrylate production considering commercial hydrophilic membranes and Amberlyst-15 ion exchange resin as catalyst and adsorbent. A mathematical model was proposed for the different configurations, coupled and integrated, performing some assumptions based on the equivalence between the different Simulated Moving Bed Reactors based technologies. After model validation, larger reactive separation sections than the one determined for the conventional SMBR process were obtained due to the continuous water removal from the reaction media by adsorption and permeation, simultaneously.

An optimisation study was performed, considering the integrated configuration, which showed to be more advantageous than the coupled configuration, by studying the effect of the switching time and performing a sensitivity analysis to the ratios between the liquid

and solid velocities in the critical PermSMBR sections (sections 1 and 4). Further optimisation was attained by reducing the unit from 4 to 3 sections eliminating the extract stream (3-sections integrated PermSMBR). The maximum performance of the reactor was achieved with a configuration 4-6-2 (columns per section) and a switching time of 4.0 min at 363 K. Comparatively to the SMBR performance, the productivity increased 36 % and the desorbent consumption was reduced 98 %.

Finally, a design algorithm was suggested for the 3-sections integrated PermSMBR scaling up at industrial scale. All units were dimensioned including a distillation column that was suggested for the raffinate treatment. Two different scenarios were considered for the process integration with eluent recovery and the most suitable scenario comprises the use of the distillation column top stream as part of the feed solution to the 3-sections integrated PermSMBR unit leading to 100 % of n-butanol recovery.

7.5. Notation

Abbreviations

AAc	Acrylic Acid	-
A-15	Amberlyst 15 ion exchange resin	
BAc	Butyl Acrylate	-
CL	Tube Layout Constant	
CTP	Tube Pass Constant	
DBE	Dibuthoxyethane	
DEE	Dietoxyethane	
DC	Distillation Column	
ER	Eluent Recovery	
FBR	Fixed-Bed Adsorptive Reactor	-
gPROMS	general PROcess Modelling System	
LDF	Linear Driving Force	
OCFEM	Orthogonal Collocation in Finite Elements	

PermSMBR	Simulate Moving Bed Membrane Reactor	
RSR	Reactive Separation Region	-
SMB	Simulated Moving Bed	-
SMBR	Simulated Moving Bed Reactor	-
SR	Separation Region	-
PermSMBR-3s	Simulate Moving Bed Membrane Reactor with 3 sections (integrated configuration)	

Symbols

a	Liquid phase activity	-
A_m	Membrane area per unit module volume	$m^2_{membrane}.m^{-3}_{bulk}$
A_{mod}	Membrane module area	m^2
$A_{t,m}$	Equivalent area to the total of membranes inside of a module	m^2
B	Bottom flow rate (relative to reboiler)	$m^3.min^{-1}$
C	Clearance (relative to shell and tube design)	-
C_i	Liquid phase concentration	$mol.m^{-3}$
$Conv$	Reaction Conversion	%
C_p	Liquid phase concentration inside the particle	$mol.m^{-3}$
D	Distillate flow rate (relative to condenser)	$m^3.min^{-1}$
D_{ax}	Axial dispersion coefficient	$m^2.s^{-1}$
$DesC$	Desorbent Consumption	$m^3_{n\text{-}Butanol}.kg^{-1}_{BAc}$
d_{int}	Internal diameter of a tubular membrane	m
D_M	Molecular diffusivity	$m^2.s^{-1}$
d_{out}	Tube outside diameter	m
$D_{S,\text{mod}}$	Shell diameter (relative to a module)	m
$d_{t,m}$	Equivalent diameter to the total membranes inside of a module	m
F	Flow rate (relative to distillation column)	$m^3.min^{-1}$
H_{tower}	Tower height	m
J	Permeate molar flux	kg. $(m^{-2}\ h^{-1})$

k_L	Global mass transfer coefficient	$m.s^{-1}$
L_b	Fixed-bed column length	m
L_m	Membrane length	m
L_{tower}	Tower length	m
N	Number of trays	-
N_m	Number of membranes	-
N_{mod}	Number of membranes modules	-
N_F	Feed tray of distillation column	-
P_e	Peclet number	-
P_{Ext}	Extracte purity	%
P_{Perm}	Permeate pressure	bar
P_{Raff}	Raffinate purity	%
$Prod$	Productivity	$kg_{BAc}.(m_{ads}^{-3}\ day^{-1})$
P_t	Tube pitch (relative to shell and tube design)	in
$\bar{q}$	Solid phase concentration in equilibrium with the fluid concentration inside the particle	$mol.m^{-3}$
Q	Volumetric flow rate (relative to PermSMBR unit)	$m^3.min^{-1}$
Q_m	Membrane permeance	$kg.(m^{-2}\ h^{-1}\ bar^{-1})$
R_{actual}	Reflux ratio	-
R_e	Reynolds number	-
Sc	Schmidt number	-
Sh	Sherwood number	-
r_p	Particle radius	m
$r_{t,m}$	Equivalent radius to the total membranes inside of a module	m
$t^*_{integrated}$	Switching time	min
$t^*_{coupled}$	Switching time of coupled configuration	min
t^*_{SMBR}	Switching time of SMBR	min
$\overline{t_{r,\mathrm{mod}}}$	Average of retention time in a membrane module	min
T	Temperature	K
U_s	Solid velocity	$m.s^{-1}$

u_j	Liquid velocity	$m.s^{-1}$
u_s	Superficial velocity	$m.s^{-1}$
V_M	Molar volume	$m^3.mol^{-1}$
V_{mod}	Volume of a membranes module	m^3
x	Liquid phase molar fraction	-
x_B	Composition of the light compound in bottom	-
x_D	Composition of the light compound in	-
y	Vapour phase molar fraction	-
z_F	Composition of the light compound in the	-

Greek Letters

γ	Interstitial velocities ratio	-
ε	Bulk porosity	-
ε_p	Catalyst/adsorbent particle porosity	-
ρ_b	Bulk density	$kg.m^{-3}$

Subcripts

0	Relative to initial conditions	-
b	Bulk	-
EL	Eluent	-
Ext	Extract	-
F	Feed	-
i	Relative to a species	-
j	Relative to a section of PermSMBR unit	-
m	Membrane	-
out	At the outlet of the fixed-bed column	-
p	Particle	-
perm	Permeate	-
Raff	Raffinate	-
Rec	Recycle	-

t	Tonnes	-

7.6. References

1. Stankiewicz, A. I.; Moulijn, J. A., Process intensification: Transforming chemical engineering. *Chemical Engineering Progress* **2000,** 96, 22-33.

2. Stankiewicz, A., Reactive separations for process intensification: an industrial perspective. *Chem Eng Process* **2003,** 42, 137-144.

3. Silva, V. M. T. M.; Pereira, C. S. M.; Rodrigues, A. E., PermSMBR—A new hybrid technology: Application on green solvent and biofuel production. *AIChE Journal* **2011,** 57, (7), 1840-1851.

4. Pereira, C. S. M.; Rodrigues, A. E., New sorption enhanced reaction technologies (SMBR and PermSMBR) for the production of diesel blends and green solvents. *Chimica Oggi* **2013,** 31, (3), 64-67.

5. Constantino, D. S. M.; Faria, R. P. V.; Rodrigues, A. E., Chapter Four - Sorption-Enhanced Reaction With Simulated Moving Bed Reactor and PermSMBR Technologies. In *Advances in Chemical Engineering*, Lemonidou, A. A., Ed. Academic Press 2017; Vol. 51, pp 261-330.

6. Pereira, C. S.; Rodrigues, A. E., Process intensification: New technologies (SMBR and PermSMBR) for the synthesis of acetals. *Catalysis today* **2013,** 218, 148-152.

7. Pereira, C. S. M.; Silva, V. M. T. M.; Rodrigues, A. E., Green Fuel Production Using the PermSMBR Technology. *Industrial & Engineering Chemistry Research* **2012,** 51, (26), 8928-8938.

8. Wijmans, J. G.; Athayde, A. L.; Daniels, R.; Ly, J. H.; Kamaruddin, H. D.; Pinnau, I., The role of boundary layers in the removal of volatile organic compounds from water by pervaporation. *Journal of Membrane Science* **1996,** 109, (1), 135-146.

9. Lévêque, A., *Les Lois de la transmission de chaleur par convection*. Dunod: 1928.

10. Himmelblau, D. M., Reaction kinetics and reactor design (Butt, John B.). *Journal of Chemical Education* **1980,** 57, (10), A297.

11. Eryener, D., Thermoeconomic optimization of baffle spacing for shell and tube heat exchangers. *Energy Conversion and Management* **2006,** 47, (11), 1478-1489.

12. Thulukkanam, K., *Heat exchanger design handbook*. CRC press: 2013.

8. Economical Evaluation

A straightforward procedure was followed to determine the main costs involved in each process intensification strategy studied at industrial scale for the butyl acrylate synthesis. In order to compare all proposed schemes, the same calculation basis was used to assess the respective economic viability. In this Chapter, key economic indicators are presented, including the economic potential, production and investment costs for all process intensification strategies studied. Finally, a comparison with other process intensification alternatives, available in the open literature, is performed.

A part of this Chapter is adapted from Constantino, D. S. M.; Pereira, R. P. V.; C. S. M.; Faria; Loureiro, J. M.; Rodrigues, A. E., Enhanced Simulated Moving Bed Reactor Process for Butyl Acrylate Synthesis: Process Analysis and Optimization. *Ind. Eng. Chem. Res.* 2016, 55 (40), pp 10735-10743. DOI: 10.1021/acs.iecr.6b02474.

8.1. Introduction

As mentioned in Chapter 2, different process intensification strategies have emerged for butyl acrylate (BAc) production. Among them, some process schemes were scaled up at industrial scale and their economic viability was evaluated [1-3], including the Reactor-Separator-Recycle (with one recycle) presented by Moraru et al.[1], the reactive distillation column (RD) coupled with a decanter and flash [2], and the RD coupled with a decanter presented by Niesbach et al [3]. The first authors presented a reduction on the production cost of 38 % (836 €.t_{BAc}^{-1}), in relation to the market reference price of BAc [3] (1350 €.t_{BAc}^{-1}), for the Reactor-Separator-Recycle process, which comprises one fixed-bed reactor (FBR) and two distillation columns (more details are described in Chapter 2, *section 2.6*). A reduction of 43.5 % (762 €.t_{BAc}^{-1}) was achieved with a RD coupled with a decanter and a flash vessel while Niesbach et al. determined a reduction of 37 % (855 €.t_{BAc}^{-1}) using a RD column with a decanter.

In this Chapter, a brief economic analysis, for each Simulated Moving Bed Reactor (SMBR) based process investigated in this thesis at industrial scale (the conventional SMBR, enhanced SMBR and Simulated Moving Bed Membrane Reactor with 3 sections, PermSMBR-3s), is performed in order to evaluate the respective feasibility and competitiveness. For that, a calculation basis, similar to the one described by other authors [1], is used for a fair comparison of the different processes schemes, including the ones available in the open literature. Finally, a summary of the main key economic parameters for all process intensification strategies for BAc production is presented, which showed that the conventional SMBR is the most attractive process with promising economic indicators.

8.2. Calculation Basis

The fundamental economic parameters of each process integration strategy at industrial scale were calculated. In this section, the procedure and assumptions

considered are described using the enhanced simulated moving bed reactor (presented in Chapter 6) as reference case.

Capital (*CAPEX*, capital expenditure), and operating (*OPEX*, operating expenditure) costs are the two major categories of costs involved in a project [4]. For the total investment cost, the equipment dimensions, material of construction and operating pressure are crucial. Thus the different equipments involved in the enhanced SMBR were taken into account, including the FBR (7.9 %), SMBR (10.2 %), membrane pervaporation (PERV) unit (24.4 %), distillation column (15.9 %), trays (1.8 %), reboiler (5.8%), condenser (6.0 %), heat exchangers (25.4 %), all pumps required (1.4 %) and a feed vessel (1.2 %).

All the equipment costs were estimated based on equations described in Dimian et al. [4] (Equations (8.1)-(8.4)), with exception of the cost of the pumps which were determined following a procedure described by Timmerhaus and Peters (through equation (8.5)) [5].

$$C_{Vessels/Columns} = \left(M\,\&\,S/280\right)\left(957.9D^{1.066}H^{0.82}\right)\left(2.18+F_mF_p\right) \tag{8.1}$$

$$F_p = 1 + 0.0074(P - 3.84) + 0.00023(P - 3.48)^2). \tag{8.2}$$

$$C_{Trays} = \left(M\,\&\,S/280\right)97.2D^{1.55}\left(F_t+F_m\right)N_t \tag{8.3}$$

$$C_{HEx} = \left(M\,\&\,S/280\right)\left(474.7\cdot A^{0.65}\right)\left(2.29+F_m\left(F_d+F_p\right)\right) \tag{8.4}$$

$$C_{Equipment\_A} = C_{Equipment\_B}\left(\frac{capacity\_A}{capacity\_B}\right)^n \tag{8.5}$$

where the exponent *n* used was 0.34, which corresponds to pumps with a capacity range of 2-100 gallons per minute (gpm), or 0.33 for higher capacities, according to the literature [5].

The cost of vessels, reactors (SMBR and FBR) and columns were obtained from equation (8.1) using the Marshall and Swift (M&S) equipment cost index of 2011, 1536.5, which was also considered by Moraru et al [1]. All equipment was considered to be made of stainless steel (SS), so $F_{m,}$ (material correction factor) is 2.25 (in equation

(8.1)). F_p is the pressure factor and can be determined by equation (8.2) for which atmospheric pressure operation was considered. For the trays cost estimation (internals of distillation column) equation (8.3) was used, where F_t is the tray factor that is 0 for sieve trays while F_m is 1.7 for SS material [4] and N_t is the number of trays. A cost estimation of shell and tubes heat exchangers was determined through equation (8.4), where $F_{m,}$ is 3.75 for SS/SS materials (shell/tubes), $F_{d,}$ is the design factor being 1.35 for kettle reboiler and 0.80 for fixed-tube sheet while F_p is the correction factor for the design pressure being 0 for pressure (P) lower than 10 bar [4]. Afterwards, the *CAPEX* was calculated by adding all costs of the major equipment involved in each process. In the enhanced SMBR process case, a value of 3.87 M € was determined, which represents 57.8 €.t_{BAc}^{-1} considering the production capacity of the respective process, 67,000 t_{BAc}.$year^{-1}$.

The operating or production costs (61.1 M €.$year^{-1}$), $C_{Production}$, were calculated from equation (8.6) which includes the amortisation cost (0.9 %), $C_{Amortisation}$, the utilities costs (2.4 %), the reactants costs (95.0 %) as well as the packing of the reactors (1.7 %).

For the reactants cost, $C_{reactants}$, the prices of acrylic acid (614.5 €.t^{-1}) and n-butanol (628.8 €.t^{-1}) provided in the open literature [3] were considered, resulting in a total of 58.0 M €.$year^{-1}$. An amount of 43.5 tonnes of catalyst/adsorbent (Amberlyst-15 ion exchange resin, A-15) is required for packing both FBR and SMBR (considering the FBR volume of 82.7 m^3 and the SMBR volume of 28.9 m^3). The price of A-15 was calculated based on the Sigma-Aldrich's price (70.4 €.kg^{-1}) and the packing replacement was considered at the end of 3 years. For the utilities costs, $C_{Utilities}$, in enhanced SMBR case the cost of steam (72.2 %), cooling water (4.1 %), waste water treatment (22.4 %) and electricity (1.3 %) were taken into account. For that, the prices reported by Moraru et al.[1] were considered: 7.01 €.GJ^{-1} for steam (6 bar), 0.65 €.GJ^{-1} for cooling water and 0.45 €.$kg_{organics}^{-1}$ for waste water. Cooling water at 293 K was considered for coolers and condensers and steam at 6 bar, for the reboilers. For the electricity cost estimation a value of 0.125 €.kWh^{-1} was considered according to the Eurostat data (half-yearly electricity prices) for industry from European Commission home page [6]. The yearly cost of all pumps were estimated based on the procedure described by Turton et al.[7] (12 units were considered in this process). The design of all heat exchangers was based on a heat transfer coefficient of 700 kcal.$(m^{-2}.h^{-1}.K^{-1})^1$. As a result, the total cost of utilities required, for BAc production by means of the enhanced SMBR process, is about 1.49 M €.$year^{-1}$.

Finally, the specific product cost (912 €.t_{BAc}^{-1}), $C_{SpecificProduct}$, was calculated from equation (8.7) while the amortisation cost, $C_{Amortisation,}$ gave a total value of approximately 552,961 €.$year^{-1}$ from equation (8.8). The payback period was standardised to 7 years for all processes. The Economic Potential of each process is calculated from equation (8.9) where $C_{Product}$ is the market reference price (1350 €.t_{BAc}^{-1}).

$$C_{Production} = C_{Amortisation} + C_{Utilities} + C_{Reactants} + C_{Packing} \quad (8.6)$$

$$C_{specificProduct} = C_{Production} / P.Capacity \quad (8.7)$$

$$C_{Amortisation} = CAPEX / Payback\ Period \quad (8.8)$$

$$Ec.Potential = C_{Product} \times P.Capacity - C_{Production} \quad (8.9)$$

8.3. Results and Discussion

8.3.1. CAPEX

All equipment considered in each process intensification strategy, as well as their respective dimensions and costs, are presented in Table 8.1 to Table 8.3, for conventional SMBR, enhanced SMBR and 3s- integrated PermSMBR, respectively. With respect to distillation columns, the dimensions were obtained from ASPEN PLUS software (Version 8.6). A residence time of 10 min was considered for mixers sizing and the hall-full criteria was used [1]. According to the results, either in the conventional SMBR or in the enhanced SMBR, the most expensive equipment are the heat exchanger required for heating of the eluent stream and the pervaporation unit used for the n-butanol dehydration, where each one represents over 20 % of the *CAPEX* in both processes. This fact is naturally due to the large flow rates treated by each equipment being both flow rates higher than 2000 L.min^{-1}. Indeed, the main disadvantage of these processes (conventional and enhanced SMBR) is the large amount of eluent (n-butanol) required for the solid regeneration.

On the other hand, in the PermSMBR-3s case, the equipment which has the higher contribution for the *CAPEX* value is the set of membrane modules of the PermSMBR-3s (reactor), representing 97 % of the total *CAPEX* value. This reactor comprises 12 membrane modules with a specific area of 1022 m^2 (each module), so its cost was calculated based on a commercial value provided by Pervatech Company (Netherlands) and taking into account its dimensions (12 membrane modules). Regarding the remaining reactors in the conventional SMBR and enhanced SMBR, the respective costs were estimated from equation (8.1) based on their dimensions, which were determined in Chapter 5 and Chapter 6, respectively.

Table 8.1. Major equipment costs and sizes considered in the Conventional Simulated Moving Bed Reactor process.

Equipment	Q ($L.min^{-1}$)	D (m)	H (m)	A (m^2)	Cost (M €)
Mixing Tank	118	0.93	2.79	-	0.045
HEx (feed stream)	118	-	-	5.85	0.039
HEx (eluent stream)	2397	-	-	523	1.009
HEx (condenser)	68.0	-	-	75.5	0.206
HEx (reboiler)	122	-	-	42.9	0.199
HEx (final product)	122	-	-	4.42	0.045
SMBR (N = 12)	-	2.23	0.615	-	0.393
Distillation Column	200.5	1.55	40	-	0.682
Trays (N_t = 48)	-	1.55	-	-	0.077
PERV (N_m = 29,500)	2314	0.007	1.0	649	0.835
Pumps (12 units)	-	-	-	-	0.055
CAPEX Total (M €)					3.586

Table 8.2. Major equipment costs and sizes considered in the Enhanced Simulated Moving Bed Reactor process.

Equipment	Q ($L.min^{-1}$)	D (m)	H (m)	A (m^2)	Cost (M €)
Mixing Tank	130	0.96	2.88	-	0.047
HEx (feed stream)	130	-	-	6.29	0.041
HEx (eluent stream)	2280	-	-	437	0.898
HEx (condenser)	112	-	-	8.51	0.231
HEx (reboiler)	167	-	-	51.8	0.225
HEx (final product)	167	-	-	5.75	0.054
SMBR (N = 12)	-	2.23	0.62	-	0.393
FBR	130	7.25	2.00	-	0.303
Distillation Column	262	1.55	35	-	0.612
Trays (N_t = 42)	-	1.55	-	-	0.068
PERV (N_m = 35,600)	2148	0.007	1.0	785	0.945
Pumps (11 units)	-	-	-	-	0.055
CAPEX Total (M €)					3.872

Table 8.3. Major equipment costs and sizes considered in the Simulated Moving Bed Membrane Reactor with 3 sections, PermSMBR-3s process.

Equipment	Q ($L.min^{-1}$)	D (m)	H (m)	A (m^2)	Cost (M €)
Mixing Tank	134	0.97	2.90	-	0.048
HEx (feed stream)	134	-	-	6.08	0.040
HEx (eluent stream)	42.2	-	-	1.85	0.026
HEx (condenser)	46.0	-	-	56.9	0.172
HEx (reboiler)	126	-	-	33.4	0.169
HEx (final product)	126	-	-	4.84	0.481
PermSMBR (N_{mod} = 12, N_m = 83,000)	-	0.007	0.56	1022.5	39.26
Distillation Column	153	1.23	13	-	0.212
Trays (N_t = 19)	-	1.23	-	-	0.021
Pumps (9 units)	-	-	-	-	0.055
CAPEX Total (M €)					40.48

8.3.2. OPEX

An overview of the total operating expenditure or production cost of the conventional SMBR (a) enhanced SMBR (b) and PermSMBR-3s (c) is displayed in Figure 8.1. Although in the PermSMBR-3s case the cost of the reactants has less impact in the overall production cost, it is noticed that this cost is predominant in all cases, representing 85 % of the total production cost in PermSMBR-3s and 95 % in the remaining process. Other important aspect is the amortisation cost that is significantly higher in PermSMBR-3s process, above ten times greater than the other SMBR based processes. Other costs involve the utilities and packing of reactors. For the first one, the global energy determined for each process through an energy balance was splitted by cooling or heating requirements and the same prices of steam and cooling water used by Moraru et al [1] were considered, as described previously (see *Section 8.2*). Moreover, the electricity required for all pumps was estimated assuming an efficiency of 85 %. The enhanced SMBR is the

process that requires higher packing costs since it includes two reactors and, from the industrial point of view, this process may be less attractive due to larger maintenance compared with the remaining processes. However, other key indicators must be taken into account for the processes competitiveness and viability evaluation, as the economic potential, for instance, which is discussed in *Section 8.3.3*.

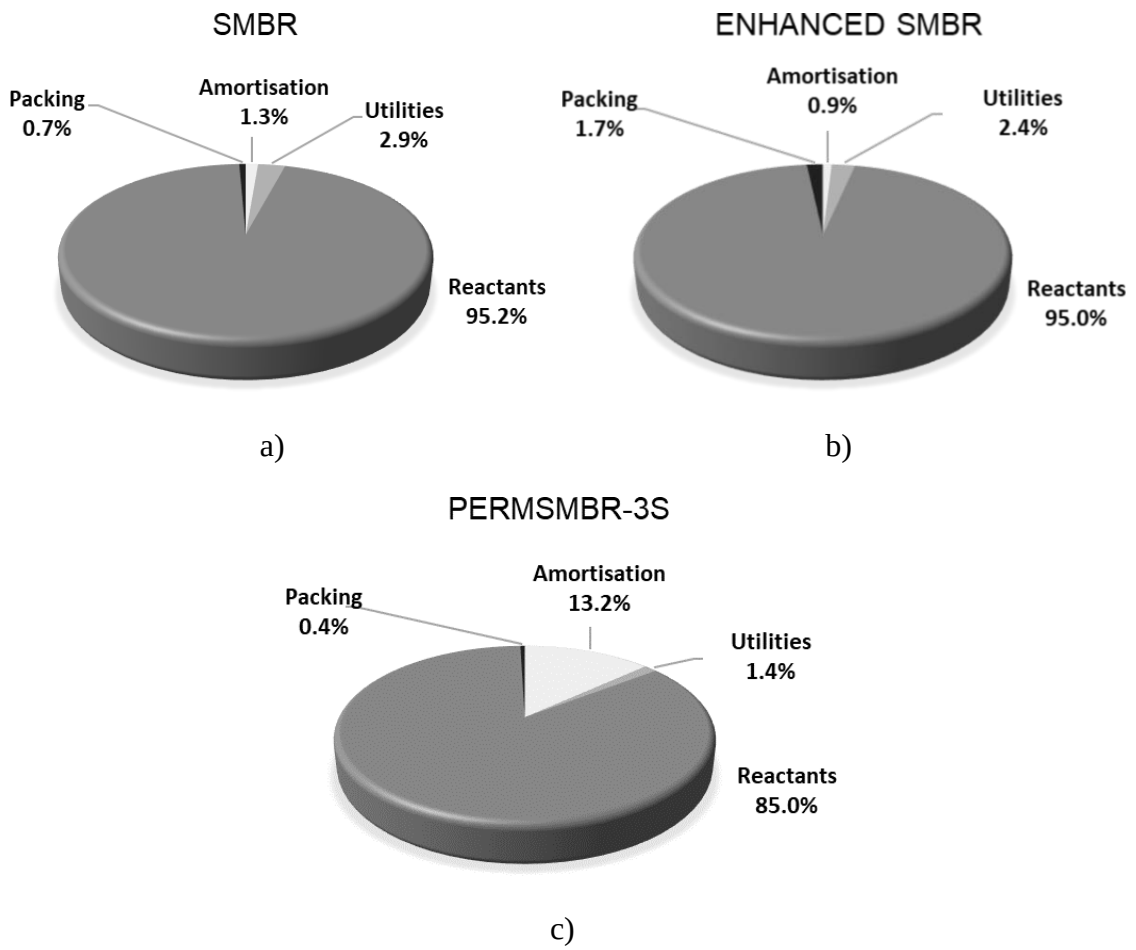

Figure 8.1. Overview of the production costs for each SMBR based process: a) Conventional SMBR (39.3 M €.year^{-1}), Enhanced SMBR (61.1 M €.year^{-1}) and PermSMBR-3s (43.3 M €.year^{-1}).

8.3.3. Competitiveness

8.3.3.1. SMBR based cyclic processes

A direct comparison of the main indicators of the SMBR based cyclic processes studied can be observed in Figure 8.2, where *CAPEX*, production cost and economic potential are represented for each process. According to the results, the conventional SMBR is the most attractive process with the highest economic potential and the lowest production cost. Moreover, the results led to conclude that PermSMBR-3s requires the largest investment while the enhanced SMBR has the most expensive production due, mainly, to the great amount of reactants required and A-15 for the packing of the two reactors (FBR and SMBR). Regarding the economic potential, PermSMBR-3s and the enhanced SMBR present very similar values, 491 €.t_{BAc}^{-1} and 454 €.t_{BAc}^{-1}, respectively.

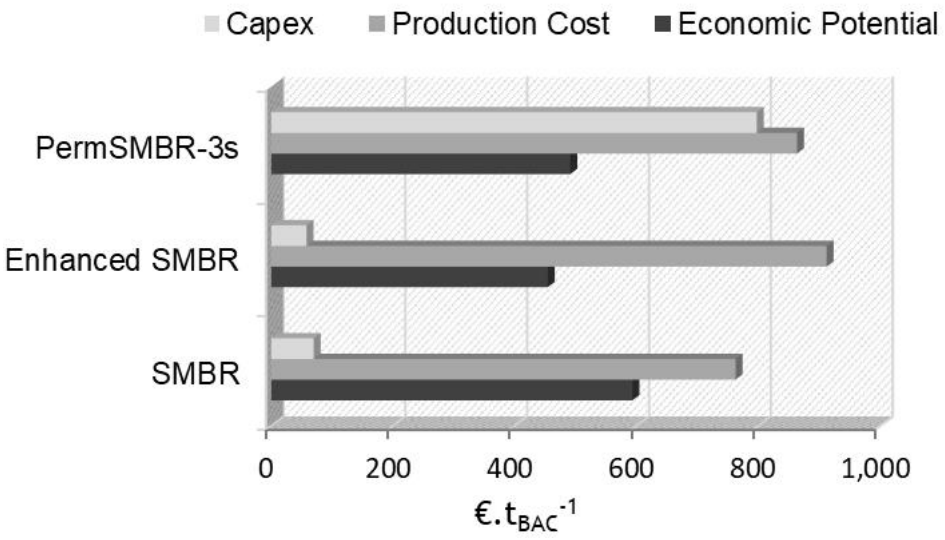

Figure 8.2. Comparison of the main economic indicators for the different Simulated Moving Bed Reactor based processes: Conventional SMBR, Enhanced SMBR and PermSMBR-3s.

8.3.3.2. SMBR based cyclic processes vs other process intensification strategies

A summary of the main economic indicators determined for each process is presented in Table 8.4. In order to have an idea about the competitiveness of the SMBR based processes, results of other process intensification strategies proposed in the open literature for the synthesis of BAc were also considered, including RD with decanter [3], RD with decanter and flash [2] and Reactor-Separation-Recycle (one recycle) [1]. All indicators were normalised by the respective production capacities ($t_{BAc}.year^{-1}$). In a general way, all process intensification processes using heterogeneous catalysis present very competitive specific product cost with significant reductions, from 32.5 % to 43.6 %, relatively to the market reference price of BAc (1350 €.t_{BAc}^{-1}).

Table 8.4. Summary of the key economic indicators for the different PI strategies for the synthesis of BAc and comparison with PI strategies available in the open literature.

Process parameters/ Process	SMBR	Enhanced SMBR	PermSMBR-3s	RD with Decanter [3]	RD with Decanter and Flash [2]	Reactor-Separation-Recycle [1]
P. Capacity ($\times 10^3$) ($t_{BAc}.year^{-1}$)	51.5	67.0	50.2	20.0	20.6	20.5
Energy ($\times 10^3$) ($kJ.kg_{BAc}^{-1}$)	1.80	1.87	1.18	1.69	-	-
CAPEX (€.t_{BAc}^{-1})	69.5	57.8	797	238	231	191
$C_{Reactants}$ (€.t_{BAc}^{-1})	725	866	734	743	714	707
$C_{Utilities}$ (€.t_{BAc}^{-1})	21.8	22.2	11.7	76.6	15.0	101
$C_{Amortisation}$ (€.t_{BAc}^{-1})	9.95	8.25	114	34.4	33.0	27.3
$C_{Specifc Product}$ (€.t_{BAc}^{-1})	762	911	863	855	762	836
Ec.Potential (€.t_{BAc}^{-1})	593	454	491	496	588	473

Although different methodologies might have been used for the estimation of the operating costs, the conventional SMBR process shows the most promising indicators, with the best economic potential (593 €.t_{BAc}^{-1}) and one of the lowest specific product cost (762 €.t_{BAc}^{-1}), even comparing with the processes proposed by other authors. According

to this brief economic analysis, RD coupled with a decanter and flash presents a similar specific product cost to the conventional SMBR; however it requires an investment 3.4 times higher than the conventional SMBR. Regarding the enhanced SMBR, it is the process that attains the highest production capacity (67,000 $t_{BAc}.year^{-1}$) with the smallest capital investment.

8.4. Conclusions

A brief economic analysis was performed to assess the viability and competitiveness of all Simulated Moving Bed Reactor based processes studied at industrial scale. For that, a straightforward procedure was used based on similar methodologies used in the literature. Furthermore, a summary of the several key economic indicators was presented for all process intensification strategies studied as well as for those proposed by other authors. The results showed that all the alternatives using heterogeneous catalysis present very competitive specific product cost, all of them below the market reference price of butyl acrylate, allowing to reduce its specific product cost from 33 % to 44 %, approximately. Moreover, it is possible to conclude that the conventional simulated moving bed reactor and the enhanced simulated moving bed reactor require lower capital expenditure to reach much higher production capacity when compared with reactive distillation based processes.

Finally, although different methodologies may have been used for the estimation of the operating costs, the highest economic potential indicator belongs to the conventional Simulated Moving Bed Reactor process (593 $€.t_{BAc}^{-1}$) with one of the lowest specific product cost, 762 $€.t_{BAc}^{-1}$. These results suggest that the conventional Simulated Moving Bed Reactor process is the most economically attractive solution for the synthesis of butyl acrylate at industrial scale among all alternative processes proposed, so far, in the literature.

8.5. Notation

Abbreviations

AAc	Acrylic Acid	-
A-15	Amberlyst 15 Ion Exchange Resin	-
BAc	Butyl Acrylate	-
FBR	Fixed-Bed Reactor	-
HEx	Heat Exchanger	-
M	Millions	
PERV	Pervaporation	-
RD	Reactive Distillation	-
SMBR	Simulated Moving Bed Reactor	-
PermSMBR-3s	Simulated Moving Bed Membrane Reactor with 3 sections and integrated configuration	-

Symbols

A	Area	m
$C_{Amortisation}$	Amortisation cost	€.t_{BAc}^{-1}
$CAPEX$	Capital expenditure	€.t_{BAc}^{-1}
$C_{Equipment}$	Equipment cost	€
C_{HEx}	Cost of heat exchanger	€
$C_{Reactants}$	Reactants cost	€.t_{BAc}^{-1}
$C_{Production}$	Production cost	€.t_{BAc}^{-1}
$C_{SpecificProduct}$	Specific product cost	€.t_{BAc}^{-1}
C_{Trays}	Trays cost	€
$C_{Utilities}$	Utilities cost	€.t_{BAc}^{-1}
$C_{Vessels/Columns}$	Cost of vessels or columns	€
D	Diameter	m
$Ec.Potential$	Economic potential	€.t_{BAc}^{-1}
F_d	Design factor	-

F_m	Material correction factor	-
F_p	Pressure factor	-
F_t	Tray factor	-
H	Height	m
$M\ \&\ S$	Marshall and Swift	-
N_m	Number of membranes in a module	-
N_{mod}	Number of membrane modules	-
N_t	Number of trays	-
$OPEX$	Operating expenditure	€.t_{BAc}^{-1}
P	Pressure	bar
$P.Capacity$	Production capacity	$t_{BAc.}year^{-1}$
Q	Flow rate	$m^3.min^{-1}$

8.6. References

1. Moraru, M. D.; Bildea, C. S.; Milea, A., Design and Economic Evaluation of a Process for n-Butyl Acrylate Production. *U.P.B. Sci. Bull, Series B* **2016,** 78, 113.

2. Moraru, M. D.; Bîldea, C. S., Process for n-butyl acrylate production using reactive distillation: Design, control and economic evaluation. *Chemical Engineering Research and Design* **2017,** 125, 130-145.

3. Niesbach, A.; Kuhlmann, H.; Keller, T.; Lutze, P.; Górak, A., Optimisation of industrial-scale n-butyl acrylate production using reactive distillation. *Chem Eng Sci* **2013,** 100, 360-372.

4. Dimian, A. C.; Bildea, C. S.; Kiss, A. A., *Integrated design and simulation of chemical processes*. Elsevier: 2014; Vol. 13.

5. Peters, M. S.; Timmerhaus, K. D., *Plant design and economics for chemical engineers*. McGraw-Hill: New York, 1991.

6. European Commission Home Page. Energy prices and costs in Europe. https://ec.europa.eu/eurostat/statistics-explained/index.php/File:Half-yearly_electricity_prices_(EUR)_V2.png. (accessed on August 2016).

7. Turton, R.; Bailie, R. C.; Whiting, W. B.; Shaeiwitz, J. A., *Analysis, Synthesis, and Design of Chemical Processes*. third ed.; Prentice Hall: 2012.

9. Conclusions and Suggestions for Future Work

9.1. General Conclusions

In this work, new process intensification approaches were investigated for butyl acrylate synthesis, from the equilibrium limited esterification reaction of acrylic acid with n-butanol, based on the simulated moving bed and membrane pervaporation technologies combining them with chemical reaction. Therefore, this Thesis comprised the study of different multifunctional reactors, including a simulated moving bed reactor (conventional SMBR), Enhanced SMBR (fixed-bed reactor coupled with a SMBR) and the integration of both separation techniques (adsorption and membrane pervaporation) with chemical reaction, the simulated moving bed membrane reactor (PermSMBR). For that, the elementary units were firstly investigated separately, namely, a fixed-bed reactor and a fixed-bed membrane reactor. An ion exchange resin, Amberlyst-15, was used as catalyst and adsorbent in the dynamic study of the fixed-bed adsorptive reactor. Commercial hydrophilic silica based membranes were considered for the study of the fixed-bed membrane reactor. Afterwards, the respective cyclic adsorption processes were studied through the different mathematical models developed, taking into account the fundamental kinetic data available in the literature, multicomponent adsorption equilibrium data and multicomponent pervaporation data. Hence, the principal conclusions of this thesis are:

i) Fixed-bed Adsorptive Reactor

Dynamic adsorption experiments were carried out at 323 K and 363 K in absence of reaction to determine the multicomponent adsorption equilibrium data over Amberlyst-15 ion exchange resin. The results showed that the resin affinity towards the species involved in butyl acrylate synthesis, in descending order, is: water, n-butanol, acrylic acid

and butyl acrylate. In order to estimate the adsorption parameters, the multicomponent Langmuir adsorption isotherm was modified considering a constant volumetric monolayer capacity for all compounds. In this way, the number of estimated parameters was reduced from 8 parameters (one monolayer capacity and one equilibrium constant for each species) to 5, simplifying the parameters estimation procedure.

Afterwards, the proposed mathematical model (already with the respective multicomponent adsorption equilibrium parameters previously estimated) was validated with experimental runs involving chemical reaction at 363 K under different conditions. In summary, this sorption-enhanced reaction process showed very promising results for the sustainable butyl acrylate production since it attained conversions significantly above the equilibrium conversion.

ii) Fixed-bed Membrane Reactor

A pervaporation based hybrid process was evaluated for the synthesis of butyl acrylate using commercial hydrophilic silica membranes from Pervatech BV (Netherlands) and A-15 ion exchange resin as catalyst/adsorbent. Fundamental pervaporation data for multicomponent mixtures were measured for the compounds involved in butyl acrylate synthesis in absence of reaction at 323, 353 and 363 K. Then, the permeance as function of temperature was determined for all species.

The presence of butyl acrylate and acrylic acid severely affects the total permeate flux, due to higher mass transfer resistances in the boundary layer of the membrane. Nevertheless, the driving force for water is enhanced by increasing the temperature, since this species presents the highest vapour pressure. These conditions lead to higher permeate water mole fraction and, consequently, higher total flux since it is composed mainly by water. Hence, the compounds are selectively permeated in the following order: water > n-butanol > acrylic acid > butyl acrylate mainly due to the lower vapour pressure values for butyl acrylate and acrylic acid.

Additionally, a mathematical model was developed focusing on either the dehydration of n-butanol, as the downstream separation techniques for of the simulated moving bed reactor extract stream, or on process intensification for the synthesis of butyl acrylate by continuous water permeation and adsorption, simultaneously. Significant improvement on the reaction conversion was reached, 99.8 %, using a fixed-bed membrane reactor

(fixed-bed reactor with integrated membranes) under isothermal conditions (363 K), which is 66 % higher comparatively to the reaction conversion attained in the fixed-bed adsorptive reactor at the same operating conditions (molar ratio of 1.3 with excess of n-butanol).

iii) Simulated Moving Bed Reactor

The promising results obtained in the chromatographic reactor with Ambelyst-15 ion exchange resin led to the study of the butyl acrylate production in a Simulated Moving Bed Reactor. This process intensification strategy allows the reduction of the total number of units required comparing to the conventional process. A mathematical model was proposed to predict the concentrations profiles inside the reactor, which were assessed numerically at pilot and industrial scales taking into account the fundamental kinetic and adsorption data previously determined. After model validation at pilot scale with different experimental runs, the effect of configuration and other operating parameters were studied. Then, a SMBR was sized at industrial scale and the ideal operating conditions to reach the maximum productivity and minimum eluent consumption at industrial scale were determined, which are: Q_{EL} = 2397 L.min^{-1}, Q_{Rec} = 475 L.min^{-1}, Q_F = 118 L.min^{-1} and Q_{Ext} = 2315 L.min^{-1} at 363 K, using a configuration 2-4-4-2 (columns per section) and a switching time of 3.1 minutes.

Although promising results were observed, this kind of reactors require a large amount of eluent for the solid regeneration. Therefore, downstream units were proposed focusing on process integration in order to get a more sustainable process. All units were sized at industrial scale and different scenarios of eluent (n-butanol) recovery were investigated. The final global process attained a very competitive production capacity of 51,500 t_{BAc}.year^{-1} recycling almost all the n-butanol used as eluent. A reaction conversion of 99.8 % was obtained at cyclic steady state, with a final product purity of 99.7 mol.%.

iv) Enhanced Simulated Moving Bed Reactor

A novel process design was investigated for the synthesis of butyl acrylate at industrial scale, by coupling two reactors: a fixed-bed reactor with a SMBR. The viability of this strategy was evaluated by modelling the process according to the flow diagram proposed. The best performance was achieved with a molar feed ratio of (1:2) (n-butanol:AAc) in the fixed-bed reactor and a configuration of 2-3-5-2 in the SMBR, achieving the maximum productivity with the minimum eluent consumption for the butyl acrylate

purity required. The most suitable operating flow rates for this new process design, at 363 K are: Q_{EL} = 2280 L.min^{-1}, Q_{Rec} = 478 L.min^{-1}, Q_F = 130 L.min^{-1} and Q_{Ext} = 2148 L.min^{-1}, achieving a reaction conversion of 99.5 % and a production capacity 30 % higher (67,000 t_{BAc}.year^{-1}) than the conventional SMBR with a similar energy consumption (1.85×10^3 kJ.kg$_{BAc}^{-1}$).

v) Simulated Moving Bed Membrane Reactor

Integrating membrane pervaporation technology with chromatographic reactors can bring significant benefits for an equilibrium limited esterification reaction, as it was proved in the pervaporation membrane reactor study. Therefore, a new process approach based on the SMBR was studied by coupling it with hydrophilic silica membrane modules or integrating hydrophilic silica membranes in it, in a technology designated as simulated moving bed membrane reactor (PermSMBR). The process was investigated numerically through a mathematical model proposed and the integrated configuration reached a better performance than the coupled configuration. Since this strategy allows removing water by pervaporation and adsorption, simultaneously, the integrated configuration was reduced from 4 to 3 sections (eliminating the extract stream) in the PermSMBR-3s, which significantly reduced the amount of eluent required. Moreover, this process design requires one downstream unit less than the previous SMBR based processes. The maximum performance of the reactor, at 363 K, was achieved with a configuration 4-6-2 and a switching time of 4.0 min. Comparatively to the SMBR performance, the productivity increased 36 % and the desorbent consumption reduced 98 %.

vi) Economic Analysis

Lastly, a brief economic evaluation was performed and the principal economic indicators were determined for the different SMBR based processes. From a direct comparison, PermSMBR-3s requires the largest investment while the enhanced SMBR has the most expensive production.

The conventional SMBR process demonstrated to be the most attractive solution for the synthesis of butyl acrylate at industrial scale since it presents the highest economic potential (593 €.t_{BAc}^{-1}), even compared with other process intensification strategies proposed in the open literature. Moreover, this process enables to reach a very

competitive specific product cost, 762 €.t_{BAc}^{-1}, that represents a reduction of approximately 44 % on the market reference price of butyl acrylate (1350 €.t_{BAc}^{-1}).

9.2. Suggestions for Future Work

Although promising results were attained with the different SMBR based process intensification strategies studied in this Thesis for the synthesis of butyl acrylate, there is still a long way to be covered towards a real sustainable and competitive industrial process. Some topics must be deeper investigated in order to clarify some assumptions performed along this Thesis and /or complement some research lines that can lead to a better understanding of the results obtained. Hence, some suggestions of future work are here proposed:

i) The deactivation of the catalyst/adsorbent must be investigated since it is known that the economic viability of a process depends, among several factors, on the catalyst life cycle. Moreover, tests of membrane stability in long term operation are recommended to check the materials compatibility (including catalyst and membrane coating);

ii) Although promising results had been attained in a pervaporation hybrid process integrated with chemical reaction numerically, experimental runs must be performed in the pervaporation membrane reactor (single unit) under batch conditions in order to validate the mathematical model proposed in this Thesis;

iii) As mentioned previously, the influence of the resin shrinking combined with the high viscosity of the eluent used (n-butanol) on the SMBR performance can be mitigated by using special fixed-bed columns with dynamic adjustable pistons in order to avoid the creation of voids in the bulk during the operation. This can help to reduce the dispersion observed in the concentration profiles inside the reactor, increasing its performance. In this way, experimental runs, using these sort of columns in the SMBR at pilot scale unit should be performed and the dispersion effect re-evaluated; Another alternative would be to perform some adaptations to the unit in order to mitigate the dispersion generated by the recycling line;

iv) Additionally, SMBR design can be optimised using an objective function based on annual profit maximisation, for instance, using more advanced optimisation tools (genetic algorithms, particles swarm optimisation, etc.).

v) Finally, a study of alternative process integration configurations considering also different downstream units can be investigated.

Appendix A

A.1. Materials Safety Data

A.1.1. n-Butanol

General Information	
Product Name/ Synonymous:	n-Butanol/ Butyl Alcohol, 1-Butanol
CAS No.:	71-36-3
Molecular Formula:	$C_4H_{10}O$
Hazards Identification	
Classification according to Regulation (EC) No 1272/2008:	Danger H226-Flammable liquids (Category 3) H302- Oral acute toxicity (Category 4) H315-Skin irritation (Category 2) H318 Serious eye damage (Category 1) H336 Specific target organ toxicity -single exposure (Category 3) Central nervous system H335 Specific target organ toxicity -single exposure (Category 3) Respiratory system.
First Aid Measures	
In case of inhalation:	Move person into fresh air.
In case of eye contact:	Wash with plenty of water for at least 15 minutes and consult a physician.
In case of ingestion:	Never give anything by mouth to an unconscious person. Rinse mouth with water. Consult a physician.
Special medical attention:	No data available.

Firefighting Measures	
Extinguishing media:	Water spray, alcohol-resistant foam, dry chemical or carbon dioxide.
Special hazards:	Carbon dioxides.
Advice for firefighters:	Wear self-contained breathing apparatus for firefighting if necessary.
Additional information:	Use water spray to cool unopened containers.

Accidental Release Measures	
Personal precautions and emergency procedures:	Avoid breathing vapours, mist or gas. Ensure adequate ventilation. Beware of vapours accumulating to form explosive concentrations.
Environmental precautions:	Prevent further leakage or spillage if safe to do so. Do not let product enter drains.
Methods and materials for containment and cleaning up:	Contain spillage, and then collect with an electrically protected vacuum cleaner and place in container for disposal according to local regulations.

Handling and Storage	
Precautions for safe handling:	Avoid contact with skin and eyes. Avoid inhalation of vapour or mist. Keep away from sources of ignition.
Conditions for safe storage:	Store in cool place. Keep container tightly closed in a dry and well-ventilated place. Storage class (TRGS 510): Flammable liquids.

Exposure Controls/Personal Protection	
Eye/face protection:	Use safety glasses with side-shields. Use equipment for eye protection tested and approved under appropriate government standards EN 166 (EU).
Skin protection:	Handle with gloves (Nitrile rubber).
Body protection:	Wear Complete suit protecting against chemicals.
Respiratory protection:	Use a full-face respirator type ABEK (EN 14387).

Physical and Chemical Properties	
Appearance:	Colourless liquid.
Melting point:	-90 ºC.
Boiling point:	116 ºC.
Vapour pressure:	0.5 kPa at 20 °C.
Vapour density:	2.56 - (Air = 1.0).
Flash point:	35 °C -closed cup.
Explosion limits:	Upper explosion limit: 11.25 % (v/v) Lower explosion limit: 1.45 % (v/v).
Auto-ignition temperature:	343°C.
Decomposition temperature:	No data available.
Water solubility:	73 $g.L^{-1}$ at 25 °C.
Stability and Reactivity	
Reactivity:	No data available.
Chemical stability:	Stable under recommended storage conditions
Possibility of hazardous reactions:	No data available.
Possible hazardous decomposition products:	No data available.
Conditions to avoid:	Heat, flames and sparks.
Incompatible materials:	Oxidizing agents, alkali metals, bases, strong acids, halogens.
Toxicological Information	
Toxicity:	Acute. LD50 Oral -Rat -790 mg/kg LC50 Inhalation -Rat -4 h -8000 ppm LD50 Dermal -Rabbit -3.400 mg/kg.
Skin corrosion/ irritation:	Skin -Rabbit Result: Skin irritation -24 h

Toxicological Information	
Eye damage/irritation:	Eyes -Rabbit Result: Blindness (OECD Test Guideline 405)
Specific target organ toxicity (single exposure)	May cause respiratory irritation. May cause drowsiness or dizziness.
Specific target organ toxicity (repeated exposure)	No data available
Carcinogenicity:	No component of this product present at levels greater than or equal to 0.1% is identified as probable, possible or confirmed human carcinogen by IARC

A.1.2. Acrylic Acid

General Information	
Product Name/ Synonymous:	Acrylic Acid/ Propenoic Acid, Ethylenecarboxylic Acid.
CAS No.:	79-07-7
Molecular Formula:	$C_3H_4O_2$

Hazards Identification	
Classification according to Regulation (EC) No 1272/2008:	H226-Flammable liquids (Category 3) H302- Oral acute toxicity (Category4) H332- Inhalation acute toxicity (Category 4) H312- Dermal acute toxicity (Category 4) H314-Skin corrosion (Category 1A) H335-Specific target organ toxicity-single exposure (Category 3), Respiratory system H400-Acute aquatic toxicity (Category1).

First Aid Measures	
In case of inhalation:	Move person into fresh air.
In case of eye contact:	Rinse thoroughly with plenty of waterfor at least 15 minutes and consult a physician.
In case of ingestion:	Never give anything by mouth to an unconscious person. Rinse mouth with water. Consult a physician.

First Aid Measures

Special medical attention:	No data available.

Firefighting Measures

Extinguishing media:	Use water spray, alcohol-resistant foam, dry chemical or carbon dioxide.
Special hazards:	Carbon oxides. Flash back possible over considerable distance.
Advice for firefighters:	Wear self-contained breathing apparatus for firefighting if necessary.
Additional information:	Use water spray to cool unopened containers

Accidental Release Measures

Personal precautions and emergency procedures:	Avoid breathing vapours, mist or gas. Ensure adequate ventilation. Beware of vapours accumulating to form explosive concentrations.
Environmental precautions:	Prevent further leakage or spillage if safe to do so. Discharge into the environment must be avoided.
Methods and materials for containment and cleaning up:	Contain spillage, and then collect with an electrically protected vacuum cleaner and place in container for disposal according to local regulations.

Handling and Storage

Precautions for safe handling:	Avoid contact with skin and eyes. Avoid inhalation of vapour or mist. Keep away from sources of ignition.
Conditions for safe storage:	Store in cool place. Keep container tightly closed in a dry and well-ventilated place. Storage class (TRGS 510): Flammable liquids.

Exposure Controls/Personal Protection

Eye/face protection:	Use safety glasses with side-shields. Use equipment for eye protection tested and approved under appropriate government standards EN 166 (EU).
Skin protection:	Use proper glove removal technique (without touching glove's outer surface) to avoid skin contact with this product. Wash and dry hands.
Body protection:	Wear complete suit protecting against chemicals.

Exposure Controls/Personal Protection	
Respiratory protection:	Use a full-face respirator type ABEK (EN 14387).

Physical and Chemical Properties	
Appearance:	Colourless liquid.
Melting point:	14 ºC
Boiling point:	141 ºC
Vapour pressure:	0.5 kPa at 20 °C 5.3 kPa at 60 °C
Vapour density:	2.5 (Air = 1.0)
Flash point:	46 °C-closed cup
Explosion limits:	Upper explosion limit: 13.7 % (v/v) Lower explosion limit: 2.0 % (v/v).
Auto-ignition temperature:	438 ºC
Decomposition temperature:	No data available
Water solubility:	Completely miscible

Stability and Reactivity	
Reactivity:	No data available.
Chemical stability:	Stable under recommended storage conditions.
Possibility of hazardous reactions:	Reacts violently in contact with acids, amines, driers, polymerisation accelerators and easily oxidised materials. Polymerisation can occur.
Possible hazardous decomposition products:	Hazardous decomposition products formed under fire conditions- Carbon oxides.
Conditions to avoid:	High temperatures. Tends to polymerize.
Incompatible materials:	Strong oxidizing agents, strong bases, oxygen, polymerising initiators, peroxides.

Toxicological Information	
Toxicity:	Acute. LD50 Oral-Rat-357 mg/kg (Acrylic acid LC50 Inhalation-Rat-male and female-4 h-> 5.1 mg/l (Acrylic acid)
Skin corrosion/ irritation:	Skin-Rabbit (Acrylic acid) Result: Causes severe burns.-3 min
Eye damage/irritation:	Eyes-Rabbit (Acrylic acid) Result: Corrosive-18-24 h
Specific target organ toxicity (single exposure)	No data available
Specific target organ toxicity (repeated exposure)	No data available
Other toxic effects on humans	Very hazardous in case of skin contact, eye contact (corrosive). Hazardous in case of skin contact (corrosive), inhalation (lung corrosive).
Carcinogenicity:	IARC: Group 3. Not classifiable as to its carcinogenicity to humans.

A.1.3. Butyl Acrylate

General Information	
Product Name/ Synonymous:	Butyl Acrylate/ Butyl prop-2-enoate, Butyl ester of acrylic acid
CAS No.:	141-32-2
Molecular Formula:	C_7-H_{12}-O_2
Hazards Identification	
Classification according to Regulation (EC) No 1272/2008:	H226-Flammable liquids (Category 3) H319-Serious eye damage/eye irritation (Category 2) H315-Skin corrosion/irritation (Category 2) H335-Specific target organ toxicity - Single exposure Respiratory tract irritation (Category 3) H317-Sensitisation - Skin (category 1).

First Aid Measures	
In case of inhalation:	Move person into fresh air.
In case of eye contact:	Rinse thoroughly with plenty of waterfor at least 15 minutes and consult a physician.

First Aid Measures	
In case of ingestion:	Rinse mouth out with water. Consult a physician.
Special medical attention:	No data available.

Firefighting Measures	
Extinguishing media:	Dry chemical powder, alcohol-resistant foam, carbon dioxide. Do not use a heavy water stream.
Special hazards:	Fire: Flammable liquid and vapour. Explosion: May form flammable/ explosive vapour-air mixture.
Advice for firefighters:	Do not attempt to take action without suitable protective equipment.
Additional information:	No data available.

Accidental Release Measures	
Personal precautions and emergency procedures:	Remove ignition sources. Use special care to avoid static electric charges.
Environmental precautions:	Avoid release to the environment.
Methods and materials for containment and cleaning up:	Collect spillage. On land, sweep or shovel into suitable containers. Soak up spills with inert solids, such as clay or diatomaceous earth as soon as possible.

Handling and Storage	
Precautions for safe handling:	Take precautionary measures against static discharge. Use only non-sparking tools. Avoid breathing dust/fume/gas/mist/vapours/spray. Use only outdoors or in a well-ventilated area.
Conditions for safe storage:	Keep container tightly closed.

Exposure Controls/Personal Protection	
Eye/face protection:	Use safety glasses with side-shields. Use equipment for eye protection tested and approved under appropriate government standards EN 166 (EU).
Skin protection:	Nitrile rubber gloves. Use proper glove removal technique (without touching glove's outer surface) to avoid skin contact with this product. Wash and dry hands.
Body protection:	Wear complete suit protecting against chemicals.
Respiratory protection:	Use a full-face respirator type ABEK (EN 14387).

Physical and Chemical Properties	
Appearance:	Colourless liquid.
Melting point:	-64.6 ºC
Boiling point:	145 ºC
Vapour pressure:	0.44 kPa at 20 ºC
Vapour density:	4.4 (Air = 1.0)
Flash point:	36 ºC
Explosion limits:	Upper explosion limit: 0.13% (v/v) Lower explosion limit: 0.099 % (v/v).
Auto-ignition temperature:	293 ºC
Decomposition temperature:	No data available.
Water solubility:	Slightly soluble

Stability and Reactivity	
Reactivity:	Reactive with oxidizing agents, acids, alkalis. The product may undergo hazardous decomposition, condensation or polymerisation.
Chemical stability:	Stable only if stored and handled under recommended conditions. Must contains an inhibitor, hydroquinone monomethyl ether (10 to 120 ppm). It may polymerise on exposure to light and upon heating.
Possibility of hazardous reactions:	Hazardous polymerisation can occurs.
Possible hazardous decomposition products:	Hazardous decomposition products formed under fire conditions-Carbon oxides

Stability and Reactivity	
Conditions to avoid:	Heat, flames and sparks.
Incompatible materials:	Strong acids, strong oxidizing agents, strong bases.

Toxicological Information	
Toxicity:	Acute toxicity
	LD50Oral-Rat-900 mg/kg (Butyl acrylate)
	LC50 Inhalation-Rat-4 h-2730 ppm (Butyl acrylate)
	Remarks:
	Sense Organs and Special Senses (Nose, Eye, Ear, and Taste): Lungs, Thorax, or Respiration: Dyspnea.
Skin corrosion/ irritation:	LD50 Dermal-Rabbit-1,796 mg/kg (Butyl acrylate)
	Rabbit; 24 h uncovered.
	Results: moderate to marked erythema
Eye damage/irritation:	Rabbit; 0.5 ml.
	Results: moderate to severe corneal injury; iritis in 2/5
Specific target organ toxicity (single exposure)	May cause respiratory irritation.
Specific target organ toxicity (repeated exposure)	Prolonged and repeated overexposure to butyl acrylate vapour may result in damage to the tissues of the nose and upper respiratory tract. The contact of the skin with butyl acrylate may cause sensitization and an allergic skin reaction.
Carcinogenicity:	IARC: Group 3. Not classifiable as to its carcinogenicity to humans.

Appendix B

B.1. Calibration Curves

Different calibration curves were determined for different chromatographic columns in different stages of this project. Therefore, in this *Appendix*, the different calibration curves determined for binary and multicomponent mixtures with the CpWax57CB chromatographic column are presented in Figure B.1 and Figure B.2, respectively and the calibration curves for multicomponent mixtures with the Stabilwax column are presented in and Figure B.3.

For binary mixtures analysis, several standards were prepared for each compound with a known composition of the respective compound with isopropanol, which was used as solvent. The respective calibration curves were determined by injecting a fixed volume of each standard and considering the average area of at least three analysis of each standard. For all compounds, the response factor, f_i, corresponds to the slope of the respective function n_i / n_{IS} vs A_i / A_{IS}, which are presented in Figure B.1

For multicomponent mixtures analysis, several quaternary mixtures were prepared. The calibration curve for each compound was obtained considering n-butanol as solvent, as it happens in the Simulated Moving bed Reactor and in the Fixed-Bed Adsorptive Reactor experiments, where n-butanol is always present in large concentrations since it is used as eluent. In this way, the response factor, f_i, corresponds to the slope of the respective function $n_i / n_{n\text{-}butanol}$ vs $A_i / A_{n\text{-}butanol}$, which are represented in Figure B.2 and Figure B.3, for CpWax57CB and Stabilwax, respectively. Regarding the n-butanol, the response factor is the slope of $n_{n\text{-}butanol} / n_{total}$ vs $A_{n\text{-}butanol}$ in both cases.

B.1.1. CpWax57CB chromatographic column

B1.1.1. Binary mixtures

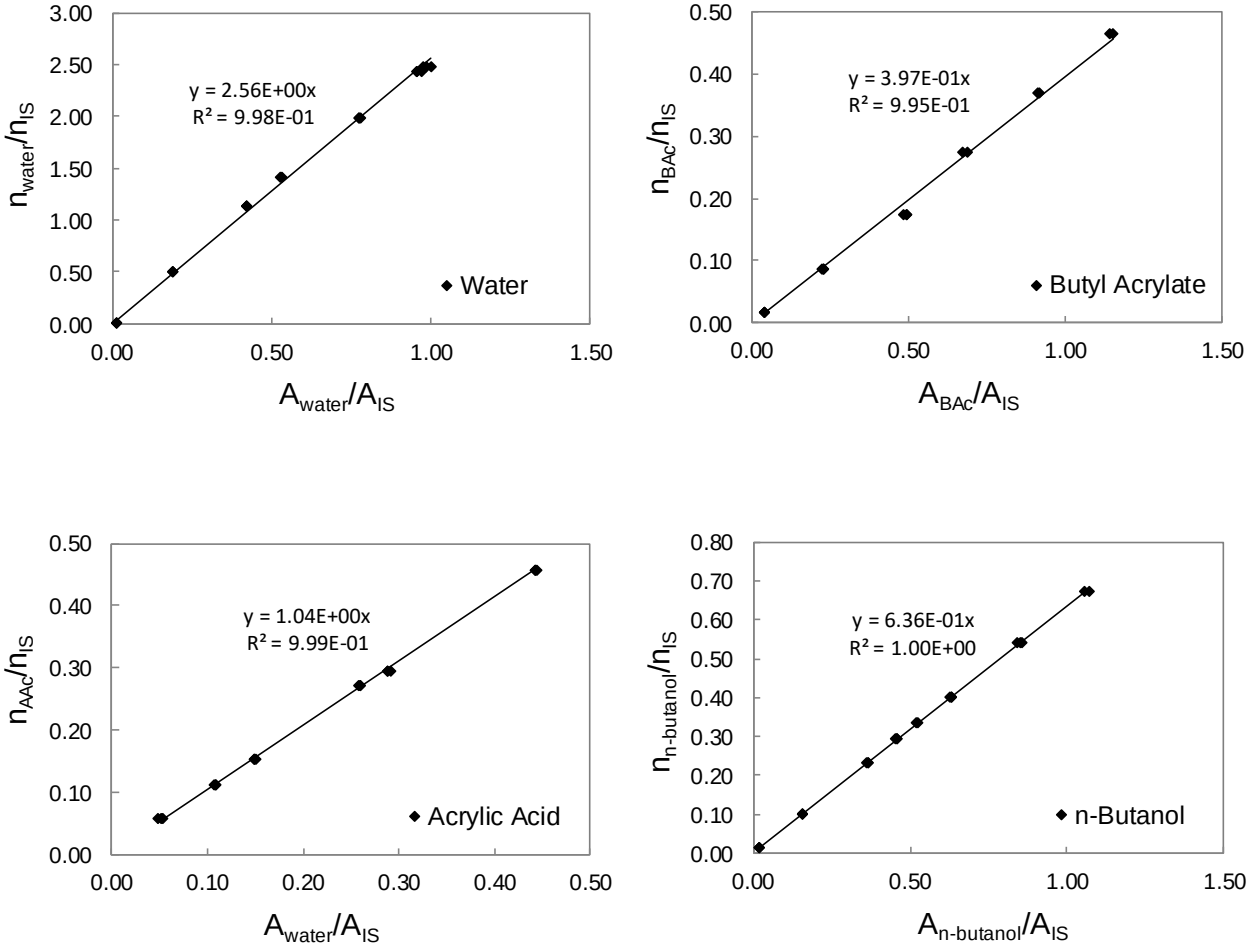

Figure B.1. Calibration curves using the CpWax57CB chromatographic column for binary mixtures analysis.

B1.1.2. Multicomponent mixtures

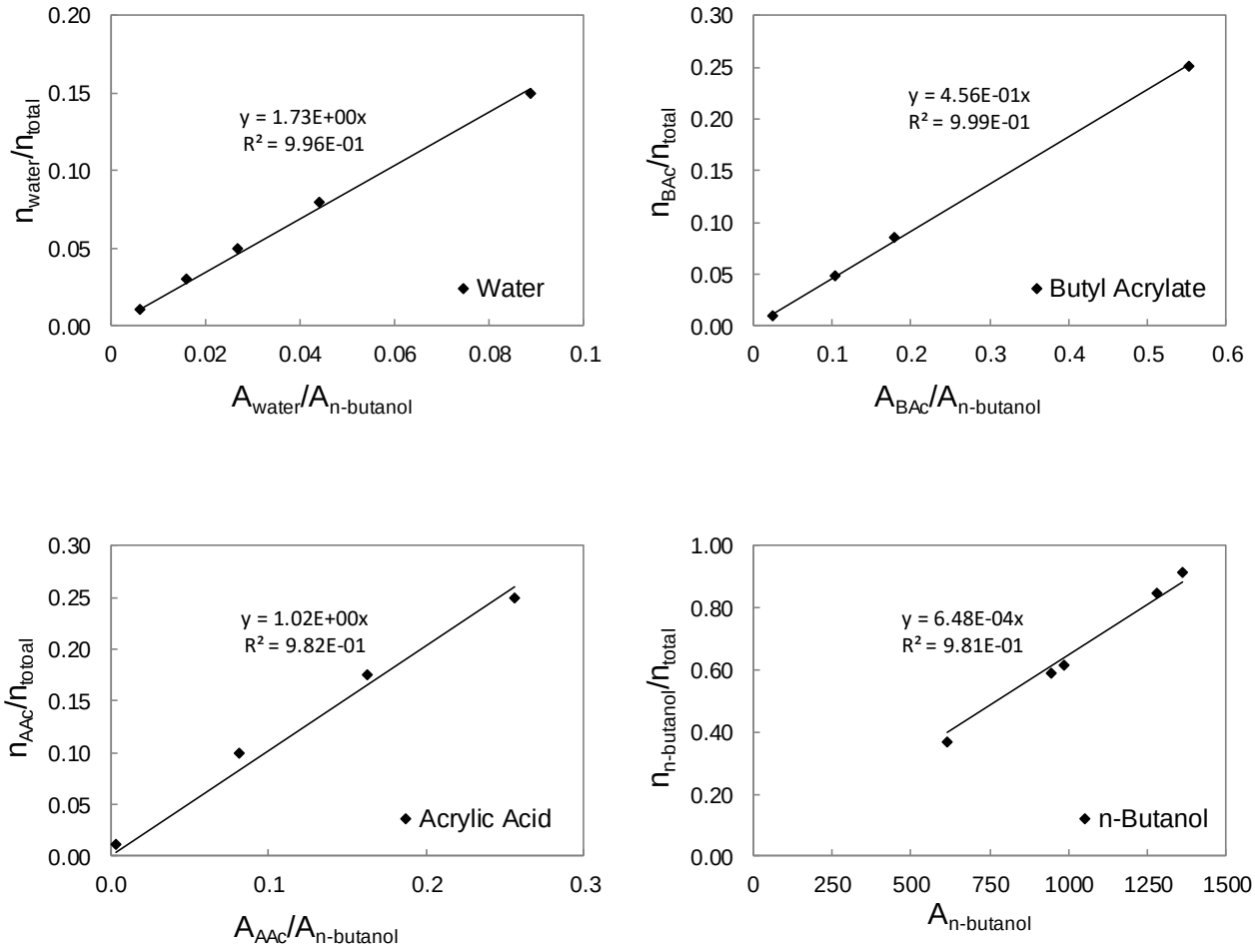

Figure B.2. Calibration curves using the CpWax57CB chromatographic column for multicomponent mixtures analysis.

B.1.2. Stabilwax chromatographic column

B1.2.1. Multicomponent mixtures

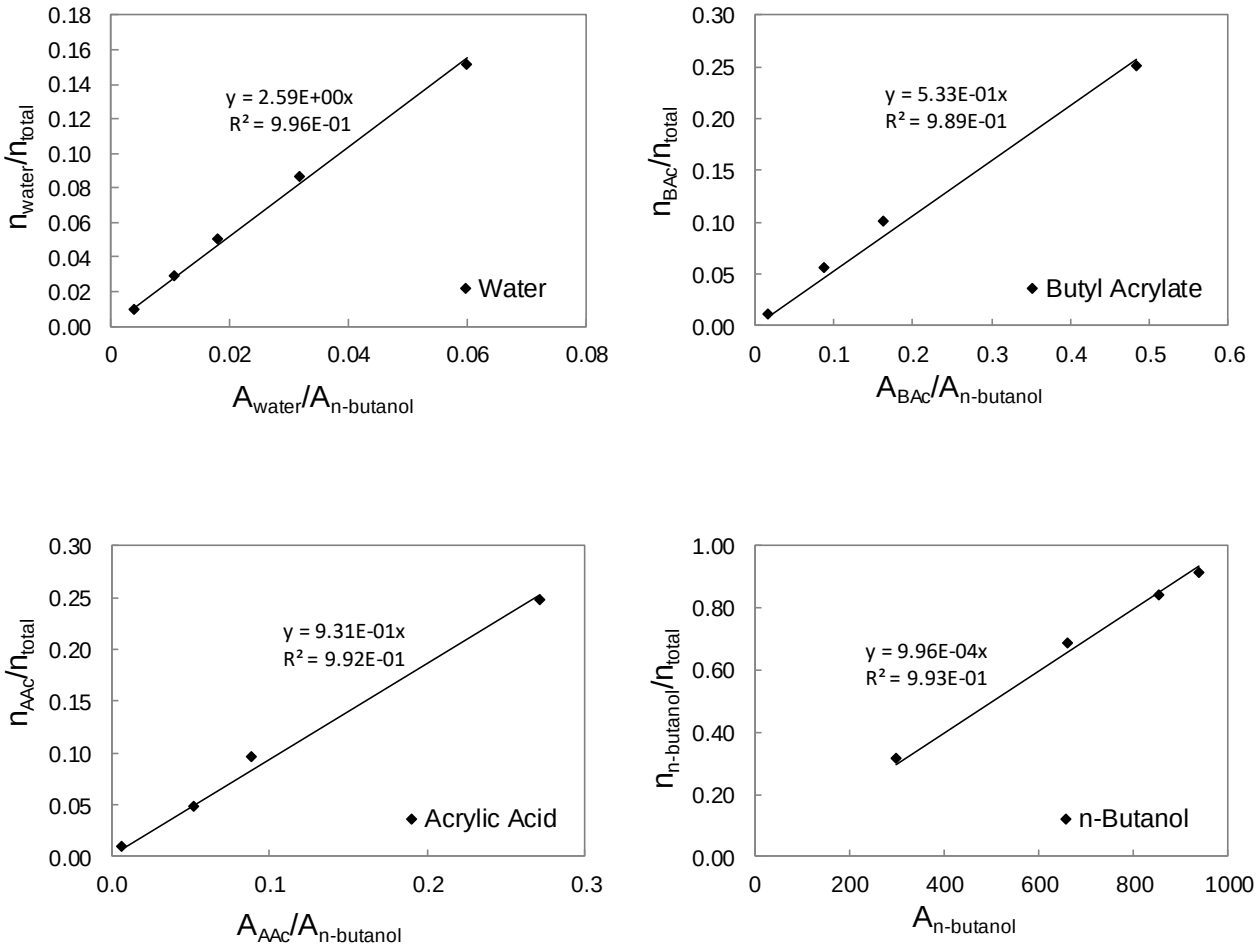

Figure B.3. Calibration curves using the Stabilwax chromatographic column for multicomponent mixtures analysis.

B.1.3. Quantification method and validation

New binary and quaternary mixtures with known concentrations were prepared in order to validate the analytical methods used to quantify the compositions of each species in the different mixtures. Then, the molar fraction of all compounds in

binary mixtures, x_i, were obtained according to equation (B.1), while the molar composition of each species in multicomponent mixtures were obtained with equation (B.2). In the n-butanol case, its molar composition in multicomponent mixtures was obtained according to equation (B.3).

$$x_i = \frac{f_i\left(A_i / A_{IS}\right)}{\sum_j^{NC} f_j (A_j / A_{IS})} \quad (B.1)$$

$$x_i = \frac{f_i\left(A_i / A_{n\text{-}butanol}\right)}{\sum_j^{NC} f_j (A_j / A_{n\text{-}butanol})} \quad (B.2)$$

$$x_{n\text{-}butanol} = \frac{f_{n\text{-}butanol} A_{n\text{-}butanol}}{\sum_j^{NC} x_j} \quad (B.3)$$

Some examples of the binary and multicomponent mixtures with the respective real and estimated compositions are shown in Table B.1 to Table B.5 .

Table B.1. Example of n-butanol/water analysis.

Compound	x_{real}	$x_{estimated}$	Error (%)
n-Butanol	0.434	0.428	-0.6
Water	0.566	0.572	0.6

Table B.2. Example of n-butanol/butyl acrylate analysis.

Compound	x_{real}	$x_{estimated}$	Error (%)
n-Butanol	0.757	0.753	-0.4
Butyl Acrylate	0.243	0.247	0.4

Table B.3. Example of butyl acrylate/acrylic acid analysis.

Compound	x_{real}	$x_{estimated}$	Error (%)
Butyl Acrylate	0.654	0.656	0.2
Acrylic Acid	0.346	0.344	-0.2

Table B.4. Example of water/acrylic acid analysis.

Compound	x_{real}	$x_{estimated}$	Error (%)
Water	0.752	0.748	-0.3
Acrylic Acid	0.248	0.252	0.3

Table B.5. Example of a multicomponent mixture analysis.

Compound	x_{real}	$x_{estimated}$	Error (%)
n-Butanol	0.648	0.642	-0.6
Water	0.102	0.096	-0.6
Butyl Acrylate	0.100	0.108	0.8
Acrylic Acid	0.150	0.154	0.4

Appendix C

C.1. Binary Adsorption Experiments at 323 K

Breakthrough curves for non-reactive pairs were measured at 323 K. The results are presented in the following Figure C.1 to Figure C.4.

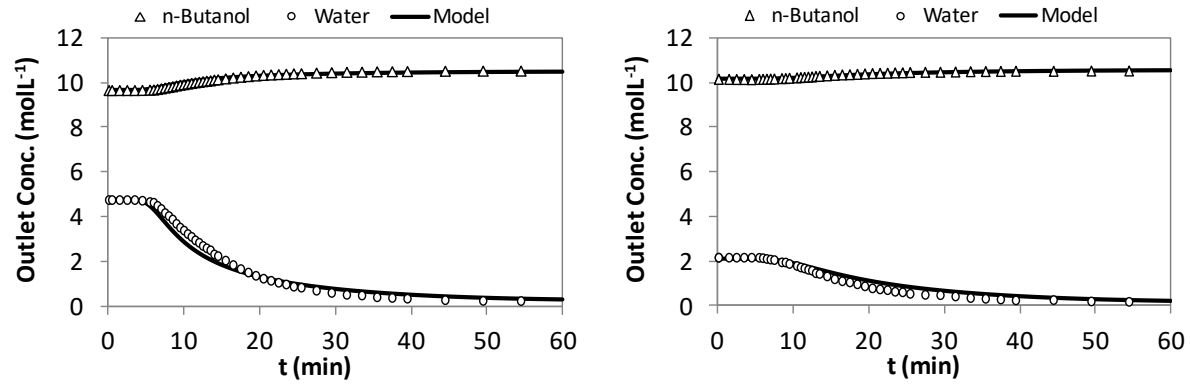

Figure C.1. Breakthrough curves for n-butanol displacing n-butanol/water mixtures at 7.5 mLmin^{-1} and 323 K: a) (67/33) mol % and b) (80/20) mol %; Top-down direction.

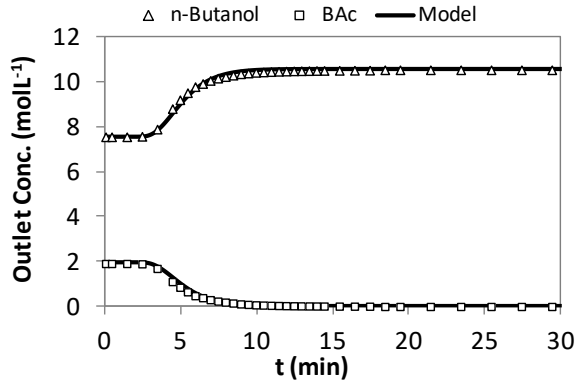

(a

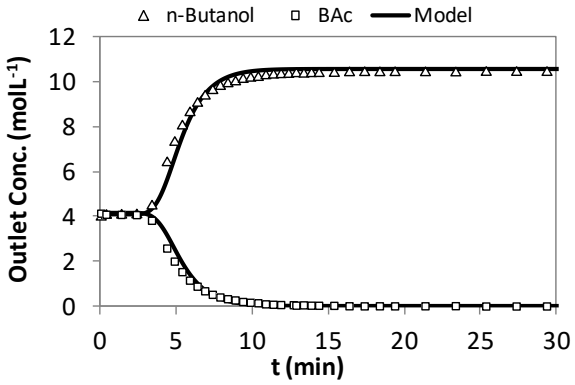

b)

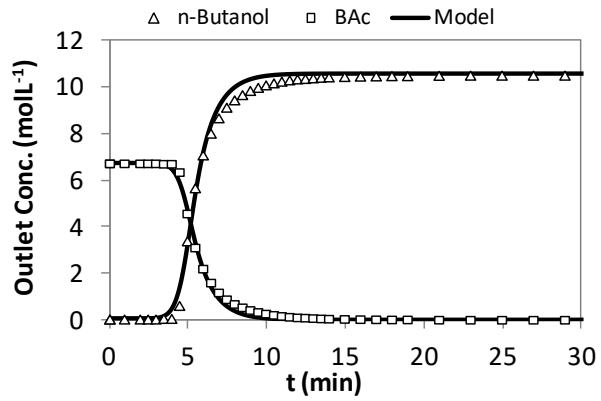

c)

Figure C.2. Breakthrough curves for n-butanol displacing n-butanol/BAc mixtures at 7.5 mLmin^{-1} and 323 K: a) (20/80) mol %, b) (50/50) mol % and c) (0/100) mol %; Bottom-up direction.

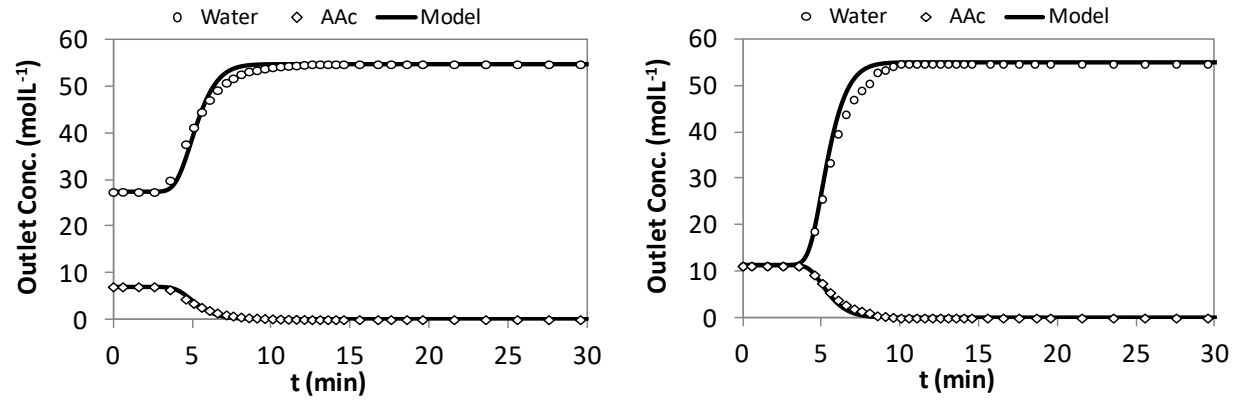

Figure C.3. Breakthrough curves for water displacing AAc/water mixtures at 7.5 mLmin^{-1} and 323 K a) (20/80) mol % and b)(50/50) mol %; Top-down direction.

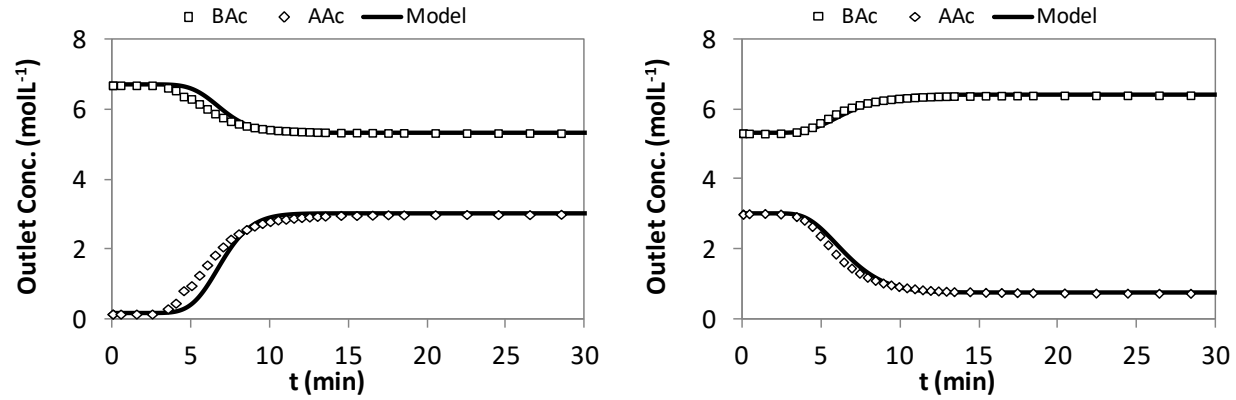

Figure C.4. Breakthrough curves for a) AAc/BAc mixture (35/65) mol % displacing BAc pure and b) AAc/BAc mixture (10/90 mol % displacing AAc/BAc mixture (35/65) mol % at 7.5 mLmin^{-1} and 323 K; Bottom-up direction.

.

Appendix D

D.1. Ternary System: n-Butanol/Butyl Acrylate/ Water

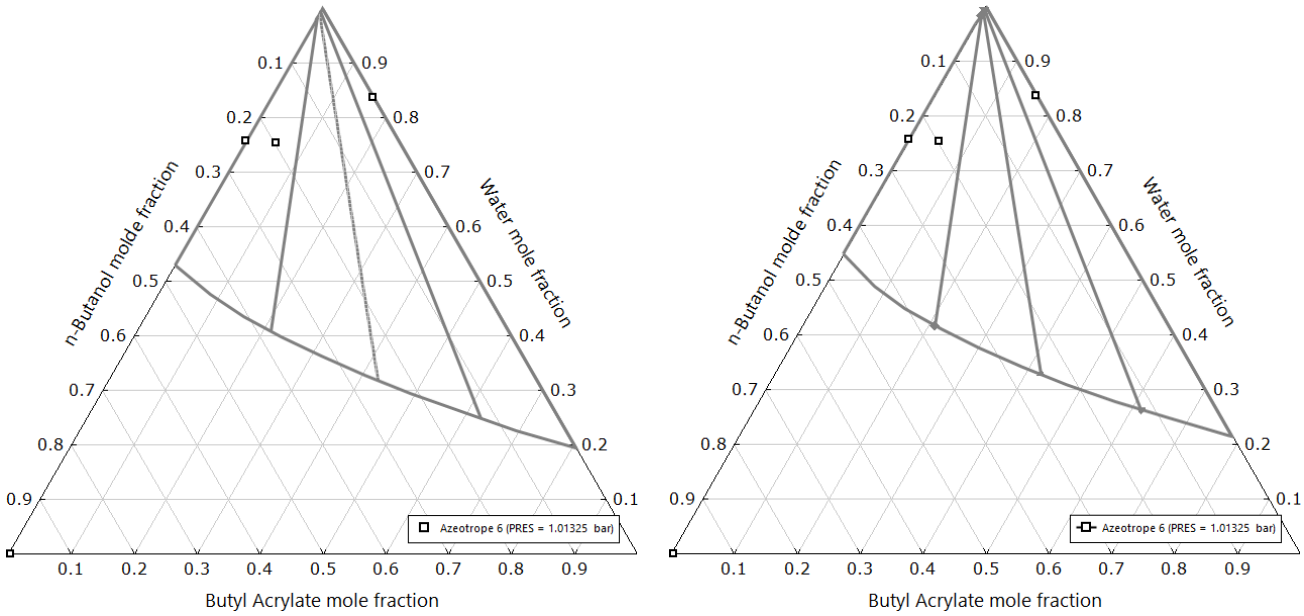

a) T = 323 K b) T = 363 K

Figure D.1. Ternary diagram for n-Butanol/Butyl Acrylate/Water system, using the modified UNIFAC Dortmund group contribution model.

D.2. Permeate stream composition for multicomponent mixtures

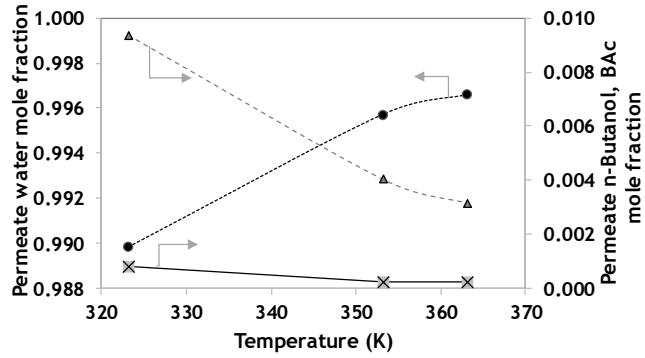

a)

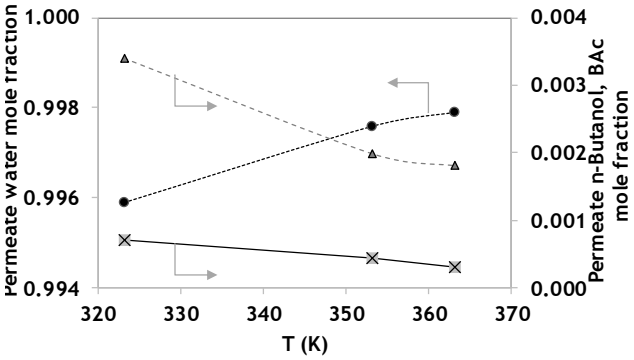

b)

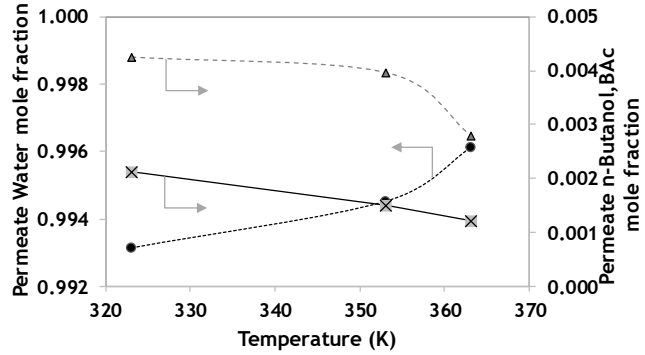

c)

Figure D.2. Permeate stream composition as a function of temperature for the ternary mixtures: a) T1, b) T2, c) T3 (circles: water, triangles: n-butanol, squares: butyl acrylate).

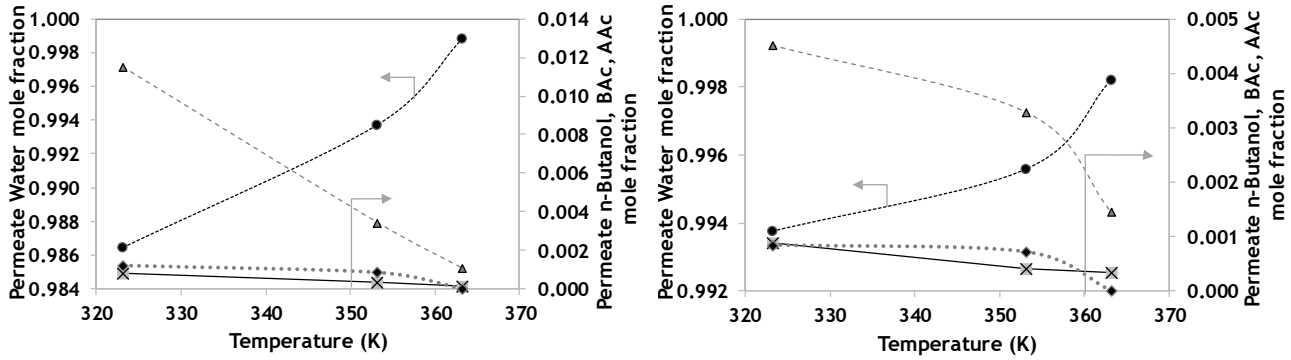

a) b)

Figure D.3. Permeate stream composition as a function of temperature for the quaternary mixtures: a) Q1, b) Q2 (circles: water; triangles: n-butanol; Squares: butyl acrylate, diamonds: acrylic acid).

D.3. Activation Energy, Pre-Exponential Factor and Permeance Data

Table D.1. Activation energy for each compound in the different systems.

System	$E_{perm,\ water}$ (kJ.mol^{-1})	$E_{perm,\ n\text{-}butanol}$ (kJ.mol^{-1})	$E_{perm,\ BAc}$ (kJ.mol^{-1})	$E_{perm,\ AAc}$ (kJ.mol^{-1})
Binary	-28.37	-11.20	-	-
Ternary	-36.38	-28.49	-7.90	-
Quaternary	-21.21	-49.97	-41.05	-9.37
Overall	-30.53	-26.64	-20.85	-9.37

Table D.2. Pre-exponential factor for each compound in the different systems.

System	$Q_{0,\ water}$ (mol.($s^{-1}.m^{-2}.Pa^{-1}$)	$Q_{0,\ n\text{-}butanol}$ (mol.($s^{-1}.m^{-2}.Pa^{-1}$)	$Q_{0,\ BAc}$ (mol.($s^{-1}.m^{-2}.Pa^{-1}$)	$Q_{0,\ AAc}$ (mol.($s^{-1}.m^{-2}.Pa^{-1}$)
Binary	1.07E-10	5.51E-10	-	-
Ternary	4.97E-12	1.21E-13	2.30E-10	-
Quaternary	6.18E-10	4.80E-17	8.37E-16	5.17E-10
Overall	3.90E-11	5.66E-13	1.72E-12	5.17E-10

Table D.3. Permeance of each compound in the different systems at 363 K.

System	Q_{water} (mol.$s^{-1}.m^{-2}.Pa^{-1}$)	$Q_{n\text{-}butanol}$ (mol.$s^{-1}.m^{-2}.Pa^{-1}$)	Q_{BAc} (mol.$s^{-1}.m^{-2}.Pa^{-1}$)	Q_{AAc} (mol.$s^{-1}.m^{-2}.Pa^{-1}$)
Binary	1.29E-06	2.25E-08	-	-
Ternary	8.51E-07	1.51E-09	3.15E-09	-
Quaternary	6.94E-07	7.38E-10	6.71E-10	1.15E-08
Overall	9.58E-07	3.83E-09	1.71E-09	1.15E-08

D.4. Fixed-Bed Reactor vs Fixed-Bed Membrane Reactor: influence of reactant molar ratio

Table D.4. FBR vs FBMR using different reactant molar ratios (A = n-butanol and B = Acrylic Acid).

($r_{A/B}$)	X_{FBR} (%)	X_{FBMR} (%)	C_{BAc_FBR} ($mol.L^{-1}$)	C_{BAc_FBMR} ($mol.L^{-1}$)
1.0	53.2	93.8	3.11	5.51
1.2	57.5	98.1	3.01	5.18
1.3	59.4	98.7	2.96	4.96
1.4	61.2	99.0	2.90	4.74
3.0	77.4	99.4	2.10	2.71

Appendix E

E.1. Effect of the Feed Flux Direction

Additional two fixed-bed reactor experiments were performed using two columns of the pilot scale LICOSEP unit connected in series. In the first experimental run the FBR was fed at 10 $mL.min^{-1}$ in a top-to-down configuration while in the second experimental run the FBR was fed in a bottom-to-up configuration, at the same flow rate. Both experiments were carried out at 323 K and an equilibrium feed mixture diluted in n-butanol, similar to the conditions inside of the SMBR taking into account the eluent stream, was used as feed solution. Changes in the bulk conditions were observed during both experimental FBR runs: in the first one (top-to-down configuration) after 5 min of feeding the solution, a void was observed at the beginning of each column as can be observed in Figure E.1 a); during the second experimental run (bottom-to-up) a bumpy bulk was visible along the columns (Figure E.1 b). Similar effects occur in the LICOSEP pilot scale unit depending on the section flow rates, mainly in section 1 where the section flow rate is even higher (more than 50 $mL.min^{-1}$) comprising the recycle and the eluent flow rates, simultaneously ($Q_1 = Q_{EL} + Q_{Rec}$). Nevertheless, the comparison between the concentration profiles obtained in both experimental FBR runs is shown in Figure E.2, adsorption (a) and regeneration (b) steps, where the results reproducibility is clear. So, in this case, the feed flux direction is not crucial for the sorption-enhanced reactions either in FBR or in the SMBR since flow rates from 10 $mL.min^{-1}$ lead to unstable bulk conditions but with the same effect on the reactors' performance.

a) b)

Figure E.1. Bulk conditions during the experimental runs depending on the feed flow direction: a) Top-to-down and b) Bottom-to-up.

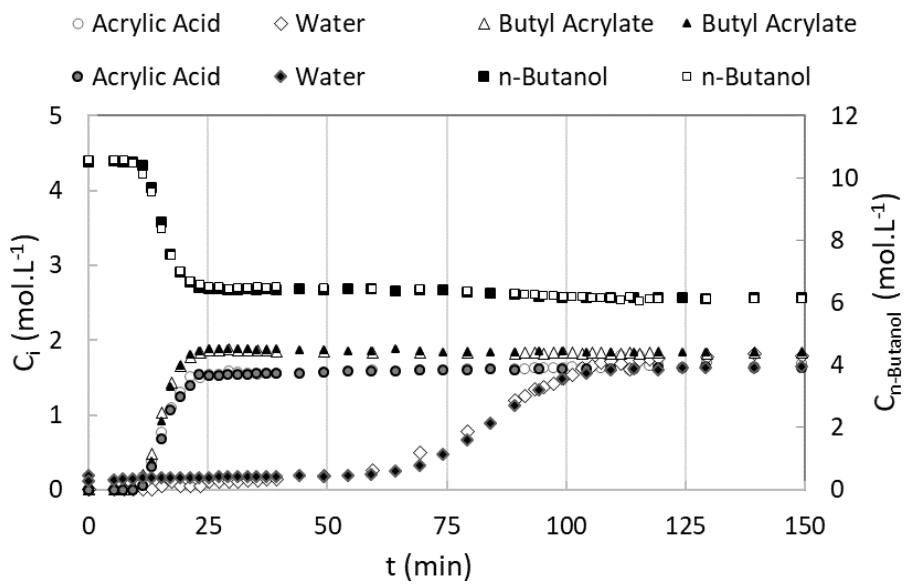

a)

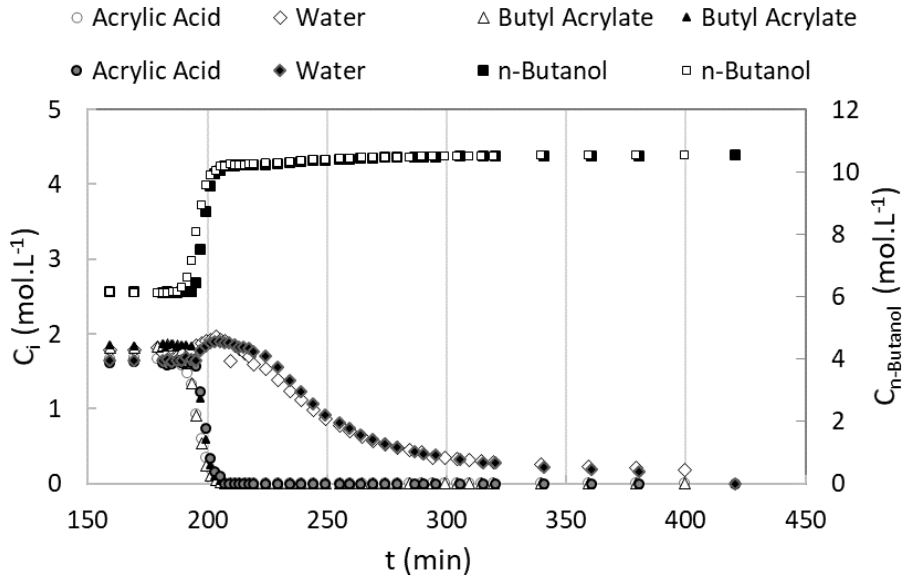

b)

Figure E.2. Experimental concentration histories obtained at the outlet of a Fixed-Bed Reactor operating a 323 K and using different feed flow directions at 10 mL.min^{-1}: top to down (dark symbols) and bottom to up (white symbols): a) adsorption step and b) regeneration step.

E.2. Dispersion Effect on the SMBR Performance

Different simulation runs of SMBR operating a 323 K were performed, with the respective mathematical model described in *Section* 5.3, using the same operating conditions of the experimental run SMBR03 using different Peclet number values in order to analyse its effect on the reactor performance. The results are displayed in Figure E.3, where it is possible to compare both theoretical concentrations histories with the experimental data. In Table E.1 are presented the respective performance parameters. The grey profile, simulated with higher Peclet number, presents more compressive fronts allowing a better separation between BAc and AAc in the raffinate port (column 10). However, when there is higher dispersion (lower Peclet number) it is noticed a significant effect on AAc and BAc concentration profiles, decreasing the respective concentrations and expanding it through section 3 contaminating the raffinate stream.

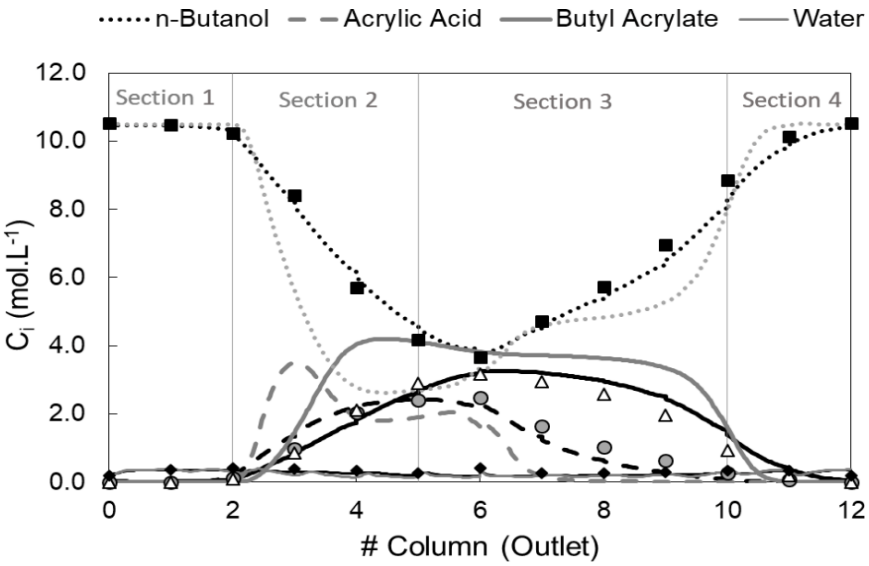

Figure E.3. Theoretical concentration profiles in SMBR LICOSEP unit at the middle of the switching time (3.1 min) at 323 K and at cyclic steady state (13th cycle) under similar conditions of the experimental run SMBR03 considering different Peclet number values: grey profile simulated with Peclet 143 and black profile simulated with Pe 10. The points represent the experimental data.

Table E.1.Dispersion effect on the performance parameters obtained in the SMBR for the same simulated operating conditions (similar to the experimental run SMBR03).

Simulated Conditions	Run SMBR03	
Q_F (mL.min^{-1})	2.0	
Q_{Ext} (mL.min^{-1})	25.0	
Q_{El} (mL.min^{-1})	29.0	
Q_{Rec} (mL.min^{-1})	23.0	
Performance Parameters	*Pe* = 143	*Pe* = 10
P_{Ext} (%)	42.3	42.8
P_{Raff} (%)	85.0	79.2
Conv (%)	20.5	27.6
Prod ($kg_{BAc}.(L_{ads}^{-1}.day^{-1})$)	1.8	1.6
DesC ($L_{n\text{-}butanol}.kg_{BAc}^{-1}$)	26.8	29.8

E.3. Thermophysical data for butyl acrylate system

Thermophysical data for all compounds present in BAc system are available in open literature [1] and the fundamental parameters required to determine those data are described in this section.

The enthalpy of vaporisation of each compound is displayed in Table E.2 as well as the respective parameters required for its determination, including the boiling (T_b) and critical temperature (T_c), according to the equation:

$$\Delta H_v\ (kJ.mol^{-1}) = A \times \left(1 - \frac{T_b}{Tc}\right)^n \qquad (E.1)$$

Table E.2. Parameters required for determination of vaporisation enthalpy of each compound.

Compound	T_b (K)	T_c (K)	A	n	ΔH_v (kJ.mol^{-1})
n-butanol	390.8	562.9	63.02	0.318	43.20
Acrylic Acid	414.2	615.0	62.98	0.351	42.50
Butyl Acrylate	421.0	598.0	55.78	0.327	37.50
Water	373.2	647.1	54.00	0.440	40.30

In Table E.3, values of density, molecular weight and molar volume can be observed. The density is determined by the following equation:

$$\rho(g.cm^{-3}) = AB^{-\left(1-\frac{T}{Tc}\right)^{n}} \qquad (E.2)$$

Table E.3. Parameters required for determination of density as well as for determination of the molecular volume of each compound at 363 K.

Compound	A	B	n	ρ_i (g.cm^{-3})	MM (g.mol^{-1})	V_M (cm^3.mol^{-1})
n-butanol	0.2689	0.2667	0.2457	0.7492	74.12	98.90
Acrylic Acid	0.3465	0.2581	0.3070	0.9702	72.06	74.30
Butyl Acrylate	0.2995	0.2584	0.3084	0.8258	128.2	155.2
Water	0.3471	0.2740	0.2857	0.9656	18.00	18.70

The viscosity of the fluid is given by the equation (E.3) and the respective constants for each compound are presented in Table E.4, while the mixture viscosity is given by the equation (E.4) where x_i is the molar composition of the compound i in the mixture.

$$\mu_i(cP) = 10^{\left(A+\frac{B}{T}+CT+DT^2\right)} \qquad (E.3)$$

Table E.4. Parameters [2]required for determination of viscosity of each compound at 363 K.

Compound	A	B	C	D	μ_i (cP)
n-butanol	-5.397	1.326×10^{3}	0.0062	-5.506×10^{-6}	0.6013
Acrylic Acid	-15.42	2.354×10^{3}	0.0336	-2.735×10^{-5}	0.4559
Butyl Acrylate	-6.931	1.169×10^{3}	0.0135	-1.234×10^{-5}	0.3658
Water	-11.62	1.949×10^{3}	0.0216	-1.599×10^{-5}	0.3125

$$\mu_m(cP) = exp\left[\sum_{i=1}^{n} x_i \ln(\mu_i)\right] \qquad (E.4)$$

Regarding the heat capacity, it can be determined for each compound from the following equation (E.5) and the respective values determined at 363 K can be found in Table E.5.

$$C_{p,i}\left(J.(mol^{-1}.K^{-1})\right) = A + BT + CT^2 + DT^3 \qquad (E.5)$$

Table E.5. Parameters required for determination of heat capacity of each compound at 363 K.

Compound	A	B	C	D	$Cp_{,i}$ ($J.mol^{-1}.K^{-1}$)
n-butanol	127.2	5.228E-01	-1.536E-03	2.216E-06	220.6
Acrylic Acid	84.15	5.300E-01	-1.362E-03	1.729E-06	179.5
Butyl Acrylate	144.3	7.740E-01	-2.126E-03	2.902E-06	284.0
water	-22.42	0.8770	-2.570E-03	2.484E-06	76.03

References

1. Yaws, C. L., *Thermophysical Properties of Chemicals and Hydrocarbons (Electronic Edition)*. Knovel 2010.

2. Yaws, C. L., Yaws' Handbook of Thermodynamic and Physical Properties of Chemical Compounds. In Knovel.